

**COORDINATION OF GEOLOGICAL AND ENGINEERING RESEARCH IN SUPPORT  
OF GULF COAST CO-PRODUCTION PROGRAM**

*FITZGERALD, R.E., MORTON, R.A., DOBRIAN, M.E., & SAH, H.R. (EDS.)*

**Annual Report**

**(May 1, 1984 - July 31, 1985)**

**Prepared for the Gas Research Institute  
Contract No. 5084-212-0924**

**July 1985**

**Bureau of Economic Geology  
and  
Center for Energy Studies  
The University of Texas at Austin  
Austin, Texas 78713**

DISCLAIMER

LEGAL NOTICE This report was prepared by the Bureau of Economic Geology as an account of work sponsored by the Gas Research Institute (GRI). Neither GRI, members of GRI, nor any person acting on behalf of either:

- a. Makes any warranty or representation, express or implied, with respect to the accuracy, completeness, or usefulness of the information contained in this report, or that the use of any apparatus, method, or process disclosed in this report may not infringe privately owned rights; or
- b. Assumes any liability with respect to the use of, or for damages resulting from the use of, any information, apparatus, method, or process disclosed in this report.

<b>REPORT DOCUMENTATION PAGE</b>	<b>1. REPORT NO.</b> GRI 85/0145	<b>2.</b>	<b>3. Recipient's Accession No.</b>
<b>4. Title and Subtitle</b> Coordination of Geological and Engineering Research in Support of Gulf Coast Co-Production Program		<b>5. Report Date (contract period)</b> May 1984 - July 1985	
<b>7. Author(s)</b> R. J. Finley, R. A. Morton, M. H. Dorfman, K. Sepehrnoori		<b>6.</b>	
<b>9. Performing Organization Name and Address</b> Bureau of Economic Geology The University of Texas at Austin University Station, Box X Austin, Texas 78713		<b>8. Performing Organization Rept. No.</b>	
<b>12. Sponsoring Organization Name and Address</b> Gas Research Institute 8600 West Bryn Mawr Avenue Chicago, Illinois 60631		<b>10. Project/Task/Work Unit No.</b>	
<b>15. Supplementary Notes</b> Original research using industry and regulatory body data.		<b>11. Contract(C) or Grant(G) No.</b> (C) 5084-212-0924 (Gas (G) Research Institute)	
<b>16. Abstract (Limit: 200 words)</b> The objective of this investigation was to evaluate the mechanism of secondary gas recovery by co-production in a slightly geopressed watered-out reservoir (Hitchcock N.E. field). This involved making a geologic interpretation of the field and defining the reservoir parameters for reservoir engineering and modeling analysis. The excellent reservoir parameters of the Frio 'A' sandstone are due to its distributary-mouth-bar origin. Slight salinity reductions during production may be evidence of contemporaneous shale dewatering. Geochemical data indicate that the hydrocarbons had a deep source and were introduced by very saline brines. Numerical simulation of the Hitchcock N.E. field is being carried out by modeling the physical dimensions of the field, determining reservoir properties, and matching simulated pressures with historical measures. The historical and simulated measures match has not yet been achieved satisfactorily. Hence no attempt was made to simulate the future performance of the Hitchcock N.E. field. Studies at the Delee No. 1 well show that there are large short-term variations in mud and mud-filtrate resistivity while a well is being drilled. Boron concentrations in the Frio 'A' sandstone are high and must be corrected for when interpreting some types of neutron logs.		<b>13. Type of Report &amp; Period Covered</b> Research 1984-1985	
<b>17. Document Analysis a. Descriptors</b> geologic analysis, shale dewatering, source hydrocarbons, numerical simulation, mud resistivity, boron concentration		<b>14.</b>	
<b>b. Identifiers/Open-Ended Terms</b> evaluation of co-production mechanism, Hitchcock N.E. field, Texas Gulf Coast depleted reservoirs			
<b>c. COSATI Field/Group</b>			
<b>18. Availability Statement:</b> Release unlimited	<b>19. Security Class (This Report)</b> unclassified	<b>21. No. of Pages</b> 211	
	<b>20. Security Class (This Page)</b> unclassified	<b>22. Price</b>	

## CONTENTS

### RESEARCH SUMMARY

PART 1: Structure, facies, and internal properties of the Frio 'A' reservoir, Hitchcock N.E. field, Galveston County, Texas, and Subsidence and subsurface faulting in the Houston-Galveston area, Texas--a result of deep fluid withdrawal?  
by M.P.R. Light and Thomas E. Ewing

STRUCTURE, FACIES, AND INTERNAL PROPERTIES OF THE FRIO 'A' RESERVOIR, HITCHCOCK N.E. FIELD, GALVESTON COUNTY, TEXAS	1
INTRODUCTION	1
REGIONAL SETTING	7
STRUCTURE	8
STRATIGRAPHY	17
Depositional environment of the Frio 'A' sandstone	17
Facies influence on reservoir continuity	20
Facies influence on porosity and permeability	20
Diagenetic modification of porosity and permeability	22
SHALE DEWATERING	23
Original fluid migration	23
Shale dewatering from burial effects	34
Shale dewatering during production	45
SHALE PYROLYSIS DATA	47
CONCLUSIONS	55
IMMEDIATE RESEARCH PLANS	60
SUBSIDENCE AND SUBSURFACE FAULTING IN THE HOUSTON-GALVESTON AREA, TEXAS--A RESULT OF DEEP FLUID WITHDRAWAL?	63
INTRODUCTION	63
FAULTING IN THE CAPLEN AREA	63
EAST BAY FAULT SYSTEM	67

GENOA-WEBSTER FAULT SYSTEM	69
A MODEL TO BE TESTED	72
ACKNOWLEDGMENTS	73
REFERENCES	74
APPENDIX	81
<p>PART 2: Numerical simulation of the Hitchcock N.E. field, Galveston County, Texas by C. M. Lea, D. B. Voorhis, C. K. Mamum, B. H. Caudle, and K. Sepehrnoori</p>	
ABSTRACT	119
INTRODUCTION	121
HITCHCOCK N.E. FIELD GEOLOGY AND THE PHYSICAL DIMENSIONS OF THE RESERVOIR	122
Geology	122
Hitchcock N.E. field reservoir	124
Reservoir dimensions	129
Aquifer dimensions	132
FLUID DATA, PETROPHYSICAL DATA, AND ITS USE AS INPUT DATA	132
Fluid data	132
Petrophysical data	136
ADJUSTMENT OF RESERVOIR PROPERTIES AND GRID BLOCK CONFIGURATIONS TO MATCH HISTORICAL PRESSURES	145
FINAL NOTE	150
ACKNOWLEDGMENTS	154
REFERENCES	155
APPENDICES	156
APPENDIX A	156
APPENDIX B	164
APPENDIX C	181

PART 3: Research in well logging,  
by H. F. Dunlap, James H. Dupree, Jr.,  
and Tom A. Lowe

RESEARCH IN WELL LOGGING--Discussion	203
EFFECT OF MAKEUP WATER AND MUD ADDITIVES ON FLUID RESISTIVITY	205
ABSTRACT	205
INTRODUCTION	205
THE EXPERIMENT	206
USE OF ION SELECTIVE ELECTRODES	208
CONCLUSIONS	211
ACKNOWLEDGMENTS	211
REFERENCES	211
Figures	
1. Hitchcock N.E. field location map	9
2. Depth versus drill-stem test pressures, Hitchcock N.E. field	10
3. Equilibrium temperatures, Hitchcock N.E. field	11
4. Regional depositional setting of the Hitchcock N.E. field	12
5. Regional distribution of the Frio 'A' sandstone aquifer and location of the Hitchcock N.E. field	14
6. Structure map on top of the Frio 'A' pay zone	15
7. Log of the Frio 'A' sandstone interval in the S. G. R. Delee No. 1 well	16
8. Log facies map of the Hitchcock N.E. field	18
9. Frio 'A' sandstone thickness map showing location of Hitchcock N.E. field	19
10. Frio diagenetic sequence in Brazoria County	24

11. Naphthene fraction from shale extracts expressed as time-temperature indices (TTI) versus depth for the Pleasant Bayou No. 1 well and oil from Prets No. 1 well compared to the burial history maturity profiles for both these wells in TTI	26
12. Stylized stratigraphic dip section across the Texas Gulf Coast showing the relative position of the GCO/DOE Pleasant Bayou geopressedured geothermal test wells	27
13. Burial history diagram of the Hitchcock N.E. field	28
14. Maturation profile of the Delee No. 1 well based on vitrinite reflectance data compared to a maturation profile for the Hitchcock N.E. field using Lopatin's method	29
15. Temperature profiles in a geopressedured zone	30
16. Natural logarithm of the naphthene fraction in shale extracts versus the natural logarithm of the time-temperature integral for the Pleasant Bayou No. 1 geothermal test well	32
17. KFC diagram showing the elemental compositions of Anahuac and Frio shales compared to pure clay end members	41
18. Estimated concentration of illite, silica, and alumina versus depth in the Delee No. 1 well, Hitchcock N.E. field	42
19. Strontium versus chloride in formation water, Brazoria and Galveston Counties	48
20. $\delta D$ SMOW versus depth in formation water, Brazoria and Galveston Counties	49
21. Concentration of short chain aliphatic acids versus depth in formation water, Brazoria and Galveston Counties	50
22. Key for pyrolysis data interpretation with average values from the Delee No. 1 well	54
23. Van Krevelen diagram showing the source rock quality of Anahuac and Frio shales from the Delee No. 1 well	56
24. Pyrolysis maturity diagram showing immature nature of the Delee No. 1 shales	57
25. Histograms of the canonical variable for $\delta^{13}C$ aromatics versus $\delta^{13}C$ saturates	58
26. Canonical variable versus pristane/phytane ratios	59
27. Surface faulting and subsidence in the Caplen and Robinson Lake areas, as detected on 1982 aerial photographs taken for the General Land Office, and subsurface faults at about 7,000 ft from well data	65

28. Production of oil and gas versus depth in Caplen field through 1979	66
29. East Bay fault system compared with subsurface structure	68
30. Stratigraphic section from Caplen to High Island, showing continuity of Lower Miocene sandstone reservoirs	70
31. Genoa-Webster fault system compared with subsurface structure	71

#### Tables

1. Isotope analyses of hydrocarbons and formation waters, Hitchcock N.E. field	6
2. Porosity and permeability results from the S. G. R. Delee No. 1 well	21
3. Disproportionation reaction for naphthenes	33
4. Inductively coupled plasma (ICP) analyses of shale samples from the S. G. R. Delee No. 1 well	38
5. Brine analysis results, Phillips Prets No. 1 well	46
6. Results of Rock-Eval pyrolysis	51

## RESEARCH SUMMARY

**Title** Coordination of Geological and Engineering Research in Support of Gulf Coast Co-Production Program

**Contractor** Bureau of Economic Geology and Center for Energy Studies, The University of Texas at Austin, GRI Contract No. 5084-212-0924

**Principal Investigator** R. J. Finley/R. A. Morton/M. H. Dorfman/K. Sepehrnoori

**Report Period** May 1, 1984 - July 31, 1985

**Objectives**

- To evaluate the mechanism of secondary gas recovery by co-production in a slightly geopressured watered-out reservoir. This involved making a geologic interpretation of the field and defining the reservoir parameters adequately for reservoir engineering and modeling analysis.
- To investigate the potential for shale dewatering occurring as a result of fast pressure drawdown during co-production of gas and water.
- To investigate the hydrocarbon sources of gas and condensate, i.e., whether they are locally derived or have migrated from deeper levels.
- To numerically simulate the future performance of the Hitchcock N.E. field.
- To evaluate the possibility of quantitative gas saturation calculation using several current open-hole logs.
- To evaluate sanding prediction using compressional and shear wave velocities from the digital sonic log run in open hole.
- To continue the study of short-term variation in mud and mud filtrate resistivity.
- To advise on logging programs in the Delee No. 1 well.

**Technical Perspective** The Hitchcock N.E. field was reviewed in a regional context, especially the facies and structure of the Frio 'A' sandstone. Emphasis was on the facies influence on reservoir continuity, porosity, and permeability as well as on the diagenetic modification of porosity and permeability. Shale dewatering was examined in the context of three types of fluid movement: original migration of hydrocarbons, shale dewatering from burial, and pressure drawdown due to production. The source of the gas and condensate is being investigated by a number of geochemical techniques.

Numerical simulation of the Hitchcock N.E. field is being carried out by completing four separate tasks. These tasks are:

- (1) Model physical dimensions of the field through grid block configurations based upon subsurface maps of the Hitchcock N.E. field.
- (2) Gather and determine the reservoir fluid properties and petrophysical properties of the reservoir rock.
- (3) Adjust the reservoir properties and the grid block configuration of the field to allow simulated pressures to match historical pressures.
- (4) Use the reservoir description which resulted in the best pressure match to simulate the future performance of the Hitchcock N.E. field.

Gas affects porosity estimates from the neutron log and from the density log differently. This has long been used as a qualitative gas indicator in open-hole log interpretation. It was intended to evaluate the use of these logs, along with the gamma spectrometry tool and the lithodensity log, as a quantitative measure of gas saturation in the Delee No. 1 well. There are no good methods presently available for estimating gas saturation quantitatively from well logs.

#### Results

The Hitchcock N.E. field, which produces from the Frio 'A' or 9,100 ft sandstone, is defined by a northwest-plunging anticline of moderate relief. It is truncated on its southeast flank by a major fault downthrown several hundred feet to the south. Several minor faults displace the original pay zone and may influence enhanced gas recovery efforts in the reservoir.

The Frio 'A' sandstone, which occurs at the top of the Frio Formation in the Chocolate Bayou area, forms part of a constructive delta lobe in the Hitchcock N.E. field. It consists of a stacked sequence of distributary-mouth-bar sandstones that grades into a thin delta destructional unit and is overlain by the transgressive shallow-marine Anahuac shale. Marine reworking of the Frio 'A' sandstone has resulted in its broad lateral extent and internal continuity, although thin shale breaks vertically partition the reservoir. Much of the preserved excellent porosity (+30%) and permeability (+1,000 md,  $0.99 \mu\text{m}^2$ ) in the Frio 'A' sandstone is due to its distributary-mouth-bar origin. The porosity and permeability were subsequently modified by diagenetic reactions.

The Frio 'A' aquifer extends some 8 mi southwest of the Hitchcock N.E. field to the Alta Loma and Sarah White fields. It is confined on its northern and southern flanks by major growth faults. The continuity of the Frio 'A' sandstone has bearing on any plans to control water influx by drilling additional guard wells below the

gas-water contact. However, reservoir modeling suggests that the faults are not sealing during co-production pressure drawdown.

Variable areas of indurated authigenic kaolinite zones developed in the Frio 'A' sandstone adjacent to thin shale units probably result from fluids emitted from the shales that have a consistent illite-smectite composition. Slight reductions in salinity during production at the Prets No. 1 well may be evidence of contemporaneous dewatering of shales.

Shale pyrolysis data indicate that the Anahuac and Frio shales are of too poor a quality and are too immature to have generated appreciable hydrocarbons. Furthermore, isotope data for the Prets No. 1 condensates imply a marine organic source for these fluids. Thermal and hydrocarbon maturity data indicate that the Upper Frio was subjected to an extended period of hot, extremely saline, basinal-fluid flow. This fluid flow appears to have introduced the hydrocarbons and caused albitization of feldspars and formation of carbonate cements.

At the time this report was written, a satisfactory pressure match of historical pressures had not been achieved. Hence, no attempts were made to simulate the future performance of the Hitchcock N.E. field.

No data were gathered for quantitative gas saturation calculations or on compressional and shear wave velocities as no open-hole logs were run at the Delee No. 1 well. However, studies at the Delee No. 1 well show that there are large short-term variations in mud and mud-filtrate resistivity while a well is being drilled. University of Texas personnel were present at the Delee No. 1 well site when the cased hole logs were run, and advised on logs to be included in this package.

The boron concentration in the Frio 'A' sand was found to be unexpectedly high (10 to 44 ppm) and must be corrected for when interpreting some types of neutron logs.

#### Technical Approach

Base maps and a selected number of well logs were acquired in order to prepare new cross sections and maps illustrating the stratigraphic characteristics of the Frio 'A' sandstone. Depositional systems and constituent facies were defined from maps and cross sections in conjunction with published information (Galloway and others, 1984). Detailed geologic mapping of the Frio 'A' sandstone and a detailed description of a core cut in the Delee No. 1 well were conducted to estimate the size, extent, and compartmentalization of the reservoir for simulation purposes. Shale Frio 'A' sandstone compositional changes were examined by a number of techniques at the Frio 'A' sandstone boundary for evidence supporting shale dewatering and the diagenetic history of Frio sandstones. Forty shale samples were subjected to total organic carbon and Rock-Eval pyrolysis analyses. These data give an indication of the quantity of hydrocarbons in the shales (and hence available during shale dewatering) and the shale

thermal maturity. Detailed gas chromatography-mass spectrometry analyses are currently being done on samples of gas and condensate from the Prets No. 1 and Delee No. 1 wells. These data should have bearing on the source of the hydrocarbons. The hydrogen and oxygen isotope ratios of formation waters coexisting with hydrocarbons in the Prets No. 1 and Delee No. 1 wells are being measured and will be used to define the source of the waters.

Most of the reservoir properties and the transmissibility across the fault blocks within the hydrocarbon reservoir are adequately defined. Satisfactory pressure matches of historical data were obtained over a 10-yr period; however, when the simulation was extended to a 30-year period large variations between simulated pressures and historical pressures resulted. The large variations between simulated pressures and historical pressures within the 10- to 30-yr timeframe are believed to be caused by inaccuracies in the definition of the field's aquifer size and the aquifer's petrophysical properties. Simulation runs indicate that the aquifer size of the field is between 2.4 billion barrels and 3.99 billion barrels and that the aquifer permeability is approximately 400 millidarcys (md).

The latest simulation runs, which are currently being processed, are evaluating an aquifer size of 2.8 billion barrels and an aquifer permeability of 400 millidarcys (md). These values for the size of the aquifer and the hydrocarbon reservoir are expected to allow a closer match between historical and simulated pressures.

Once a satisfactory match between simulated and historical pressures has been achieved, simulation runs will be made to project the future performance of the Hitchcock N.E. field under various production scenarios. These forecasts will be incorporated in a final report of the work described herein.

During the drilling of Secondary Gas Recovery Delee No. 1 well, Hitchcock N.E. field, Galveston County, Texas, it was possible to sample the mud and mud makeup water daily and also to obtain samples of barite, bentonite, lignosulfonate, and other additives used in the mud. However, it proved impossible to monitor the volume of mud makeup water added. Water was added to the mud in several places, and it was not possible to devise a system for measuring daily water additions. An ideal system would use a water meter installed so as to measure only mud makeup water, not water used in washing down the rig floor, etc. Such data may be obtained in the Texas Oil and Gas Co. Bruce No. 1 well, Alta Loma N. field, Galveston County, Texas.

Project  
Implications

Results of these projects are an important part of the GRI Co-Production Research Program to locate and evaluate reservoirs where research production tests can be conducted. The best possible geological mapping and definition of reservoir properties are necessary for the reservoir engineering studies designed to enhance gas production. These detailed geochemical studies on the reservoir rock and fluid have also provided improved understanding

of the possible sources of the gas and of how the fluids have migrated in the reservoir system.

PART 1

STRUCTURE, FACIES, AND INTERNAL PROPERTIES OF THE FRIO 'A' RESERVOIR,  
HITCHCOCK N. E. FIELD, GALVESTON COUNTY, TEXAS

and

SUBSIDENCE AND SUBSURFACE FAULTING IN THE HOUSTON-GALVESTON AREA,  
TEXAS--A RESULT OF DEEP FLUID WITHDRAWAL?

by M. P. R. Light and Thomas E. Ewing

assisted by W. D'Attilio

· July 1985

Bureau of Economic Geology  
W. L. Fisher, Director  
The University of Texas at Austin  
Austin, Texas 78713

STRUCTURE, FACIES, AND INTERNAL PROPERTIES OF THE FRIO 'A' RESERVOIR,  
HITCHCOCK N.E. FIELD, GALVESTON COUNTY, TEXAS

by M. P. R. Light

INTRODUCTION

Investigations into the feasibility of gas production from watered-out reservoirs have developed from research into the production of gas from hot brines in geopressed aquifers along the Gulf Coast (Dorfman, 1982). Watered-out gas reservoirs were predicted to become more important as an economic source of natural gas (Dorfman, 1982). Co-production of watered-out, hydro pressured gas reservoirs and geopressed prospects appears to be economically viable (Gregory and others, 1983). Co-production of oil with geopressed gas could significantly improve the economic prospects of gas utilization, thus improving the reserves of both energy resources (Weres and others, 1984).

As part of GRI's Unconventional Natural Gas Research Program, the Bureau of Economic Geology and the Center for Energy Studies, both located at The University of Texas at Austin, have contributed to a joint project on the Hitchcock N.E. field (Galveston County). This project, entitled "Coordination of Geological and Engineering Research in Support of Gulf Coast Co-Production," involved the following research objectives.

(1) Placing the Hitchcock N. E. field in a regional context, especially the facies and structure of the Frio 'A' reservoir sandstone. In 1984 the Frio 'A' (9,100 ft or top Frio) sandstone was correlated in more than 200 electric logs over the Hitchcock, Hitchcock N.E., Alta Loma, Sarah White, and Chocolate Bayou oil and gas fields. Regional sandstone distribution (thickness and percentage) maps and facies maps have been drawn that relate the Hitchcock N.E. field to the Chocolate Bayou field (Brazoria County) to the west. The Frio 'A' sandstone is represented by two units in many areas, and these units have been mapped separately and in combination. The sandstone distribution and facies maps allow an assessment to be made of the depositional environment of the Frio 'A' sandstone.

(2) Detailed geologic mapping (of structure, gross sandstone thickness, and net sandstone thickness above original gas-water contact) of the Frio 'A' sandstone in the Hitchcock N.E. field was needed to understand the size, extent, and compartmentalization of the reservoir for simulation purposes. Local cross sections were constructed over the Hitchcock N.E. field to determine the degree of reservoir compartmentalization. A search was made for thin shale breaks/permeability barriers that may be important during rapid drawdown relative to long-term primary production. The completed maps were made available to researchers at the Center for Energy Studies who then modeled the Hitchcock N.E. reservoir using the pressure drawdown enhancement technique.

(3) An examination was made of the potential for shale dewatering occurring as a result of fast pressure drawdown during co-production of gas and water. This shale water would help to replenish pressure. This analysis entails discriminating between three types of fluid movement:

- a) Original migration of hydrocarbons from the source and emplacement in the trap;
- b) Shale dewatering as a consequence of compaction and pressure/temperature increase due to burial effects; and
- c) Shale fluid flow (dewatering) during production.

In 1984 the Secondary Gas Recovery Delee No. 1 co-production well penetrated the Frio 'A' (9,100 ft) reservoir sandstone in the Hitchcock N.E. field. One hundred and thirty feet (40 m) of core were cut over this depleted gas-condensate accumulation, of which the upper 34.5 ft (10.5 m) consisted of the overlying Anahuac Formation shales. A detailed correlation between rate of penetration of the drill bit and the induction logs had been maintained before coring to accurately fix the core position. Cuttings samples were also collected over the whole interval from lower Miocene to total depth in this well. A detailed core description was made on site, and the core was examined under ultraviolet light for the presence of liquid hydrocarbons. The availability of shale samples at some

distance from, adjacent to, and within the Frio 'A' sandstone as a result of this coring allowed shale dewatering to be investigated by several approaches.

Shale compositional changes were examined at the Frio 'A' sandstone boundaries and in adjacent thin shale layers within the reservoir using Scanning Electron Microscope (SEM) and Energy Dispersive Spectrometer (EDS) techniques, X-ray diffraction, inductively-coupled-plasma analysis (elemental), and detailed core descriptions at the Bureau's laboratories. Shale compositions were estimated and a large number of cross plots and ternary diagrams constructed of elemental composition, elemental ratios, and other parameters. These data were then examined for any phenomena that could cause shale dewatering.

Compositional changes within the Frio 'A' sandstone were also investigated using the SEM-EDS technique as well as by doing a detailed core description. Thin shale or permeability barriers were recorded during this procedure. A search was made for zones showing excessive authigenic cementation, which might be evidence of either shale dewatering or original fluid movement during migration of hydrocarbons into the reservoir. This information was combined with diagenetic models of the Frio Formation and used to decipher the diagenetic history of the Frio 'A' sandstone. The clay composition, sequence, and distribution affect permeability variation and quality in the reservoir.

Detailed petrographic work is still to be done on the samples analyzed by SEM-EDS. Four samples of sandstone also underwent inductively-coupled-plasma elemental analysis to estimate the concentrations of certain elements with large neutron-capture cross sections. These data were made available to Dr. Henry F. Dunlap for calibration of certain logs in the Delee No. 1 well.

(4) An investigation was conducted on the source of the gas and condensate in the Frio Formation, with particular emphasis on the Hitchcock N.E. field. This is a continuation of an integrated geologic study of the Pleasant Bayou-Chocolate Bayou area, Brazoria County, Texas, sponsored by the U.S. Department of Energy. The purpose of this

research was to determine whether the hydrocarbons present in the Hitchcock field are locally derived by shale dewatering or have migrated up from deeper levels. Should the hydrocarbons have a local derivation, there could be an additional influx from the shales by fast pressure drawdown during production. Methods followed in this investigation are outlined below.

The thermal maturation of the Anahuac shales, shale stringers within the Frio 'A' sandstones, and Frio shales below the Frio 'A' sandstone was studied. Vitrinite reflectance analyses were conducted on 40 shale samples from this interval by Robertson Research (U.S.) Inc. (see appendix). Vitrinite reflectance data were combined with modeled thermal maturity using the present geothermal gradient in the Hitchcock N.E. field area and with hydrocarbon maturity using the naphthene concentration in the oils to estimate the depth at which the hydrocarbons formed. Shale samples near the Frio 'A' sandstone were examined for the thermal effects of migrating hot-hydrocarbon-bearing fluids.

Forty shale samples underwent total organic carbon and Rock-Eval pyrolysis analyses by Geochem Laboratories, Inc. (see appendix). These data indicate the quantity of hydrocarbons present in the shales (and hence available during shale dewatering), the amount released by pyrolysis, the relative amount of oxygen and hydrogen in the kerogen, and its thermal maturity. Kerogen quality and hydrocarbon productivity relate to the local derivation of hydrocarbons in the Hitchcock N.E. field.

Detailed gas chromatography-mass spectrometry analyses are currently being done by Geochem Laboratories, Inc., on samples of gas and condensate from the Phillips Prets No. 1 and S. G. R. Delee No. 1 wells, Hitchcock N.E. field. It was hoped that these data would be available at the time of writing this report. However, considerable delay in starting production on the Delee No. 1 well has resulted in only preliminary analyses being available. The entire analysis procedure is outlined in the appendix.

The C<sub>4</sub>-C<sub>7</sub> gasoline-range and C<sub>15</sub>+ paraffin-naphthene (P-N) gas chromatography analyses and C<sub>15</sub>+ gas chromatography-mass spectrometry analyses will be correlated with

Geochem source rock extract analyses at the Pleasant Bayou No. 1 well (Brazoria County) over the entire sampled interval (2,072 ft to 16,500 ft; 630 m to 5,030 m). These analyses should indicate whether or not the hydrocarbons are derived from Oligocene sediments.

The C<sub>4</sub>-C<sub>6</sub> gasoline-range data have been and will be used to estimate the maturity of the sediments using the methods of Young and others (1977). Biomarker analyses will be used to investigate the geological environment of the source rocks and hence to assist in fixing its probable location when combined with depth data from other work.

Detailed carbon and hydrogen isotope analyses of the gases and condensates from the Prets No. 1 and Delee No. 1 wells are being conducted by Coastal Science Laboratories, Inc. (table 1). These data will give an estimate of the temperature of formation (maturity of the source rock) and the depositional environment of the source rocks. It may be possible to estimate the effects of migration and mixing using the methods of Schoell (1983). Geothermal gradient and vitrinite reflectance data from the Hitchcock N.E. field have been combined with hydrocarbon maturity in estimating a depth of hydrocarbon generation.

Hydrogen and oxygen isotope ratios of the formation waters coexisting with the hydrocarbons in the Prets No. 1 and Delee No. 1 wells are being measured and will be compared to isotopic ratios from authigenic cements in Brazoria County and other oil fields in the Gulf Coast (Loucks and others, 1981). Some data already exist and are discussed in this report. Isotopic data are used to define the source of the waters (table 1).

The nickel and vanadium contents of the oils at the Prets No. 1 and Delee No. 1 wells are being measured by Geochem Laboratories, Inc., and will be of use when additional work is done on oil-source rock correlations in the Frio and older formations.

This report presents the results of investigations into the structural, stratigraphic, facies, and diagenetic controls of porosity and permeability in the Hitchcock N.E. field. These data bear on the size and continuity of the field, the best location for guard wells to

Table 1. Isotope analyses of hydrocarbons and formation waters, Hitchcock N. E. field.

$\delta^{13}\text{C}$  and  $\delta^2\text{H}$ , methane:

$\delta^{13}\text{C}$ , gas components ( $\text{C}_2$ ,  $\text{C}_3$ ,  $\text{C}_4$ ,  $\text{C}_5$ ,  $\text{CO}_2$ ):

$\delta^{13}\text{C}$ , condensate:

$\delta^{18}\text{O}$  and  $\delta^2\text{H}$ , water:

Isotopes	Large Component from Shale Dewatering	Large Component from Basinal Brines
Oxygen $\delta^{18}\text{O}$	Heavy $\delta^{18}\text{O}$ for quartz overgrowing indicates formation at shallower depths	$\delta^{18}\text{O}$ constant in formation fluid with depth - no indication of source of formation fluid
Hydrogen $\delta\text{D}$	Constant?	$\delta\text{D}$ becomes depleted with increasing depth of formation fluid
Carbon $\delta^{13}\text{C}$	Constant?	$\delta^{13}\text{C}$ becomes depleted over temperature range $212^\circ$ to $215^\circ\text{F}$ ( $100^\circ$ to $120^\circ\text{C}$ ) and then increases with increasing depth
$\delta^{18}\text{O}$ V's $\delta\text{D}$		Distinguishing genetic groups of waters
$\delta^{18}\text{O}$ V's $\delta^{13}\text{C}$		Distinguishing genetic groups of waters
Sulfur $\delta^{34}\text{S}$		Formation water source identification

reduce water influx into this depleted reservoir, and the degree of shale dewatering occurring during pressure drawdown.

## REGIONAL SETTING

Hitchcock N.E. field lies beneath part of the townsites of Hitchcock and LaMarque in Galveston County 15 mi (9 km) northwest of the City of Galveston (fig. 1). The producing reservoir (Frio 'A', or 9,100 ft) sandstone is widely distributed in a belt parallel to the Texas coastline and has produced from many fields along the Texas and southern Louisiana Gulf Coast (Anderson and others, 1984).

The Frio 'A' sandstone occurs below the T2 marker horizon at the top of the Oligocene Frio Formation. The geostatic gradient is about 0.6 psi/ft (13.6 kPa/m) at the level of the Frio 'A' reservoir (fig. 2), which has an average temperature of 215°F (101°C) (fig. 3). However, the top of the geopressured zone occurs about 7,200 ft (2,200 m) below sea level at the Hitchcock N.E. field, 400 ft (120 m) below the top of the Anahuac Formation (fig. 2). This reservoir is slightly geopressured in contrast to the Mt. Selman co-production test, which was normally pressured.

Hitchcock N.E. field is located on the seaward fringe of the Houston delta system (fig. 4). The following discussion of the regional geology is from Galloway and others (1982). Several minor, laterally coalesced, vertically repetitive deltaic cycles compose the Houston delta system, which is the main locus of terrigenous accumulation in the Frio. Elongate to lobate deltas formed during the most regressive phases in the Lower Frio and more arcuate deltas during periods of general transgression and shoreline retreat in the Upper Frio (Galloway and others, 1982).

During Middle Frio deposition, deltas were supplied by large fluvial channel systems (Chita-Corrigan fluvial system) 16 to 20 mi (25 to 33 km) north and west of the Hitchcock

N.E. field. Net-sand isopachs show that the positions of the fluvial axes changed substantially with time (Galloway and others, 1982).

Platform-delta sequences from 50 to 300 ft (15 to 90 m) thick characterize the Middle and Upper Frio in the Houston delta system. Blocky sandstones record the development of multistoried wave-reworked sandstones of recurrent delta destructional phases. The deltas became smaller as successive lobes shifted landward. Transgression and wave reworking produced thick time-transgressive blanket sandstones. There was constant switching of the delta lobes, destructional marine reworking, and inundation of the abandoned sites (Galloway and others, 1982).

Upper Frio depositional style was strongly influenced by Anahuac marine transgression. This shale wedge, which pinches out updip, marks the invasion of a comparatively sediment starved shelf and contains a neritic fauna. In part it was deposited contemporaneously with and is indistinguishable from the Upper Frio prodelta muds (Galloway and others, 1982).

## STRUCTURE

During Frio deposition, growth faulting produced a closely spaced pattern of strike-parallel, broadly arcuate fractures (Galloway and others, 1982). The Frio 'A' aquifer at the Hitchcock N. E. field occurs within an ovoid fault block that is 10.5 mi (17 km) long and 4.6 mi (7 km) wide (fig. 5). Isolated circular to ovoid areas of thick sand accumulation may represent sites of major growth faulting or salt-withdrawal basins (Galloway and others, 1982). The fault block lies within an area characterized by deeply buried salt diapirs (T. E. Ewing, personal communication, 1985).

The Hitchcock N.E. field is defined by a northwest-plunging anticline of moderate relief (fig. 6). It is truncated on its southeast flank by a major northeast-trending growth

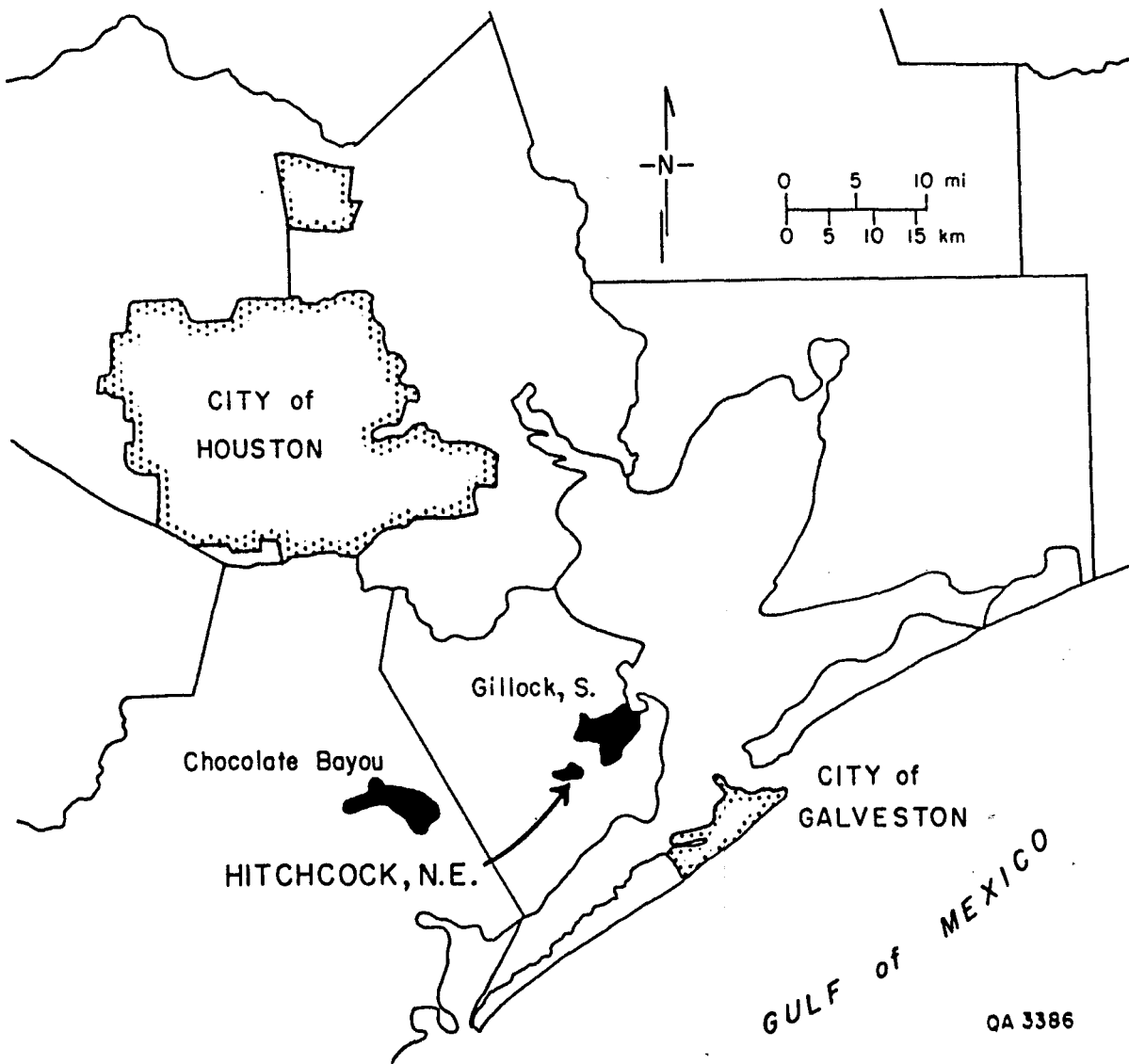


Figure 1. Hitchcock N.E. location map (modified from Anderson and others, 1984).

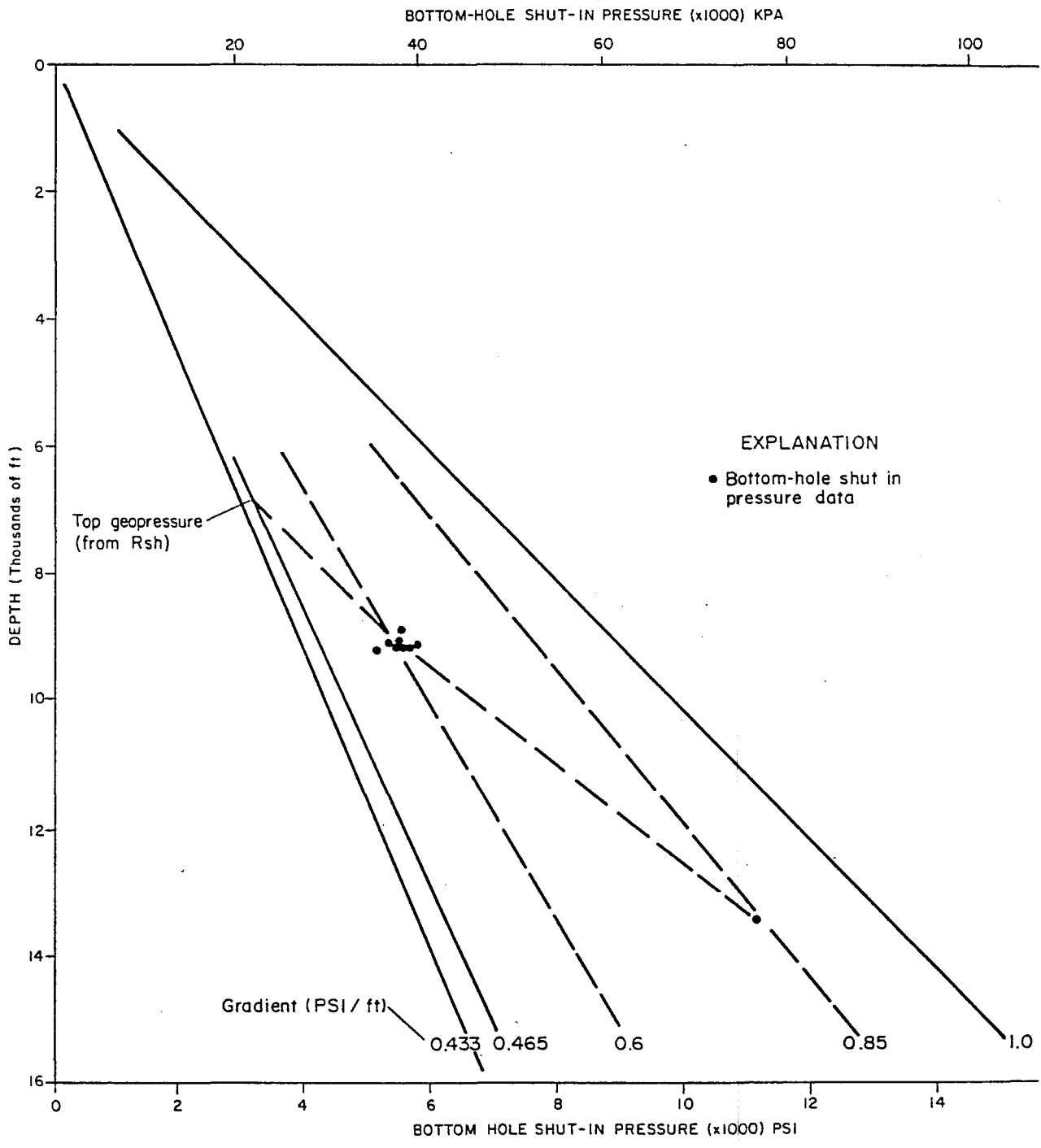


Figure 2. Depth versus drill stem test pressures, Hitchcock N.E. field.

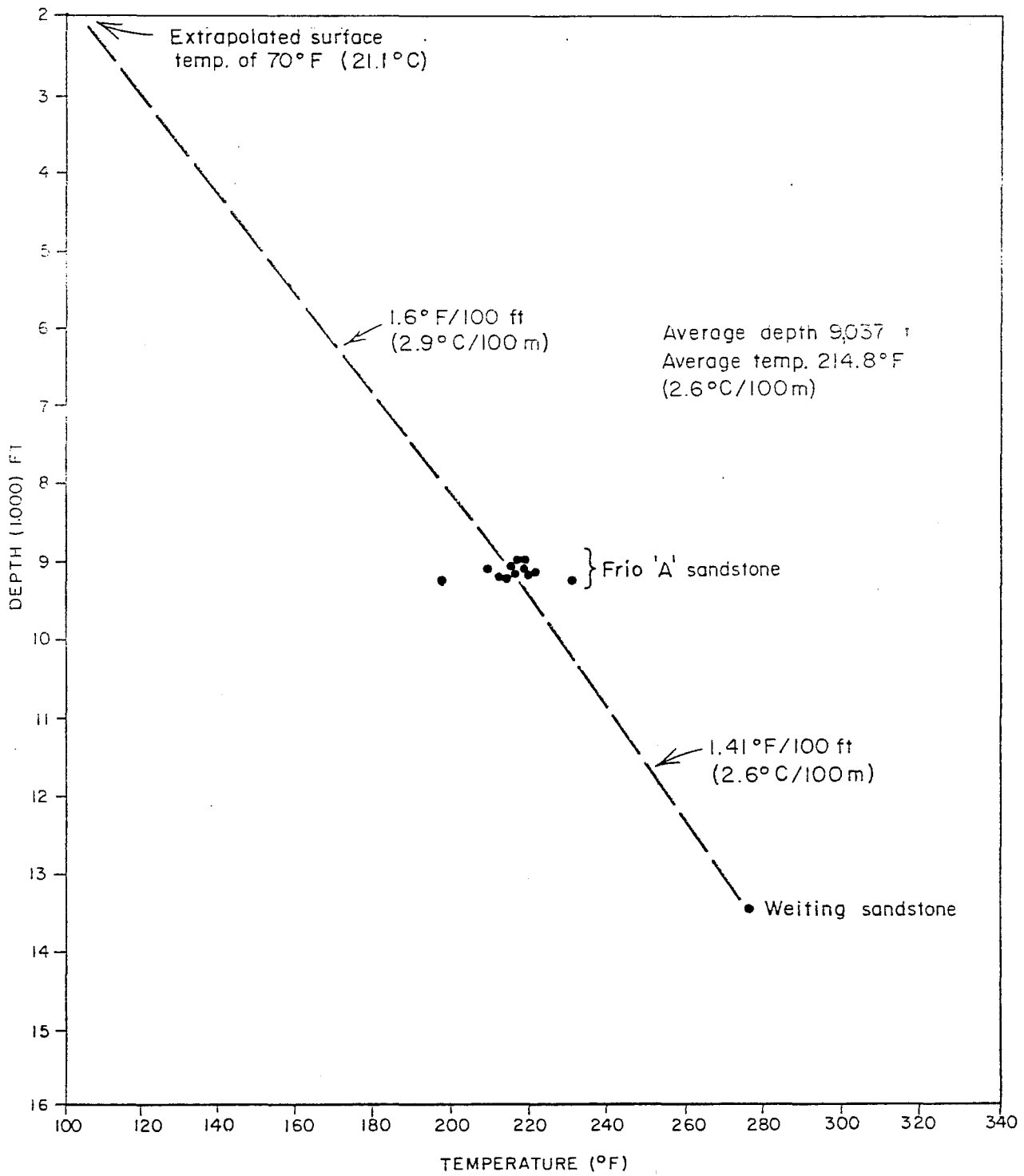


Figure 3. Equilibrium temperatures, Hitchcock N.E. field.

FRIO DEPOSITIONAL SYSTEMS

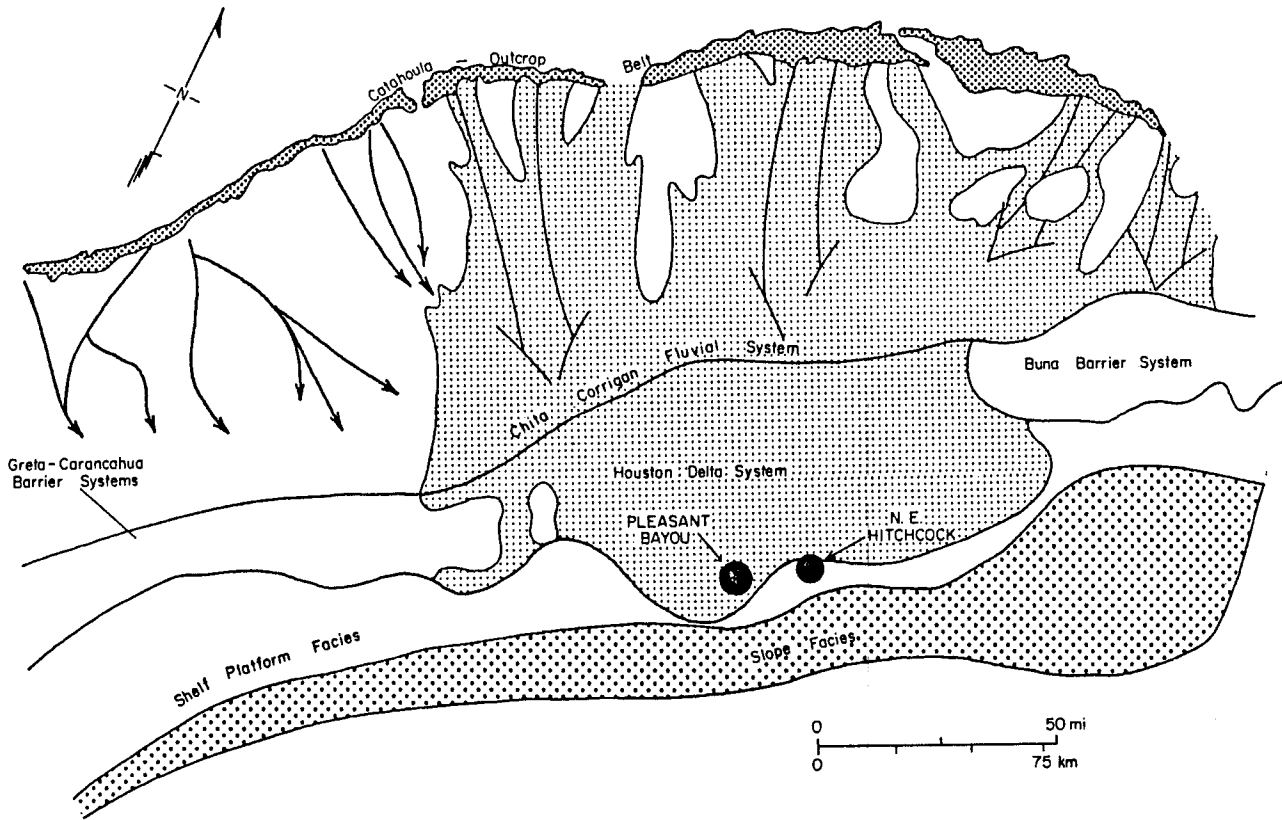


Figure 4. Regional depositional setting of the Hitchcock N.E. field. (Modified from Galloway, Hobday, and Magara, 1982.)

fault with several hundred feet of throw. This fault forms the southern boundary of the reservoir and aquifer (figs. 5 and 6).

A fault wedge upthrown some 50 ft (15 m) forms the northwest sector of the field. This wedge formed contemporaneously with Frio 'A' sandstone deposition; sandstone thickness and facies change markedly across it. Three other arcuate northeast-trending normal faults dissect the east flank of the reservoir and have throws that vary from 30 to 60 ft (9 to 18 m) (fig. 6). The two western faults appear to have isolated the Cockrell No. 1-Lowell Lemm well from both the Phillips No. 1 Prets well to the west and other wells to the east (Anderson and others, 1984; W. A. Parisi, personal communication, 1984; fig. 6).

A major east-west scissor fault (concave to the north) lies directly south of the Secondary Gas Recovery (S. G. R.) No. 1 Delee well (fig. 6). Although its throw exceeds 100 ft (30 m) in the west, its displacement decreases to 30 ft (9 m) over the crest of the structure (fig. 6). Two other en echelon scissor faults dissect the original Frio 'A' pay zone in the southern part of the Hitchcock N.E. anticline (fig. 6). However, the throw on these faults is less than 50 ft (15 m) on the western flank of the reservoir (fig. 6). These scissor faults do not disrupt the reservoir continuity, which is evident from the subsurface pressure history. The whole region underwent an almost even pressure drop from the Phillips No. 1 Delaney (De) in the north to the Phillips No. 1 Sundstrom (S) in the south over the 24-yr period from 1957 to 1981 (Anderson and others, 1984).

Cores from the S. G. R. No. 1 Delee well indicate that thin shale and other permeability breaks appear to stratify the Frio 'A' reservoir (fig. 7). Larger shale breaks are also evident on electric logs from the Phillips No. 1 Prets and Thompson wells. Some of these breaks are clearly permeability barriers, as they formed basal seals onto which heavier hydrocarbons have accumulated from gravity settling. This local vertical partitioning and the minor faults that isolate parts of the Frio 'A' reservoir possibly explain the different oil-gas dew points and oil percentages found in pressure-volume-temperature relationship (PVT) analyses of fluids from the Prets and Thompson wells. The location and

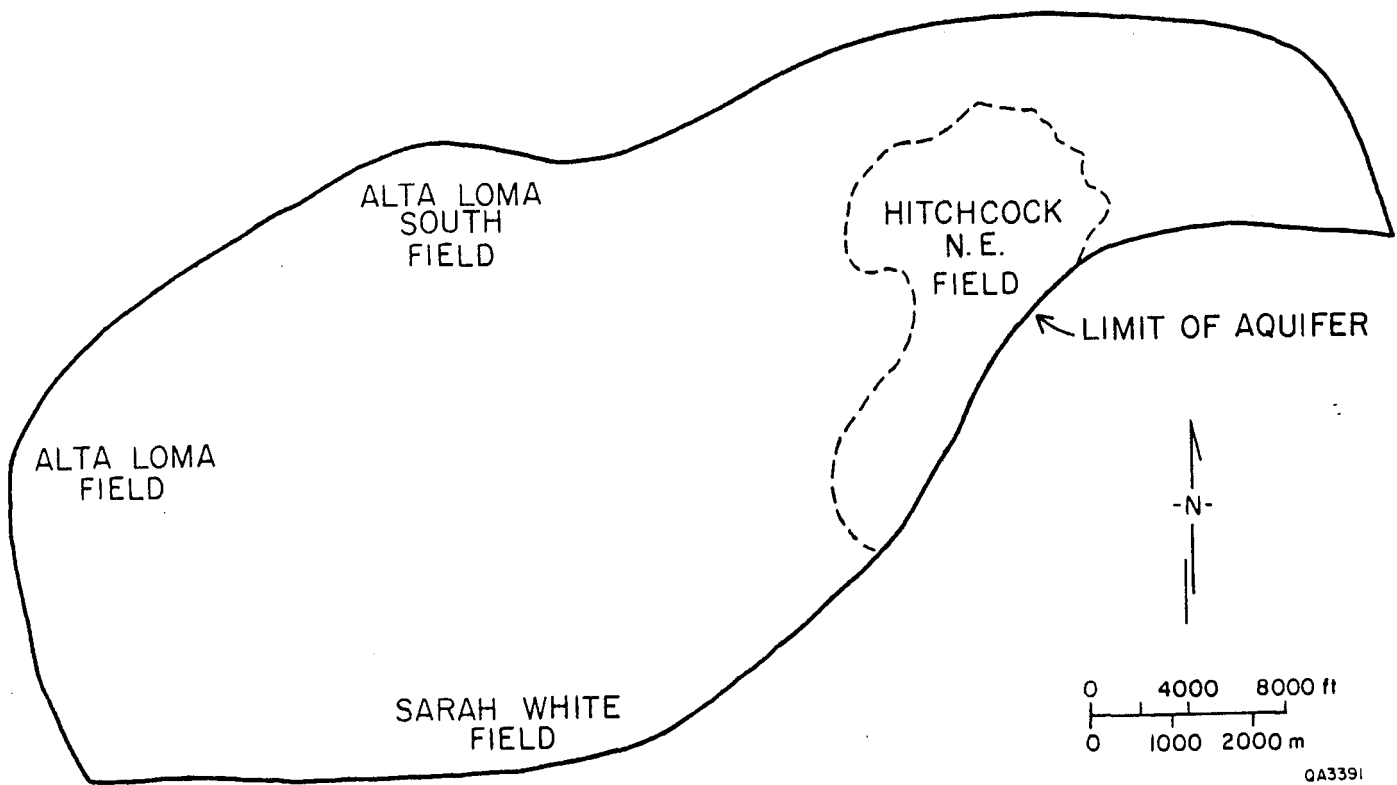


Figure 5. Regional distribution of the Frio 'A' sandstone aquifer and the location of the Hitchcock N.E. field.

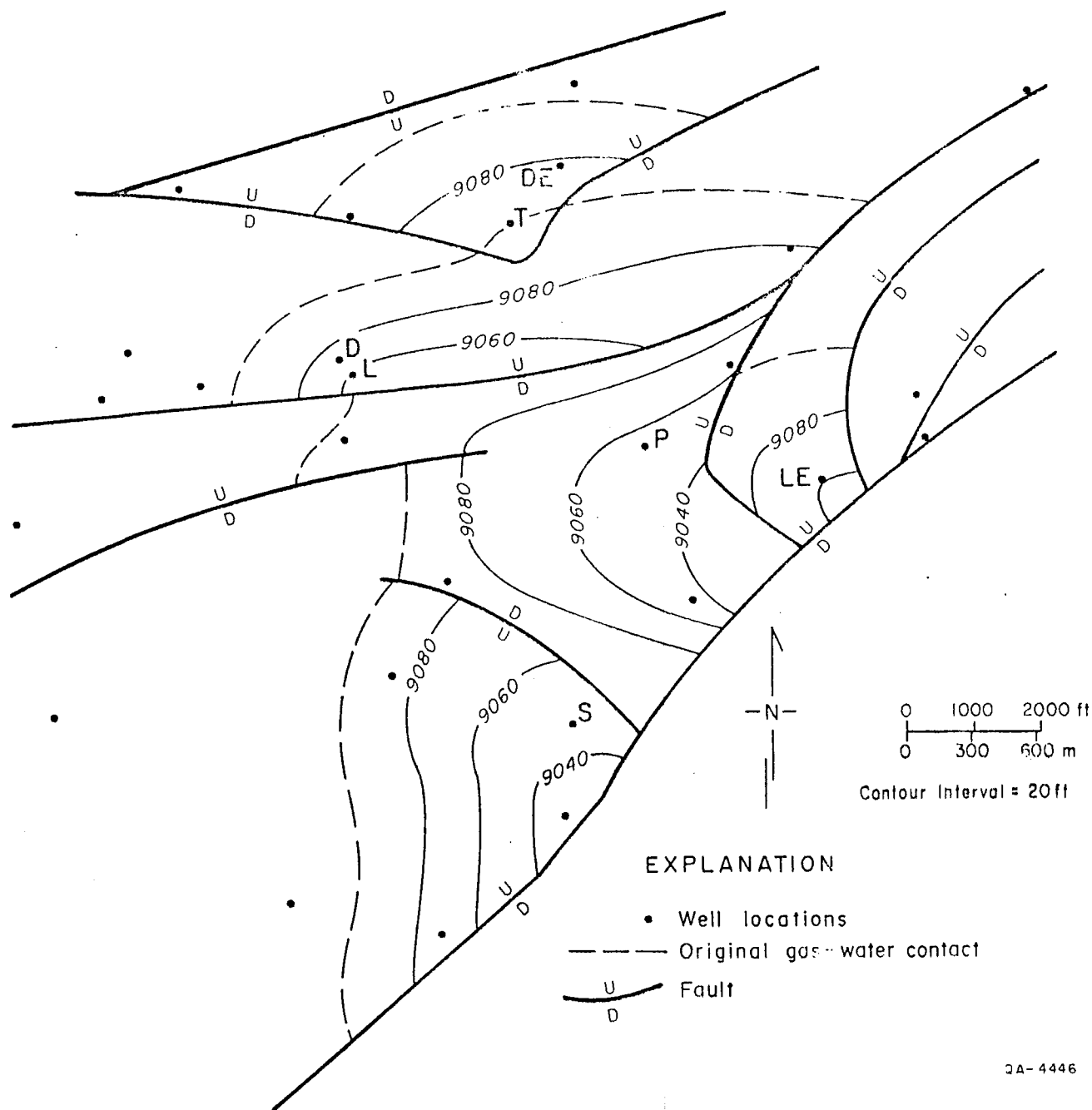


Figure 6. Structure map on top of the Frio 'A' pay zone. Lettered oil well locations are Phillips No. 1 Delaney (DE), Thompson (T), Louise (L), Prets (P), Sundstrom (S), Secondary Gas Recovery No. 1 Delee (D), and Cockrell No. 1 Lowell Lemm (LE).

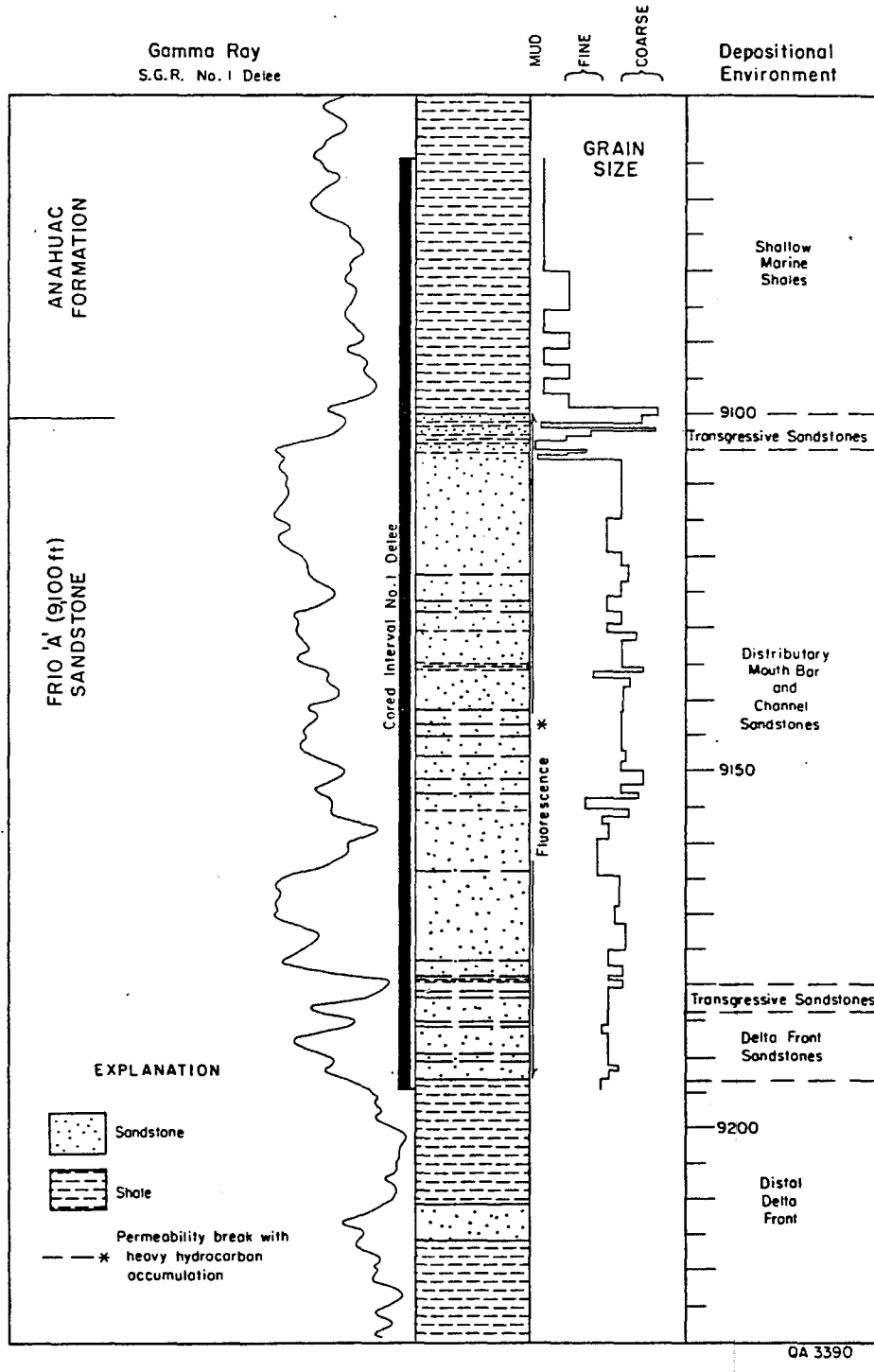


Figure 7. Log of the Frio 'A' sandstone interval in the S. G. R. Delee No. 1 well. The gamma ray response, grain size, and depositional environment are indicated.

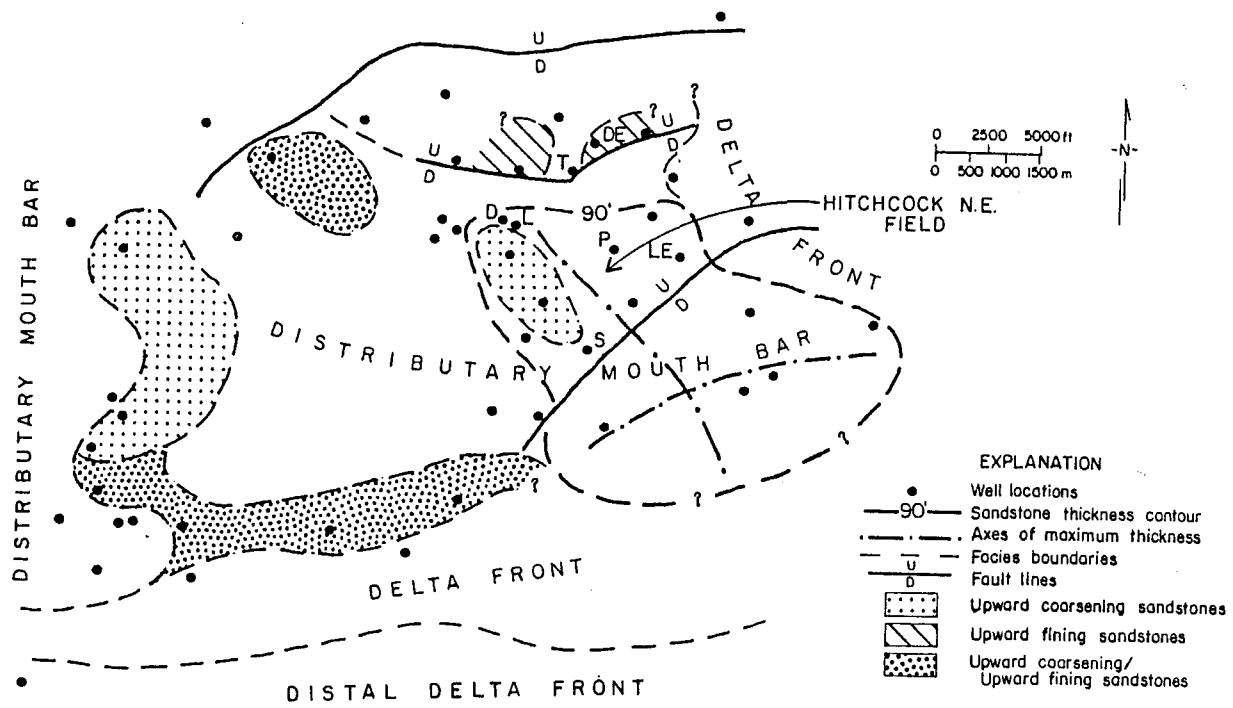
throw of these minor faults and the position of shale breaks will influence enhanced gas recovery. Detailed mapping of the fault plane and juxtaposition of thin sandstone units should assist in identifying isolated sections of the reservoir and the best location for guard wells to reduce water influx into the reservoir.

## STRATIGRAPHY

### Depositional Environment of the Frio 'A' Sandstone

In the Hitchcock N.E. field, the Frio 'A' sandstone consists of a stacked sequence of distributary-mouth-bar sandstones and thin delta destructional units and is overlain by the transgressive Anahuac shale (fig. 7). The facies distribution of the Frio 'A' sandstone was analyzed using spontaneous potential (SP) profiles in an area extending from the Hitchcock N.E. field in the east to the Pleasant Bayou field 11.5 mi (18.4 km) to the west. All major sandstone systems in the Hitchcock N.E. area exhibit a transition from thick, composite upward-coarsening sandstones updip to serrate sandstones downdip (fig. 8). The well-defined lobate to elongate net-sandstone thickness pattern (fig. 9) is evidence of deposition in a high-constructive lobate delta.

A distributary appears to have prograded 3 mi (5 km) southeastward from the fault wedge forming the northwest flank of the Hitchcock N.E. field during deposition of the Frio 'A' sandstone. This distributary progressively formed a major distributary-mouth-bar deposit on the southern downthrown block of the fault wedge. Further progradation resulted in deposition of a thickened sandstone on the downthrown southeast side of the major growth fault forming the southern boundary of the Hitchcock N.E. reservoir (figs. 8 and 9). Spontaneous potential profiles of distributary mouth bars are thinner and generally upward-fining within the northwest fault wedge, indicating their proximity to the distributary system. Thicker, composite upward-coarsening SP profiles are present in the south



QA3389

Figure 8. Log facies map of the Hitchcock N.E. field (modified from Tyler, 1984).

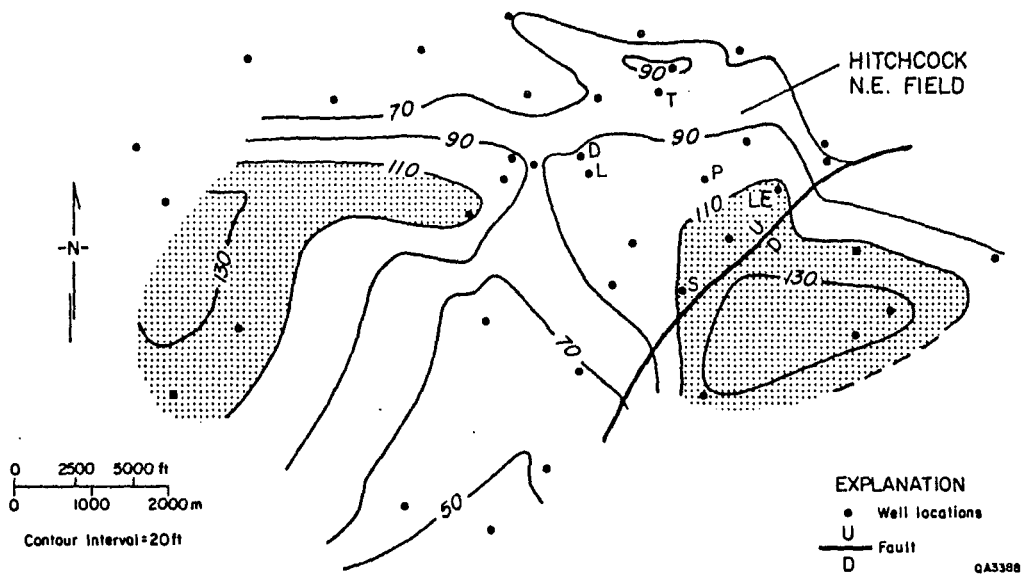


Figure 9. Frio 'A' sandstone thickness map showing location of Hitchcock N.E. field.

and east of the Hitchcock N.E. field. Continuous delta-front sandstones occur in more distal positions (fig. 8).

#### Facies Influence on Reservoir Continuity

Normally distributary-mouth-bar sandstones are composed of cross-stratified sandstones and silts displaying a wide variety of primary sedimentary structures (Coleman and Prior, 1980). The general lack of such structures and the massive nature of the Frio 'A' sandstone in the Hitchcock N.E. field is considered to be evidence of vigorous marine reworking. This strong marine influence resulted in the broad lateral extent and good internal continuity of the 'A' sandstone. Continuity of the Frio 'A' sandstone over the whole region must be considered in the placement of guard wells to control water influx.

The northeast orientation of the major growth faults strongly influenced sandstone thickness trends in the Frio 'A' aquifer as well as routes of water movement from the southwest. Hence guard wells should be located between fracture systems on the southwest side of the reservoir to effectively reduce the influx of water. Any attempts to isolate the Hitchcock N.E. field from the aquifer by fracturing and grouting must take account of the preferential orientation of fracture systems in the region. Should fracture systems accidentally be formed in the field, the flow characteristics of the reservoir may be severely affected by grouting.

#### Facies Influence on Porosity and Permeability

Modern and ancient distributary mouth bars are commonly composed of medium- to fine-grained, well-sorted sand having large primary sedimentary structures. Thus they are favorable potential reservoirs for hydrocarbons (Coleman and Prior, 1980; Morton and others, 1983). Much of the preserved excellent porosity ( $\pm 30$  percent) and permeability ( $\pm 1,000$  md,  $0.99 \mu\text{m}^2$ ) in the Frio 'A' sandstone is due to its distributary-mouth-bar origin (table 2).

Table 2. Porosity and permeability results from the S.G.R. No. 1 Delee well.

Core Depth Feet BKB.	Porosity %	Horiz. Perm. Md	Cycles
9101.5	10.9	1.7	↑
9106.5	24.9	442	
9108.5	30.6	265	
9113.1	26.2	328	
9116.0	25.9	624	
9119.3	27.8	717	
9122.3	27.2	1193	
9125.6	23.5	158	
9128.6	26.1	29	
9131.4	29.9	644	
9134.7	28.5	1017	
9137.3	28.7	918	
9140.4	22.4	1121	
9143.3	30.0	815	
9146.3	28.7	2911	
9149.4	30.9	3709	
9152.2	29.5	4446	
9155.7	27.7	79	
9158.3	25.3	204	
9161.4	31.1	1044	
9164.4	25.4	22	
9167.6	32.1	1885	
9170.2	29.5	572	
9173.2	32.0	1761	
9175.4	29.0	977	
9178.1	29.2	2266	
9182.1	28.0	1452	
9186.2	33.7	1493	
9189.2	28.2	1382	
9192.1	30.8	1134	

The permeability and porosity pattern of the Frio 'A' sandstone in the S. G. R. No. 1 Delee core shows a general upward decrease that is normally characteristic of an upward-fining pattern (pattern 2, Morton and others, 1983) (table 1). However, grain size measurements of the mouth-bar sandstones in the cored interval indicate a consistent medium grain size (fig. 7). This implies either an upward decrease in sorting or an increase in diagenetic cements.

Within the massive distributary-mouth-bar sandstones, the upward decrease in permeability appears to be controlled by an increase in the calcite cement content, though very thin carbonaceous layers are occasionally present. The lower mouth-bar sandstones, which contain only minor calcareous streaks, display permeabilities up to 1,000 md ( $0.99 \mu\text{m}^2$ ), whereas in the shallower well-cemented mouth-bar sandstone permeability is only a few hundred millidarcys.

Porosity and permeability are indirectly related to internal stratification because sediment structures are partly controlled by grain size (Pryor, 1973; Morton and others, 1983). In Oligocene sandstones the relative ranking of permeabilities from highest to lowest corresponds to (1) foresets and large-scale troughs, (2) horizontal and low-angle, parallel-inclined stratification, and (3) small-scale troughs and ripple stratification (Morton and others, 1983). This relationship is demonstrated by the difference in permeability between the upper calcite-cemented distributary-mouth-bar sandstones and the overlying transgressive sandstones. Permeabilities in the massive to indistinctly laminated mouth-bar sandstones are an order of magnitude greater than permeabilities in the transgressive sandstones. The latter sandstones are well stratified, more poorly sorted, and commonly coarser grained (fig. 7).

#### Diagenetic Modification of Porosity and Permeability

Primary porosity and permeability at the Hitchcock N.E. field were subsequently modified by diagenetic reactions and leaching by organic acids. On the basis of regional

investigations of diagenesis, the following parageneses are indicated (Loucks and others, 1981). Early clay coats formed around quartz grains and feldspars were leached. This was followed by euhedral quartz overgrowth development and secondary leaching of pore spaces (fig. 10). Remaining feldspars were then albitized and kaolinite crystallized in leached pore spaces (Loucks and others, 1981) (fig. 10). At the Hitchcock N.E. field, iron-chlorite formation appears to postdate quartz overgrowths and framboidal pyrite on which it has formed. Radiating calcium sulfate crystals have formed on quartz overgrowths and appear to be related to crystallization of fluids during drying of the core. Gypsum is unstable at the Frio 'A' reservoir temperatures and pressures (Blatt and others, 1972).

Oil is present throughout the S. G. R. No. 1 Delee core from both above and below the original gas-water contact at  $\pm 9,105$  ft (2,775 m) BMSL (figs. 3 and 4). Phillip L. Randolph (personal communication, 1984) suggested that this oil is possibly being expelled from geopressed shale below the Frio 'A' sandstone.

#### SHALE DEWATERING

The potential for shale dewatering occurring as a result of pressure drawdown during production has been examined. This entails discriminating between three types of fluid movement.

- a) Original migration of hydrocarbons from source and emplacement in a trap.
- b) Shale dewatering as a consequence of compaction and pressure/temperature increase during burial.
- c) Shale fluid flow (dewatering) during production.

#### Original Fluid Migration

Maturation data in shales can be used as an indicator of hot fluid flow in adjacent sandstones (Light, 1985; Tyler and others, 1985).

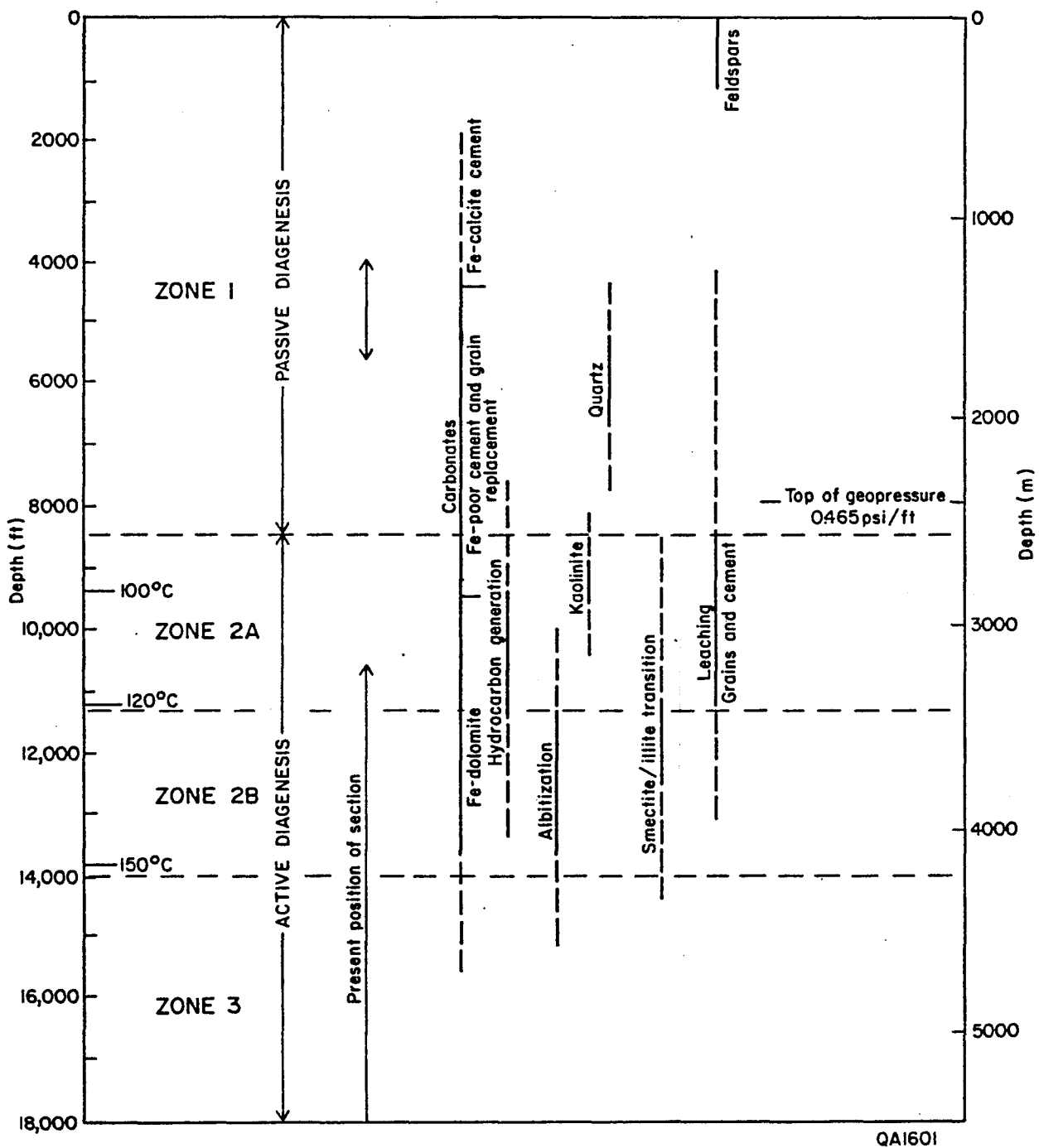


Figure 10. Frio diagenetic sequence in Brazoria County, modified from Loucks and others (1981) and Milliken and others (1981).

The Pleasant Bayou geopressured-geothermal test wells in Brazoria County display a maturity anomaly that cannot arise as a consequence of simple conduction (Ewing and others, 1984). The corrected maturity in the Upper Frio (above T5) appears much higher than that indicated when the present (and apparent regional) geothermal gradient is applied to the burial history of those strata (fig. 11) (Ewing and others, 1984). In contrast, the maturity of the Lower Frio (below T5) is consistent with the present geothermal gradient (fig. 11). The higher thermal maturity of the Frio (T2 to T5 succession) is believed to be a consequence of heating by updip migration of hot basinal fluids formed during compaction and diagenesis of slope shales (fig. 12) (Burst, 1969; Ewing and others, 1984). A reduction to almost normal pressure in the Upper Frio may have allowed fluid migration to occur, while fluid movement would have been slower or static in the highly geopressured Lower Frio (pre-T5 succession) (fig. 12). Consequently, the maturity of the Lower Frio was not increased (Tyler and others, 1985).

Maturity data from the Delee No. 1 well (Hitchcock N.E. field) suggest, however, that the Anahuac shales tend to be more mature above the Frio 'A' sandstone than are Frio shales within the reservoir. This is evident when the thermal maturity estimated by vitrinite reflectance is compared to the theoretical thermal maturity using Lopatin's method (Waples, 1980) and a burial history model (figs. 13 and 14). An anomaly of this kind may be related to higher geopressure and consequent increased geothermal gradient in the Anahuac (fig. 15) (Lewis and Rose, 1970), but it clearly is not a result of increased geothermal gradient as a result of hot fluid flow in the Frio 'A' sandstone. The thermal anomaly above the Frio 'A' sandstone occurs some 1,000 ft (305 m) shallower in the Delee No. 1 well than the anomaly in the Pleasant Bayou test wells (Ewing and others, 1983), and hot upwelling fluids may have cooled to ambient temperatures by the time they reached these shallower levels. Evidence of a deep source for the Delee No. 1 fluids will therefore have to be sought in hydrocarbon compositional and isotopic data.

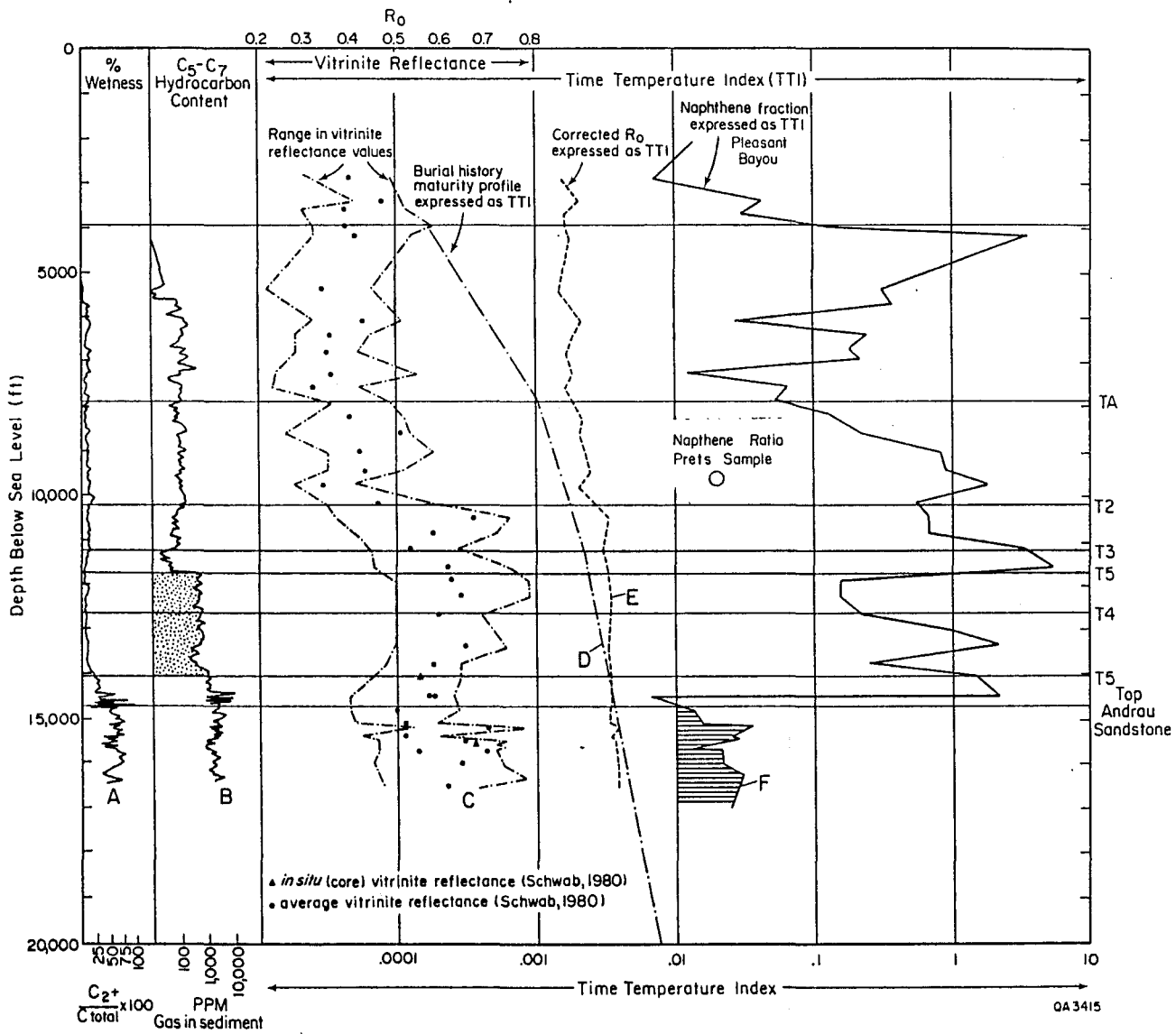
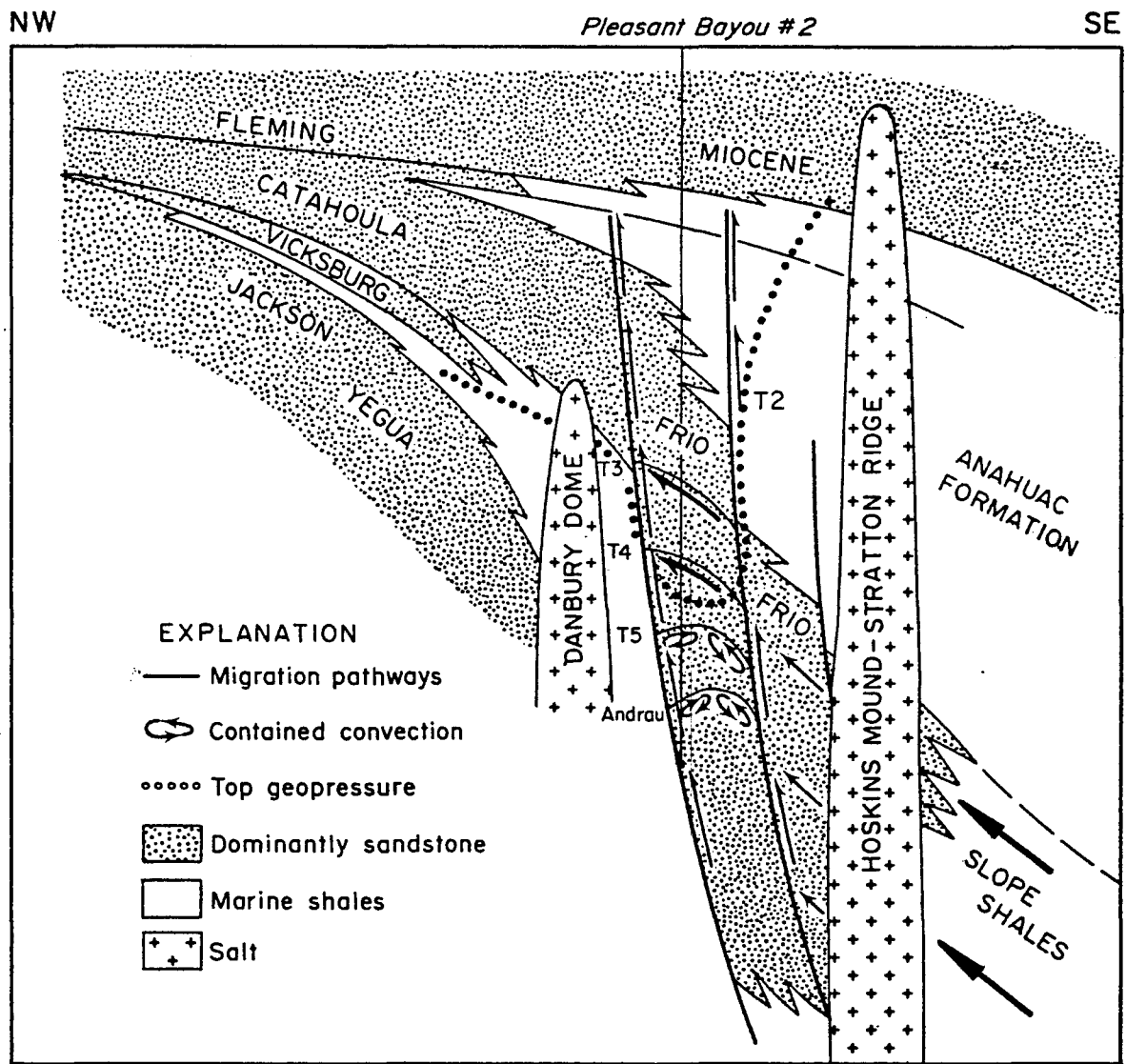


Fig. 13

Figure 11. Naphthene fraction from shale extracts expressed as time-temperature indices (TTI) vs. depth for the Pleasant Bayou No. 1 well and oil from Prets No. 1 well compared to the burial history maturity profiles for both these wells in TTI. The corrected vitrinite reflectance (expressed in TTI) and uncorrected vitrinite reflectance are shown as well as percent wetness, and C<sub>5</sub>-C<sub>7</sub> hydrocarbon content in 1 million volumes of sediment (Brown, 1980).



QA3414

Figure 12. Stylized stratigraphic dip section across the Texas Gulf Coast showing the relative position of the GCO/DOE Pleasant Bayou geopressured geothermal test wells (modified from Galloway, Hobday and Magara, 1982).

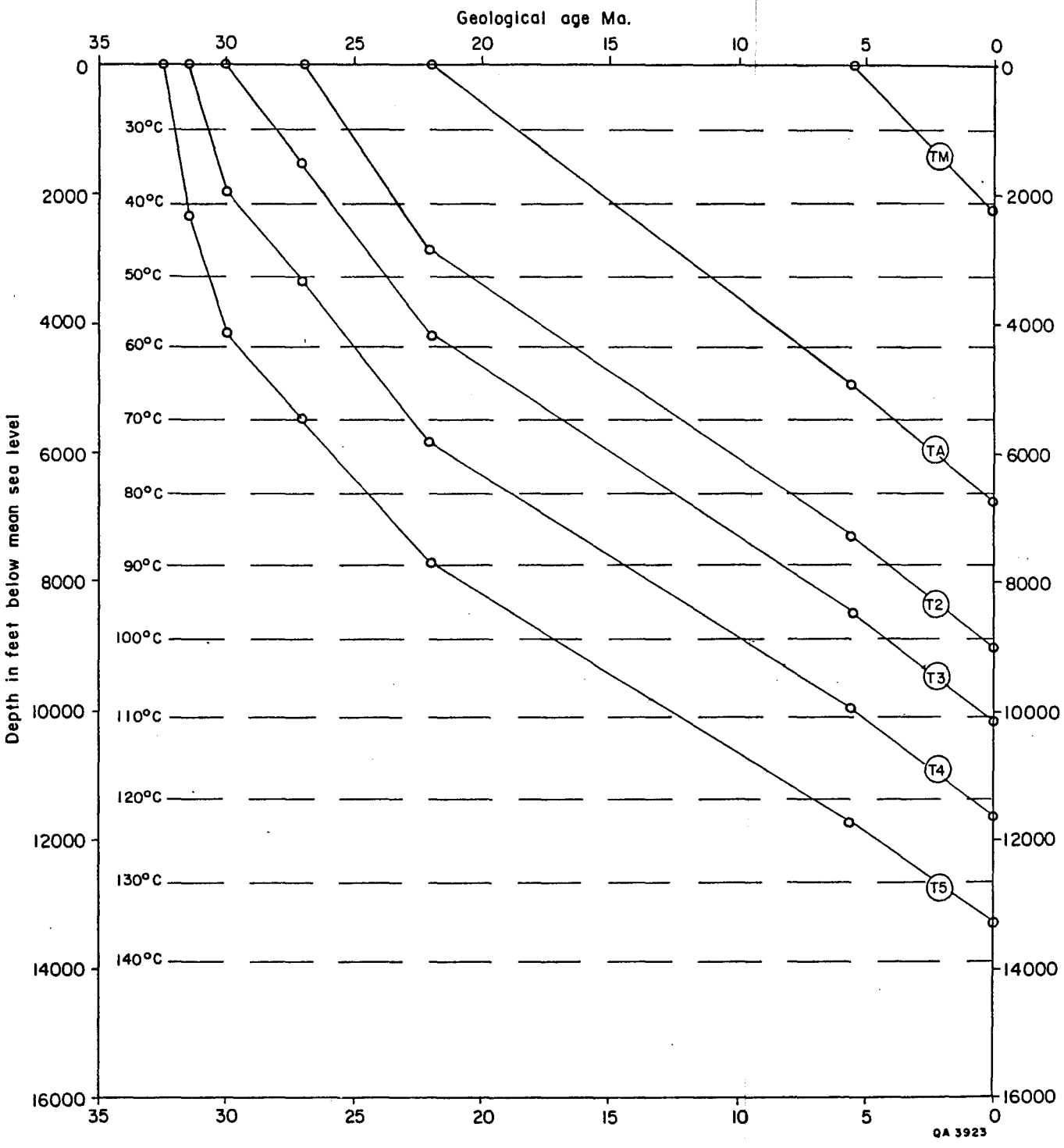


Figure 13. Burial history diagram for the Hitchcock N.E. field.

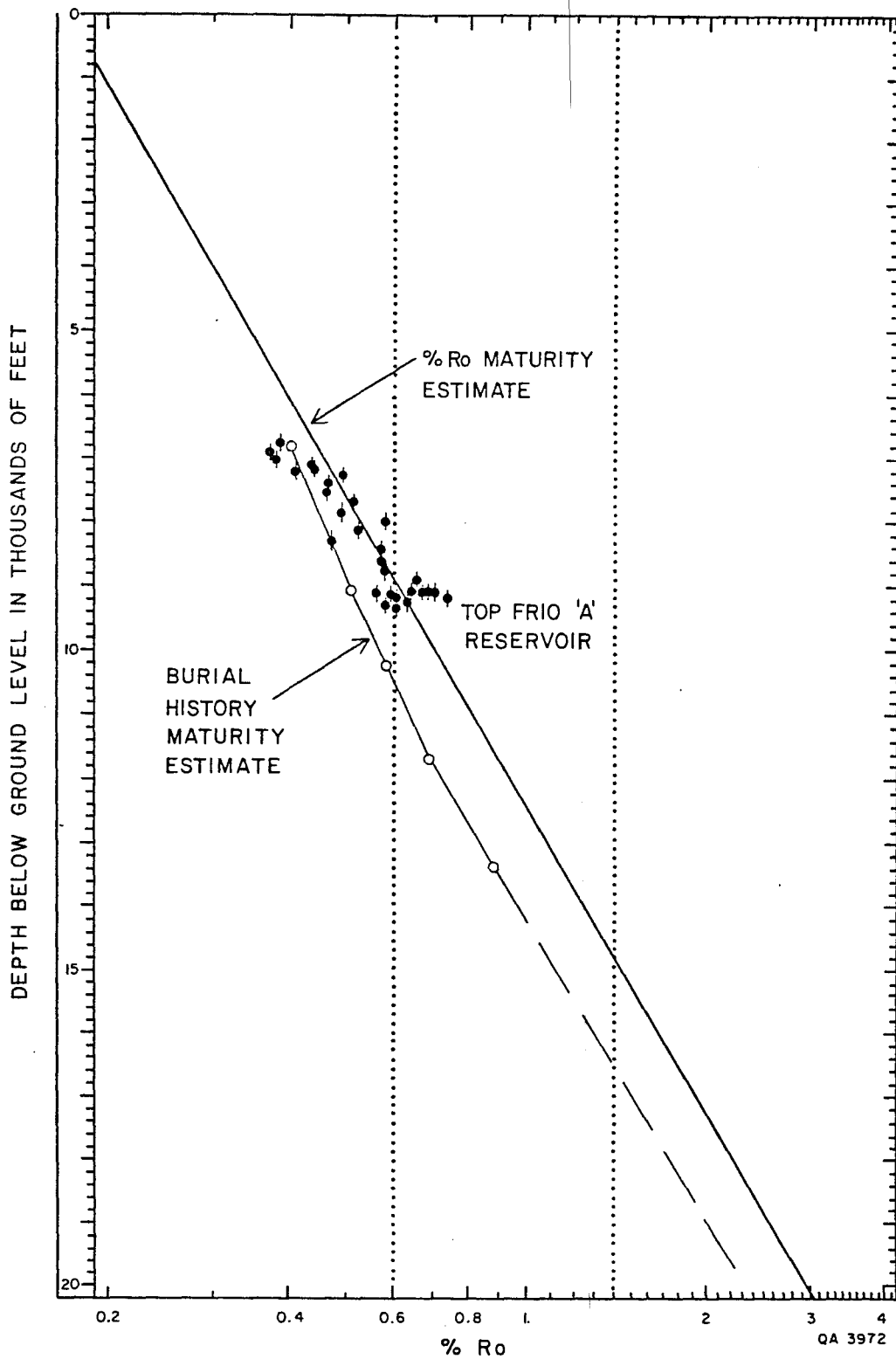
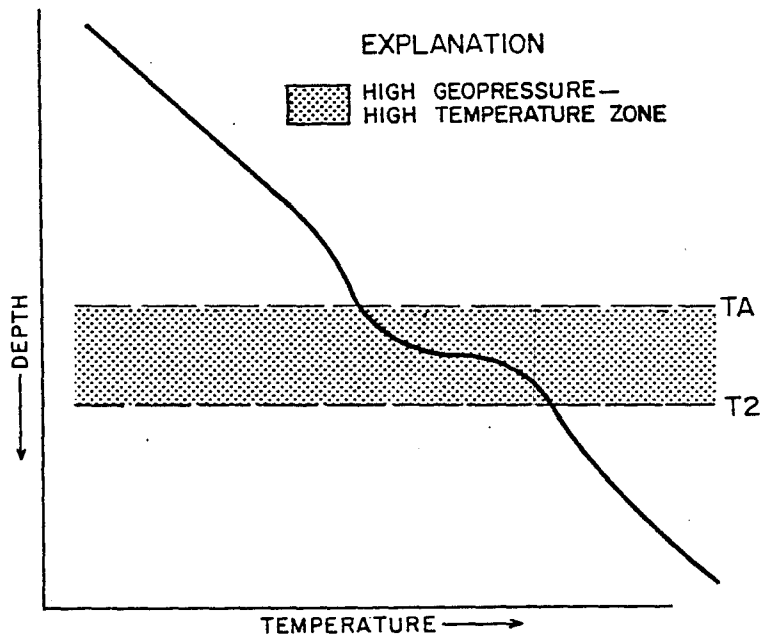


Figure 14. Maturation profile of the Delee No. 1 well based on vitrinite reflectance data compared to a maturation profile for the Hitchcock N.E. field using Lopatin's method.



QA-3476

Figure 15. Temperature profiles in a geopressured zone, modified from Lewis and Rose (1970).

The composition of the hydrocarbons in oil changes as they mature, and this variation may be used to estimate the time of oil formation (Young and others, 1977). Calculation of hydrocarbon ages for the gasoline-range hydrocarbons is based on the apparent disproportionation of naphthenes to create paraffins and aromatics (table 3) (Light and others, in preparation).

Young and others (1977) used 10 naphthenes (cyclopentane to ethylcyclopentane), 17 paraffins (isopentane to n. heptane), and 2 aromatics (benzene and toluene) in their calculations. They were unable to improve the accuracy of the method by deleting certain individual compounds or groups of compounds. Detailed C<sub>4</sub>-C<sub>7</sub> hydrocarbon extract analyses from cuttings from the Pleasant Bayou test wells (Brazoria County) and gas/condensate/oil from the Prets No. 1 well (Hitchcock N.E. field) are available. These analyses include only 9 naphthenes, 16 paraffins, and 2 aromatics (Brown, 1980). Though the calculated ages (fig. 16) of the Delee No. 1 and Pleasant Bayou test wells are not directly compatible with Young and others' (1977) data, the error is probably small because almost the complete suite of gasoline-range hydrocarbons was considered. The calculated age of the Prets No. 1 gasoline-range hydrocarbons is older than the age of the formation in which they occur.

The hydrocarbon-age calculation method assumes that the disproportionation reaction of naphthenes depends on the effects of time and temperature. Naphthene concentration (C<sub>n</sub>) is related to time and temperature by the following equation (equation 5, table 3).

Natural logarithm C<sub>n</sub> = intercept + slope x (time-temperature integral (TTI)) (Young and others, 1977).

This equation has been calibrated to gasoline-range hydrocarbons in clastic reservoirs (Young and others, 1977).

When the naphthene fractions of the Pleasant Bayou No. 1 well and Prets No. 1 well are expressed as TTI and are plotted against depth the highly geopressured Lower Frio (pre-T5 marker horizon) and some of the shallow Miocene have high naphthene concentra-

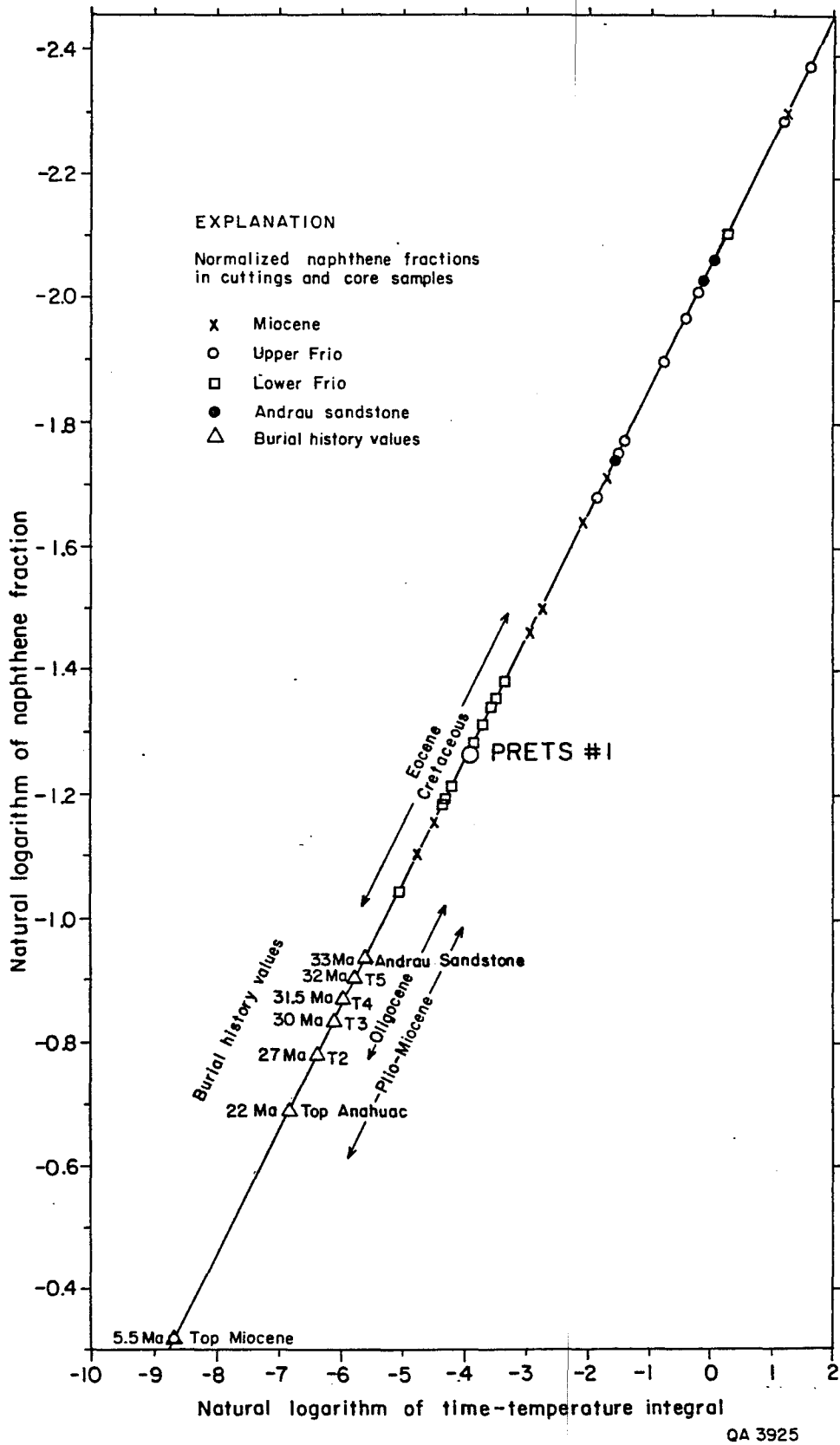


Figure 16. Natural logarithm of the naphthene fraction in shale extracts versus the natural logarithm of the time-temperature integral for the Pleasant Bayou No. 1 geothermal test well. For comparison the natural logarithm of the naphthene fraction of oil from the Plets No. 1 well is shown. Age ranges of the naphthene fractions are from Young and others, 1977.

Table 3. Disproportionation reaction for naphthenes.

Disproportionation reaction for naphthenes

$$4N = 3P + 1A \quad (1) \quad (\text{Reznikov, 1967})$$

Normalized naphthene concentration

$$C_n = \frac{N}{N+P+A} \quad (2)$$

Time rate change of concentration

$$\frac{dC}{dt} = -KC \quad (3)$$

Reaction rate "constant"

$$K = be^{-\frac{E}{RT}} \quad (4)$$

Natural logarithm of normalized naphthene concentration

$$\text{Ln}C_n = -b \int_{t=0}^{t=t} e^{-\frac{E}{RT}} dt + a \quad (5)$$

Time temperature index

$$\text{TTI} = \int_{t=0}^{t=t} e^{-\frac{E}{RT}} dt \quad (6) \quad (\text{equations 2-6 from Young and others, 1977})$$

N = naphthenes

R = universal gas constant

P = paraffins

T = absolute temperature °K

A = aromatics

b = constant

C<sub>n</sub> = normalized naphthene concentration

t = time at which reaction concentration is C

K = reaction rate constant at temperature t

e = base of natural logarithmic system

E = activation energy of the reaction

a = constant (equal to LnC at t=0)

tions (i.e., low maturity or TTI). Conversely, most of the Miocene, Anahuac, and Upper Frio samples show low naphthene concentrations (i.e., high maturity or TTI). The high maturities (TTI) shown by the hydrocarbons above the T5 marker horizon (Miocene, Upper and Middle Frio) compared to the thermal maturity of their containing sediments derived from the burial history indicate that these fluids have migrated up from more deeply buried, more mature source rocks (fig. 11). High geopressure below the T5 marker horizon probably arrested fluid flow, and the hydrocarbons present are more locally derived. The discrepancy between the hydrocarbon maturity data and the burial history maturity profile below T5 in the Lower Frio Formation may represent a standard error in the calculation of the maturity (TTI) from naphthene concentration.

An anomalous concentration of C<sub>5</sub>-C<sub>7</sub> gasoline-range hydrocarbons in the T3 to T5 succession in a zone of relatively low wetness is consistent with the idea that they have been introduced (Brown, 1980). The thermal maturity (vitrinite reflectance) above the top of the Frio is lower than the maturity of the hydrocarbons in their containing rocks (fig. 11). This discrepancy is probably a consequence of the fluids having lost their heat to the surrounding formations by the time they reached these shallower levels (fig. 11).

#### Shale Dewatering from Burial Effects

Shales tend to be water wet due to the preferential adsorption of water on grain surfaces because of strong electrostatic forces active between the fine clay grains and pore fluids (Hinch, 1980). Adsorption causes "dynamic" structuring of the water close to the mineral grain surfaces (Hinch, 1980). The structured water close to the grain surfaces, though highly mobile on a molecular scale, is immobile in a hydrodynamic sense.

Shale water is lost by compaction due to burial until about only 10 layers of water molecules separate the clay grains near the top of geopressed shale (Hinch, 1980). After this, movement of the hydrated ions is inhibited because they are close in size to the average pore size and the shales maintain a constant porosity (Hinch, 1980). However,

Newton (in Hinch, 1980) noted that hydrocarbon accumulations in the Gulf Coast are associated with waters having slightly subnormal salinity. This may be a result of dewatering of the surrounding geopressured shales (Hinch, 1980). Sandstones at the Frio 'A' level in the Delee No. 1 well are geopressured (geopressure gradient of 0.6 psi/ft), whereas geopressure starts at 7,200 ft (2,200 m) some 1,900 ft (580 m) shallower than the producing reservoir (fig. 2). We can therefore expect the shales surrounding the Frio 'A' sandstone at the Delee No. 1 well to have already entered a zone of fairly constant porosity and for the shale water to average around 2 to 10 layers separating clay grains (Hinch, 1980). Hinch (1980) stated that the generation of hydrocarbons in the geopressured zone can result in an increase in water content. However, the low total organic carbon (TOC) content of the shales in the Delee No. 1 well (averaging 0.35 percent TOC) and immaturity of the woody hydrocarbons make water production difficult (see section on shale pyrolysis data).

The content of structural water within the shale can be estimated by analysis of hydrogen and carbon contents of the products of shale pyrolysis at very high temperatures. These analyses will be done at the Mineral Studies Laboratory at the Bureau of Economic Geology in the next control period. Plots of carbon and hydrogen contents of shale organic material pyrolyzed at different temperatures should form a straight line that will intercept the hydrogen axis at 0 percent carbon, and will indicate the remaining amount of hydrogen tied up in structured water. This structured water, which can be compared to the bound water estimated by log analysis, may be used to estimate the maximum amount of water available for shale dewatering.

Smectite begins to alter to illite when temperatures have exceeded 194° to 212° F (90° to 100° C) and when potassium and aluminum are present in the pore waters (Foscolos and others, 1976; Powell and others, 1978). The temperature at the level of the Frio 'A' sandstone is close to this value (215° F; 101° C) in the Hitchcock N.E. field (fig. 3) (Light, 1985).

Previous workers suggested that during the transformation of smectite to illite a mixed-layer silicate formed in which aluminum substituted for silicon in the tetrahedral position, promoting a charge deficit that resulted in potassium being adsorbed on the clay surface. This potassium was believed to displace calcium, magnesium, or iron while water sloughed off into the solution (Foscolos and others, 1976; Powell and others, 1978). These changes were believed to be recognized by a reduction of the  $d_{001}$  spacing of a Ca-saturated smectite from 1.56 to 1.20  $\mu\text{m}$  in the mixed-layer clay (Foscolos and Powell, 1980).

The amount of water lost by dehydration during the smectite-illite transition was estimated to be 270 to 290 mg/g of clay (Mooney and others, 1952), which represents 10 to 15 percent of the compacted bulk volume of argillaceous sediments (Burst, 1969). This period of apparent clay dehydration coincides with a maturity level of 0.5 percent  $R_o$  (Foscolos and others, 1976; Powell and others, 1978). The maturity at the Delee No. 1 well at the level of the Frio 'A' sandstone exceeds this amount ( $\pm$  0.6 percent  $R_o$ , fig. 14).

Anahuac shales overlying the sandstones in the Delee No. 1 well were initially analyzed by X-ray diffraction to find evidence to support clay dewatering during production. Nadeau and others (1984) have, however, demonstrated that materials representing commonly interstratified clay minerals are composed of aggregates of fundamental particles whose X-ray diffraction patterns result from interparticle diffraction. What was taken formerly to be randomly interstratified smectite-illite is composed of primary populations of illite and smectite particles (Nadeau and others, 1984). During diagenesis, smectite particles become unstable and dissolve while illite particles are formed (Nadeau and others, 1984). When the smectite is completely gone, the remaining population consists of elementary illite and thicker illite particles, which when examined under XRD appear to be regularly interstratified smectite-illite with 50 percent or more illite (Nadeau and others, 1984). Consequently, the reduction in the (XRD)  $d_{001}$  spacing during the smectite-illite transformation can no longer be taken as an indication of the

amount of water lost by dehydration but rather is a measure of the change in elementary illite particle size.

Inductively-coupled plasma (ICP) elemental analyses were conducted by the Mineral Studies Laboratory at the Bureau of Economic Geology on seven shale samples from above, within, and at the base of the Frio 'A' sandstone (table 4). These data were used in place of the XRD information to estimate the illite content of the shales. A ternary diagram showing the relative percentages of  $K_2O$  to  $CaO$  and  $Na_2O$  and  $Fe_2O_3$  and  $MgO$  in the shales was constructed. These shale compositions were then compared to those of pure clay end members, from which the approximate illite percentage and the silica concentration in the shales were estimated (fig. 17) (Deer and others, 1969). The illite percentage appears to be fairly erratic in the clays and lies mainly between 50 and 70 percent, whereas the silica content of the shales is more consistent (fig. 17).

The transformation of smectite to illite is potentially important if water and ions released by this reaction migrate into sandstones where they may affect diagenesis (Loucks and others, 1981). Boles and Franks (1979) showed that smectite-illite transformation reactions with aluminum as an immobile component release significantly more cations (silica release increases more than five times) than do reactions in which aluminum is considered a mobile component (Loucks and others, 1981). Provisional data had suggested that the aluminum had been mobile in the shales directly overlying the Frio 'A' sandstone (fig. 18) in the Delee No. 1 well. However additional SEM-EDS analyses of the clay fraction over this interval indicate that it has a very consistent smectite-illite composition. The apparent decrease in alumina appears to be entirely due to an increase in the content of detrital components in the clay (mostly quartz), a consequence of the upward-fining nature of the upper boundary of the Frio 'A' sandstone. Aluminum can therefore be considered immobile in the smectite-illite transformation reaction. This reaction in the Anahuac shales directly above the Frio 'A' sandstones would release significant amounts of silica and other elements to the reservoir. The transformation reaction is as follows:

Table 4. Inductively coupled plasma (ICP) analyses for shale samples from the S. G. R. Delee No. 1 well.

<u>SAMPLE NO.</u>		<u>2</u>	<u>1</u>	<u>10</u>	<u>9</u>
<u>LAB. NO.</u>		<u>84-822</u>	<u>84-824</u>	<u>84-854</u>	<u>84-855</u>
<u>LOC ID</u>		<u>9092'</u>	<u>9070'</u>	<u>9194' 3"</u>	<u>9179' 11"</u>
		<u>SHALE</u>	<u>SHALE</u>	<u>SHALE</u>	<u>SHALE</u>
SiO <sub>2</sub>	(Wt %)	63.95	62.76	66.76	61.27
Na <sub>2</sub> O	"	1.71	1.66	2.04	1.73
K <sub>2</sub> O	"	2.60	2.71	3.15	3.33
MgO	"	2.14	2.11	1.78	2.08
CaO	"	1.31	1.58	1.58	3.39
Al <sub>2</sub> O <sub>3</sub>	"	18.59	17.87	16.49	16.33
Fe <sub>2</sub> O <sub>3</sub> (T)	"	5.33	5.74	4.00	4.13
TiO <sub>2</sub>	"	0.84	0.83	0.77	0.82
MnO	"	0.03	0.05	0.01	0.02
P <sub>2</sub> O <sub>5</sub>	"	<0.25	<0.25	<0.25	<0.25
TOTAL		96.50	95.31	96.58	93.10
Sr	"	250	280	160	270
Ba	"	460	360	290	430
Zr	"	180	180	510	210

LOC ID (Location identification) depth footage from Delee No. 1 well, Hitchcock N.E. field.

Table 4. (continued)

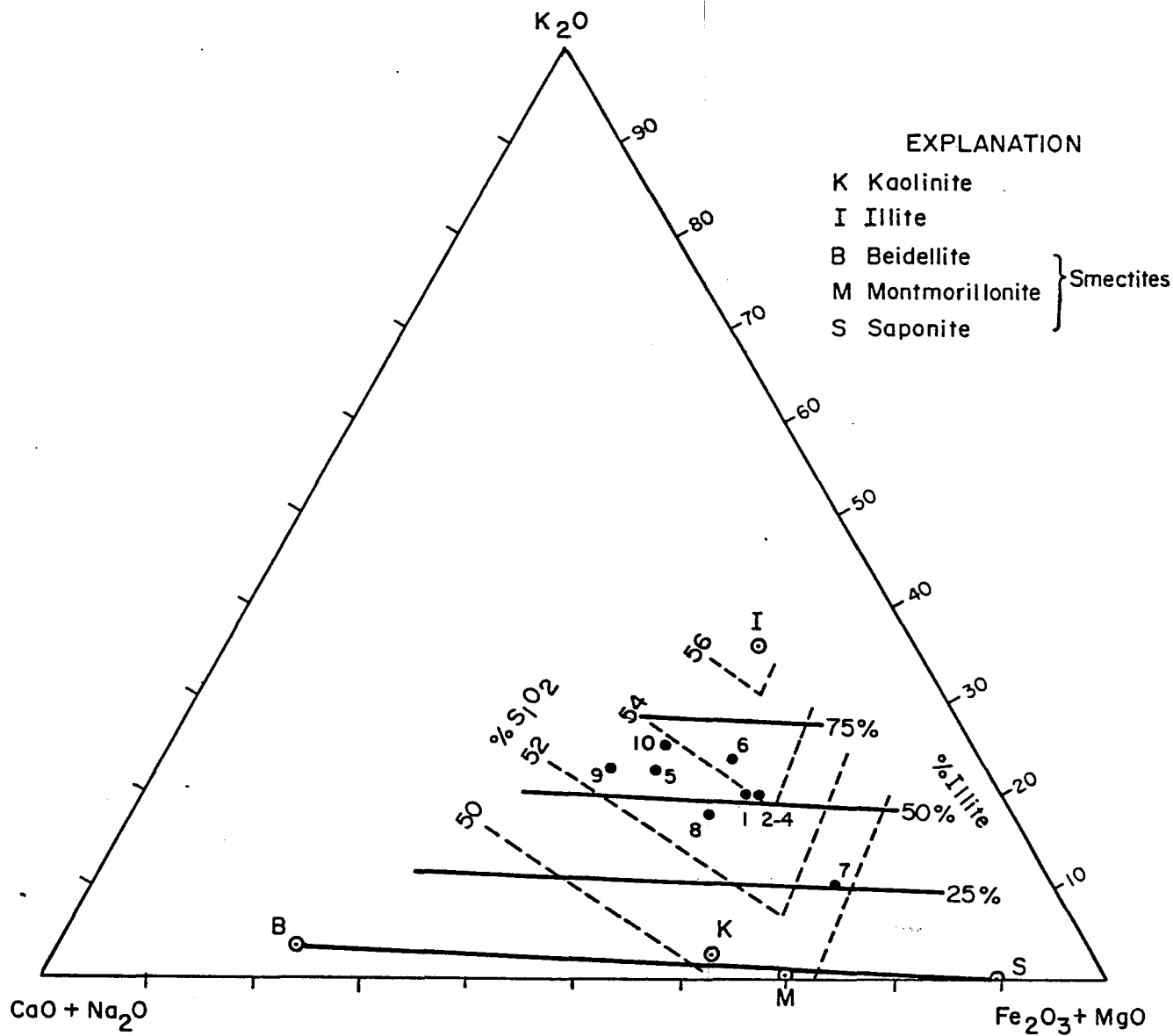
<u>SAMPLE NO.</u>		8	6	7	5
<u>LAB. NO.</u>		84-817	84-819	84-819(FINE)	84-821
<u>LOC ID</u>		9100' 10.75"	9100' 6"	9100' 6"	9099' 5.5"
		<u>SHALE</u>	<u>SHALE</u>	<u>SHALE</u>	<u>SHALE</u>
SiO <sub>2</sub>	(Wt %)	76.76	70.24	61.69	67.75
Na <sub>2</sub> O	"	1.56	1.24	0.56	2.05
K <sub>2</sub> O	"	1.91	2.15	2.60	2.68
MgO	"	1.30	1.30	2.63	1.82
CaO	"	1.50	0.83	0.70	1.67
Al <sub>2</sub> O <sub>3</sub>	"	10.95	12.97	19.92	16.50
Fe <sub>2</sub> O <sub>3</sub>	"	4.49	3.49	6.10	3.83
TiO <sub>2</sub>	"	0.36	0.55	0.86	0.73
MnO	"	0.02	0.01	0.01	0.01
P <sub>2</sub> O <sub>5</sub>	"	<0.25	<0.25	<0.25	<0.25
TOTAL		98.85	92.78	95.07	97.04
Sr	"	260	250	150	300
Ba	"	450	1,020	740	410
Zr	"	*80	150	160	200

LOC ID (Location identification) depth footage from Delee No. 1 Well,  
Hitchcock N.E. field.

Table 4. (continued)

<u>SAMPLE NO.</u> <u>LAB. NO.</u>		<u>DUPLICATES</u>		Cody Shale USGS SCO-1 Found	<u>QUALITY ASSURANCE</u>		
		3 84-822 9092 <sup>a</sup> Run 1	4 SHALE Run 2		Accepted	Green River Shale-USGS SGR-1 Found	Accepted
SiO <sub>2</sub>	(Wt %)	64.36	63.53	62.81	62.3?	28.73	28.3?
Na <sub>2</sub> O	"	1.71	1.71	0.90	0.9?	3.00	3.0?
K <sub>2</sub> O	"	2.60	2.59	2.74	2.7?	1.50	1.6?
MgO	"	2.14	2.14	2.63	2.6?	4.25	4.5
CaO	"	1.31	1.31	2.65	2.6?	8.57	7.2?
Al <sub>2</sub> O <sub>3</sub>	"	18.62	18.55	13.63	13.6?	6.53	6.5?
Fe <sub>2</sub> O <sub>3</sub> (T)	"	5.34	5.32	5.32	5.1?	3.05	3.2?
TiO <sub>2</sub>	"	0.84	0.83	0.62	0.64?	0.26	0.26?
MnO	"	0.03	0.03	0.05	0.05?	0.03	0.03?
P <sub>2</sub> O <sub>5</sub>	"	<0.25	<0.25	* 0.21	0.29?	<0.25	0.4?
Sr	"	255	257	216	200?	502	500?
Ba	"	457	465	570	500?	260	300?
Zr	"	199	171	100	150?	<41	70?

LOC ID (Location identification) depth footage from Delee No. 1 Well,  
Hitchcock N.E. field.



QA-3479

Figure 17. KFC diagram showing the elemental compositions of Anahuac and Frio shales compared to pure clay end members (Deer, Howie, and Zussman, 1969). The estimated illite and silica concentration in the clays is also shown.

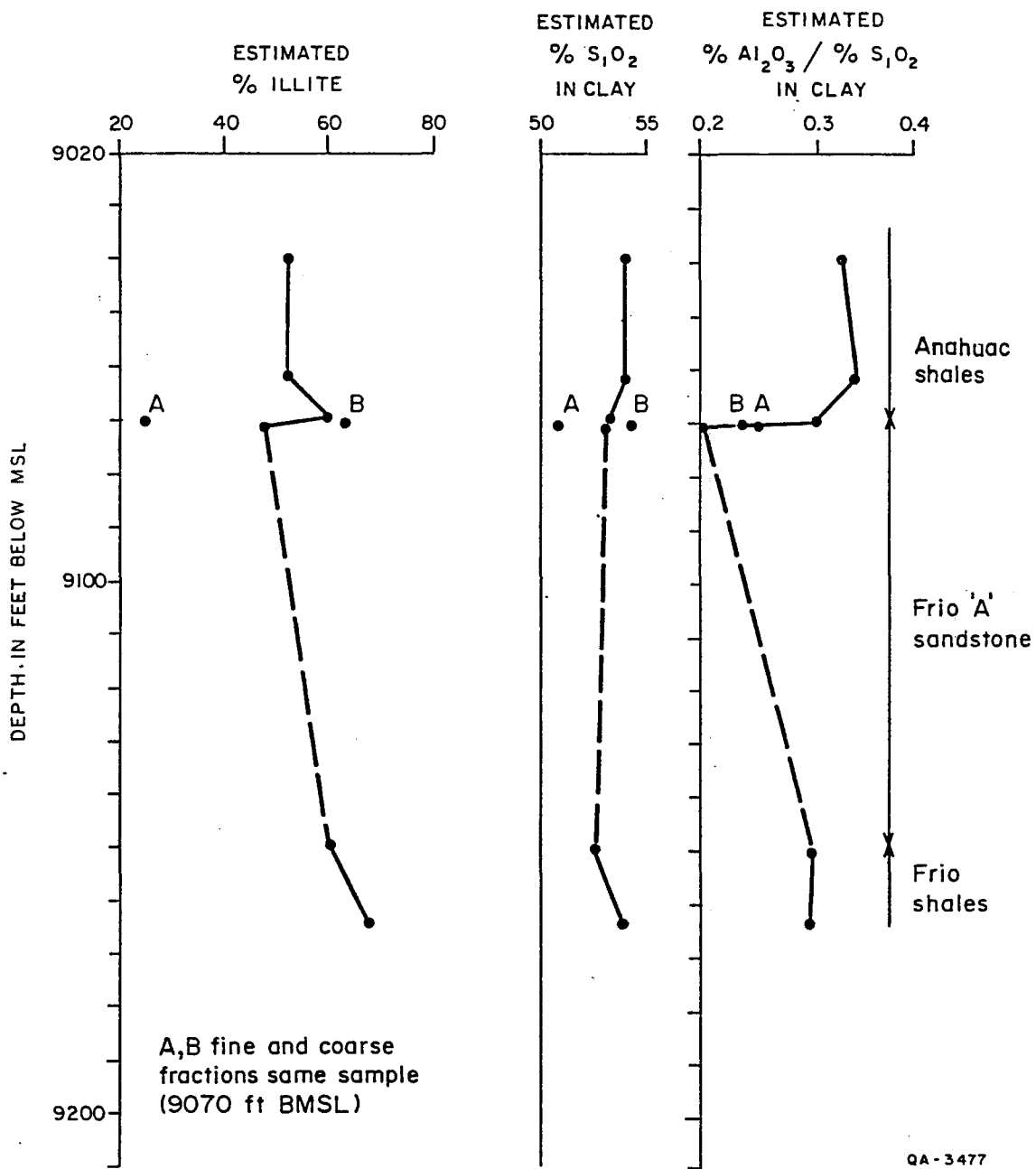


Figure 18 Estimated concentrations of illite, silica, and alumina versus depth in the Delee No. 1 well, Hitchcock N.E. field.

Smectite + Al<sup>3+</sup> + K<sup>+</sup> = illite + amorphous Si<sup>4+</sup> + various amounts of Ca<sup>2+</sup>,  
Mg<sup>2+</sup>, Fe<sup>2+</sup> and interlayer H<sub>2</sub>O (Hower and others, 1976)

The clay water containing amorphous silica probably migrated into the Frio 'A' sandstones during dewatering where the silica crystallized as authigenic quartz overgrowths (Morton, 1983). These authigenic quartz overgrowths formed at temperatures of 167° to 176° F (75° to 80° C) in Brazoria County (Loucks, and others, 1981).

Kaolinized feldspars and authigenic kaolinite cement are present throughout most of the Frio 'A' reservoir in the Delee No. 1 well. There does not seem to be a marked increase in kaolinite content in the upper parts of the reservoir as would be expected if major introduction of alumina rich fluids had occurred as a result of the smectite-illite transformation. However, a thin shale layer (9,179 to 9,182 ft; 2,798 to 2,799 m) near the base of the Frio 'A' reservoir is surrounded by a very indurated sandstone which contains spotty patches of authigenic kaolinite cement. The spotty zone is some 20 inches thick above the shale but only 4 inches thick below the shale, and is the best evidence of the introduction of fluids formed by clay dewatering, which resulted in crystallization of authigenic kaolinite in the sandstones. Crystallization of abundant kaolinite in the adjacent sandstones has greatly reduced their reservoir quality.

Authigenic kaolinite is abundant in sandstones in the depth range of 8,000 ft (2,438 m) to at least 17,700 ft (5,395 m) in Brazoria County (Loucks and others, 1981; Ewing and others, 1983). In general, precipitation of kaolinite postdates formation of quartz overgrowths and subsequent leaching of calcite and formation of secondary porosity (Kaiser and Richmann, 1981). Major authigenic kaolinite began to crystallize in Frio sandstones in Brazoria County at around 212° F (100° C) (Loucks and others, 1981). The smectite-illite transition in the shales begins at 194° to 212° F (90° to 100° C), which is similar to the temperature of major crystallization of authigenic kaolinite (Foscolos and others, 1976; Loucks and others, 1981). The present temperature of the Frio 'A' sandstone at the

Hitchcock N.E. field is about 215°F (101°C), which indicates both that illite should have begun to form from smectite and that major authigenic kaolinite should have begun to crystallize.

Measured pH values (6.2 to 7.1) of Frio Formation waters in Brazoria County (Kharaka and others, 1979) indicate that the fluids lie within the chlorite field and not the kaolinite stability field, contradicting petrographic evidence (Kaiser and Richmann, 1981). The stability of these two minerals is primarily controlled by the pH and Mg-Fe log activity product of the fluids (Kaiser and Richmann, 1981). However, Kharaka and others (1979) showed that pH values measured at well sites and wellhead temperatures are up to 2 pH units greater than the estimated (and probable) pH in the formation itself. Hence the measured pH values of 6.9 to 7.74 at the Huff A No. 1, Delee No. 1, Thompson No. 1, and Prets No. 1 wells (Kharaka and others, 1979; Randolph, 1985) probably represent an in situ pH of 5 to 6 in the formation. Kaolinite is stable in formation waters with pH values from 5 to 6 in Brazoria County (Kaiser and Richmann, 1981), which explains its abundance in the Delee No. 1 core. The increased value of the measured pH compared to the true in situ value may result from dilution of the formation water by condensed water vapor produced with the natural gas (Kharaka and others, 1977). Dilution of formation water may account for the reports of less saline than normal water in the geopressured zone (Kharaka and others, 1977).

The relative stability of feldspar versus kaolinite was examined by Kaiser and Richmann (1981). In shallower hydro pressured waters, plagioclase is stable at temperatures of less than 214°F (100°C), whereas kaolinite is stable relative to plagioclase under geopressured conditions. The fact that the Frio 'A' sandstone is 2,000 ft (609 m) below the top of geopressure in the Hitchcock N.E. field in a zone with a geopressure gradient of 0.6 psi/ft (fig. 2) is the probable explanation of the widespread replacement of feldspar by kaolin in this reservoir.

## Shale Dewatering During Production

Little evidence is currently available that can be used to demonstrate shale fluid flow (dewatering) during production. However, formation water at the Phillips Prets No. 1 well was analyzed on three occasions, once 8 years ago (Kharaka and others, 1977) and twice in 1985 by the Institute of Gas Technology (IGT) and the University of Houston staff (Randolph, 1985). Although the quality of the early analyses and differences in the sampling points and procedures raise some questions, the slight decrease in chloride ion concentration of about 5.5 to 8.7 percent may indicate shale dewatering (table 5). Fowler (1970), using 94 water analyses from Frio sandstones in the Chocolate Bayou field, calculated the percentage change in chloride ion production over long periods of time. Reduced chloride ion production is a result of dilution of the original formation waters by waters squeezed out of the shales adjacent to the aquifers having declining pressures in the reservoir sandstones. Reductions in chloride ion concentration varied from 0.5 to 42.3 percent in 10 of the reservoirs in which shale dewatering is believed to have occurred; mean value is 18.5 percent (Fowler, 1978). The Frio 'A' sandstone showed a 12.4 percent reduction in salinity in the Chocolate Bayou field over an 18-year production period. The fact that the Hitchcock N.E. field has produced for 25 yr (Anderson and others, 1984) indicates that this amount of variation in the chloride ion concentration is to be expected if major shale dewatering did occur due to pressure drawdown. To more accurately investigate the effects of shale dewatering during the co-production of the Hitchcock N.E. field, the time-dependent variation of the elemental composition of brine produced at the Delee No. 1 well should be measured. This investigation should be done over a long time interval and analyses should be made periodically to determine if the concentrations of major, trace, and rare-earth elements change systematically. These concentrations can be related to the effects of shale dewatering or to water introduction from deeper levels (water drive from a large aquifer or leaky faults). It may be possible by measuring the amount of elemental variation to estimate the volume of water being added by shale

Table 5. Brine analyses results, Phillips Prets No. 1 well.

Sampling Point	Kharaka and others, 1977	Southern Pet. Lab. Inc., 1982	University of Houston, 1984	IGT, 1985
	?	Brine Tank	Prets Separator	Prets Separator
TDS	44,600	38,700		44,000
Li	4.0			3.56
Na	17,000	14,400		16,800
K	160			120
Rb	0.40			
Ca	470	511		420
Mg	85	79		70.4
Sr	35			37.0
Ba	16	<1		16.8
Fe	0.1	15		11.3
Mn	0.4			0.5
B	41			
NH <sub>3</sub>	17.0			15.0
H <sub>2</sub> S	0.62			
HCO <sub>3</sub>	643	687		
CH <sub>3</sub> COO	750			
Cl	25,200	23,000	25,000	23,800
Br	25			
I	15			
SO <sub>4</sub>	34	20		10.4
SiO <sub>2</sub>	65			64
pH	6.9			7.74
δ D	-14.5 SMOW			

elemental concentrations in mg/L

dewatering and thus to estimate the reduction in pressure depletion of the reservoir during rapid pressure drawdown.

Iron content in the formation fluids increases to 15 mg/L in the Prets No. 1 well (table 5). This iron may be derived from oxidation of casing in the production wells over the long (25 yr) production period of the Hitchcock N.E. field. However, the data available only apply to the last 8 yr of production.

The variation of elemental abundance, compounds, and isotopes was plotted against both depth and chlorine content of wells in Brazoria and Galveston Counties. Most elements show a trend with depth and values from the Prets No. 1 well tend to plot on the opposite end of the trend compared with those from the Pleasant Bayou geopressured geothermal wells (fig. 19) (Kharaka and others, 1977).

The  $\delta D$  (deuterium/hydrogen) value becomes depleted with depth in Brazoria and Galveston Counties (fig. 20) (Kharaka and others, 1977) and the variation in  $\delta D$  over time in the Delee No. 1 well should indicate whether shale dewatering is occurring or the fluids are more deeply sourced. A similar but larger variation is shown by the concentration of short chain aliphatic acids ( $C_2-C_5$ ) (fig. 21) (Kharaka and others, 1977).

#### SHALE PYROLYSIS DATA

Forty shale samples from the Anahuac and Frio Formations in the Delee No. 1 well underwent total organic carbon and Rock-Eval pyrolysis analyses by Geochem Laboratories, Inc. The total organic carbon (TOC) in shales averaged 0.35 percent (range 0.17 to 1.06), which indicates that these shales are very poor hydrocarbon source rocks (table 6a and b). One sample from 6,863 ft (2,092 m) had a TOC of 1.06 percent whereas a thin coaly shale within the top of the Frio 'A' sandstone at 9,104 ft 5 inches contained 0.58 percent TOC. Total organic carbon contents of Frio shales beneath the Frio 'A' sandstone are variable (0.20 to 0.44 percent TOC) but on average are lean (mean = 0.33 percent TOC).

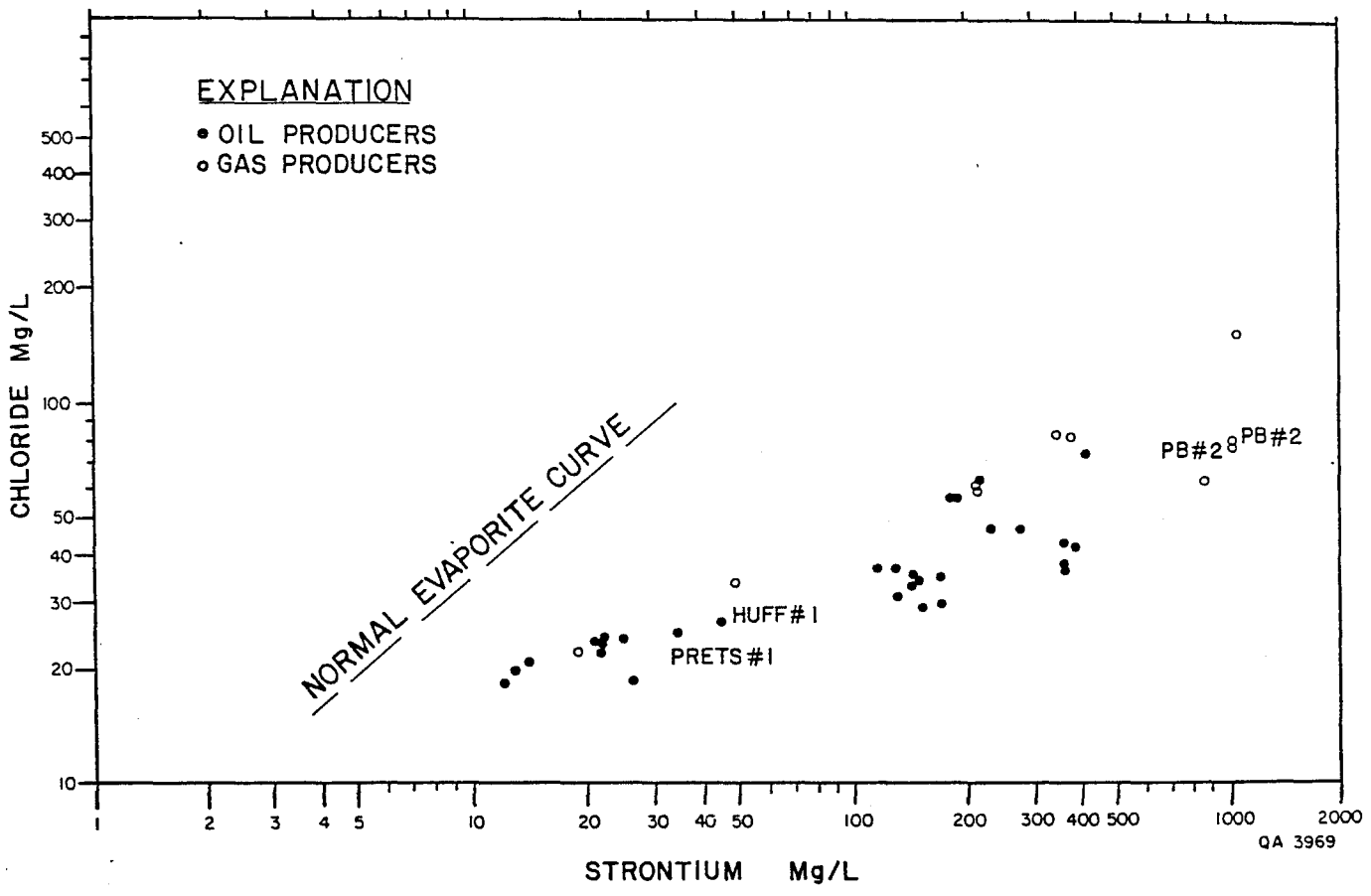


Figure 19. Strontium versus chloride in formation water, Brazoria and Galveston Counties (data from Kharaka and others, 1977). Positions of the Prets No. 1 and Pleasant Bayou geopressured-geothermal test wells are shown for comparison. Normal evaporite curve from Collins, 1975.

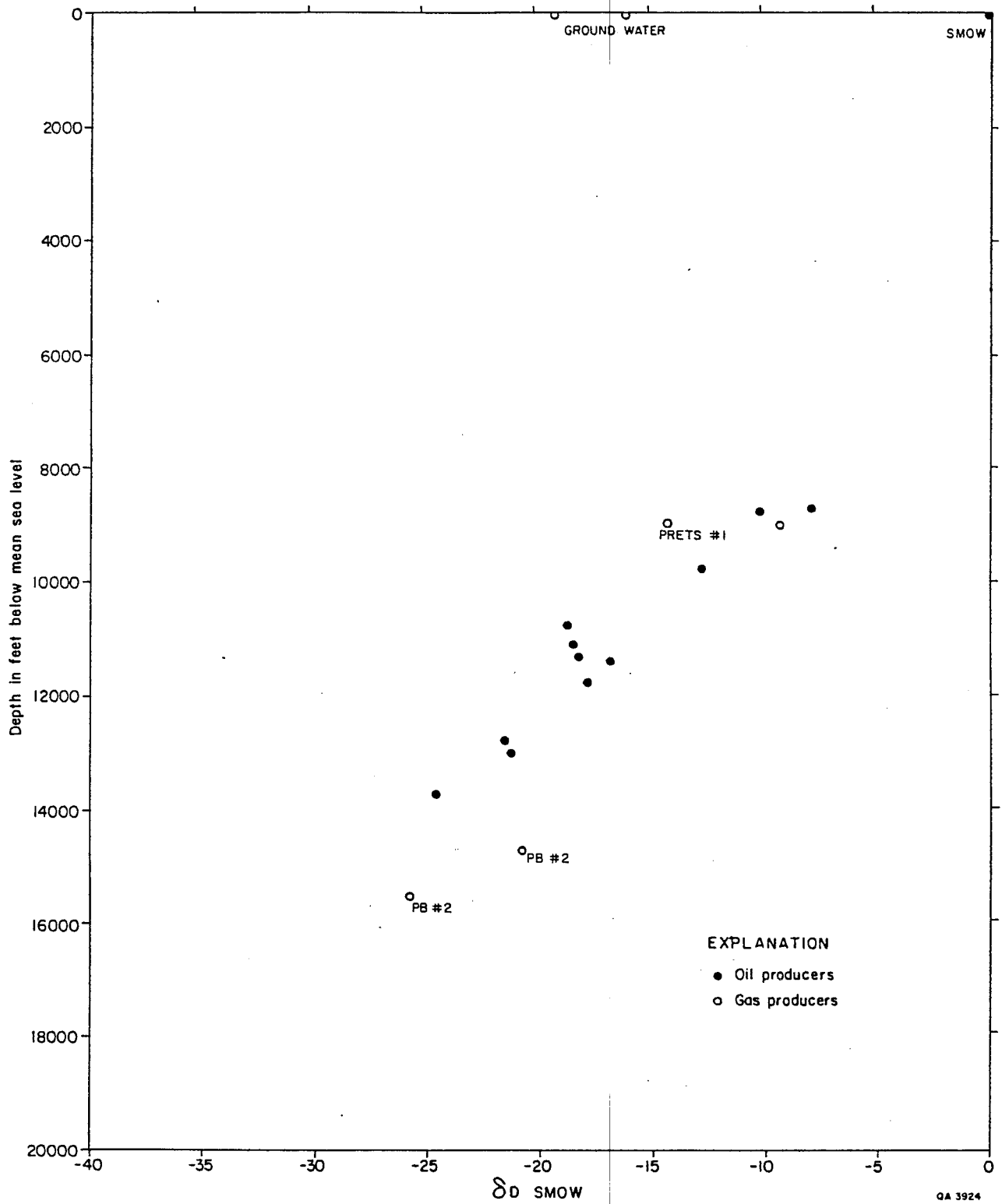


Figure 20.  $\delta D$  SMOW versus depth in formation water, Brazoria and Galveston Counties (data from Kharaka and others, 1977). Positions of the Prets No. 1 and Pleasant Bayou geopressured-geothermal test wells are shown for comparison.

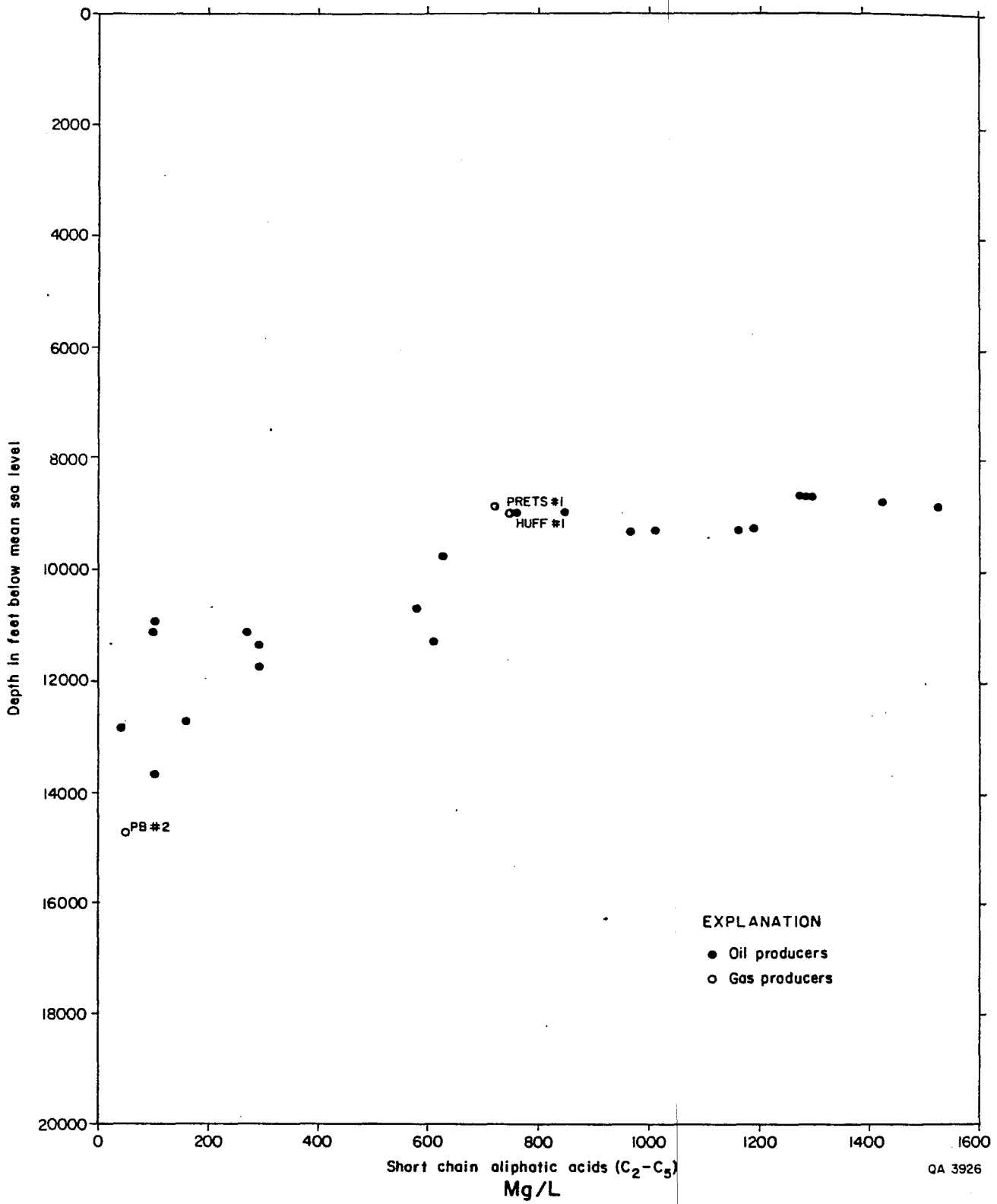


Table 6a.

## RESULTS OF ROCK-EVAL PYROLYSIS

GeoChem Sample No.	Depth Interval (Feet)	Tmax (c)	S <sub>1</sub> (mg/g)	S <sub>2</sub> (mg/g)	S <sub>3</sub> (mg/g)	PI	PC*	T.O.C. (wt.%)	Hydrogen Index	Oxygen Index
3013-001	6758	409	0.02	0.30	1.41	0.06	0.02	0.85	35	165
3013-002	6863	430	0.02	0.26	1.42	0.07	0.02	1.06	24	133
3013-003	6887	416	0.01	0.05	0.48	0.17	0.00	0.36	13	133
3013-004	7020	391*	0.02	0.07	0.48	0.25	0.00	0.28	25	171
3013-005	7113	386*	0.01	0.11	0.57	0.08	0.01	0.47	23	121
3013-006	7176	415*	0.01	0.09	0.53	0.10	0.00	0.35	25	151
3013-007	7216	375*	0.02	0.09	0.79	0.20	0.00	0.34	26	232
3013-008	7262	405*	0.02	0.08	0.42	0.20	0.00	0.32	25	131
3013-009	7294	354*	0.00	0.06	0.45	0.00	0.00	0.34	17	132
3013-010	7392	410*	0.02	0.08	0.44	0.20	0.00	0.33	24	133
3013-011	7534	354*	0.03	0.07	0.36	0.30	0.00	0.27	25	133
3013-012	7679	395*	0.01	0.14	0.50	0.07	0.01	0.39	35	128
3013-013	7858	394*	0.01	0.07	0.35	0.12	0.00	0.26	26	134
3013-014	7990	377*	0.00	0.06	0.36	0.00	0.00	0.27	22	133
3013-015	8126	415*	0.01	0.07	0.32	0.12	0.00	0.27	25	118
3013-016	8304	413	0.02	0.09	0.28	0.20	0.00	0.30	30	93
3013-017	8432	385*	0.03	0.10	0.36	0.25	0.01	0.30	33	120
3013-018	8602	409*	0.02	0.08	0.22	0.20	0.00	0.27	29	81
3013-019	8759	406*	0.02	0.09	0.21	0.20	0.00	0.30	30	70
3013-020	8913	415*	0.02	0.14	0.48	0.12	0.01	0.64	21	75
3013-021	8999	360*	0.01	0.07	0.28	0.12	0.00	0.31	22	90
3013-022	9070	337*	0.03	0.08	0.24	0.30	0.00	0.30	26	80
3013-023	9083.5	423*	0.03	0.07	0.25	0.30	0.00	0.20	35	125
3013-024	9092	376*	0.02	0.06	0.20	0.25	0.00	0.23	26	86
3013-025	9099'5.5"	323*	0.02	0.03	0.14	0.50	0.00	0.17	17	82
3013-026	9100	329*	0.02	0.08	0.28	0.20	0.00	0.22	36	127
3013-027	9100 6"	314*	0.02	0.05	0.17	0.33	0.00	0.17	29	100
3013-028	9100 7.25"	299*	0.02	0.07	0.25	0.25	0.00	0.17	41	147
3013-029	9101	318*	0.02	0.09	0.28	0.20	0.00	0.21	42	133

\*The S2 value, or quantity of kerogen pyrolyzed to bitumen, is insufficient to produce a valid Tmax

T.O.C. = Total organic carbon, wt.%  
 S1 = Free hydrocarbons, mg HC/g of rock  
 S2 = Residual hydrocarbon potential  
 (mg HC/g or rock)

S<sub>3</sub> = CO<sub>2</sub> produced from kerogen pyrolysis  
 (mg CO<sub>2</sub>/g of rock)  
 PC\* = 0.083 (S1 + S2)  
 Hydrogen  
 Index = mg HC/g organic carbon

Oxygen  
 Index = mg CO<sub>2</sub>/g organic carbon  
 PI = S1/S1 + S2  
 Tmax = Temperature Index, degrees C.

Table 6b.  
RESULTS OF ROCK-EVAL PYROLYSIS

GeoChem Sample No.	Depth Interval (Feet)	Tmax (c)	S <sub>1</sub> (mg/g)	S <sub>2</sub> (mg/g)	S <sub>3</sub> (mg/g)	PI	PC*	T.O.C. (wt.%)	Hydrogen Index	Oxygen Index
3013-030	9104 5"	421	0.04	0.40	0.38	0.09	0.03	0.58	68	65
3013-031	9179 11"	403*	0.02	0.07	0.20	0.25	0.00	0.21	33	95
3013-032	9194 3"	425	0.03	0.20	0.19	0.14	0.01	0.35	57	54
3013-033	9262	423	0.01	0.21	0.49	0.05	0.01	0.44	47	111
3013-034	9288	416	0.01	0.15	0.32	0.06	0.01	0.37	40	86
3013-035	9302	401*	0.01	0.12	0.35	0.08	0.01	0.34	35	102
3013-036	9340	302*	0.01	0.03	0.44	0.25	0.00	0.20	15	220
3013-037	9351	336*	0.01	0.10	0.37	0.10	0.00	0.27	37	137
3013-038	9367-9371	377*	0.03	0.29	0.30	0.09	0.02	0.43	67	69
3013-039	9370-9392	333	0.27	0.76	0.47	0.26	0.08	0.43	176	109
3013-040	9392-9402	343	0.02	0.15	0.31	0.12	0.01	0.29	51	106

52

\*The S<sub>2</sub> value, or quantity of kerogen pyrolyzed to bitumen, is insufficient to produce a valid Tmax.

T.O.C.	= Total organic carbon, wt.%	S <sub>3</sub>	= CO <sub>2</sub> produced from kerogen pyrolysis (mg CO <sub>2</sub> /g of rock)	Oxygen Index	= mg CO <sub>2</sub> /g organic carbon
S <sub>1</sub>	= Free hydrocarbons, mg HC/g of rock	PC*	= 0.083 (S <sub>1</sub> + S <sub>2</sub> )	PI	= S <sub>1</sub> /S <sub>1</sub> + S <sub>2</sub>
S <sub>2</sub>	= Residual hydrocarbon potential (mg HC/g or rock)	Hydrogen Index	= mg HC/g organic carbon	Tmax	= Temperature Index, degrees C.

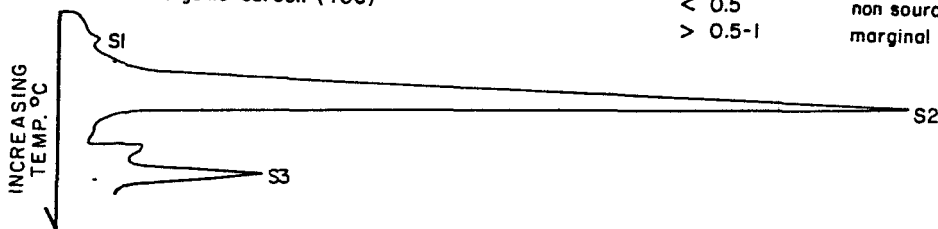
Rock-Eval pyrolysis is a technique used to evaluate the maturity of source rocks, a procedure that involves heating a shale sample in the absence of oxygen to break down large hydrocarbon molecules into smaller ones (Milner, 1982; Dutton, in press). Dutton (in press) outlined the pyrolysis procedure. As the temperature is gradually increased, the sample will first give off hydrocarbons (S1) that are already present in the rock either in a free or adsorbed state (Tissot and Welte, 1978). When the temperature is raised further, kerogen in the sample will generate new hydrocarbons (S2), imitating in the laboratory the natural process of hydrocarbon generation. Finally, the CO<sub>2</sub> that is generated during pyrolysis is measured (S3) as an indication of the type of kerogen in the sample, whether it is humic (oxygen-rich) or sapropelic (hydrogen-rich) (Hunt, 1979). Thermal maturity is measured by comparing the temperature of maximum evolution of thermally cracked hydrocarbons (T-max°C) versus the proportion of free hydrocarbons (S1) in the sample compared to total hydrocarbons (S1 + S2), that is, T-max°C versus S1/(S1 + S2). An example of the various peaks and a key for interpreting the pyrolysis data are given in figure 22 (Dow and Page, 1981).

Source potential (values of S2) of the shales in the Delee No. 1 well averages 0.13 mg/g (range 0.03 to 0.76 mg/g), well below the 2.5 mg/g upper limit for poor source potential (tables 6a and 6b, fig. 22). The thin coaly shale within the top of the Frio 'A' sandstone has a slightly better source potential of 0.4 mg/g, whereas deeper Frio shales at 9,370 to 9,392 ft (2,856 to 2,863 m) have source potentials of 0.76 mg/g. Source potential values indicate that it is extremely unlikely that the condensate in the Frio 'A' reservoir could have been derived from either Anahuac or Frio shales.

The S2/S3 ratio provides a general indication of kerogen quality (type) and reveals whether oil or gas is likely to be generated (Dow and Page, 1981). Dry gas generating kerogens have S2/S3 values of less than 2.5. Delee No. 1 well S2/S3 values average 0.35 (range 0.1 to 1.6), which suggests that the kerogen is a poor source even for dry gas (fig. 22).

KEY FOR PYROLYSIS DATA INTERPRETATION:

			DELEE #1
Source potential—values of S2	< 2.5	poor	0.13
	2.5-5.0	marginal	
	> 5.0	good	
Petroleum type—values of S2/S3	< 2.5	dry gas	0.35
	2.5-5.0	wet gas	
	> 5.0	oil	
Generation zones—values of T-max (°C)	< 435	immature	0.435
	435-470	oil	
	450+	gas	
Productivity index—high values of S1/(S1+S2) indicate migrated hydrocarbons			
Total organic carbon (TOC)	< 0.5	non source	0.35
	> 0.5-1	marginal	



QA 3921

Figure 22. Key for pyrolysis data interpretation (Dow, 1981) with average values from the Delee No. 1 well.

Hydrogen and oxygen index data on shales in the Delee well indicate that the kerogen is type III, consisting essentially of woody and coaly material (fig. 23). The T-max°C values for all these samples are less than 815°F (435°C), indicating that this lignitic material is immature (fig. 24). However, many of the samples contained such a small quantity of organic matter (kerogen) that it was insufficient to produce a valid T-max°C.

Estimated  $\delta^{13}\text{C}$  values were made for the aromatics and the saturates in oil from the Prets No. 1 well by Coastal Science Laboratories, Inc., Austin, Texas. Calculations of the canonical variable from these data and pristane-phytane ratios (figs. 25 and 26) indicate that the Prets No. 1 oil is correctly classified as a nonwaxy oil sourced from marine organic matter. This is in contrast to the terrigenous nature of the kerogen in the Anahuac and Frio shales and implies that these oils have been sourced from other (deeper) formations.

### CONCLUSIONS

The high porosity ( $\pm 30$  percent) and permeability ( $\pm 1,000$  md,  $0.99 \mu\text{m}^2$ ) of the Frio 'A' reservoir in the Hitchcock N.E. field are largely the result of deposition in a distributary-mouth-bar complex. As a consequence of extensive marine reworking, the lateral extent of this sandstone will allow free access to water influx from the southwest extension of this aquifer.

Location of the Hitchcock N.E. field on the northeast side of the large faulted Frio 'A' aquifer isolated to the north and south by northeast-trending fault systems has bearing on the best location of guard wells below the gas-water contact to control water influx.

Minor faults that dissect the Hitchcock N.E. field may locally isolate certain parts of the pay zone where shale or permeability breaks are present. Knowledge of the position and extent of these zones will also control the best placement of guard wells. However,

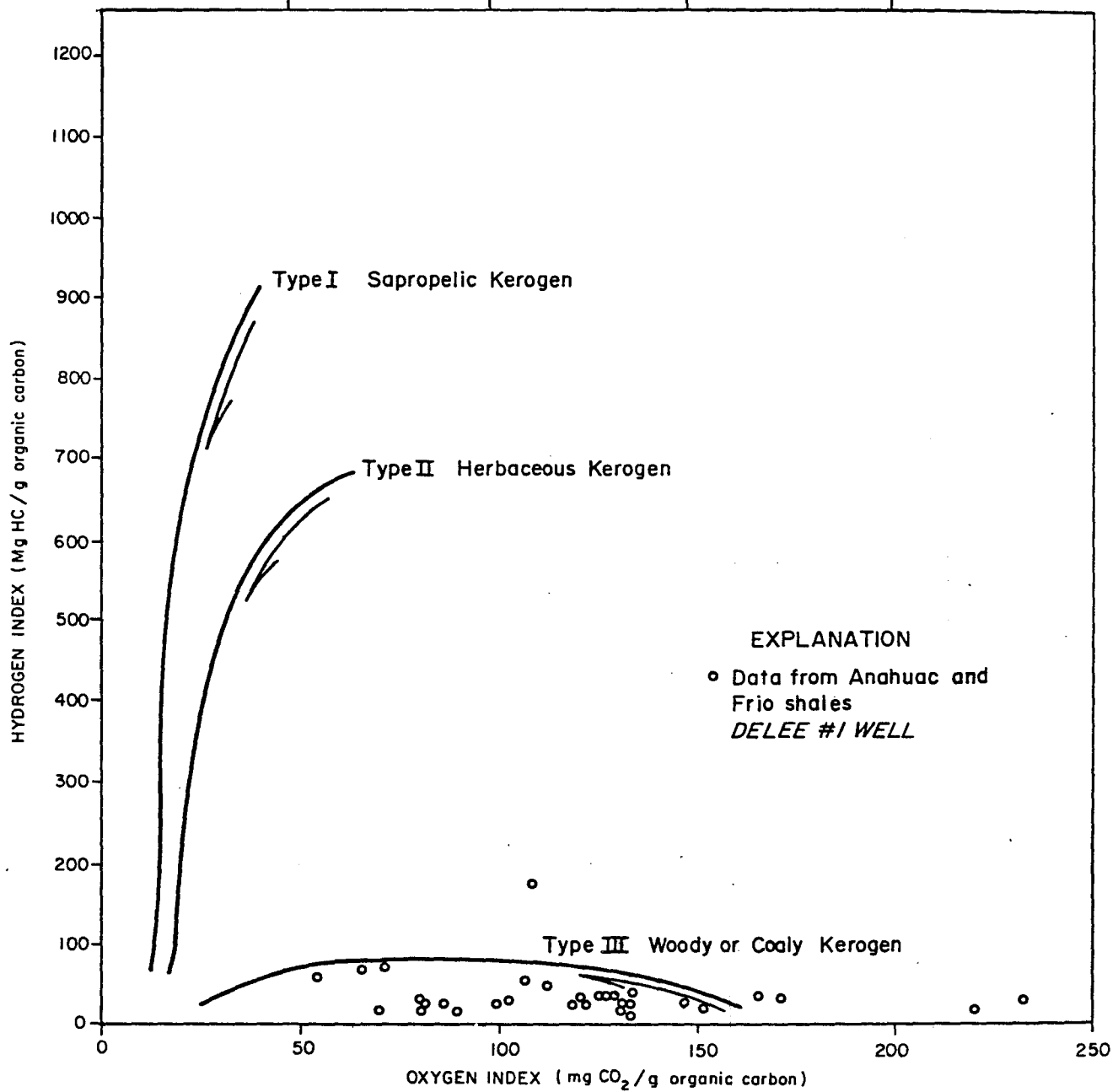


Figure 23. Van Krevelen diagram showing the source rock quality of Anahuac and Frio shales from the Delee No. 1 well.

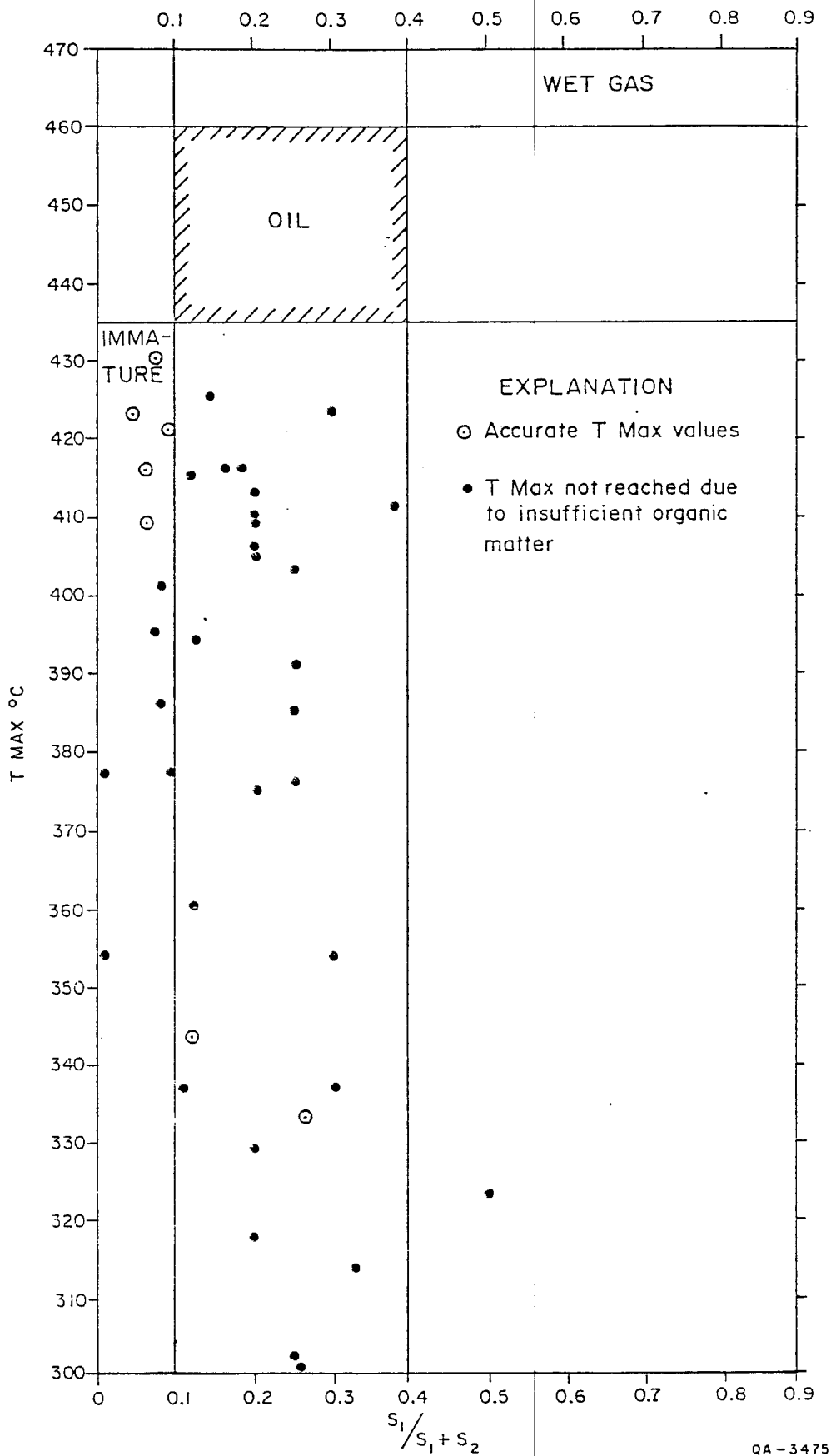


Figure 24. Pyrolysis maturity diagram (T-Max°C versus S1/S1 + S2) showing immature nature of the Delee No. 1 shales.

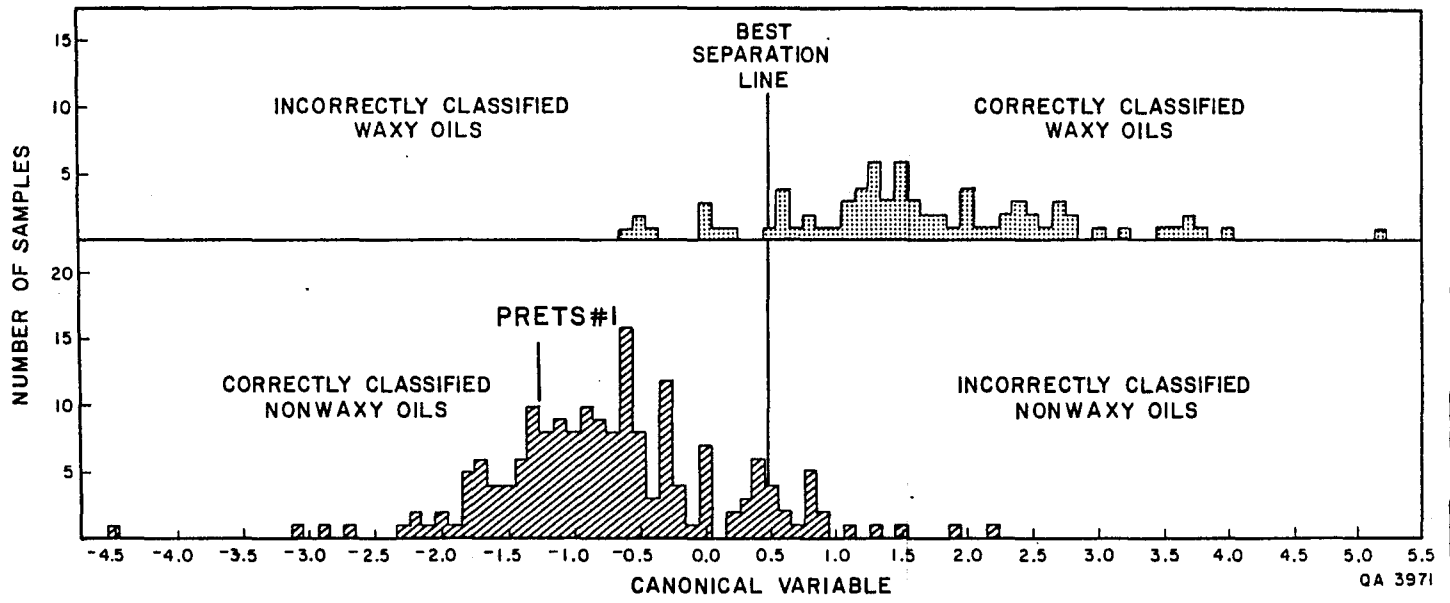


Figure 25. Histograms of the canonical variable (CV) for  $\delta^{13}\text{C}$  aromatics versus  $\delta^{13}\text{C}$  saturates from Sofer, 1984. The Prets No. 1 oil plots within the non-waxy oils.

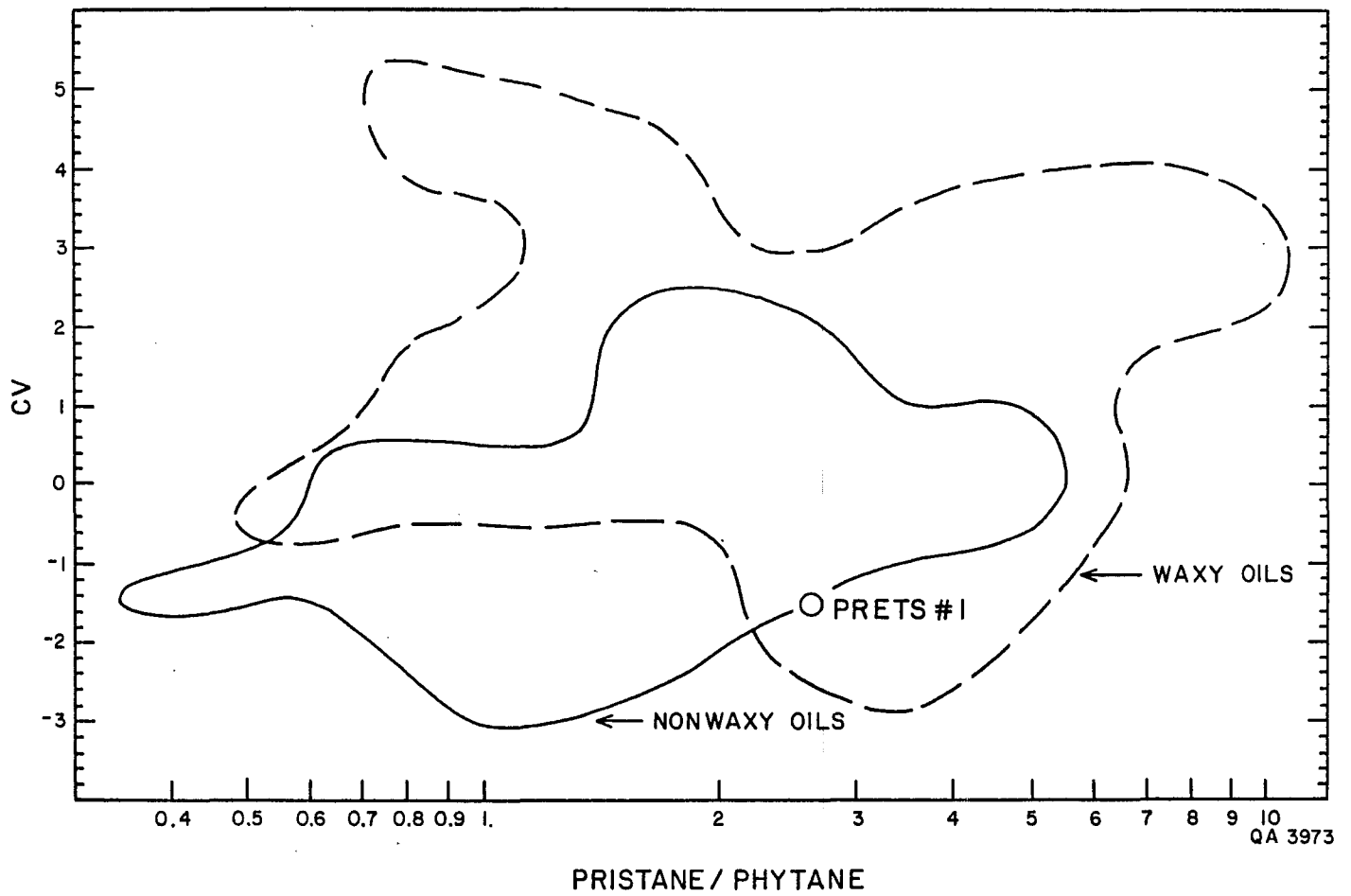


Figure 26. Canonical variable (CV) versus pristane/phytane (Pr/Ph) ratios. Taken from Sofer, 1984. The position of the Prets No. 1 oil is shown.

reservoir modeling suggests that the faults are not sealing during the fairly long timeframe of pressure drawdown during co-production.

Vitrinite reflectance at the Pleasant Bayou geopressured geothermal test wells, supported by hydrocarbon maturation and isotope data, indicates that the Upper Frio was subjected to an extended period of hot, extremely saline, basinal-fluid flow. This fluid flow appears to have introduced hydrocarbons into these sandstones, caused albitization of the feldspars, and formed the carbonate cements.

Elemental composition data on Anahuac and Frio shales at the Delee No. 1 well indicate that they have a consistent smectite-illite composition. No clear evidence was found for shale dewatering. However, spotty indurated authigenic kaolinite zones, developed in the Frio 'A' sandstone adjacent to thin shale units, probably result from fluids emitted from the shales. Slight reduction in salinity during production at the Prets No. 1 well may be evidence of contemporaneous dewatering of shales.

Shale pyrolysis data indicate that the Anahuac and Frio shales contain coaly or woody kerogen of very poor hydrocarbon source quality. Furthermore, all the samples appear to be immature. In contrast, isotope data indicate that the Prets No. 1 condensates are derived from marine organic matter, further supporting a deep source for these fluids.

#### IMMEDIATE RESEARCH PLANS

Initial research by the Bureau of Economic Geology will be to screen previously unidentified candidate reservoirs for enhanced gas recovery during the next contract period. Work on this project has begun. In the process of identifying these reservoirs we will refine previously used criteria and will develop new criteria that can be applied in selecting potential co-production reservoirs. The best 10 ( $\pm 2$ ) fields will be selected for detailed reservoir evaluation. These data will be made available to groups contracted to the Gas Research Institute that are conducting reservoir simulation. They will determine

the total reservoir initial volume and estimate the recoverable gas reserves using the co-production of gas and water pressure drawdown enhancement procedure.

Work on the Delee No. 1 well will be continued but on a reduced scale. The shale Frio 'A' sandstone boundary will be examined using scanning electron microscopy and petrographic studies. These data bear on fluid migration and shale dewatering.

Gas chromatography-mass spectrometry and isotope analyses of hydrocarbons and formation fluids from the Prets and Delee wells are still to be received from Geochem Laboratories and Coastal Science Laboratories, respectively. These data will be statistically compared by computer with hydrocarbon extract data from shales from the Pleasant Bayou test wells for the entire Frio, Anahuac, and Miocene sequence (16,500 ft [5,029 m] total). This procedure will aid in locating the source of the hydrocarbons.

We propose that detailed major, trace, and rare-earth element analyses be conducted periodically on produced fluids from the Delee No. 1 well and on the shales surrounding the Frio 'A' sandstone. These data should indicate the amount of shale dewatering that is occurring as a result of the pressure drawdown during the co-production of gas and water.

# SUBSIDENCE AND SURFACE FAULTING IN THE HOUSTON-GALVESTON AREA, TEXAS--A RESULT OF DEEP FLUID WITHDRAWAL?

by Thomas E. Ewing

## INTRODUCTION

The environmental effects of the production of geopressed geothermal fluids have been extensively considered in recent years. Various researchers have concluded that surface subsidence and fault reactivation are the most significant non-spill hazards of long-term production (Gustavson and Kreitler, 1976). Since long-term tests of geopressed geothermal test wells will not be available for some time, a useful approach for evaluating these hazards is to examine cases where subsidence or fault reactivation is caused by fluid production at intermediate depths (2,000 to 10,000 ft [610 to 3,050 m]), searching for principles that can be extrapolated to deep, high-volume production.

Examination of high-altitude aerial photographs showed that active faulting in the Texas Coastal Zone (where subtle elevation changes are most easily noted) is limited to the area northeast of Matagorda County in the Houston salt-structure province. Subsidence in the area of the Caplen oil field, Galveston County, was noted earlier on low-altitude photographs (R. A. Morton, personal communication, 1984). However, upon closer study it appears that this feature is probably linked with additional faulting to the north, forming a fault system similar to the one in the Genoa-Webster area southeast of Houston.

## FAULTING IN THE CAPLEN AREA

Surface faulting in the Caplen area (fig. 1) is easily visible on 1982 aerial photographs. Fault scarps have formed across a major washover fan on Bolivar Peninsula. Two conspicuous scarps bound a sector showing no subsidence. Subsidence east and south of these two scarps has been sufficient to flood most of the central part of the fan, and only a few levees of distributary channels are above the water. Levees of this sort are

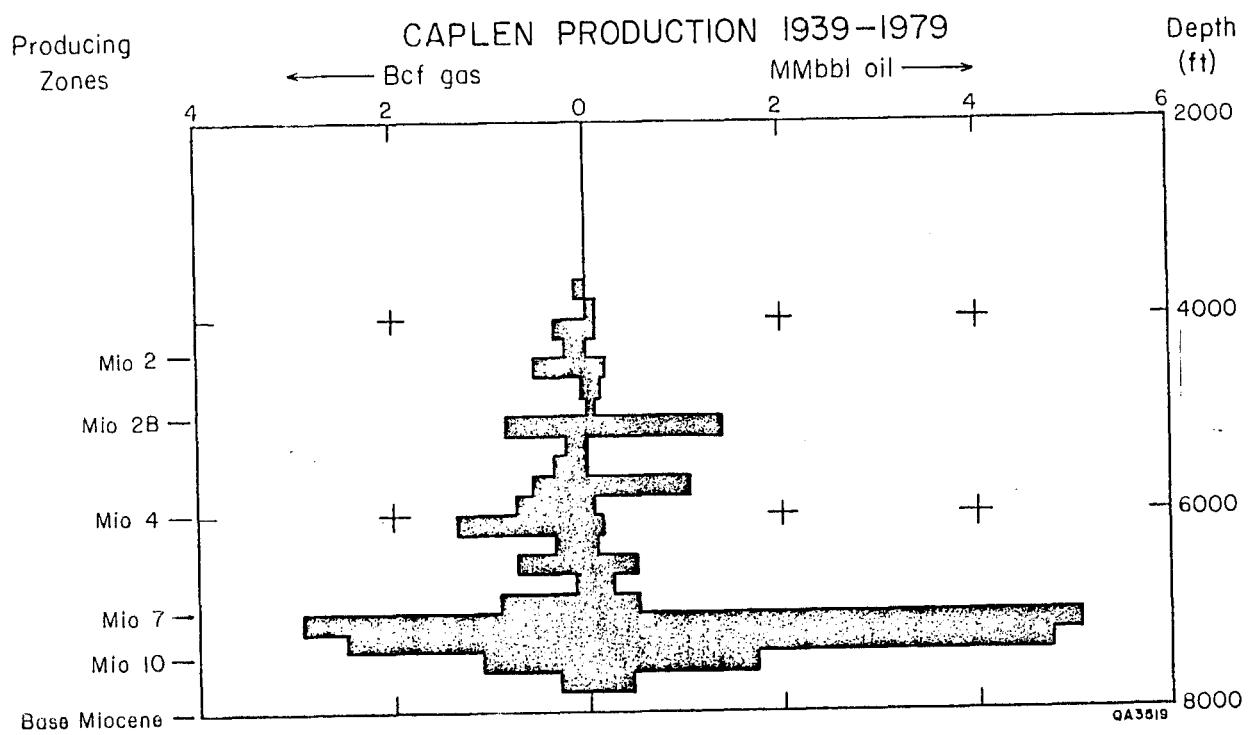


Figure 27. Surface faulting and subsidence in the Caplen and Robinson Lake areas, as detected on 1982 aerial photographs taken for the General Land Office, and subsurface faults at about 7,000 ft from well data. Faults in East Bay from Verbeek and Clanton (1981, their fig. 3a).

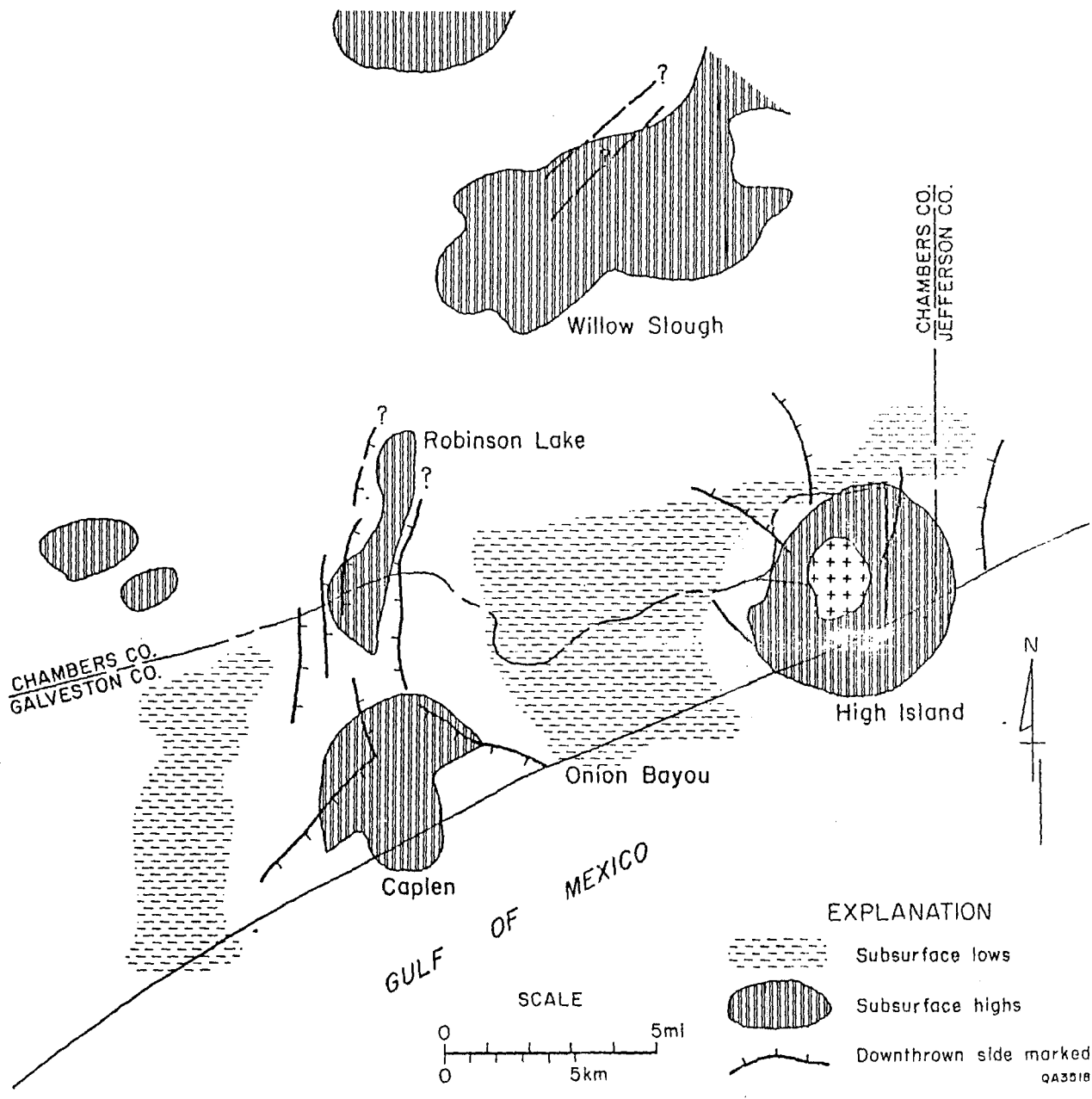


Figure 28. Production of oil and gas versus depth in Caplen field through 1979. Data from International Oil Scouts Association (1983).

## EAST BAY FAULT SYSTEM

Faults in the Caplen area are apparently connected with active normal faults observed to the north in the Robinson Lake area (fig. 27). Photographs of that area clearly show fault scarps in 1982 and (inconspicuously) in 1956, but not in 1930. The faults transect beach-ridge complexes along East Bay. The scarps outline a complex graben, with more down-to-the-east than down-to-the-west faults. In East Bay, which separates the two areas of surface faulting, faults extending to the seabed can be mapped using high-resolution seismic reflection data. These faults are traceable northward into onshore faults, as noted by Verbeek and Clanton (1981), but only a short data gap separates them from the Caplen faults.

The Robinson Lake - East Bay faults are not associated with significant fluid production. A few gas wells are found (Robinson Lake gas field), but production is minor.

Taken as a whole, the East Bay system forms a gently arcuate graben from Robinson Lake to Caplen field, where it apparently divides into southwest- and southeast-trending half-grabens (fig. 29). The northeast limit of the complex is indefinite at present, owing to cultivation and the absence of diagnostic wetland vegetation. The graben system is located over a subsurface high that bounds two basinal areas. To the east is the major salt-withdrawal basin located west of High Island salt dome; basin-rimming normal faults are mapped on the Robinson Lake-Caplen high.

The only significant fluid production within the fault system is that from the 7,000-ft (2,134-m) level of Caplen field--at the system's southern extremity. However, more than 200 million bbl of oil and similar quantities of water have been produced from Miocene sandstones at High Island salt dome. Ground-water production in the area is insignificant, as all subsurface waters have salinities of greater than 3,000 ppm (Petitt and Winslow, 1957; Wesselman, 1971).

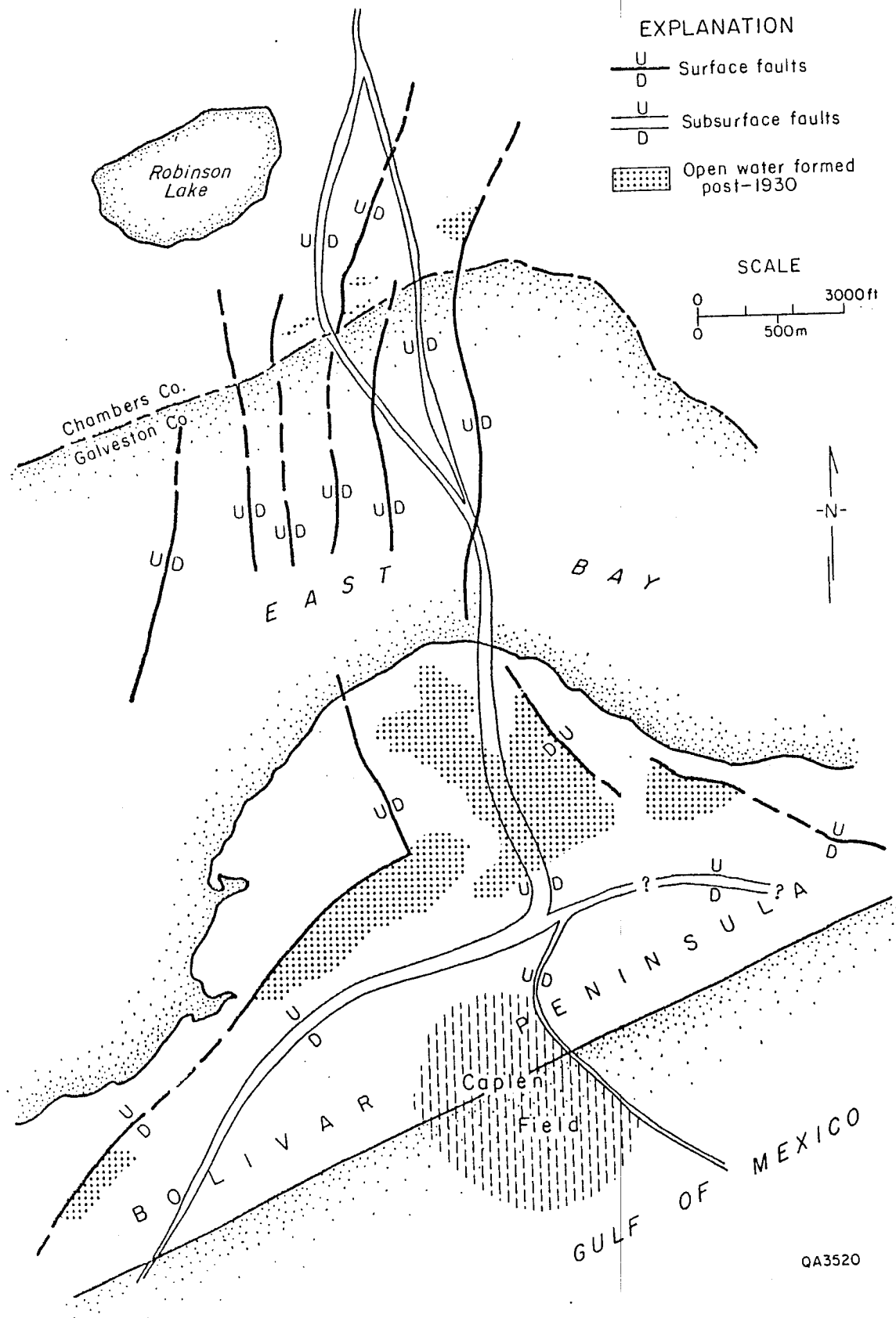


Figure 29. East Bay fault system compared with subsurface structure. The faults form grabens on subsurface highs rimming the Onion Bayou salt-withdrawal basin.

If this faulting is humanly induced (as its post-1930 development seems to indicate), the only cause appears to be fluid withdrawals through oil and gas wells. Furthermore, the only significant production that could affect the entire fault complex is that of High Island. From High Island to the East Bay fault system the Lower Miocene sandstone reservoirs show excellent lateral continuity (fig. 30). The major producing zones (7 and 9) at Caplen can be correlated in detail with zones on the west and southwest flanks of High Island dome. Production at High Island is from many sandstones, but Lower Miocene sandstones correlative to zones 7 through 10 are major reservoirs there as well (Miocene "2-3," "4," and "5").

#### GENOA-WEBSTER FAULT SYSTEM

The geometry of the East Bay fault system bears close resemblance to the well-studied surface faults southeast of Houston, here called the Genoa-Webster fault system. In this area, graben-bounding faults active since the 1930s form an irregular horseshoe open to the northeast around a salt-withdrawal basin, here called the Genoa basin. The faults have formed above the salt-cored subsurface ridges and domes of South Houston, Mykawa, Webster, and Clear Lake (fig. 31). Other surface faulting is present to the northeast at Goose Creek (where faulting has been closely tied to oilfield activities since the 1920s), to the north at Clinton, and to the south at Hastings. The area has undergone major amounts of deep fluid withdrawal (over 1,200 million bbl of oil alone), mostly from the Upper Frio (Marg-Frio) sandstone at 6,000 to 7,000 ft (1,829 to 2,134 m) depth. This sandstone forms an easily correlatable unit, up to 600 ft (183 m) thick, of substantial lateral continuity.

This fault complex, however, lies near the center of a major regional bowl of subsidence. The Genoa basin corresponds closely to the center of most rapid historic subsidence (Gabrysch and Bonnet, 1975; Kreitler, 1977). The bowl has been convincingly attributed to withdrawal of ground water from shallow, unconsolidated aquifers. This has

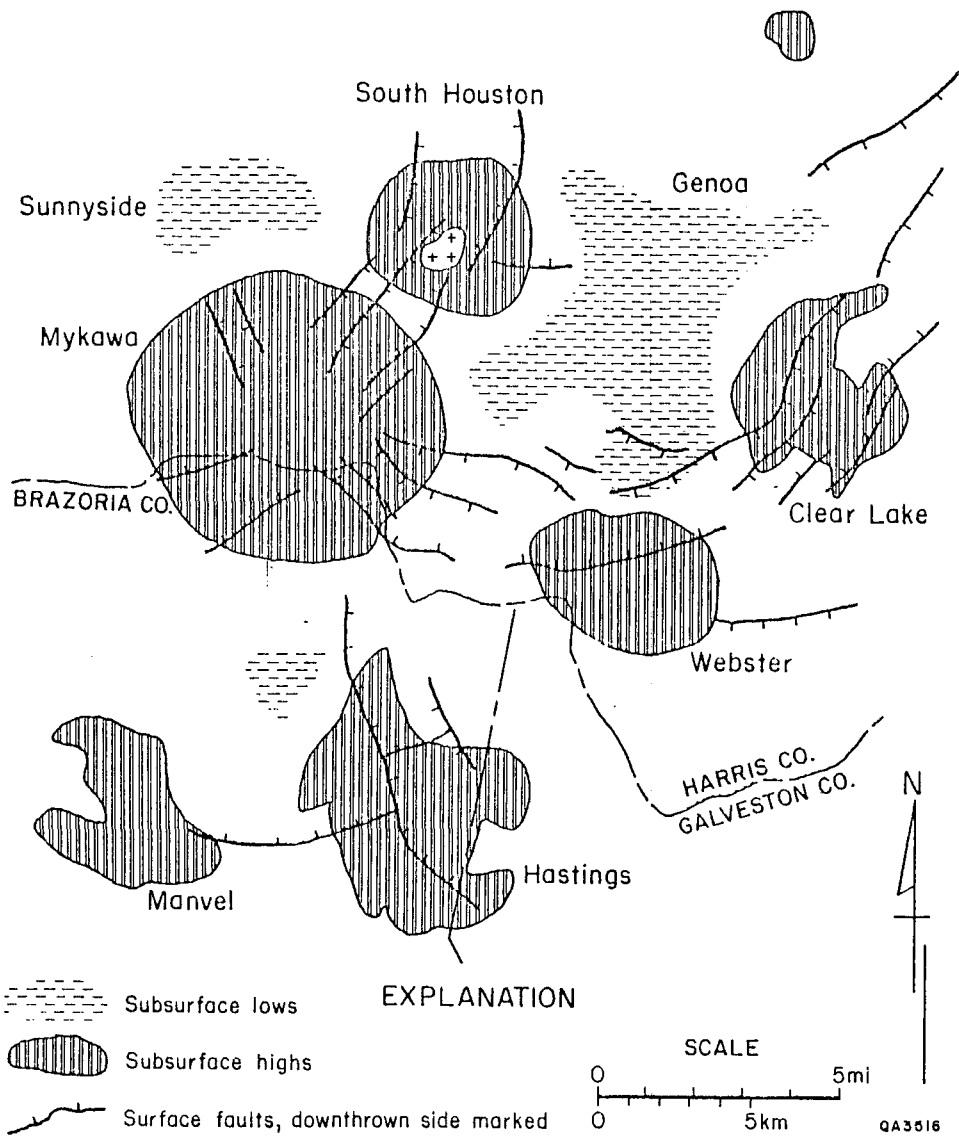


Figure 30. Stratigraphic section from Caplen to High Island, showing continuity of Lower Miocene sandstone reservoirs.

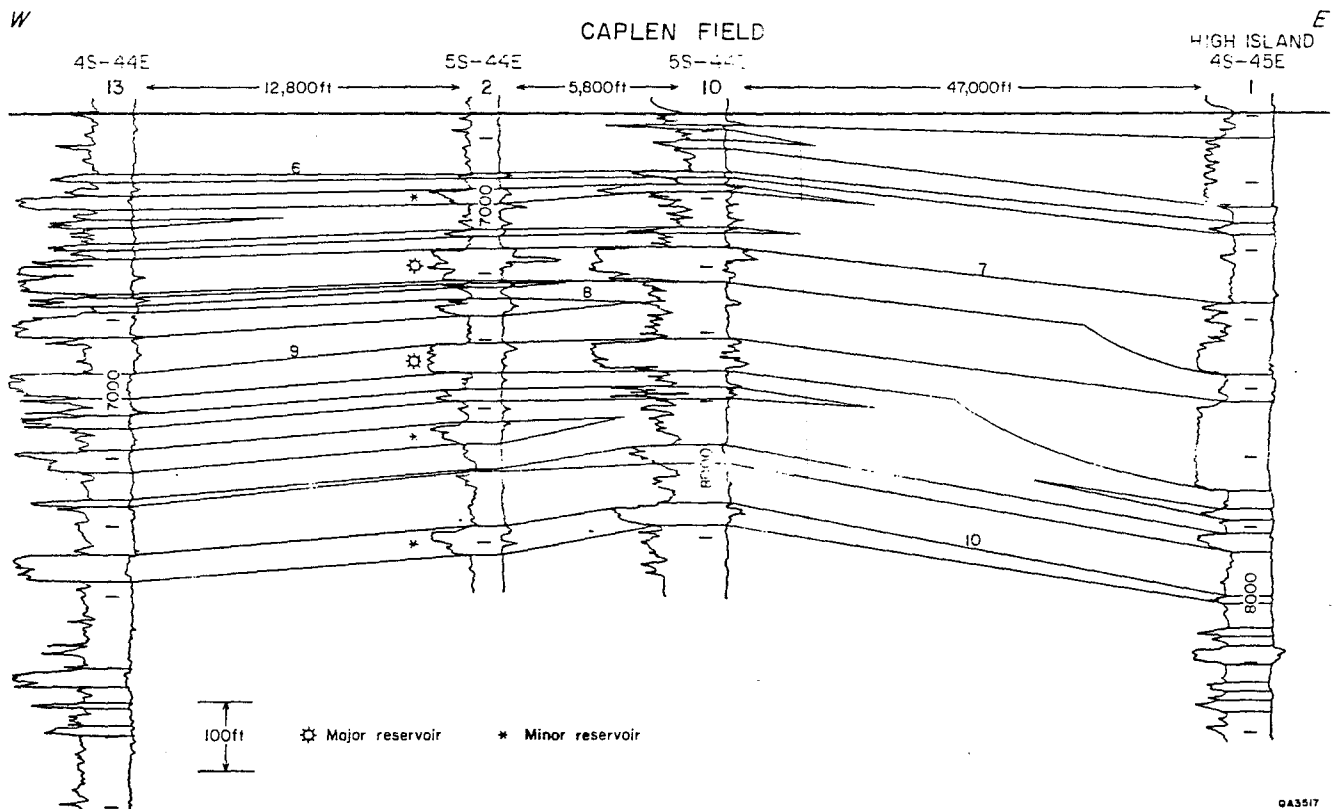


Figure 31. Genoa-Webster fault system compared with subsurface structure. These faults form grabens rimming the Genoa salt-withdrawal basin.

led previous workers to attribute fault reactivation to differential subsidence in the shallow section (Kreitler, 1977), rather than to an oilfield-induced effect. From first-order releveling in the area, oilfield-related subsidence has been shown to be minor, on the order of inches (Holzer and Bluntzer, 1984).

The question then arises: why does the graben system so neatly outline the shape of the Genoa salt-withdrawal basin? The ridges and basins appear to have only a very slight expression at shallow horizons, except for the shallow salt piercement at South Houston dome. Would shallow fluid withdrawals cause such a pattern?

#### A MODEL TO BE TESTED

The two fault systems are similar in geometry and timing. They might possibly represent responses to different types of fluid withdrawal, shaped by similar subsurface structural conditions. Alternatively, though, they may be responses to the same humanly induced compaction--which would be related to withdrawal of subsurface fluids from depths of 4,000 to 8,000 ft (1,220 to 2,433 m). Furthermore, the faulting is not restricted to the immediate vicinity of producing oil and gas fields, but is a regional response, as is shown by the faulting at Robinson Lake.

One possible factor is regional depressuring of continuous sandstone bodies within the salt-withdrawal basins. Most of the prolific Gulf Coast reservoirs are known to have produced from a strong water drive, caused by large aquifer systems (Galloway and others, 1983). Large-volume production from permeable sandstones may cause a slight regional reduction in regional aquifer pressure, leading to both reservoir and aquiclude compaction over a wide area. Such widespread compaction would be efficiently translated into surface subsidence (Geertsma, 1973). Compaction within the withdrawal basins may set up tension over the surrounding salt ridges, leading to the generation of grabens over them.

This is only a preliminary conjecture. Additional study is, however, warranted. The Pleasant Bayou geothermal reservoir, for example, is located within a major salt-withdrawal basin. Could large-volume, long-term fluid production from this much deeper aquifer create graben faults similar to those at Genoa and East Bay? Additional work should include quantitative modeling of the amount of regional depressuring and resultant compaction expected, as well as modeling for predicting the fault movements resulting from both regional and local compaction.

#### ACKNOWLEDGMENTS

Funding for this research was provided by the Gas Research Institute under contract no. 5084-212-0924.

We wish to thank R. A. Morton, W. E. Galloway, W. R. Kaiser, and N. Tyler for valuable discussions and assistance in the project and Z. S. Lin for general engineering concepts. We gratefully acknowledge assistance given by L. L. Anderson, K. P. Peterson, and W. A. Parisi of Eaton Industries of Houston, Inc. XRD and ICP analyses were done at the Mineral Studies Laboratory by Steven W. Tweedy under the direction of David W. Koppenaar. The manuscript was reviewed by R. J. Finley and typed by Dorothy C. Johnson and Shelley G. Gilmore under the direction of Lucille C. Harrell. Illustrations were drafted by Tom Byrd, Jamie McClelland, Nan Minchow, Linda Morace, Richard Platt, and Annie Kubert, under the direction of Richard L. Dillon. The manuscript was edited by Amanda R. Masterson and the report was designed by Margaret L. Evans. Text illustration photography was by James A. Morgan.

## REFERENCES

- Anderson, L. L., Peterson, K. P., and Parisi, W. A., 1984, Enhanced production from a slightly geopressured water-drive gas condensate field: Presented at 1984 SPE/DOE/GRI Unconventional Gas Recovery Symposium, Pittsburgh, PA, p. 341-344.
- Blatt, H., Middleton, G., and Murray, R., 1972, Origin of sedimentary rocks: Englewood Cliffs, New Jersey, Prentice-Hall, 634 p.
- Boles, J. R., and Franks, S. G., 1979, Clay diagenesis in Wilcox sandstones of southwest Texas, implications of smectite diagenesis on sandstone cementation: *Journal of Sedimentary Petrology*, v. 49, no. 1, p. 55-70.
- Brown, S. W., 1980, Hydrocarbon source facies analysis, Department of Energy and General Crude Oil Company Pleasant Bayou No. 1 and 2 wells, Brazoria County, Texas, in *Proceedings, Fourth Conference on Geopressured Geothermal Energy: The University of Texas at Austin*, p. 132-152.
- Burst, J. F., 1969, Diagenesis of Gulf Coast clayey sediments and its possible relationship to petroleum migration: *American Association of Petroleum Geologists Bulletin*, v. 53, no. 1, p. 73-93.
- Coleman, J. M., and Prior, D. B., 1980, Deltaic sand bodies a 1980 short course: *American Association of Petroleum Geologists Continuing Education Course Note Series 15*, 171 p.
- Collins, A. G., 1975, *Geochemistry of oil field waters*: New York, Elsevier, 496 p.
- Deer, W. A., Howie, R. A., and Zussman, J., 1969, *An introduction to the rock-forming minerals*: London, Longmans, 528 p.
- Dorfman, M. H., 1982, The outlook for geopressured/geothermal energy and associated natural gas: *Journal of Petroleum Technology*, p. 1915-1919.

- Dow, W. G., and Page, M. M., 1981, Geochemical evaluation of the Cameron Park and Development Company #1, Cameron County, Texas: Report No. 284 prepared for The University of Texas at Austin, Bureau of Economic Geology, by Robertson Research (U.S.), Inc., 36 p.
- Dutton, S. P., in press, Organic geochemistry of the Pennsylvanian and Lower Permian Palo Duro Basin, Texas: The University of Texas at Austin, Bureau of Economic Geology Geological Circular.
- Ewing, T. E., Light, M. P. R., and Tyler, N., 1984, in Ewing, T. E., Tyler, N., Morton, R. A., and Light, M. P. R., Consolidation of geologic studies of geopressured geothermal resources of Texas: The University of Texas at Austin, Bureau of Economic Geology, report prepared for the U.S. Department of Energy, Contract No. DE-AC08-79ET27111, p. 90-142.
- Foscolos, A. E., and Powell, T. G., 1980, Mineralogical and geochemical transformation of clays during burial catagenesis and their relation to oil generation: Canadian Society of Petroleum Geologists, Memoir 6, p. 153-172.
- Foscolos, A. E., Powell, T. G., and Gunther, P. R., 1976, The use of clay minerals, inorganic and organic geochemical indicators for evaluating the degree of diagenesis and oil generating potential of shales: *Geochimica et Cosmochimica Acta*, v. 40, p. 953-960.
- Fowler, W. A., Jr., 1970, Pressures, hydrocarbon accumulations and salinities, Chocolate Bayou field, Brazoria County, Texas: *Journal of Petroleum Technology*, v. 22, p. 411-423.
- Gabrysch, R. K., and Bonnet, C. W., 1975, Land-surface subsidence in the Houston-Galveston region, Texas: Texas Water Development Board Report 188, 19 p.
- Galloway, W. E., Ewing, T. E., Garrett, C. M., Jr., Tyler, N., and Bebout, D. G., 1983, Atlas of major Texas oil reservoirs: The University of Texas at Austin, Bureau of Economic Geology, Special Publication, 139 p.

- Galloway, W. E., Hobday, D. K., and Magara, K., 1982, Frio Formation of the Texas Gulf Coast Basin - depositional systems, structural framework, and hydrocarbon origin, migration, distribution and exploration potential: The University of Texas at Austin, Bureau of Economic Geology Report of Investigations No. 122, 78 p.
- Geertsma, J., 1973, Land subsidence above compacting oil and gas reservoirs: *Journal of Petroleum Technology*, v. 25, p. 734-744.
- Gregory, A. R., Lin, Z. S., Reed, R. S., Morton, R. A., and Rogers, L. A., 1983, Watered-out gas reservoirs profitable via enhanced recovery: *Oil and Gas Journal*, v. 81, no. 11, p. 55-60.
- Gustavson, T. C., and Kreidler, C. W., 1976, Geothermal resources of the Texas Gulf Coast: Environmental concerns arising from the production and disposal of geothermal waters: The University of Texas at Austin, Bureau of Economic Geology Geological Circular 76-7, 35 p.
- Hinch, H. H., 1980, The nature of shales and the dynamics of hydrocarbon expulsion in the Gulf Coast tertiary section, in Roberts, W. H., and Cordell, R. J., eds., *Problems in petroleum migration: American Association of Petroleum Geologists Studies in Geology*, v. 10, p. 1-18.
- Holzer, T. L., and Bluntzer, R. L., 1984, Land subsidence near oil and gas fields, Houston, Texas: *Ground Water*, v. 22, no. 4, p. 450-459.
- Hower, J., Eslinger, E. V., Hower, M. E., and Perry, E. A., 1976, Mechanism of burial metamorphism of argillaceous sediment, 1.: mineralogical and chemical evidence: *Geological Society of America Bulletin*, v. 87, no. 5, p. 725-737.
- Hunt, J. M., 1979, *Petroleum geochemistry and geology*: San Francisco, W. H. Freeman, 617 p.
- International Oil Scouts Association, 1983, *International oil and gas development*, v. 49-50, part II (review of 1978-1979), 932 p.

- Kaiser, W. R., and Richmann, D. L., 1981, Predicting diagenetic history and reservoir quality in the Frio Formation of Brazoria County, Texas, and Pleasant Bayou test wells, in Proceedings, Fifth Conference on Geopressured Geothermal Energy: The University of Texas at Austin, p. 67-74.
- Kharaka, Y. K., Lies, M. S., Wright, V. A., and Carothers, W. W., 1979, Geochemistry of formation waters from Pleasant Bayou No. 2 well and adjacent areas in coastal Texas, in Proceedings, Fourth Conference on Geopressured Geothermal Energy: The University of Texas at Austin, p. 11-45.
- Kharaka, Y. K., Callender, E., and Carothers, W. W., 1977, Geochemistry of geopressured-geothermal waters from the Texas Gulf Coast, in Meriwether, J. R., ed., Third geopressured-geothermal energy conference: Lafayette, Louisiana, University of Southwestern Louisiana, v. 1, G-121-G-165.
- Kreitler, C. W., 1977, Fault control of subsidence, Houston, Texas: Ground Water, v. 15, no. 3, p. 203-214.
- Lewis, C. R., and Rose, S. C., 1970, A theory relating high temperatures and overpressures: Journal of Petroleum Technology, v. 22, no. 1, p. 11-16.
- Light, M. P. R., Ewing, T. E., and Tyler, N., in preparation, Thermal history and hydrocarbon anomalies in the Frio Formation, Brazoria County, Texas--an indicator of fluid flow and geopressure history: The University of Texas at Austin, Bureau of Economic Geology, report prepared for the U.S. Department of Energy, Contract No. DE-AC08-79ET27111, p. 90-142.
- Light, M. P. R., 1985, Maturity anomalies, fluid flow, and permeability preservation in Frio and Anahuac Formations, Upper Texas Gulf Coast (abs.): American Association of Petroleum Geologists Bulletin, v. 69, no. 2, p. 279.
- Loucks, R. G., Richmann, D. L., and Milliken, K. L., 1981, Factors controlling reservoir quality in Tertiary sandstones and their significance to geopressured geothermal

- production: The University of Texas at Austin, Bureau of Economic Geology Report of Investigations No. 111, 41 p.
- Milliken, K. L., Land, L. S., and Loucks, R. G., 1981, History of burial diagenesis determined from isotopic geochemistry, Frio Formation, Brazoria County, Texas: American Association of Petroleum Geologists Bulletin, v. 65, no. 8, p. 1397-1413.
- Milner, C. W. D., 1982, Geochemical analyses of sedimentary organic matter and interpretation of maturation and source potential, in How to assess maturation and paleotemperatures: Society of Economic Paleontologists and Mineralogists Short Course 7, p. 217-252.
- Mooney, R. W., Keenan, A. G., and Wood, L. A., 1952, Adsorption of water vapor by montmorillonite. 1. heat of desorption and application of BET theory: Journal of the American Chemical Society, v. 74, p. 1367-1371.
- Morton, J. P., 1983, Age of clay diagenesis in the Oligocene Frio Formation, Texas Gulf Coast: The University of Texas at Austin, Ph.D. dissertation, 33 p.
- Morton, R. A., Ewing, T. E., and Tyler, N., 1983, Continuity and internal properties of Gulf Coast sandstones and their implications for geopressed fluid production: The University of Texas at Austin, Bureau of Economic Geology Report of Investigations No. 132, 70 p.
- Nadeau, P. H., Wilson, M. J., McHardy, W. J., and Tait, J. M., 1984, Interstratified clays as fundamental particles: Science, v. 225, p. 923-925.
- Petitt, B. M., Jr., and Winslow, A. G., 1957, Geology and ground-water resources of Galveston County, Texas: U.S. Geological Survey Water-Supply Paper 1416, 156 p.
- Powell, T. G., Foscolos, A. E., Gunther, P. R., and Snowdon, L. R., 1978, Diagenesis of organic matter and fine clay minerals: a comparative study: Geochimica et Cosmochimica Acta, v. 42, p. 1181-1197.

- Pryor, W. A., 1973, Permeability-porosity patterns and variations in some Holocene sand bodies: American Association of Petroleum Geologists Bulletin, v. 57, no. 1, p. 162-189.
- Randolph, P. L., 1985, Preliminary Hitchcock N.E. well and reservoir data, April 1, 1985: Provisional report prepared for the Gas Research Institute by the Institute of Gas Technology, Chicago, 158 p.
- Reznikov, A. N., 1967, The geochemical conversion of oils and condensates in the zone of katagenesis: Geologiya Nefti i gaza, no. 5, p. 24-28.
- Schoell, M., 1983, Genetic characterization of natural gases: American Association of Petroleum Geologists Bulletin, v. 67, no. 12, p. 2225-2238.
- Schwab, K. W., 1980, Visual kerogen and vitrinite reflectance analyses of the Pleasant Bayou No. 1 well, Brazoria County, Texas, in Proceedings, Fourth Conference on Geopressured Geothermal Energy: The University of Texas at Austin, p. 85-131.
- Sofer, Z., 1984, Stable carbon isotope compositions of crude oils: application to source depositional environments and petroleum alteration: American Association of Petroleum Geologists Bulletin, v. 68, no. 1, p. 31-49.
- Tissot, B. P., and Welte, D. H., 1978, Petroleum formation and occurrence: Berlin, Springer-Verlag, 538 p.
- Tyler, N., 1984, unpublished manuscript, The University of Texas at Austin, Bureau of Economic Geology.
- Tyler, N., Light, M. P. R., and Ewing, T. E., 1985, Saline fluid flow and hydrocarbon migration and maturation as related to geopressure, Frio Formation, Brazoria County, Texas (abs.): Sixth U.S. Gulf Coast Geopressured-Geothermal Energy Conference, The University of Texas at Austin, p. 11.
- Verbeek, E. R., and Clanton, U.S., 1981, Historically active faults in the Houston metropolitan area, Texas, in Etter, E. M., ed., Houston area environmental geology:

surface faulting, ground subsidence, hazard liability: Houston Geological Society, p. 28-68.

Waples, D. W., 1980, Time and temperature in petroleum formation: application of Lopatin's method to petroleum exploration: American Association of Petroleum Geologists Bulletin, v. 64, no. 6, p. 916-926.

Weres, O., Michel, M., Harnden, W., and Newton, A., 1984, Downhole sampling of geopressured gas wells: The University of California, Lawrence Berkeley Laboratory, report prepared for the Gas Research Institute, Contract No. 5081-212-0552, 53 p.

Wesselman, J. B., 1971, Ground water resources of Chambers and Jefferson Counties, Texas: Texas Department of Water Resources Report 133, 173 p.

Young, A., Monaghan, P. H., and Schweisberger, R. T., 1977, Calculation of ages of hydrocarbons in oils--physical chemistry applied to petroleum geochemistry: American Association of Petroleum Geologists Bulletin, v. 61, no. 4, p. 573-600.

APPENDIX: Detailed listing of Geochem Labs., Inc., analyses of hydrocarbons and shales from the Prets No. 1 and Delee No. 1 wells.

#### Sample Preparation

Routine preparation - sample handling - dry cuttings: includes inventory, sieving of samples to remove cavings, crushing and grinding, compositing, and packaging.

#### Source Rock Analyses

Total organic carbon and Rock-Eval pyrolysis analysis.

#### Crude Oil Characterization

C<sub>4</sub>-C<sub>7</sub> detailed gasoline-range gas chromatographic analysis.

C<sup>15+</sup> liquid chromatographic separation, involves topping of less than C<sup>15+</sup> fraction, deasphalting and liquid chromatographic separation to isolate C<sup>15+</sup> paraffin-naphthene (P-N) hydrocarbon, C<sup>15+</sup> aromatic (AROM) hydrocarbon, and C<sup>15+</sup> N-S-O nonhydrocarbon fractions.

Desulfurization of C<sup>15+</sup> paraffin-naphthene (P-N) hydrocarbon and C<sup>15+</sup> aromatic (AROM) hydrocarbon fractions.

Nickel-vanadium elemental analysis.

API gravity and specific gravity.

GC/MS/DS analysis of C<sup>15+</sup> aromatic (AROM) hydrocarbon fraction of crude oil.

Saturate Terpene and Sterane Hydrocarbons - liquid chromatography to obtain C<sup>15+</sup> paraffin-naphthene (P-N) hydrocarbon, C<sup>15+</sup> aromatic (AROM) hydrocarbon, C<sup>15+</sup> N-S-O nonhydrocarbon.

Molecular sieve removal of n-alkanes from C<sup>15+</sup> paraffin-naphthene (P-N) hydrocarbons.

Re-isolation of n-alkanes from molecular sieves (not necessary for terpene/sterane studies).

GC/MS analysis of isolated fraction.

Monoaromatic steranes - liquid chromatography to obtain C<sup>15+</sup> paraffin-naphthene hydrocarbon, C<sup>15+</sup>aromatic (AROM) hydrocarbon, and C<sup>15+</sup>N-S-O nonhydrocarbon resins.

Monoaromatic steranes - liquid chromatography to obtain 1, 2, and 3-ring aromatic compounds.

Monoaromatic steranes - GC/MS analysis of isolated monoaromatic fraction.

Crude Oil to Crude Oil correlation - Crude Oil to Source Rock correlation - Tier II similarity analysis, cluster analysis, and ordination. Comparison with shale extract data from Pleasant Bayou No. 1 well.

Gas chromatographic analysis (glass capillary column) of C<sup>15+</sup> paraffin-naphthene (P-N) hydrocarbon.

List of isotope analyses conducted by Coastal Science Laboratories, Inc., on hydrocarbon and formation water samples from the Prets No. 1 and Delee No. 1 wells.

<u>Isotopes</u>	<u>Sample</u>
$\delta^{13}\text{C}$ and $\delta^2\text{H}$	methane
$\delta^{13}\text{C}$	gas component (C <sub>2</sub> , C <sub>3</sub> , C <sub>4</sub> , C <sub>5</sub> , CO <sub>2</sub> )
$\delta^{13}\text{C}$	condensate
$\delta^{13}\text{C}$	chromatographic fractions
$\delta^{18}\text{O}$ and $\delta^2\text{H}$	water
silica gel column chromatography	condensate

## REFLECTED LIGHT MICROSCOPY DATA

A sample of ground rock is treated successively with hydrochloric and hydrofluoric acids to concentrate the kerogen, then freeze-dried, mounted in an epoxy plug, and polished. Kerogen type is identified with the aid of blue light fluorescence.

The visual kerogen analysis data table contains visual percentage estimates of each principal kerogen type and kerogen background fluorescence data. These data are also displayed on the histograms with relative amounts of solid bitumen and coked material.

The histograms show measured reflectance values of all vitrinite present and on all material with the visual appearance of vitrinite. Shaded values (marked with \*) are those used to calculate the interpreted vitrinite reflectance maturities. Unshaded values are interpreted to be oxidized vitrinite, recycled vitrinite, or possibly misidentified material such as solid bitumen, pseudo-vitrinite, or semifusinite. When samples analyzed contain no vitrinite or nonindigenous vitrinite or have an insufficient number of readings to allow a reliable maturity determination to be made, then the mean value for that sample is shown as N.D. (Not Determined). Alternate maturity calculations are possible on a few samples. The histograms are identified by a Robertson Research sequence number (RRUS No.) and depth or other notation.

### ABBREVIATIONS USED IN VISUAL KEROGEN ANALYSIS DATA SHEET AND HISTOGRAMS

Am	=	Amorphous Kerogen
Ex	=	Exinite
Vit	=	Vitrinite
Inert	=	Inertinite
R <sub>o</sub>	=	Vitrinite Reflectance Mean in Immersion Oil
Bkg Fl	=	Background Fluorescence

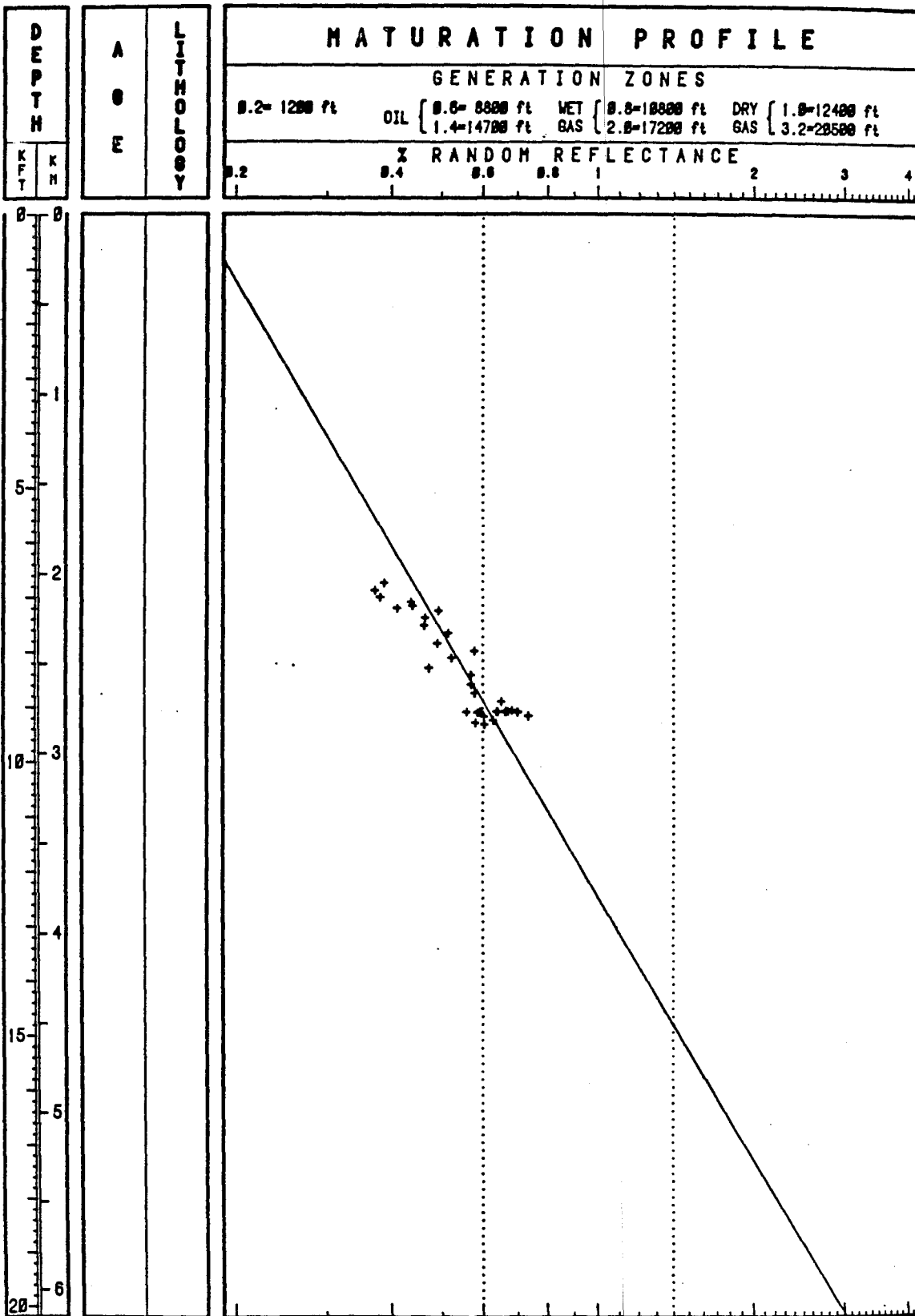
VISUAL KEROGEN ANALYSIS - REFLECTED LIGHT

DE LEE #1 - HITCHCOCK FIELD

Project No. : RRUS/845/T/844/7

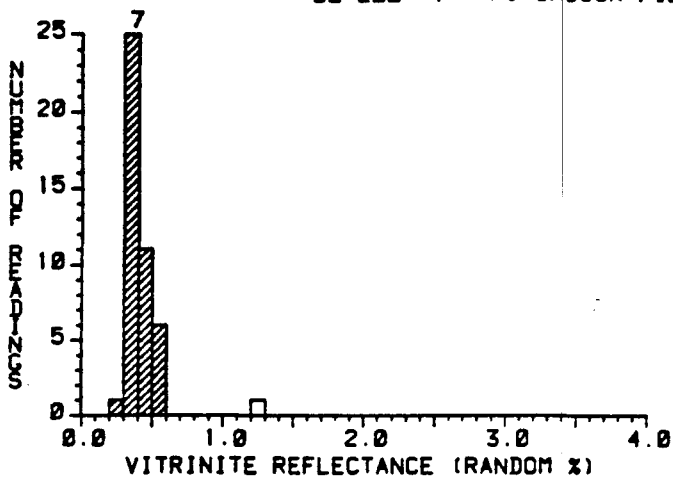
SAMPLE IDENTIFICATION				REFLECT.	KEROGEN CHARACTERISTICS					TOC
RRUS	ID /	DEPTH	(Feet)	Ro %	Am%	Ex%	Vit%	Inert%	Fluor	%
1	CTGS.	6758.0	0	0.39	5	10	65	20	None	----
2	CTGS.	6887.0	0	0.37	25	10	60	5	Low	----
3	CTGS.	7020.0	0	0.38	20	10	30	10	Low	----
4	CTGS.	7110.0	0	0.44	25	5	55	15	Low	----
5	CTGS.	7176.0	0	0.44	20	5	60	15	Med	----
6	CTGS.	7216.0	0	0.41	55	5	30	10	Med	----
7	CTGS.	7262.0	0	0.49	50	5	30	15	High	----
8	CTGS.	7392.0	0	0.46	65	5	20	10	High	----
9	CTGS.	7534.0	0	0.46	35	10	40	15	High	----
10	CTGS.	7677.0	0	0.51	60	5	30	5	Med	----
11	CTGS.	7858.0	0	0.49	35	5	50	10	Med	----
12	CTGS.	7990.0	0	0.58	70	5	20	tr	Med	----
13	CTGS.	8126.0	0	0.52	80	0	10	10	Med	----
14	CTGS.	8304.0	0	0.47	80	0	5	15	Med	----
15	CTGS.	8429.0	0	0.57	55	15	20	10	Med	----
16	CTGS.	8602.0	0	0.57	70	50	15	10	Med	----
17	CTGS.	8759.0	0	0.58	75	0	15	10	Low	----
18	CTGS.	8913.0	0	0.65	55	5	30	10	Low	----
19	CORE	9070.0	0	0.68	60	0	30	10	Low	----
20	CORE	9083.0	0	0.66	45	5	40	10	Low	----
21	CORE	9092.0	0	0.67	30	0	65	5	None	----
22	CORE	9099.0	0	0.64	25	0	65	10	Low	----
23	CORE	9100.0	0	0.70	20	10	60	10	Med	----
24	CORE	9100.5	0	0.64	55	10	30	5	Low	----
25	CORE	9100.0	0	0.59	60	5	15	20	None	----
26	CORE	9100.8	0	0.64	45	15	30	10	Low	----
27	CORE	9101.0	0	0.70	75	0	15	10	Low	----
28	CORE	9103.3	0	0.66	85	0	10	5	Med	----
29	CORE	9104.5	0	0.56	40	5	50	5	Low	----
30	CORE	9125.0	0	0.58	55	tr	35	10	Low	----
31	CORE	9141.0	0	----	95	0	5	tr	Med	----
32	CORE	9149.0	0	----	90	0	5	5	Low	----
33	CORE	9167.5	0	----	90	0	5	5	Low	----
34	CORE	9179.9	0	0.73	45	0	35	20	Low	----
35	CORE	9194.3	0	0.60	35	5	50	10	Low	----
36	CORE	9262.0	0	0.63	45	10	35	10	Low	----
37	CTGS.	9302.0	0	0.58	40	15	35	10	Med	----
38	CTGS.	9340.0	0	0.60	30	5	50	15	Low	----
39	CTGS.	9367.0	0	----	40	5	40	15	Med	----
40	CTGS.	9392.0	0	----	45	5	40	10	None	----

DE LEE #1 - HITCHCOCK FIELD



MATURATION PROFILE, BASED ON VITRINITE REFLECTANCE DATA

DE LEE #1 - HITCHCOCK FIELD



RRUS No. : 1  
 ID : CTGS.  
 DEPTH : 6758.0 F1  
 : 2059.8 M

\* = Ro MATURITY  
 # VALUES : 50  
 MEAN : 0.39  
 STD DEV : 0.07  
 MEDIAN : 0.38  
 MODE : 0.35

HISTOGRAM:  
 Range: 0- 4%  
 Increment: 0.10%

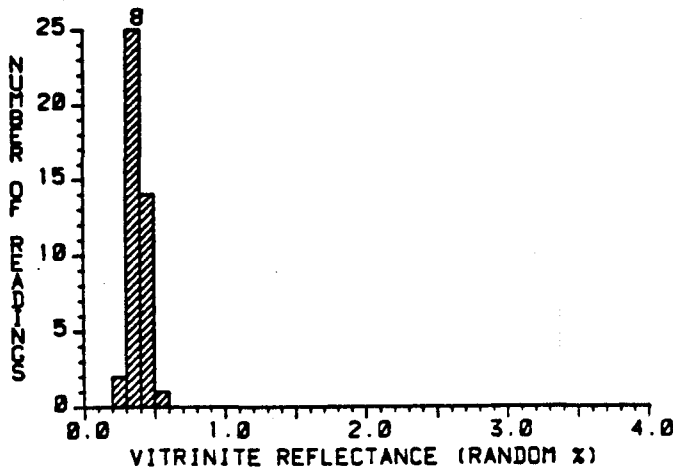
ORDERED REFLECTANCE VALUES:

*0.25	*0.32	*0.36	*0.38	*0.47	1.20
*0.30	*0.32	*0.36	*0.39	*0.47	
*0.30	*0.33	*0.36	*0.39	*0.48	
*0.30	*0.33	*0.36	*0.40	*0.48	
*0.30	*0.33	*0.37	*0.40	*0.50	
*0.31	*0.33	*0.38	*0.44	*0.51	
*0.31	*0.34	*0.38	*0.44	*0.51	
*0.31	*0.34	*0.38	*0.45	*0.52	
*0.31	*0.36	*0.38	*0.46	*0.55	
*0.32	*0.36	*0.38	*0.47	*0.56	

KEROGEN DESCRIPTION

Amorphous : 5 %  
 Exinite : 10 %  
 Vitrinite : 65 %  
 Inertinite : 20 %  
 Back Fluor : None  
 Bitumen : None  
 Coke : 1c

DE LEE #1 - HITCHCOCK FIELD



RRUS No. : 2  
 ID : CTGS.  
 DEPTH : 6887.0 F1  
 : 2099.2 M

\* = Ro MATURITY  
 # VALUES : 50  
 MEAN : 0.37  
 STD DEV : 0.05  
 MEDIAN : 0.37  
 MODE : 0.35

HISTOGRAM:  
 Range: 0- 4%  
 Increment: 0.10%

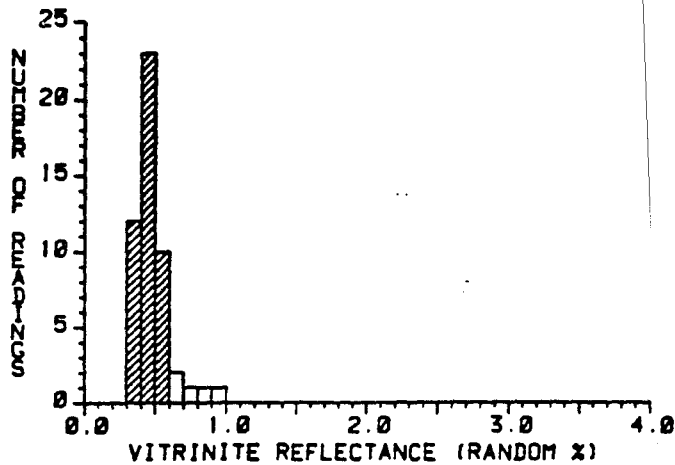
ORDERED REFLECTANCE VALUES:

*0.26	*0.33	*0.35	*0.38	*0.41
*0.29	*0.34	*0.35	*0.39	*0.42
*0.30	*0.34	*0.35	*0.39	*0.42
*0.30	*0.34	*0.36	*0.39	*0.44
*0.31	*0.34	*0.37	*0.39	*0.45
*0.31	*0.34	*0.37	*0.40	*0.45
*0.31	*0.34	*0.37	*0.40	*0.45
*0.32	*0.34	*0.37	*0.40	*0.47
*0.33	*0.35	*0.38	*0.40	*0.49
*0.33	*0.35	*0.38	*0.40	*0.51

KEROGEN DESCRIPTION

Amorphous : 25 %  
 Exinite : 10 %  
 Vitrinite : 60 %  
 Inertinite : 5 %  
 Back Fluor : Low  
 Bitumen : None  
 Coke : None

DE LEE #1 - HITCHCOCK FIELD



RRUS No. : 5  
 DEPTH : 7176.0 Ft  
 : 2187.2 M

\* = Ro MATURITY  
 # VALUES : 45

MEAN : 0.44  
 STD DEV : 0.06  
 MEDIAN : 0.44  
 MODE : 0.45

HISTOGRAM:  
 Range: 0- 4%  
 Increment: 0.10%

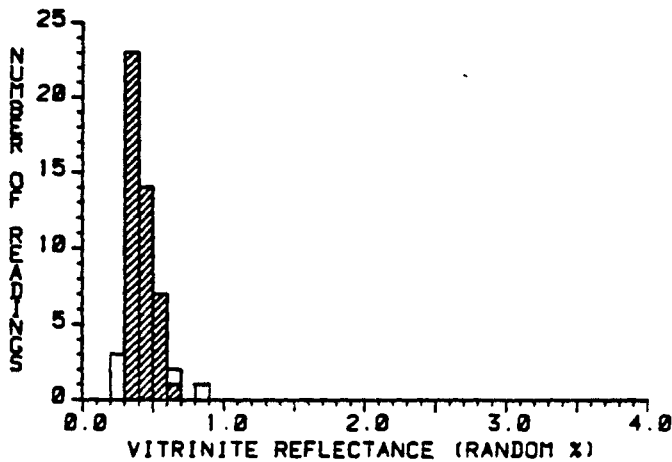
ORDERED REFLECTANCE VALUES:

*0.30	*0.30	*0.44	*0.45	*0.53
*0.30	*0.30	*0.44	*0.46	*0.53
*0.33	*0.41	*0.44	*0.48	*0.53
*0.33	*0.41	*0.44	*0.48	*0.56
*0.35	*0.41	*0.44	*0.49	*0.57
*0.37	*0.42	*0.45	*0.50	0.64
*0.38	*0.43	*0.45	*0.50	0.65
*0.38	*0.43	*0.45	*0.50	0.72
*0.38	*0.43	*0.45	*0.52	0.86
*0.38	*0.44	*0.45	*0.52	0.95

KEROGEN DESCRIPTION

Amorphous : 20 %  
 Exinite : 5 %  
 Vitrinite : 60 %  
 Inertinite : 15 %  
 Back Fluor : Med  
 Bitumen : 1r  
 Coke : None

DE LEE #1 - HITCHCOCK FIELD



RRUS No. : 6  
 ID : CTGS.  
 DEPTH : 7216.0 Ft  
 : 2199.4 M

\* = Ro MATURITY  
 # VALUES : 45

MEAN : 0.41  
 STD DEV : 0.08  
 MEDIAN : 0.39  
 MODE : 0.35

HISTOGRAM:  
 Range: 0- 4%  
 Increment: 0.10%

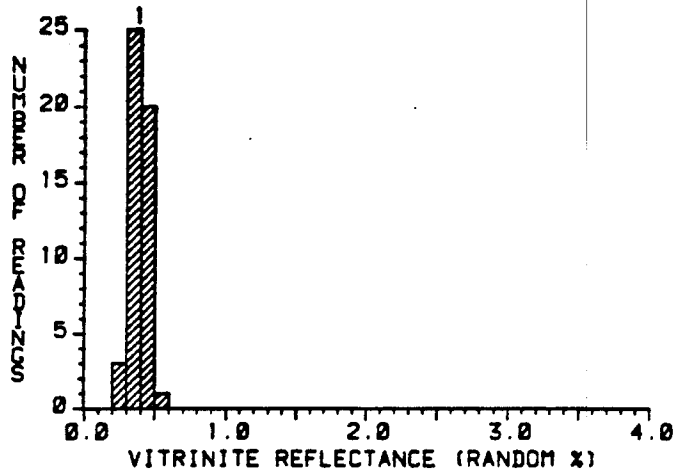
ORDERED REFLECTANCE VALUES:

0.25	*0.33	*0.38	*0.41	*0.50
0.28	*0.34	*0.38	*0.41	*0.53
0.28	*0.34	*0.38	*0.43	*0.53
*0.30	*0.35	*0.39	*0.44	*0.54
*0.30	*0.35	*0.39	*0.44	*0.54
*0.30	*0.36	*0.39	*0.44	*0.54
*0.31	*0.37	*0.40	*0.45	*0.59
*0.32	*0.37	*0.40	*0.45	*0.62
*0.33	*0.37	*0.40	*0.46	0.67
*0.33	*0.38	*0.40	*0.46	0.88

KEROGEN DESCRIPTION

Amorphous : 55 %  
 Exinite : 5 %  
 Vitrinite : 30 %  
 Inertinite : 10 %  
 Back Fluor : Med  
 Bitumen : 1r  
 Coke : None

DE LEE #1 - HITCHCOCK FIELD



RRUS No. : 3  
 ID : CTGS.  
 DEPTH : 7020.0 Ft  
 : 2130.7 M

\* = Ro MATURITY  
 # VALUES : 50  
 MEAN : 0.38  
 STD DEV : 0.06  
 MEDIAN : 0.38  
 MODE : 0.35

HISTOGRAM:  
 Range: 0- 4%  
 Increment: 0.10%

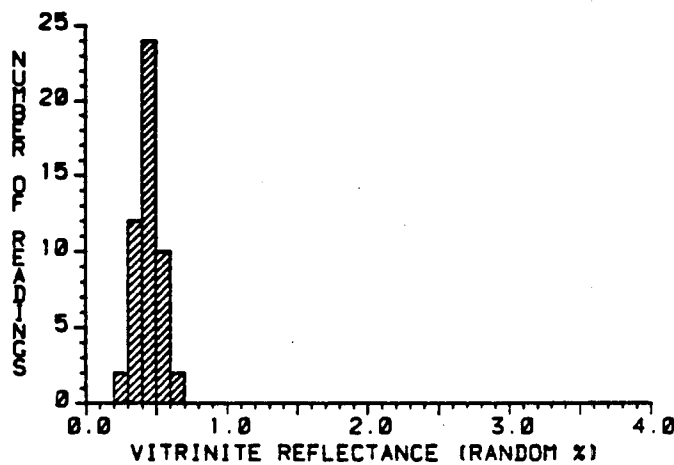
ORDERED REFLECTANCE VALUES:

*0.26	*0.33	*0.37	*0.40	*0.43
*0.27	*0.33	*0.37	*0.40	*0.43
*0.28	*0.33	*0.37	*0.40	*0.44
*0.30	*0.33	*0.37	*0.40	*0.45
*0.30	*0.35	*0.38	*0.41	*0.45
*0.31	*0.35	*0.38	*0.41	*0.46
*0.31	*0.35	*0.39	*0.41	*0.46
*0.32	*0.36	*0.39	*0.42	*0.47
*0.33	*0.36	*0.39	*0.43	*0.49
*0.33	*0.36	*0.40	*0.43	*0.52

KEROGEN DESCRIPTION

Amorphous : 20 %  
 Exinite : 10 %  
 Vitrinite : 30 %  
 Inertinite : 10 %  
 Back Fluor : Low  
 Bitumen : None  
 Coke : None

DE LEE #1 - HITCHCOCK FIELD



RRUS No. : 4  
 ID : CTGS.  
 DEPTH : 7110.0 Ft  
 : 2167.1 M

\* = Ro MATURITY  
 # VALUES : 50  
 MEAN : 0.44  
 STD DEV : 0.08  
 MEDIAN : 0.43  
 MODE : 0.45

HISTOGRAM:  
 Range: 0- 4%  
 Increment: 0.10%

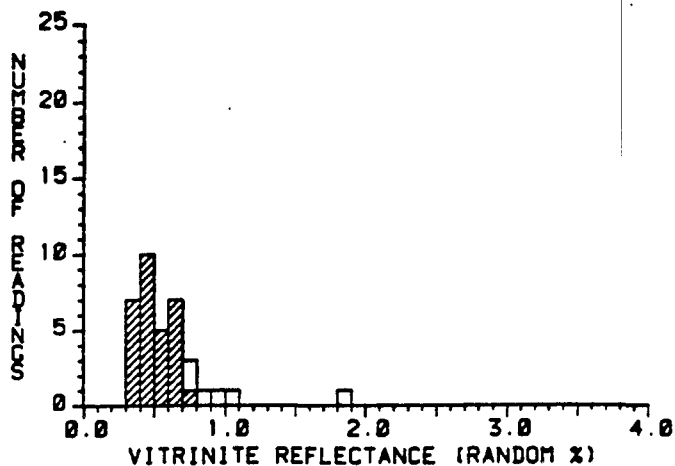
ORDERED REFLECTANCE VALUES:

*0.28	*0.38	*0.42	*0.45	*0.52
*0.29	*0.38	*0.42	*0.45	*0.52
*0.31	*0.38	*0.42	*0.45	*0.52
*0.33	*0.39	*0.42	*0.46	*0.52
*0.33	*0.40	*0.43	*0.47	*0.53
*0.34	*0.40	*0.43	*0.47	*0.53
*0.34	*0.40	*0.44	*0.48	*0.56
*0.35	*0.41	*0.44	*0.48	*0.57
*0.36	*0.41	*0.44	*0.50	*0.61
*0.37	*0.41	*0.45	*0.50	*0.62

KEROGEN DESCRIPTION

Amorphous : 25 %  
 Exinite : 5 %  
 Vitrinite : 55 %  
 Inertinite : 15 %  
 Back Fluor : Low  
 Bitumen : None  
 Coke : None

DE LEE #1 - HITCHCOCK FIELD



RRUS No. : 7  
ID : CTGS.  
DEPTH : 7262.0 Ft  
          : 2213.5 M

\* = Ro MATURITY  
# VALUES : 30  
MEAN : 0.49  
STD DEV : 0.11  
MEDIAN : 0.47  
MODE : 0.45

HISTOGRAM:  
Range: 0- 4%  
Increment: 0.10%

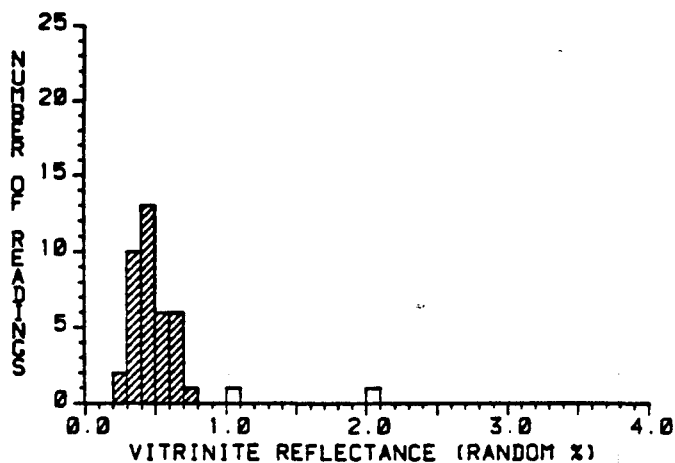
ORDERED REFLECTANCE VALUES:

*0.32	*0.42	*0.52	0.75
*0.34	*0.43	*0.54	0.79
*0.36	*0.44	*0.62	0.87
*0.37	*0.45	*0.62	0.91
*0.39	*0.46	*0.63	1.00
*0.39	*0.47	*0.64	1.83
*0.39	*0.49	*0.67	
*0.40	*0.51	*0.68	
*0.41	*0.51	*0.68	
*0.41	*0.52	*0.70	

KEROGEN DESCRIPTION

Amorphous : 50 %  
Exinite : 5 %  
Vitrinite : 30 %  
Inertinite : 15 %  
Back Fluor : High  
Bitumen : Small  
Coke : None

DE LEE #1 - HITCHCOCK FIELD



RRUS No. : 8  
ID : CTGS.  
DEPTH : 7392.0 Ft  
          : 2253.1 M

\* = Ro MATURITY  
# VALUES : 38  
MEAN : 0.46  
STD DEV : 0.11  
MEDIAN : 0.44  
MODE : 0.45

HISTOGRAM:  
Range: 0- 4%  
Increment: 0.10%

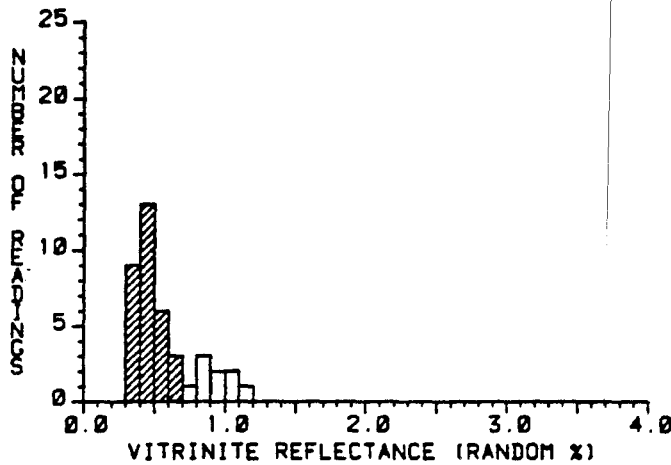
ORDERED REFLECTANCE VALUES:

*0.29	*0.38	*0.44	*0.59
*0.29	*0.38	*0.44	*0.60
*0.32	*0.40	*0.46	*0.60
*0.33	*0.41	*0.46	*0.64
*0.34	*0.41	*0.49	*0.64
*0.35	*0.41	*0.51	*0.67
*0.36	*0.42	*0.52	*0.68
*0.36	*0.43	*0.56	*0.71
*0.37	*0.43	*0.56	1.03
*0.38	*0.44	*0.57	2.00

KEROGEN DESCRIPTION

Amorphous : 65 %  
Exinite : 5 %  
Vitrinite : 20 %  
Inertinite : 10 %  
Back Fluor : High  
Bitumen : 1r  
Coke : 1r

DE LEE #1 - HITCHCOCK FIELD



RRUS No. : 9  
ID : CTGS.  
DEPTH : 7534.0 Ft  
          : 2296.4 M

\* = Ro MATURITY

# VALUES : 31  
MEAN : 0.46  
STD DEV : 0.09  
MEDIAN : 0.45  
MODE : 0.45

HISTOGRAM:  
Range: 0- 4%  
Increment: 0.10%

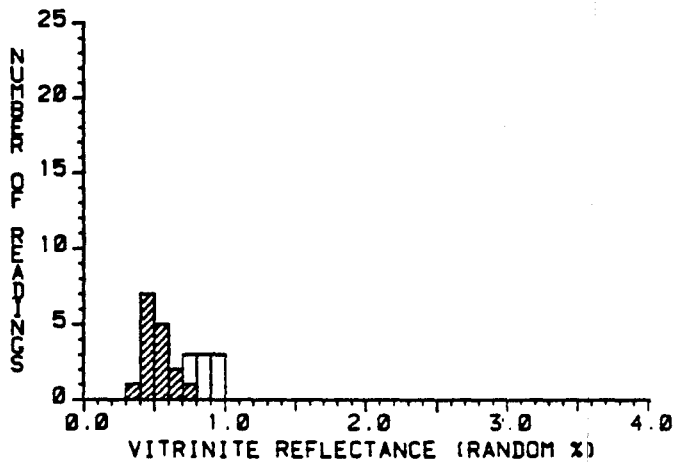
ORDERED REFLECTANCE VALUES:

*0.33	*0.41	*0.48	*0.69
*0.34	*0.43	*0.49	0.78
*0.35	*0.43	*0.52	0.83
*0.36	*0.43	*0.54	0.86
*0.37	*0.44	*0.54	0.87
*0.37	*0.45	*0.55	0.90
*0.38	*0.45	*0.55	0.95
*0.39	*0.45	*0.55	1.05
*0.39	*0.45	*0.66	1.00
*0.41	*0.48	*0.66	1.13

KEROGEN DESCRIPTION

Amorphous : 35 %  
Exinite : 10 %  
Vitrinite : 40 %  
Inertinite : 15 %  
Back Fluor : High  
Bitumen : 1r  
Coke : 1r

DE LEE #1 - HITCHCOCK FIELD



RRUS No. : 10  
ID : CTGS.  
DEPTH : 7677.0 Ft  
          : 2339.0 M

\* = Ro MATURITY

# VALUES : 16  
MEAN : 0.51  
STD DEV : 0.09  
MEDIAN : 0.50  
MODE : 0.45

HISTOGRAM:  
Range: 0- 4%  
Increment: 0.10%

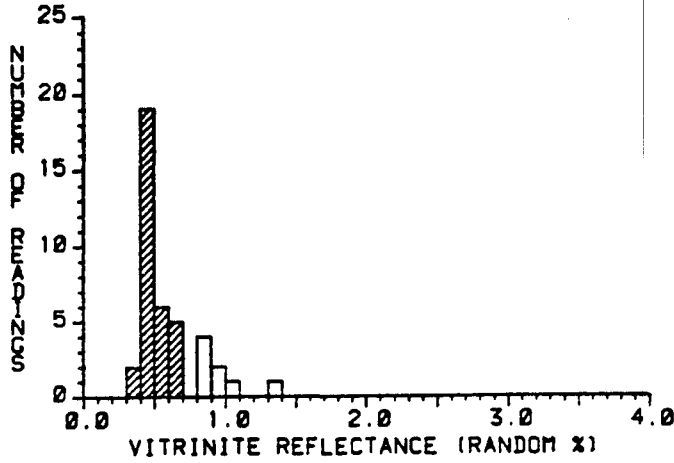
ORDERED REFLECTANCE VALUES:

*0.39	*0.53	0.87
*0.41	*0.54	0.94
*0.41	*0.55	0.98
*0.44	*0.63	0.99
*0.47	*0.69	
*0.48	*0.71	
*0.48	0.76	
*0.49	0.79	
*0.50	0.81	
*0.50	0.84	

KEROGEN DESCRIPTION

Amorphous : 60 %  
Exinite : 5 %  
Vitrinite : 30 %  
Inertinite : 5 %  
Back Fluor : Med  
Bitumen : 1r  
Coke : None

DE LEE #1 - HITCHCOCK FIELD



RRUS No. : 11  
ID : CTGS.  
DEPTH : 7858.0 Ft  
          : 2395.1 M

\* = Ro MATURITY  
# VALUES : 32  
MEAN : 0.49  
STD DEV : 0.09  
MEDIAN : 0.47  
MODE : 0.45

HISTOGRAM:  
Range: 0- 4%  
Increment: 0.10%

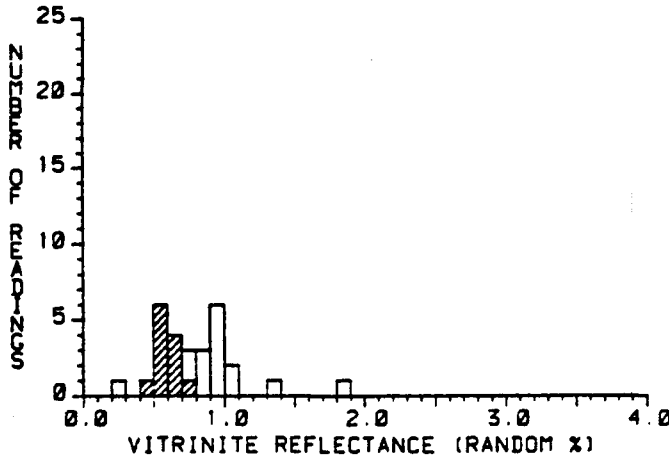
ORDERED REFLECTANCE VALUES:

*0.30	*0.44	*0.49	*0.68
*0.37	*0.45	*0.51	*0.69
*0.40	*0.45	*0.52	0.80
*0.41	*0.46	*0.53	0.83
*0.41	*0.47	*0.55	0.86
*0.41	*0.47	*0.56	0.87
*0.42	*0.47	*0.58	0.90
*0.42	*0.48	*0.60	0.93
*0.44	*0.49	*0.63	1.02
*0.44	*0.49	*0.65	1.31

KEROGEN DESCRIPTION

Amorphous : 35 %  
Exinite : 5 %  
Vitrinite : 50 %  
Inertinite : 10 %  
Back Fluor : Med  
Bitumen : 1r  
Coke : None

DE LEE #1 - HITCHCOCK FIELD



RRUS No. : 12  
ID : CTGS.  
DEPTH : 7990.0 Ft  
          : 2435.4 M

\* = Ro MATURITY  
# VALUES : 12  
MEAN : 0.58  
STD DEV : 0.07  
MEDIAN : 0.58  
MODE : 0.55

HISTOGRAM:  
Range: 0- 4%  
Increment: 0.10%

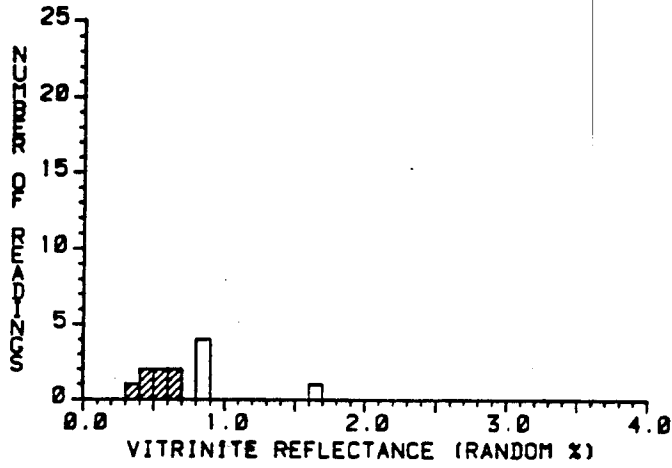
ORDERED REFLECTANCE VALUES:

0.28	*0.63	0.95
*0.46	*0.67	0.95
*0.50	*0.70	0.97
*0.51	0.76	0.99
*0.52	0.77	1.00
*0.56	0.86	1.07
*0.58	0.87	1.38
*0.58	0.89	1.82
*0.60	0.90	
*0.62	0.92	

KEROGEN DESCRIPTION

Amorphous : 70 %  
Exinite : 5 %  
Vitrinite : 20 %  
Inertinite : 2 %  
Back Fluor : Med  
Bitumen : 1r  
Coke : None

DE LEE #1 - HITCHCOCK FIELD



RRUS No. : 13  
 ID : CTGS.  
 DEPTH : 8126.0 Ft  
 : 2476.0 M

\* = Ro MATURITY  
 # VALUES : 7  
 MEAN : 0.52  
 STD DEV : 0.10  
 MEDIAN : 0.51  
 MODE : 0.65

HISTOGRAM:  
 Range: 0- 4%  
 Increment: 0.10%

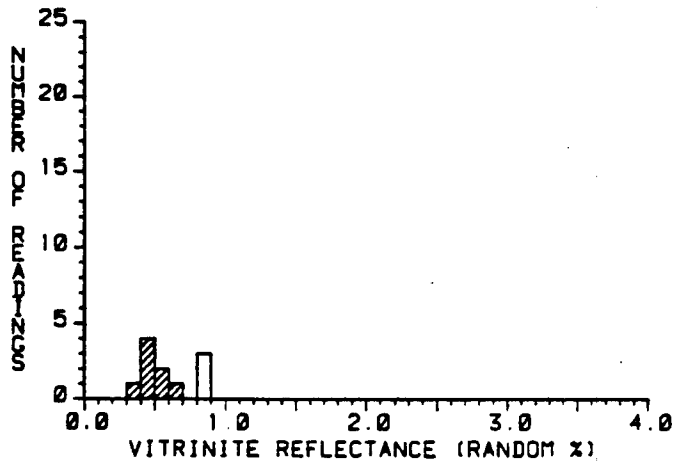
ORDERED REFLECTANCE VALUES:

\*0.38 0.85  
 \*0.44 1.69  
 \*0.49  
 \*0.51  
 \*0.52  
 \*0.65  
 \*0.66  
 0.81  
 0.82  
 0.83

KEROGEN DESCRIPTION

Amorphous : 80 %  
 Exinite : 0 %  
 Vitrinite : 10 %  
 Inertinite : 10 %  
 Back Fluor : Med  
 Bitumen : 1r  
 Coke : None

DE LEE #1 - HITCHCOCK FIELD



RRUS No. : 14.  
 ID : CTGS.  
 DEPTH : 8304.0 Ft  
 : 2531.1 M

\* = Ro MATURITY  
 # VALUES : 8  
 MEAN : 0.47  
 STD DEV : 0.08  
 MEDIAN : 0.44  
 MODE : 0.45

HISTOGRAM:  
 Range: 0- 4%  
 Increment: 0.10%

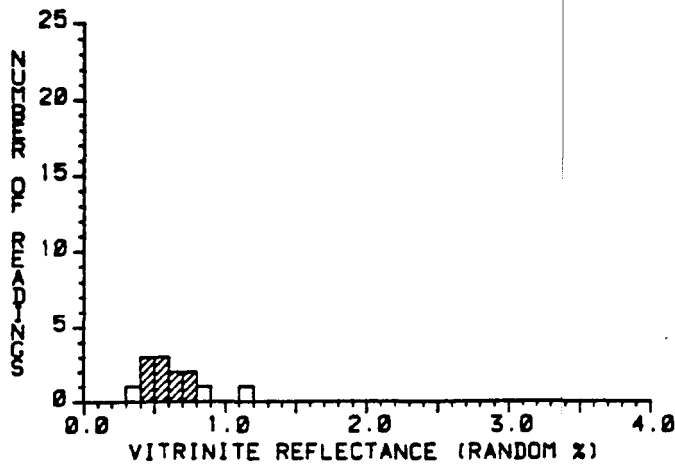
ORDERED REFLECTANCE VALUES:

\*0.37 0.89  
 \*0.40  
 \*0.42  
 \*0.44  
 \*0.44  
 \*0.50  
 \*0.50  
 \*0.61  
 0.81  
 0.87

KEROGEN DESCRIPTION

Amorphous : 80 %  
 Exinite : 0 %  
 Vitrinite : 5 %  
 Inertinite : 15 %  
 Back Fluor : Med  
 Bitumen : 1r  
 Coke : None

DE LEE #1 - HITCHCOCK FIELD



RRUS No. : 15  
 ID : CTGS.  
 DEPTH : 8429.0 Ft  
 : 2569.2 M

\* = Ro MATURITY  
 # VALUES : 10  
 MEAN : 0.57  
 STD DEV : 0.11  
 MEDIAN : 0.58  
 MODE : 0.55

HISTOGRAM:  
 Range: 0- 4%  
 Increment: 0.10%

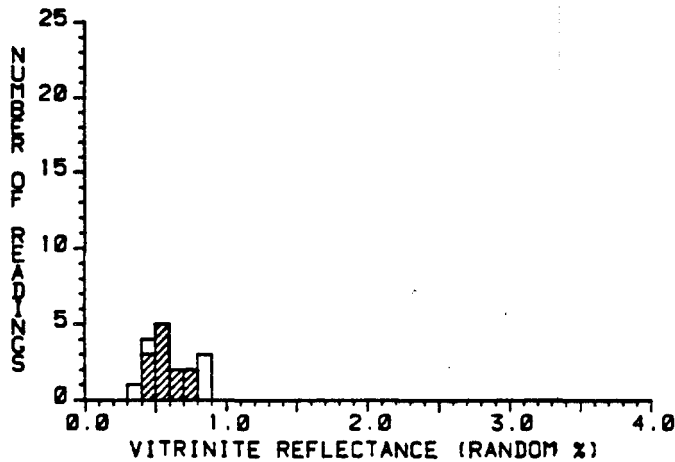
ORDERED REFLECTANCE VALUES:

0.33 \*0.72  
 \*0.41 0.85  
 \*0.43 1.12  
 \*0.46  
 \*0.53  
 \*0.53  
 \*0.58  
 \*0.61  
 \*0.69  
 \*0.72

KEROGEN DESCRIPTION

Amorphous : 55 %  
 Exinite : 15 %  
 Vitrinite : 20 %  
 Inertinite : 10 %  
 Back Fluor : Med  
 Bitumen : Small  
 Coke : None

DE LEE #1 - HITCHCOCK FIELD



RRUS No. : 16  
 ID : CTGS.  
 DEPTH : 8602.0 Ft  
 : 2621.9 M

\* = Ro MATURITY  
 # VALUES : 12  
 MEAN : 0.57  
 STD DEV : 0.10  
 MEDIAN : 0.57  
 MODE : 0.55

HISTOGRAM:  
 Range: 0- 4%  
 Increment: 0.10%

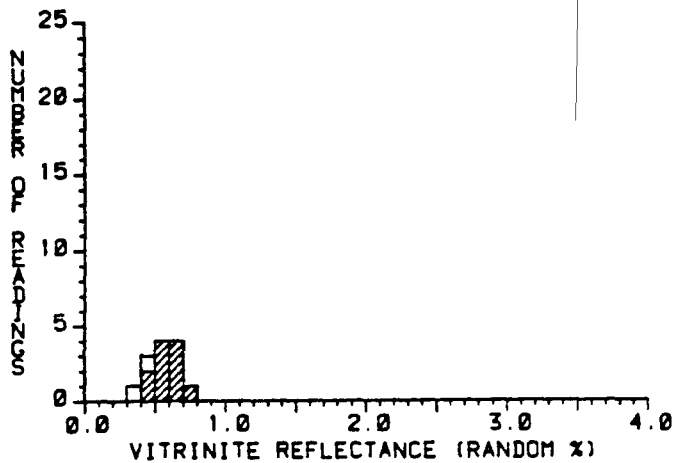
ORDERED REFLECTANCE VALUES:

0.38 \*0.60  
 0.40 \*0.60  
 \*0.44 \*0.74  
 \*0.46 \*0.76  
 \*0.46 0.83  
 \*0.50 0.87  
 \*0.55 0.88  
 \*0.56  
 \*0.57  
 \*0.59

KEROGEN DESCRIPTION

Amorphous : 70 %  
 Exinite : 50 %  
 Vitrinite : 15 %  
 Inertinite : 10 %  
 Back Fluor : Med  
 Bitumen : Small  
 Coke : None

DE LEE #1 - HITCHCOCK FIELD



RRUS No. : 17  
 ID : CTGS.  
 DEPTH : 8759.0 Ft  
 : 2669.7 M

\* = Ro MATURITY

# VALUES : 11

MEAN : 0.58  
 STD DEV : 0.10  
 MEDIAN : 0.59  
 MODE : 0.65

HISTOGRAM:  
 Range: 0- 4%  
 Increment: 0.10%

ORDERED REFLECTANCE VALUES:

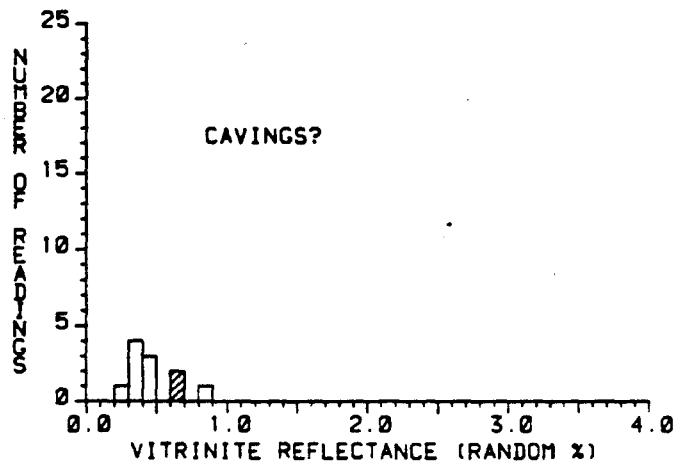
0.36 \*0.64  
 0.40 \*0.64  
 \*0.42 \*0.70  
 \*0.43  
 \*0.50  
 \*0.54  
 \*0.56  
 \*0.59  
 \*0.61  
 \*0.63

KEROGEN DESCRIPTION

Amorphous : 75 %  
 Exinite : 0 %  
 Vitrinite : 15 %  
 Inertinite : 10 %

Back Fluor : Low  
 Bitumen : 1r  
 Coke : None

DE LEE #1 - HITCHCOCK FIELD



RRUS No. : 18  
 ID : CTGS.  
 DEPTH : 8913.0 Ft  
 : 2716.7 M

\* = Ro MATURITY

# VALUES : 2

MEAN : 0.65  
 STD DEV : 0.01  
 MEDIAN : 0.66  
 MODE : 0.65

HISTOGRAM:  
 Range: 0- 4%  
 Increment: 0.10%

ORDERED REFLECTANCE VALUES:

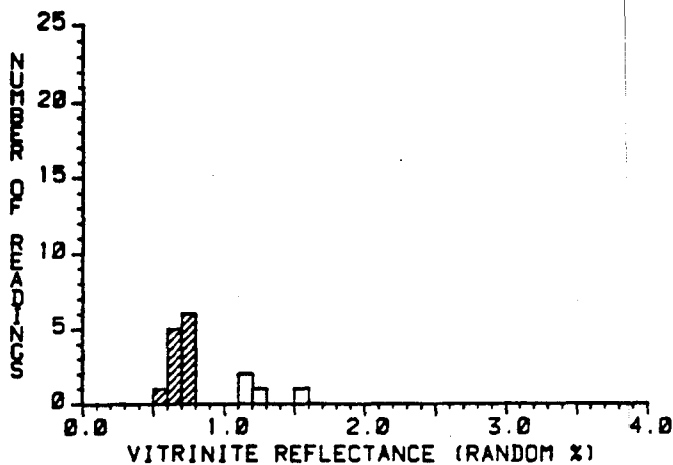
0.20 0.81  
 0.30  
 0.30  
 0.36  
 0.40  
 0.42  
 0.45  
 \*0.64  
 \*0.66

KEROGEN DESCRIPTION

Amorphous : 55 %  
 Exinite : 5 %  
 Vitrinite : 30 %  
 Inertinite : 10 %

Back Fluor : Low  
 Bitumen : Small  
 Coke : None

DE LEE #1 - HITCHCOCK FIELD



RRUS No. : 19  
 ID : CORE  
 DEPTH : 9070.0 Ft  
 : 2764.5 M

\* = Ro MATURITY  
 # VALUES : 12  
 MEAN : 0.68  
 STD DEV : 0.06  
 MEDIAN : 0.70  
 MODE : 0.75

HISTOGRAM:  
 Range: 0- 4%  
 Increment: 0.10%

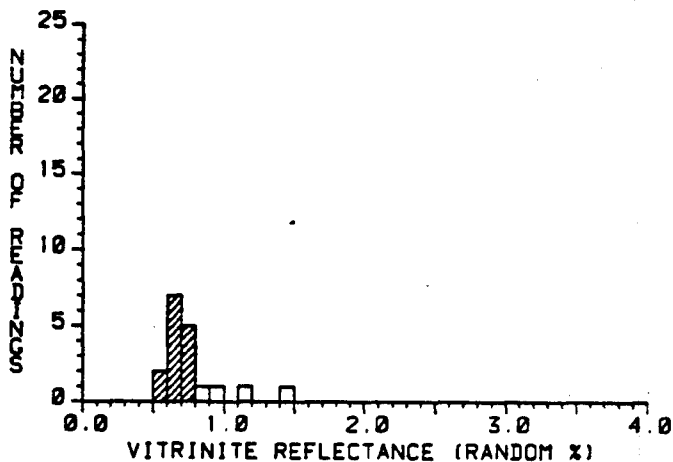
ORDERED REFLECTANCE VALUES:

\*0.58 \*0.77  
 \*0.61 \*0.78  
 \*0.64 1.12  
 \*0.65 1.15  
 \*0.65 1.23  
 \*0.66 1.55  
 \*0.70  
 \*0.70  
 \*0.72  
 \*0.72

KEROGEN DESCRIPTION

Amorphous : 60 %  
 Exinite : 0 %  
 Vitrinite : 30 %  
 Inertinite : 10 %  
 Back Fluor : Low  
 Bitumen : 1r  
 Coke : None

DE LEE #1 - HITCHCOCK FIELD



RRUS No. : 20  
 ID : CORE  
 DEPTH : 9083.0 Ft  
 : 2768.5 M

\* = Ro MATURITY  
 # VALUES : 14  
 MEAN : 0.66  
 STD DEV : 0.06  
 MEDIAN : 0.67  
 MODE : 0.65

HISTOGRAM:  
 Range: 0- 4%  
 Increment: 0.10%

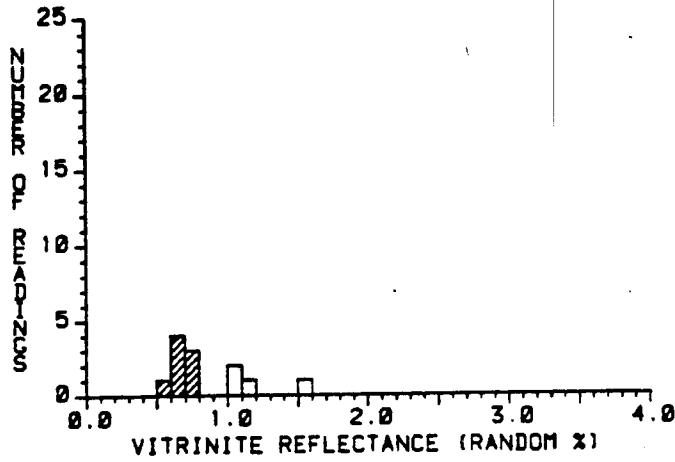
ORDERED REFLECTANCE VALUES:

\*0.55 \*0.71  
 \*0.59 \*0.73  
 \*0.61 \*0.75  
 \*0.62 \*0.78  
 \*0.62 0.83  
 \*0.63 0.92  
 \*0.65 1.14  
 \*0.67 1.43  
 \*0.68  
 \*0.70

KEROGEN DESCRIPTION

Amorphous : 45 %  
 Exinite : 5 %  
 Vitrinite : 40 %  
 Inertinite : 10 %  
 Back Fluor : Low  
 Bitumen : 1r  
 Coke : None

DE LEE #1 - HITCHCOCK FIELD



RRUS No. : 21  
ID : CORE  
DEPTH : 9092.0 Ft  
: 2771.2 M

\* = Ro MATURITY

# VALUES : 8

MEAN : 0.67  
STD DEV : 0.06  
MEDIAN : 0.68  
MODE : 0.65

HISTOGRAM:  
Range: 0- 4%  
Increment: 0.10%

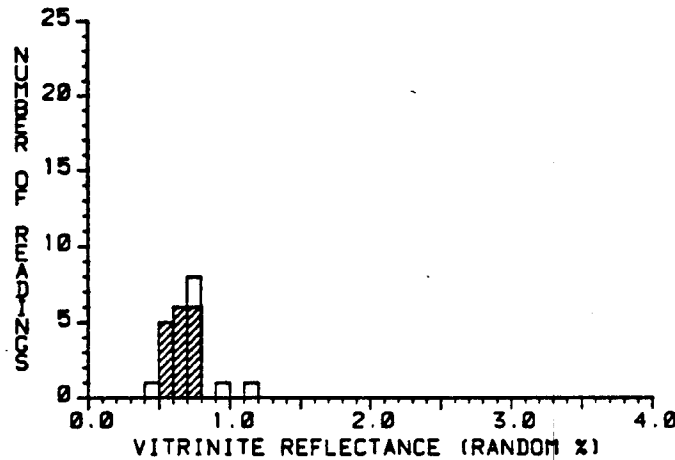
ORDERED REFLECTANCE VALUES:

\*0.53 1.16  
\*0.65 1.54  
\*0.65  
\*0.67  
\*0.68  
\*0.71  
\*0.71  
\*0.76  
1.00  
1.04

KEROGEN DESCRIPTION

Amorphous : 30 %  
Exinite : 0 %  
Vitrinite : 65 %  
Inertinite : 5 %  
Back Fluor : None  
Bitumen : None  
Coke : None

DE LEE #1 - HITCHCOCK FIELD



RRUS No. : 22  
ID : CORE  
DEPTH : 9099.0 Ft  
: 2773.4 M

\* = Ro MATURITY

# VALUES : 17

MEAN : 0.64  
STD DEV : 0.08  
MEDIAN : 0.65  
MODE : 0.75

HISTOGRAM:  
Range: 0- 4%  
Increment: 0.10%

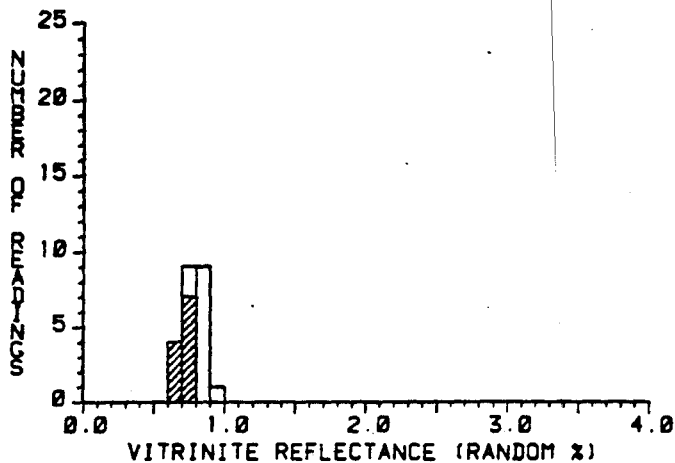
ORDERED REFLECTANCE VALUES:

0.43 \*0.65 0.93  
\*0.50 \*0.69 1.13  
\*0.51 \*0.70  
\*0.56 \*0.71  
\*0.57 \*0.71  
\*0.58 \*0.72  
\*0.60 \*0.74  
\*0.61 \*0.76  
\*0.63 0.79  
\*0.65 0.79

KEROGEN DESCRIPTION

Amorphous : 25 %  
Exinite : 0 %  
Vitrinite : 65 %  
Inertinite : 10 %  
Back Fluor : Low  
Bitumen : 1r  
Coke : None

DE LEE #1 - HITCHCOCK FIELD



RRUS No. : 23  
 ID : CORE  
 DEPTH : 9100.0 Ft  
 : 2773.7 M

\* = Ro MATURITY  
 # VALUES : 11  
 MEAN : 0.70  
 STD DEV : 0.04  
 MEDIAN : 0.71  
 MODE : 0.75

HISTOGRAM:  
 Range: 0- 4%  
 Increment: 0.10%

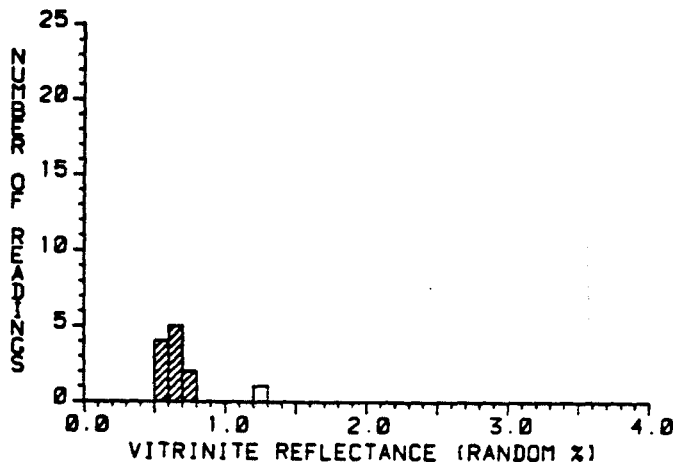
ORDERED REFLECTANCE VALUES:

*0.63	*0.74	0.88
*0.64	0.78	0.88
*0.66	0.79	0.92
*0.67	0.80	
*0.70	0.81	
*0.71	0.81	
*0.72	0.83	
*0.73	0.84	
*0.74	0.86	
*0.74	0.87	

KEROGEN DESCRIPTION

Amorphous	: 20 %
Exinite	: 10 %
Vitrinite	: 60 %
Inertinite	: 10 %
Back Fluor	: Med
Bitumen	: 1C
Coke	: None

DE LEE #1 - HITCHCOCK FIELD



RRUS No. : 24  
 ID : CORE  
 DEPTH : 9100.5 Ft  
 : 2773.8 M

\* = Ro MATURITY  
 # VALUES : 11  
 MEAN : 0.64  
 STD DEV : 0.07  
 MEDIAN : 0.67  
 MODE : 0.65

HISTOGRAM:  
 Range: 0- 4%  
 Increment: 0.10%

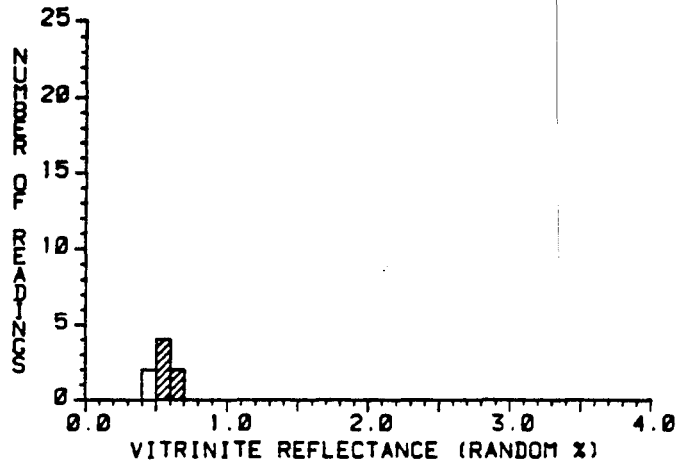
ORDERED REFLECTANCE VALUES:

*0.50	*0.75
*0.56	1.29
*0.57	
*0.58	
*0.63	
*0.67	
*0.68	
*0.69	
*0.69	
*0.71	

KEROGEN DESCRIPTION

Amorphous	: 55 %
Exinite	: 10 %
Vitrinite	: 30 %
Inertinite	: 5 %
Back Fluor	: Low
Bitumen	: None
Coke	: None

DE LEE #1 - HITCHCOCK FIELD



RRUS No. : 25  
 ID : CORE  
 DEPTH : 9100.7 Ft  
 : 2773.0 M

\* = Ro MATURITY

# VALUES : 6

MEAN : 0.59  
 STD DEV : 0.05  
 MEDIAN : 0.59  
 MODE : 0.55

HISTOGRAM:  
 Range: 0- 4%  
 Increment: 0.10%

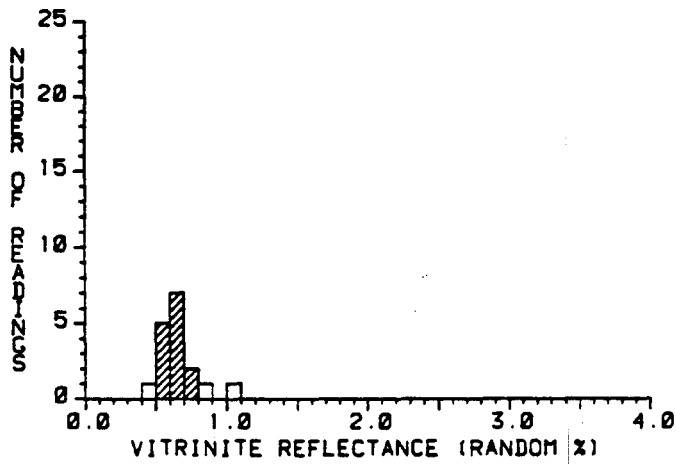
ORDERED REFLECTANCE VALUES:

0.47  
 0.47  
 \*0.54  
 \*0.55  
 \*0.56  
 \*0.59  
 \*0.63  
 \*0.68

KEROGEN DESCRIPTION

Amorphous : 60 %  
 Exinite : 5 %  
 Vitrinite : 15 %  
 Inertinite : 20 %  
 Back Fluor : None  
 Bitumen : None  
 Coke : None

DE LEE #1 - HITCHCOCK FIELD



RRUS No. : 26  
 ID : CORE  
 DEPTH : 9100.8 Ft  
 : 2773.0 M

\* = Ro MATURITY

# VALUES : 14

MEAN : 0.64  
 STD DEV : 0.06  
 MEDIAN : 0.63  
 MODE : 0.65

HISTOGRAM:  
 Range: 0- 4%  
 Increment: 0.10%

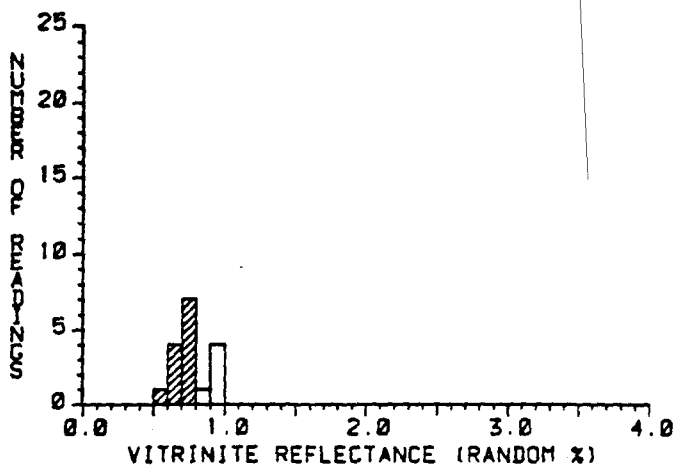
ORDERED REFLECTANCE VALUES:

0.48 \*0.66  
 \*0.56 \*0.68  
 \*0.56 \*0.69  
 \*0.57 \*0.72  
 \*0.58 \*0.77  
 \*0.59 0.87  
 \*0.62 1.00  
 \*0.63  
 \*0.63  
 \*0.65

KEROGEN DESCRIPTION

Amorphous : 45 %  
 Exinite : 15 %  
 Vitrinite : 30 %  
 Inertinite : 10 %  
 Back Fluor : Low  
 Bitumen : Small  
 Coke : None

DE LEE #1 - HITCHCOCK FIELD



RRUS No. : 27  
 ID : CORE  
 DEPTH : 9101.0 Ft  
 : 2774.0 M

\* = Ro MATURITY  
 # VALUES : 12  
 MEAN : 0.70  
 STD DEV : 0.06  
 MEDIAN : 0.72  
 MODE : 0.75

HISTOGRAM:  
 Range: 0- 4%  
 Increment: 0.10%

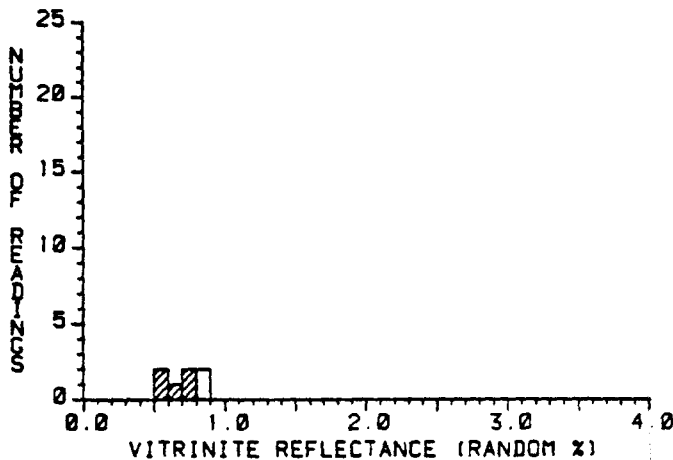
ORDERED REFLECTANCE VALUES:

\*0.58 \*0.77  
 \*0.61 \*0.78  
 \*0.65 0.83  
 \*0.66 0.90  
 \*0.67 0.93  
 \*0.70 0.94  
 \*0.72 0.99  
 \*0.74  
 \*0.75  
 \*0.77

KEROGEN DESCRIPTION

Amorphous : 75 %  
 Exinite : 0 %  
 Vitrinite : 15 %  
 Inertinite : 10 %  
 Back Fluor : Low  
 Bitumen : nr  
 Coke : None

DE LEE #1 - HITCHCOCK FIELD



RRUS No. : 28  
 ID : CORE  
 DEPTH : 9103.3 Ft  
 : 2774.7 M

\* = Ro MATURITY  
 # VALUES : 5  
 MEAN : 0.66  
 STD DEV : 0.08  
 MEDIAN : 0.66  
 MODE : 0.75

HISTOGRAM:  
 Range: 0- 4%  
 Increment: 0.10%

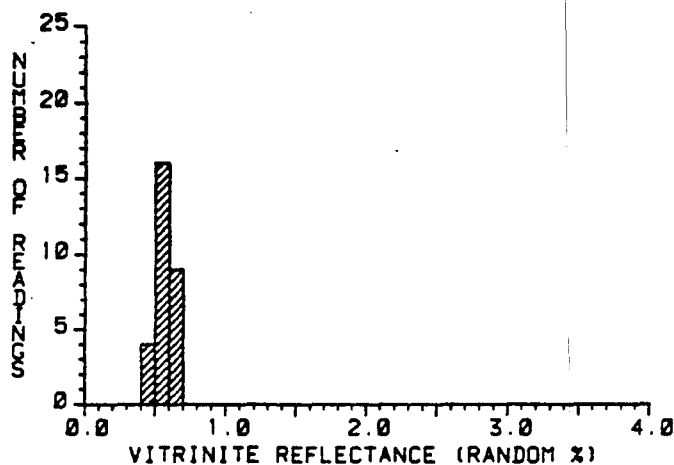
ORDERED REFLECTANCE VALUES:

\*0.57  
 \*0.58  
 \*0.66  
 \*0.74  
 \*0.76  
 0.80  
 0.84

KEROGEN DESCRIPTION

Amorphous : 85 %  
 Exinite : 0 %  
 Vitrinite : 10 %  
 Inertinite : 5 %  
 Back Fluor : Med  
 Bitumen : Small  
 Coke : None

DE LEE #1 - HITCHCOCK FIELD



RRUS No. : 29  
 ID : CORE  
 DEPTH : 9104.5 Ft  
 : 2775.1 M

\* = Ro MATURITY

# VALUES : 29  
 MEAN : 0.56  
 STD DEV : 0.05  
 MEDIAN : 0.55  
 MODE : 0.55

HISTOGRAM:  
 Range: 0- 4%  
 Increment: 0.10%

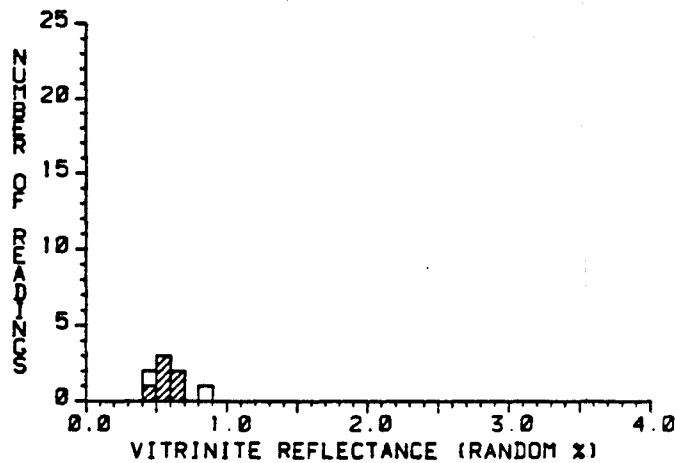
ORDERED REFLECTANCE VALUES:

\*0.45 \*0.53 \*0.60  
 \*0.46 \*0.54 \*0.60  
 \*0.49 \*0.55 \*0.61  
 \*0.49 \*0.55 \*0.61  
 \*0.51 \*0.55 \*0.61  
 \*0.51 \*0.56 \*0.62  
 \*0.52 \*0.56 \*0.63  
 \*0.53 \*0.58 \*0.64  
 \*0.53 \*0.58 \*0.65  
 \*0.53 \*0.59

KEROGEN DESCRIPTION

Amorphous : 40 %  
 Exinite : 5 %  
 Vitrinite : 50 %  
 Inertinite : 5 %  
 Back Fluor : Low  
 Bitumen : None  
 Coke : None

DE LEE #1 - HITCHCOCK FIELD



RRUS No. : 30  
 ID : CORE  
 DEPTH : 9125.0 Ft  
 : 2781.3 M

\* = Ro MATURITY

# VALUES : 6  
 MEAN : 0.58  
 STD DEV : 0.06  
 MEDIAN : 0.59  
 MODE : 0.55

HISTOGRAM:  
 Range: 0- 4%  
 Increment: 0.10%

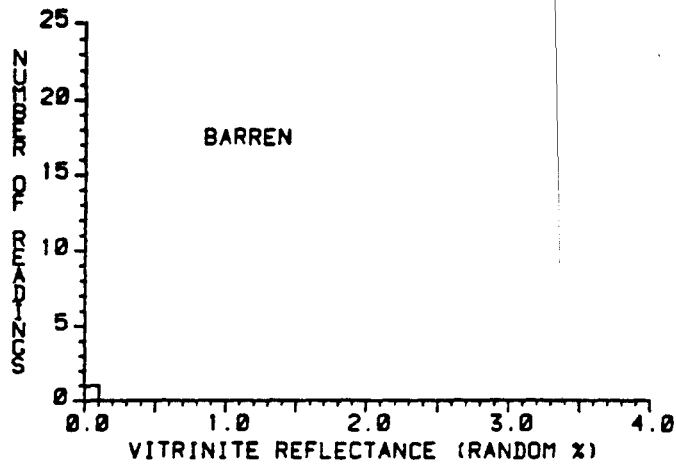
ORDERED REFLECTANCE VALUES:

0.44  
 \*0.49  
 \*0.56  
 \*0.58  
 \*0.59  
 \*0.62  
 \*0.67  
 0.80

KEROGEN DESCRIPTION

Amorphous : 55 %  
 Exinite : 1%  
 Vitrinite : 35 %  
 Inertinite : 10 %  
 Back Fluor : Low  
 Bitumen : Small  
 Coke : None

DE LEE #1 - HITCHCOCK FIELD



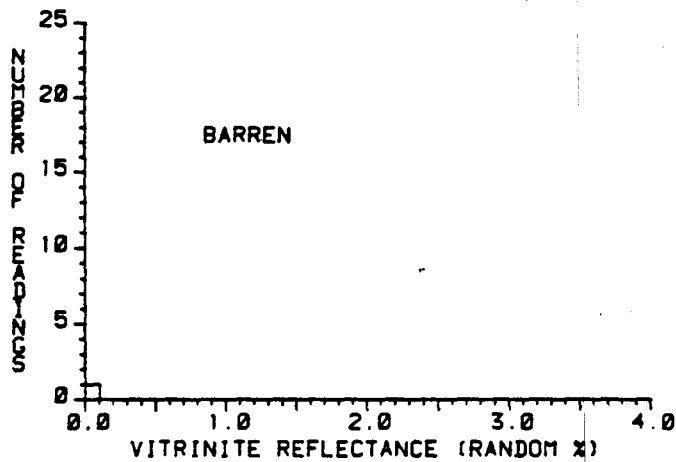
RRUS No. : 31  
 ID : CORE  
 DEPTH : 9141.0 F1  
 : 2786.2 M  
 MEAN : N.D.

HISTOGRAM:  
 Range: 0- 4%  
 Increment: 0.10%

ORDERED REFLECTANCE VALUES:  
 0.00

KEROGEN DESCRIPTION  
 Amorphous : 95 %  
 Exinite : 0 %  
 Vitrinite : 5 %  
 Inertinite : 1%  
 Back Fluor : Med  
 Bitumen : 1%  
 Coke : None

DE LEE #1 - HITCHCOCK FIELD



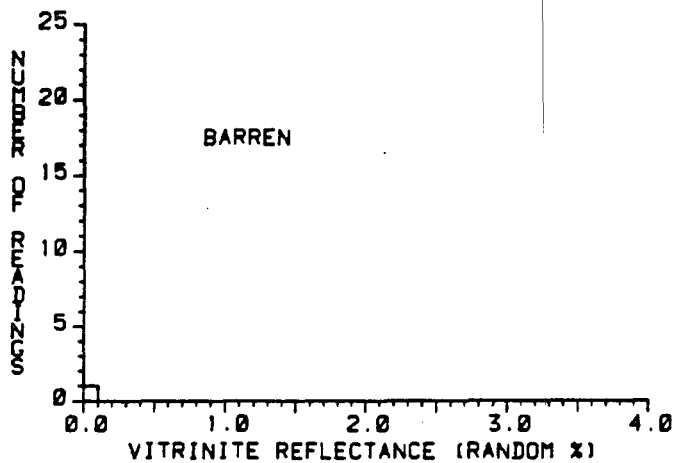
RRUS No. : 32  
 ID : CORE  
 DEPTH : 9149.0 F1  
 : 2788.6 M  
 MEAN : N.D.

HISTOGRAM:  
 Range: 0- 4%  
 Increment: 0.10%

ORDERED REFLECTANCE VALUES:  
 0.00

KEROGEN DESCRIPTION  
 Amorphous : 90 %  
 Exinite : 0 %  
 Vitrinite : 5 %  
 Inertinite : 5 %  
 Back Fluor : Low  
 Bitumen : Small  
 Coke : None

DE LEE #1 - HITCHCOCK FIELD



RRUS No. : 33  
 ID : CORE  
 DEPTH : 9167.5 Ft  
 : 2794.3 M  
 MEAN : N.D.

HISTOGRAM:  
 Range: 0- 4%  
 Increment: 0.10%

ORDERED REFLECTANCE VALUES:

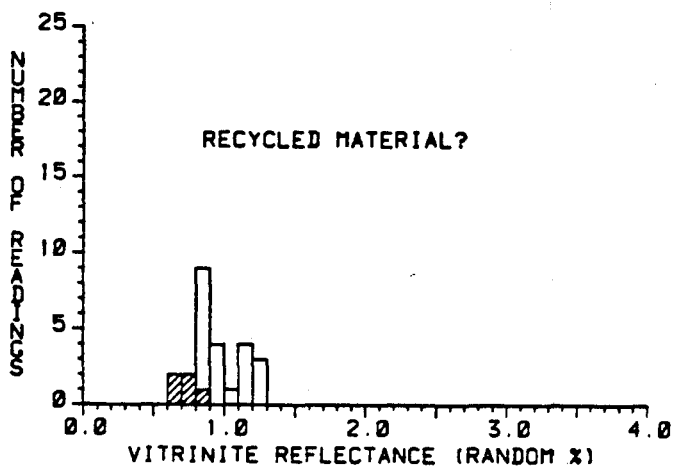
0.00

KEROGEN DESCRIPTION

Amorphous : 90 %  
 Exinite : 0 %  
 Vitrinite : 5 %  
 Inertinite : 5 %

Back Fluor : Low  
 Bitumen : 1r  
 Coke : None

DE LEE #1 - HITCHCOCK FIELD



RRUS No. : 34  
 ID : CORE  
 DEPTH : 9179.0 Ft  
 : 2798.0 M

\* = Ro MATURITY

# VALUES : 5

MEAN : 0.73  
 STD DEV : 0.07  
 MEDIAN : 0.79  
 MODE : 0.75

HISTOGRAM:  
 Range: 0- 4%  
 Increment: 0.10%

ORDERED REFLECTANCE VALUES:

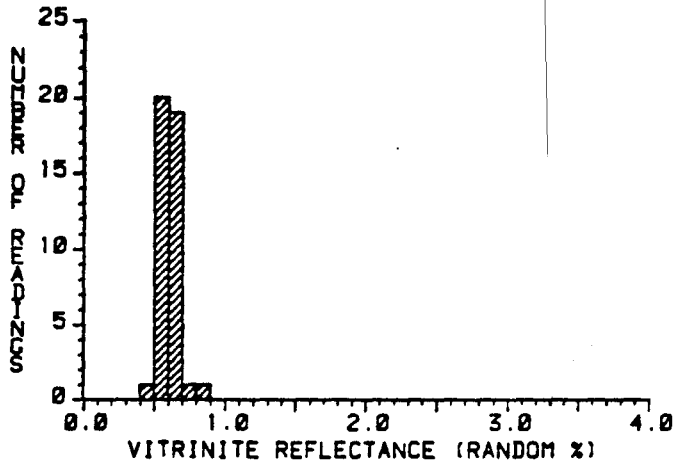
*0.62	0.84	1.14
*0.67	0.87	1.16
*0.70	0.89	1.21
*0.79	0.91	1.23
*0.80	0.93	1.26
0.82	0.93	
0.82	0.99	
0.82	1.06	
0.82	1.10	
0.82	1.12	

KEROGEN DESCRIPTION

Amorphous : 45 %  
 Exinite : 0 %  
 Vitrinite : 35 %  
 Inertinite : 20 %

Back Fluor : Low  
 Bitumen : 1r  
 Coke : None

DE LEE #1 - HITCHCOCK FIELD



RRUS No. : 35  
 ID : CORE  
 DEPTH : 9194.3 F  
 : 2802.4 M

\* = Ro MATURITY  
 # VALUES : 42  
 MEAN : 0.60  
 STD DEV : 0.06  
 MEDIAN : 0.60  
 MODE : 0.55

HISTOGRAM:  
 Range: 0- 4%  
 Increment: 0.10%

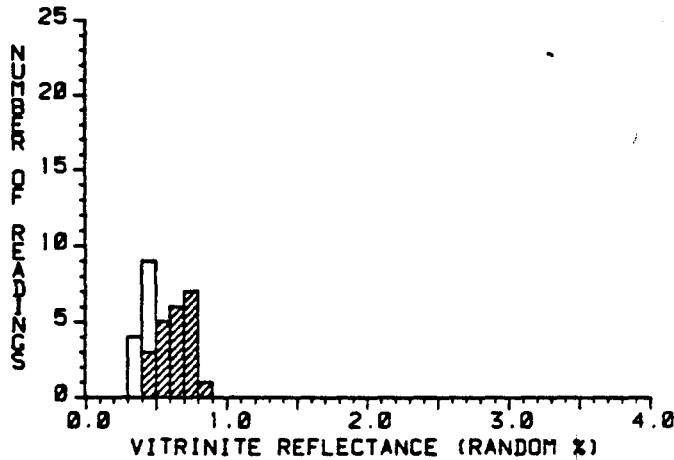
ORDERED REFLECTANCE VALUES:

*0.49	*0.56	*0.59	*0.64	*0.70
*0.50	*0.56	*0.60	*0.64	*0.83
*0.52	*0.57	*0.60	*0.64	
*0.54	*0.57	*0.61	*0.64	
*0.54	*0.57	*0.61	*0.65	
*0.54	*0.57	*0.61	*0.65	
*0.55	*0.58	*0.62	*0.66	
*0.55	*0.59	*0.63	*0.67	
*0.55	*0.59	*0.63	*0.67	
*0.56	*0.59	*0.63	*0.68	

KEROGEN DESCRIPTION

Amorphous : 35 %  
 Exinite : 5 %  
 Vitrinite : 50 %  
 Inertinite : 10 %  
 Back Fluor : Low  
 Bitumen : Small  
 Coke : None

DE LEE #1 - HITCHCOCK FIELD



RRUS No. : 36  
 ID : CORE  
 DEPTH : 9262.0 F  
 : 2823.1 M

\* = Ro MATURITY  
 # VALUES : 22  
 MEAN : 0.63  
 STD DEV : 0.10  
 MEDIAN : 0.63  
 MODE : 0.75

HISTOGRAM:  
 Range: 0- 4%  
 Increment: 0.10%

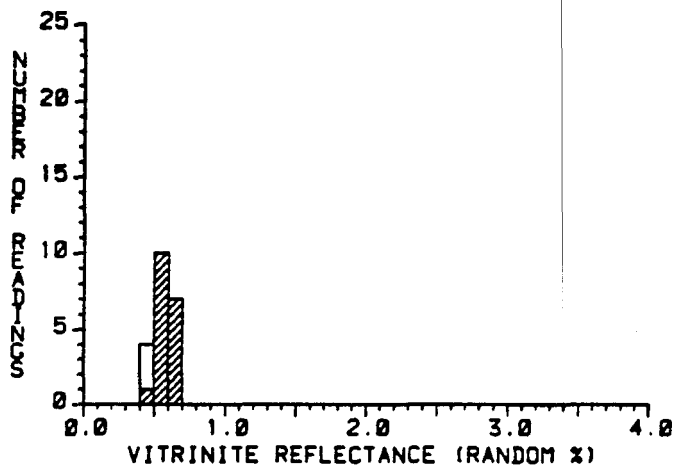
ORDERED REFLECTANCE VALUES:

0.31	*0.46	*0.63	*0.76
0.33	*0.48	*0.63	*0.81
0.37	*0.49	*0.67	
0.38	*0.50	*0.69	
0.40	*0.50	*0.70	
0.41	*0.54	*0.70	
0.42	*0.59	*0.70	
0.43	*0.59	*0.71	
0.43	*0.61	*0.71	
0.44	*0.61	*0.72	

KEROGEN DESCRIPTION

Amorphous : 45 %  
 Exinite : 10 %  
 Vitrinite : 35 %  
 Inertinite : 10 %  
 Back Fluor : Low  
 Bitumen : 1r  
 Coke : None

DE LEE #1 - HITCHCOCK FIELD



RRUS No. : 37  
 ID : CTGS.  
 DEPTH : 9302.0 Ft  
 : 2835.2 M

\* = Ro MATURITY  
 # VALUES : 18  
 MEAN : 0.58  
 STD DEV : 0.07  
 MEDIAN : 0.59  
 MODE : 0.55

HISTOGRAM:  
 Range: 0- 4%  
 Increment: 0.10%

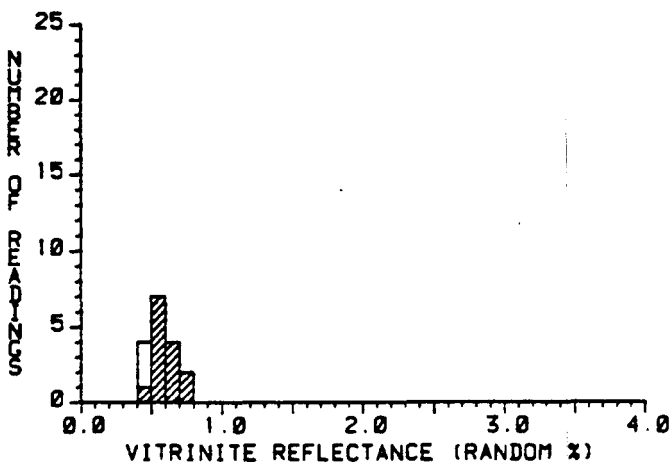
ORDERED REFLECTANCE VALUES:

0.40 \*0.54 \*0.69  
 0.45 \*0.56  
 0.47 \*0.59  
 \*0.49 \*0.59  
 \*0.50 \*0.63  
 \*0.51 \*0.63  
 \*0.51 \*0.63  
 \*0.51 \*0.65  
 \*0.52 \*0.67  
 \*0.53 \*0.67

KEROGEN DESCRIPTION

Amorphous : 40 %  
 Exinite : 15 %  
 Vitrinite : 35 %  
 Inertinite : 10 %  
 Back Fluor : Med  
 Bitumen : 1r  
 Coke : None

DE LEE #1 - HITCHCOCK FIELD



RRUS No. : 38  
 ID : CTGS.  
 DEPTH : 9340.0 Ft  
 : 2846.8 M

\* = Ro MATURITY  
 # VALUES : 14  
 MEAN : 0.60  
 STD DEV : 0.09  
 MEDIAN : 0.58  
 MODE : 0.55

HISTOGRAM:  
 Range: 0- 4%  
 Increment: 0.10%

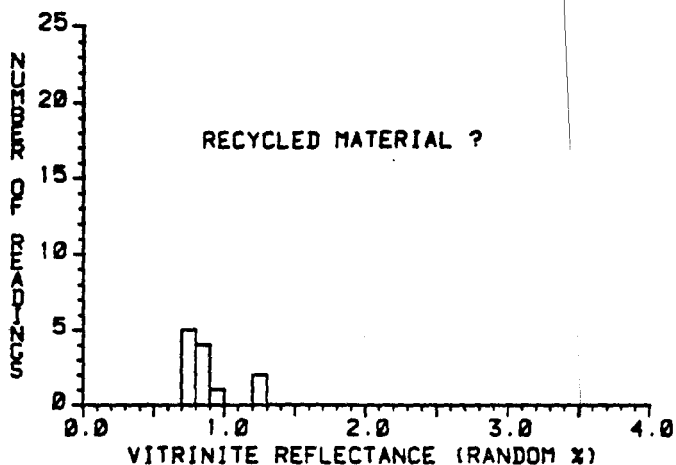
ORDERED REFLECTANCE VALUES:

0.45 \*0.58  
 0.45 \*0.61  
 0.47 \*0.63  
 \*0.48 \*0.67  
 \*0.50 \*0.68  
 \*0.53 \*0.76  
 \*0.53 \*0.78  
 \*0.56  
 \*0.56  
 \*0.58

KEROGEN DESCRIPTION

Amorphous : 30 %  
 Exinite : 5 %  
 Vitrinite : 50 %  
 Inertinite : 15 %  
 Back Fluor : Low  
 Bitumen : 1r  
 Coke : None

DE LEE #1 - HITCHCOCK FIELD



RRUS No. : 30  
 ID : CTGS.  
 DEPTH : 9367.0 Ft  
 : 2855.1 M  
 MEAN : N.D.

HISTOGRAM:  
 Range: 0- 4%  
 Increment: 0.10%

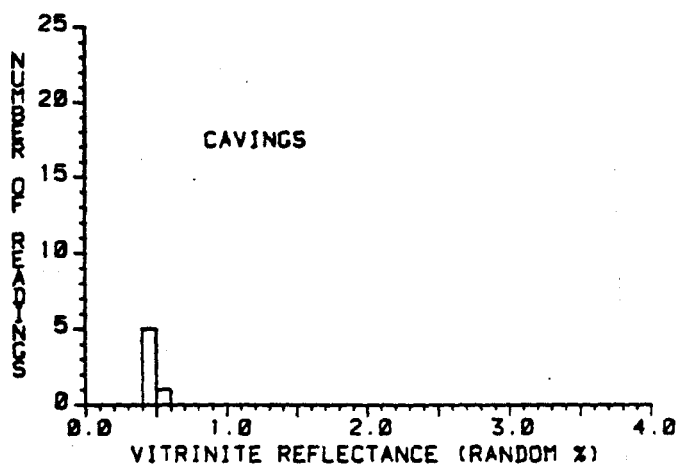
ORDERED REFLECTANCE VALUES:

0.70 1.23  
 0.72 1.25  
 0.73  
 0.74  
 0.78  
 0.81  
 0.81  
 0.82  
 0.86  
 0.89

KEROGEN DESCRIPTION

Amorphous : 40 %  
 Exinite : 5 %  
 Vitrinite : 40 %  
 Inertinite : 15 %  
 Back Fluor : Med  
 Bitumen : None  
 Coke : None

DE LEE #1 HITCHCOCK FIELD



RRUS No. : 40  
 ID : CTGS.  
 DEPTH : 9392.0 Ft  
 : 2862.7 M  
 MEAN : N.D.

HISTOGRAM:  
 Range: 0- 4%  
 Increment: 0.10%

ORDERED REFLECTANCE VALUES:

0.42  
 0.43  
 0.47  
 0.48  
 0.49  
 0.50

KEROGEN DESCRIPTION

Amorphous : 45 %  
 Exinite : 5 %  
 Vitrinite : 40 %  
 Inertinite : 10 %  
 Back Fluor : None  
 Bitumen : Tr  
 Coke : None

Detailed Compositional Data for Crude Oil

Sample No. 3013-041

GROSS OIL COMPOSITION (%)

Less than C <sub>15</sub> + Fraction	58.3
C <sub>15</sub> + Fraction	41.7

C<sub>15</sub>+ OIL COMPOSITION (%)

Asphaltene(ASPH)	1.0
Paraffin-Naphthene(P-N)	81.3
Aromatic HC(AROM)	16.7
Eluted NSO	0.5
Non-eluted NSO	0.5

DETAILED C<sub>4</sub>-C<sub>7</sub> COMPOSITION (NORM.%)

- Isobutane
- n-Butane
- Isopentane
- n-Pentane
- 2,2-Dimethylbutane
- Cyclopentane
- 2,3-Dimethylbutane
- 2-Methylpentane
- 3-Methylpentane
- n-Hexane
- Methylcyclopentane
- 2,2-Dimethylpentane
- Benzene
- 2,4-Dimethylpentane
- 2,2,3-Trimethylbutane
- Cyclohexane
- 3,3-Dimethylpentane
- 1,1-Dimethylcyclopentane
- 2-Methylhexane
- 2,3-Dimethylpentane
- 1,cis-3-Dimethylcyclopentane
- 3-Methylhexane
- 1,trans-3-Dimethylcyclopentane
- 1,trans-2-Dimethylcyclopentane
- 3-Ethylpentane
- n-Heptane
- 1,cis-2-Dimethylcyclopentane
- Methylcyclohexane
- Toluene

COMPOSITION OF C<sub>15</sub>+ SATURATE HYDROCARBONS

% n-Alkanes	36.3
% Isoalkanes	5.6
% C <sub>19</sub> & C <sub>20</sub> Isoprenoids	
% Naphthenes	58.1
Sat/Arom	4.86
Asph/NSO	1.00
CPI Index A	1.06
CPI Index B	1.08
ip-C <sub>19</sub> /ip-C <sub>20</sub>	2.69

NORMALIZED PARAFFIN DISTRIBUTION (%)

- nC<sub>15</sub>
- nC<sub>16</sub>
- nC<sub>17</sub>
- ip-C<sub>19</sub>
- nC<sub>18</sub>
- ip-C<sub>20</sub>
- nC<sub>19</sub>
- nC<sub>20</sub>
- nC<sub>21</sub>
- nC<sub>22</sub>
- nC<sub>23</sub>
- nC<sub>24</sub>
- nC<sub>25</sub>
- nC<sub>26</sub>
- nC<sub>27</sub>
- nC<sub>28</sub>
- nC<sub>29</sub>
- nC<sub>30</sub>
- nC<sub>31</sub>
- nC<sub>32</sub>
- nC<sub>33</sub>
- nC<sub>34</sub>
- nC<sub>35</sub>

MOLECULAR RATIOS

- 2-methylpentane/3-methylpentane
- isopentane/n-pentane
- cyclohexane/methylcyclopentane
- methylcyclopentane/methylcyclohexane

DETAILED C4-C7 HYDROCARBON ANALYSES

(NORMALIZED PERCENT)

GEOCHEM SAMPLE NUMBER 3013-041  
 CLIENT I.D. NO. N.E. Hitchcock Field

ISOBUTANE	4.0
N-BUTANE	5.6
ISOPENTANE	8.1
N-PENTANE	7.6
2,2-DIMETHYLBUTANE	1.0
CY CLOPENTANE	0.7
2,3-DIMETHYLBUTANE	1.6
2-METHYLPENTANE	6.1
3-METHYLPENTANE	3.7
N-HEXANE	8.2
METHY CY CLOPENTANE	3.7
2,2-DIMETHYLPENTANE	0.6
BENZENE	1.3
2,4-DIMETHYLPENTANE	0.9
2,2,3-TRIMETHYLBUTANE	0.3
CY CLOHEXANE	6.4
3,3-DIMETHYLPENTANE	0.4
1,1-DIMETHYL CY CLOPENTANE	0.7
2-METHYLHEXANE	4.6
2,3-DIMETHYLPENTANE	0.0
1, CIS-3-DIMETHYL CY CLOPENTANE	0.7
3-METHYLHEXANE	3.7
1 TRANS-3-DIMETHYL CY CLOPENTANE	0.3
1 TRANS-2-DIMETHYL CY CLOPENTANE	1.3
3-ETHYLPENTANE	0.3
2,2,4-TRIMETHYLPENTANE	0.0
N-HEPTANE	6.5
1, CIS-2-DIMETHYL CY CLOPENTANE	0.2
METHY CY CLOHEXANE	10.0
1,1,3-TRIMETHYL CY CLOPENTANE *	0.4
2,2-DIMETHYLHEXANE	0.3
ETHYL CY CLOPENTANE	0.4
TOLUENE	10.3

C4-C7 HYDROCARBON CONTENT/PPM\*\* 1.7

MOLECULAR RATIOS

2-METHYLPENTANE/3-METHYLPENTANE	1.66
ISOPENTANE/N-PENTANE	1.07
CY CLOHEXANE/METHYL CY CLOPENTANE	1.70
METHYL CY CLOPENT/METHYL CY CLOHEX	0.38

\* C8 COMPOUNDS

\*\* PPM VALUES ARE EXPRESSED AS VOLUMES OF GAS PER MILLION VOLUMES OF CUTTINGS

CRUDE OIL ANALYSIS RESULTS

GeoChem Sample No.: 3013-041  
Client Identification No.: N.E. Hitchcock Field

GROSS COMPOSITION

Less than C<sub>15+</sub> ..... 58.3%  
C<sub>15+</sub> ..... 41.7%

C<sub>15+</sub> COMPOSITION

Asphaltene (ASPH) ..... 1.0%  
Paraffin-Naphthene Hydrocarbons (P-N) ..... 81.3%  
Aromatic Hydrocarbons (AROM) ..... 16.7%  
Eluted NSO Compounds (NSO) ..... 0.5%  
Noneluted NSO Compounds (NSO) ..... 0.5%

RATIOS

$$\frac{P-N}{AROM} = 4.86$$

$$\frac{ASPH}{NSO} = 1.00$$

Saturate Hydrocarbon Analyses

Summary of Paraffin-Naphthene Distribution

Geo Chem Sample Number	Client Identification Number	% Paraffin	% Isoprenoid	% Naphthene	C-P Index A	C-P Index B	ip19/ip20
3013-041	N. E. Hitchcock Field	36.3	5.6	58.1	1.06	1.08	2.69

Saturate Hydrocarbon Analyses

Normalized Paraffin Distribution

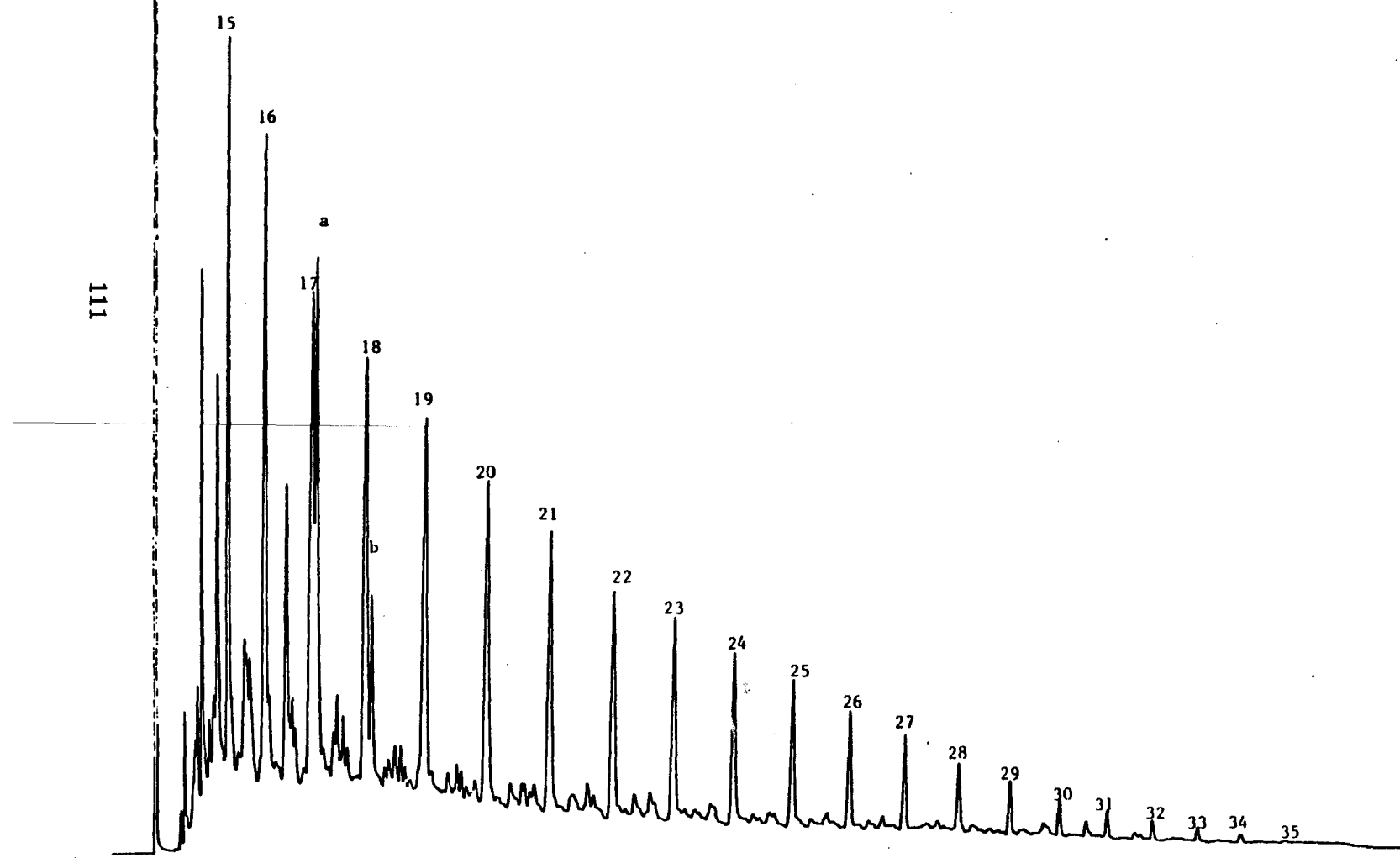
110

Geo Chem Sample Number	Client Identification Number	% nC15	% nC16	% nC17	% ip19	% nC18	% ip20	% nC19	% nC20	% nC21	% nC22	% nC23	% nC24	% nC25	% nC26	% nC27	% nC28	% nC29	% nC30	% nC31	% nC32	% nC33	% nC34	% nC35
3013-041	N.E. Hitchcock Field	14.1	12.5	9.4	9.8	8.2	3.6	7.2	6.3	5.5	4.4	4.0	3.4	2.9	2.3	1.9	1.3	1.1	0.7	0.5	0.4	0.2	0.2	0.1

C<sub>15+</sub> Paraffin-Naphthene (P-N) Hydrocarbon

GeoChem Sample No. 3013-041

Client I.D. No. N.E. Hitchcock Field



PART 2  
NUMERICAL SIMULATION OF THE HITCHCOCK N. E. FIELD,  
GALVESTON COUNTY, TEXAS

by C. M. Lea, D. B. Voorhis, C. K. Mamum, B. H. Caudle, and K. Sepehrnoori

July 1985

Center for Energy Studies  
The University of Texas at Austin  
Austin, Texas 78713

TABLE OF CONTENTS

ABSTRACT . . . . . 119

1. INTRODUCTION . . . . . 121

2. NORTHEAST HITCHCOCK FIELD GEOLOGY AND  
THE PHYSICAL DIMENSIONS OF THE RESERVOIR . . . . . 122

    2.1 Geology . . . . . 122

    2.2 Northeast Hitchcock Field Reservoir . . . . . 124

    2.3 Reservoir Dimensions . . . . . 129

    2.4 Aquifer Dimensions . . . . . 132

3. FLUID DATA, PETROPHYSICAL DATA AND ITS USE AS INPUT DATA . . . . 132

    3.1 Fluid Data . . . . . 132

    3.2 Petrophysical Data . . . . . 136

4. ADJUSTMENT OF RESERVOIR PROPERTIES AND GRID BLOCK  
CONFIGURATIONS TO MATCH HISTORICAL PRESSURES . . . . . 145

5. FINAL NOTE . . . . . 150

ACKNOWLEDGEMENTS . . . . . 154

REFERENCES . . . . . 155

APPENDICES . . . . . 156

LIST OF FIGURES

Figure 1	Structure Map of the Top of the Pay in the Northeast Hitchcock Field . . . . .	123
Figure 2	Structural Cross Section Depicting the Original Gas-Water Contact in the Northeast Hitchcock Field . . . . .	125
Figure 3	Isopach of the Gross Pay in the Frio "A" Sand of the Northeast Hitchcock Field . . . . .	126
Figure 4	Isopach of the Net Pay in the Frio "A" Sand of the Northeast Hitchcock Field . . . . .	127
Figure 5	Grid Block Configuration of the Northeast Hitchcock Field . .	131
Figure 6	N.E. Hitchcock Field Gas Viscosity Versus Pressure . . . . .	137
Figure 7	N.E. Hitchcock Field Water Viscosity Versus Pressure . . . . .	137
Figure 8	N.E. Hitchcock Field BG(RCF/SCF) Versus Pressure . . . . .	138
Figure 9	N.E. Hitchcock Field BW(RB/STB) Versus Pressure . . . . .	138
Figure 10	Imbibition-Capillary Pressure Curve, $P_{cgw}$ vs. $S_w$ . . . . .	140
Figure 11	Relative Permeability Curves $k_{rg}$ , $k_{rw}$ vs. $S_w$ . . . . .	142
Figure 12	Northeast Hitchcock Field Liquid Dropout vs. Pressure . . .	144
Figures 13-18	N.E. Hitchcock Field, Simulated Versus Actual Pressure, Wells Nos. 2, 3, 4, 5, 6, and 9 . . . . .	147-149
Figures 19-24	N.E. Hitchcock Field, Simulated Versus Actual Pressure, Wells Nos. 2, 3, 4, 5, 6, and 9 . . . . .	151-153

LIST OF TABLES

Table 1.	Listing of Well Code Numbers, Operator, and Well Name . . . . .	128
Table 2.	Hydrocarbon Reservoir and Aquifer Properties . . . . .	130
Table 3.	Condensate/Gas Ratio History . . . . .	133
Table 4.	Subsurface Pressure Data . . . . .	133
Table 5.	Gas Production History . . . . .	134
Table 6.	Water Production History . . . . .	135

LIST OF APPENDICES

Appendix A	- Structural Cross Sections . . . . .	156
Appendix B	- Calculations of Formation Volume Factors and Viscosities for the Equilibrium Gas and the Flowing Water Phase . . . . .	164
Appendix C	- Eaton Operating Co., Inc., S.G.R. No. 2 Louise Unit, Capillary Pressure Curves . . . . .	181
Appendix D	- Calculations Determining the Liquid Dropout from the Northeast Hitchcock Field Reservoir Fluid Under Conditions of Isothermal Depletion . . . . .	190
Appendix E	- Evaluation of the Northeast Hitchcock Field Aquifer Using the Method of Fetkovitch . . . . .	192
Appendix F	- Calculations determining the Amount of Liquid Hydrocarbons Dissolved in the Equilibrium Gas of the Northeast Hitchcock Field Under Conditions of Isothermal Depletion . . . . .	198

NUMERICAL SIMULATION OF THE N.E. HITCHCOCK FIELD  
GALVESTON COUNTY, TEXAS

ABSTRACT

The natural gas industry has numerous natural gas fields that have watered-out before full reserve recovery could be achieved. In many of these fields, substantial volumes of gas reserves have been left behind. Whether or not the remaining reserves in these fields can be recovered depends upon the operator's ability to economically co-produce large volumes of gas and water.

The Northeast Hitchcock Field of Galveston County, Texas is a retrograde-gas field where excessive water production has caused the abandonment of several wells. Currently, four wells are producing from this field and a fifth well has just been placed on production. One of the current producers is a well which was abandoned in 1977 because excessive water production made the well uneconomic to produce. This well has been returned to commercial production by co-producing the gas and water at high rates. Determination of the economic viability of co-producing wells requires economic analyses of the projected future production from these wells. The following report delineates the status of The University of Texas' reservoir simulation study to project the future performance of the Northeast Hitchcock Field.

NUMERICAL SIMULATION OF THE NORTHEAST HITCHCOCK FIELD

GALVESTON COUNTY, TEXAS

1. INTRODUCTION

The primary objective of this report is to present the results of work done by the University of Texas towards numerically simulating the future performance of the Northeast Hitchcock Field. The assumptions and the accuracy of the data used in developing these results are important because the end use will be a performance prediction that will be used to assess the economic viability of increasing reserve recovery from the Northeast Hitchcock Field by co-producing large volumes of formation water along with formation gas. The very nature of the co-production concept is a high risk venture since it deals with gas wells and/or gas fields where the water production has become so high that continued operations are no longer economic, i.e., "watered-out". The Northeast Hitchcock Field is a field with wells at or approaching watered-out status.

The D.O.E. "BOAST" numerical simulator<sup>1</sup> is being used to develop a forecast of future production from the Northeast Hitchcock Field. This goal is being carried out by completing the objective as four separate tasks. These tasks are to:

1. Obtain a geologic description of the field and model the field's physical dimensions through grid block configurations.
2. Gather and determine the reservoir fluid properties and the petrophysical fluid properties of the reservoir rock.
3. Use and adjust the reservoir properties and the reservoir grid block configurations to simulate a match of historical pressures.

4. Use the reservoir description having the best pressure match to simulate the future performance of the Northeast Hitchcock Field.

This report details the assumptions, the work, and the results obtained from working on tasks 1, 2, and 3. At the present time, satisfactory matches of historical pressures have not been developed. Hence, no predictions of future performance of the Northeast Hitchcock Field are available. Performance predictions will be forthcoming in a final report, after satisfactory matches of historical pressure have been achieved.

The remainder of this report details the assumptions, the work and the results obtained from work on the first three tasks.

## 2. NORTHEAST HITCHCOCK FIELD GEOLOGY AND THE PHYSICAL DIMENSIONS OF THE RESERVOIR

### 2.1 Geology

The Northeast Hitchcock Field is located in Galveston County and is immediately south of the towns of Hitchcock and La Marque. Production is from the Frio "A" sand, which is located approximately 9100 feet below sea level. The NE Hitchcock (Frio) reservoir is situated on a northwest plunging anticline that is truncated on the southeast by a regional fault. Correlation analyses of the open hole logs in the field indicate that several smaller faults exist throughout the reservoir which were created by larger regional faults along the Gulf Coast.

A structure map depicting the top of the Frio pay zone in the Northeast Hitchcock Field can be seen on Figure 1. This map provides an estimate of the location of secondary faults which were created when the larger regional fault, trending in a northeast direction, developed. Also indicated on Figure 1 is the estimated location of the original gas-water

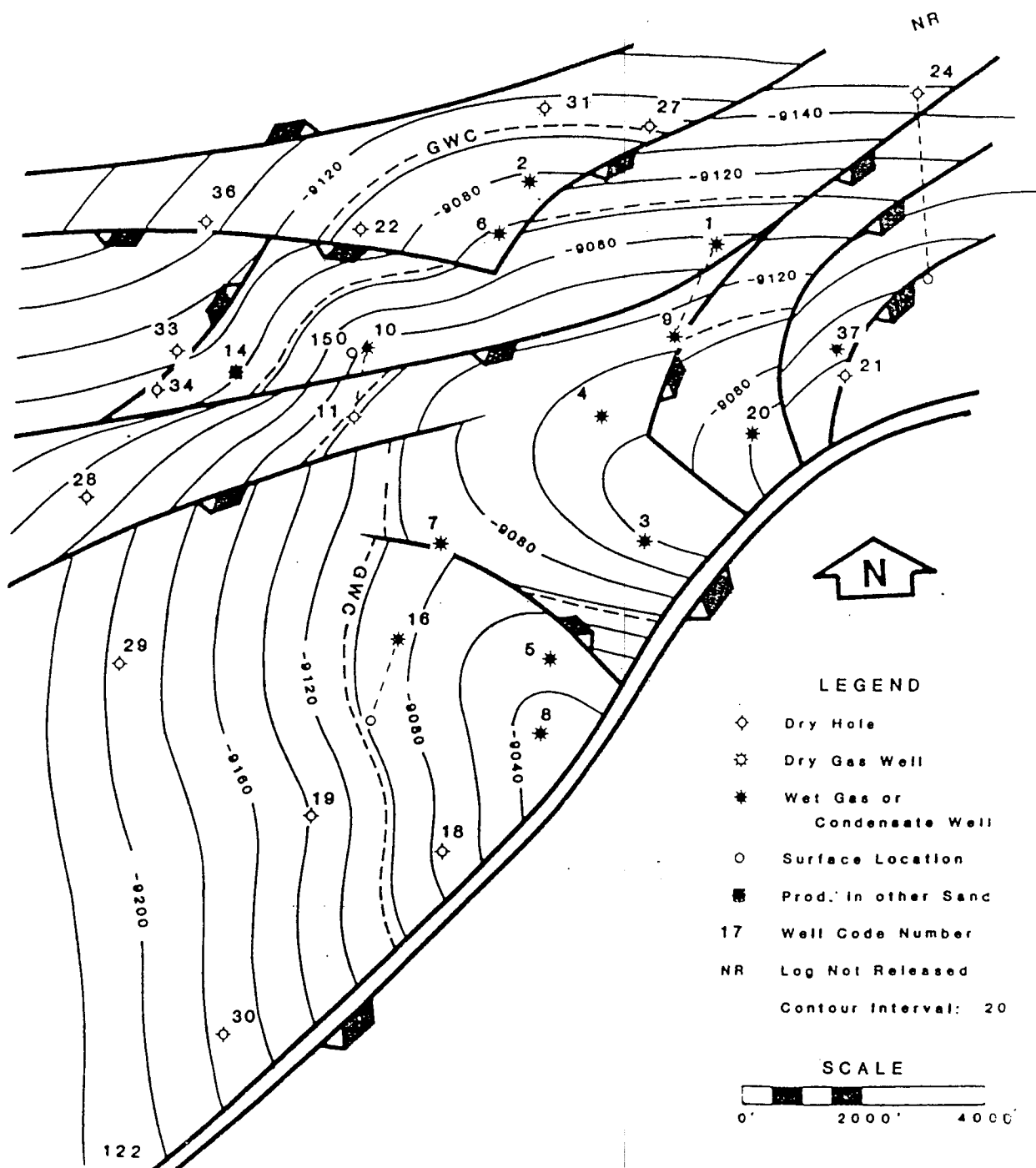


Figure 1. Structure Map of the Top of the Pay in the Northeast Hitchcock Field.<sup>3</sup>

contacts throughout the field. Analyses of the electric logs in the field indicate that the original subsea depth of the gas-water contact was around 9106 feet subsea,<sup>2</sup> as indicated on the structure map. (See Figure 2).

The depositional environment of the Frio "A" reservoir consists primarily of delta front and distributary mouth bar sands. The pay zone of the reservoir is overlain by approximately 2000 feet of Anahuac shale whereas nearly 3000 feet of Frio shale lies at the base of the Frio pay. A map depicting how the gross pay of the Frio "A" sand is distributed throughout the field is attached as Figure 3. Figure 4 presents an isopach map of the net gas sand in the Northeast Hitchcock Field. The net pay thickness for this map was derived by subtracting out the pay intervals containing shale streaks and the streaks of very tight reservoir rock from the gross pay. The net pay determination was made through the use of core data and well logs of the wells in the field.

## 2.2 Northeast Hitchcock Field Reservoir

The Northeast Hitchcock Field was discovered in September of 1957 as an over-pressured, gas-condensate reservoir. In the period from September 1957 to January 1982, twelve wells were drilled and completed in the field. Additional development began with the implementation of co-production, and the thirteenth well was drilled and completed in February 1985. As of June 1985, only five wells were producing from the Northeast Hitchcock Field. The locations of these wells are indicated on Figures 1, 3, and 4. The well name, operator, and the well code number, as used by this report, for each well in the field are detailed on Table 1.

A reservoir fluid study performed in 1959 on a recombined sample indicated that the Northeast Hitchcock Field reservoir fluid exhibits

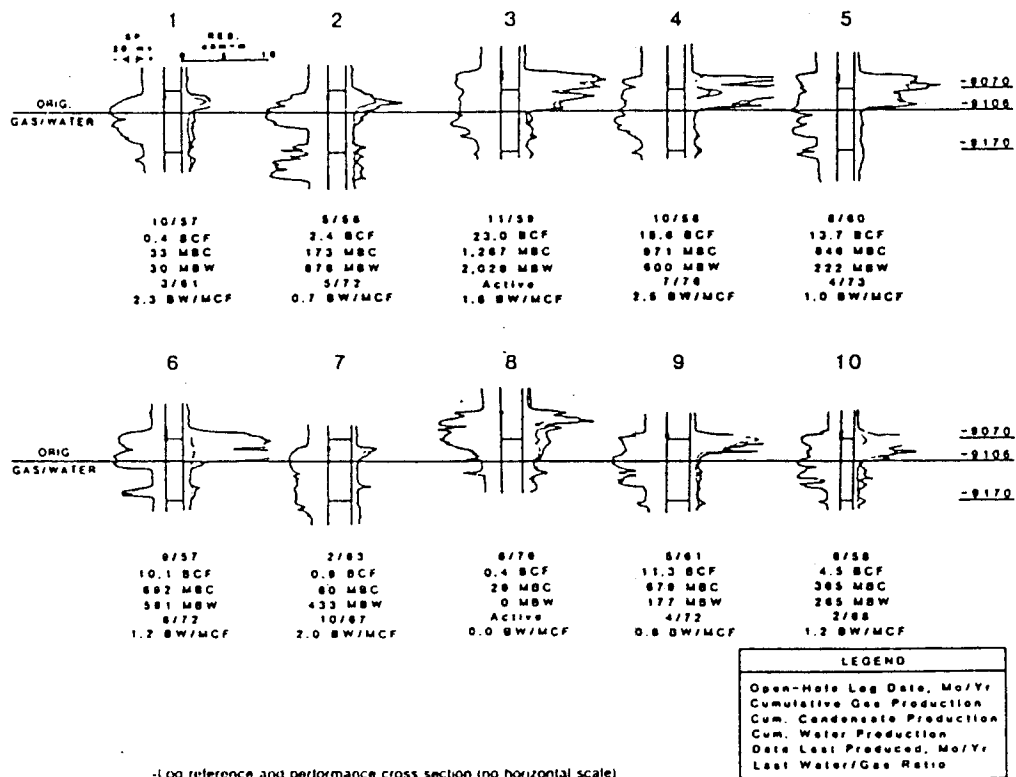


Figure 2. Structural Cross-Section Depicting the Original Gas-Water Contact in the Northeast Hitchcock Field.<sup>2</sup>

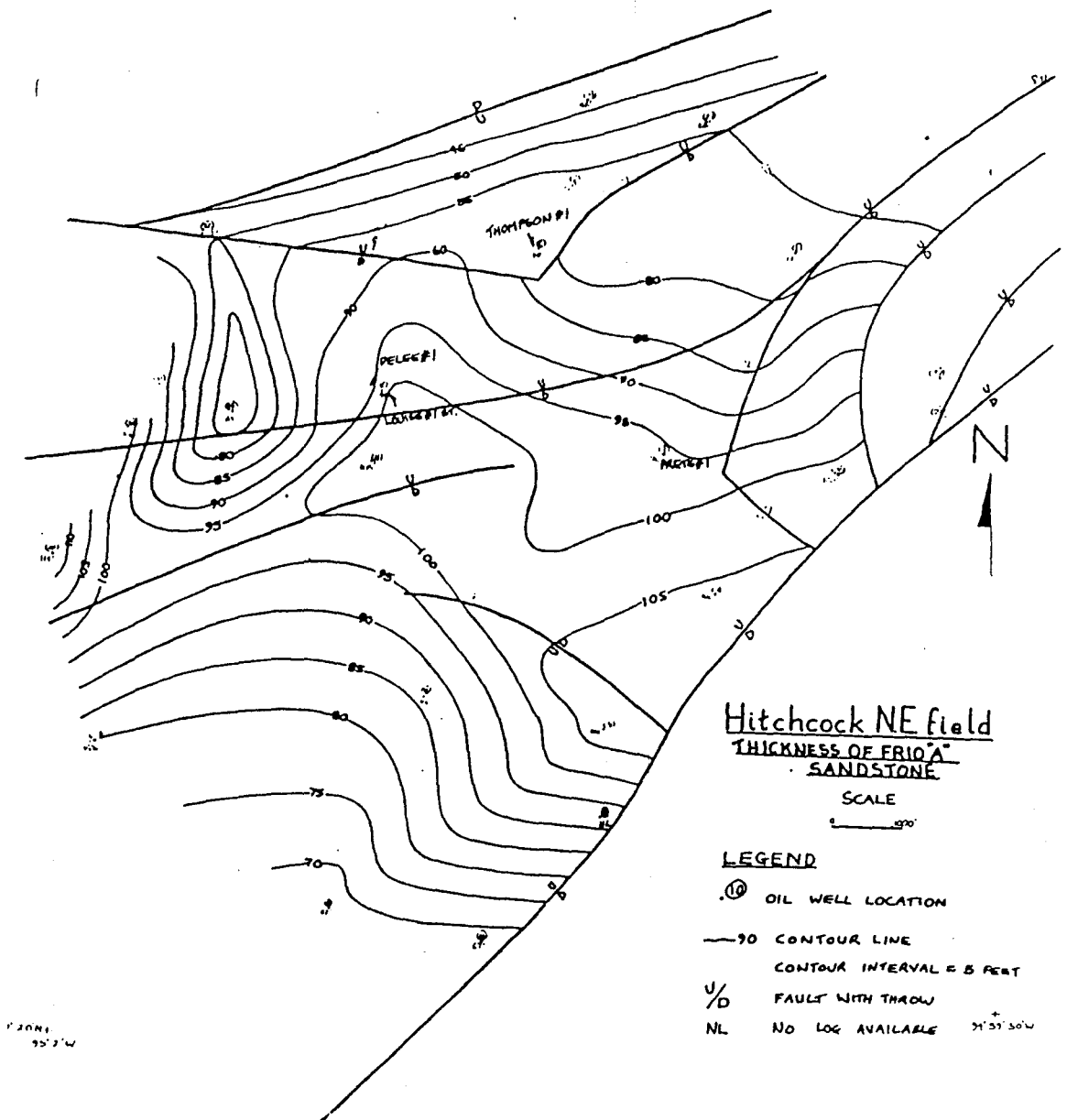
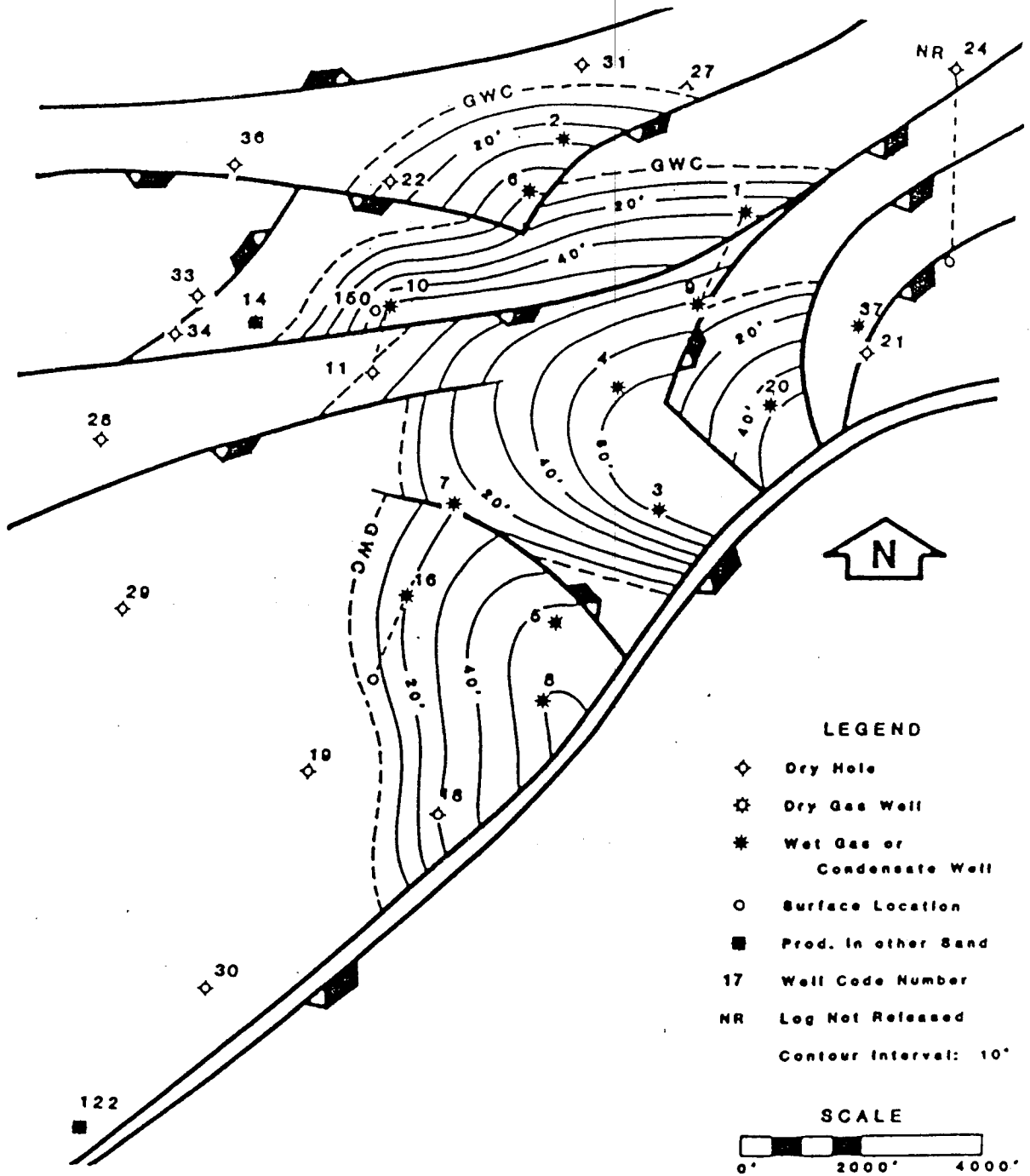


Figure 3. Isopach of the Gross Pay in the Frio "A" Sand of the Northeast Hitchcock Field.<sup>10</sup>



Isopach map of original net gas sand.

Figure 4. Isopach of the Net Pay in the Frio "A" Sand of the Northeast Hitchcock Field. <sup>3</sup>

TABLE 1

LIST OF WELL CODE NUMBERS, OPERATOR AND WELL NAME

<u>Well Code Number</u>	<u>Operator</u>	<u>Well Name</u>
1	Phillips Petroleum Co.	Davis "D" No. 1
2	Phillips Petroleum Co.	Delaney No. 1
3	Phillips Petroleum Co.	Huff "A" No. 1
4	Phillips Petroleum Co.	Pretts No. 1
5	Phillips Petroleum Co.	Sundstorm A No. 1
6	Phillips Petroleum Co.	Thompson Trustee No. 1
7	John W. Mecom	Kipfer Et Al Unit No. 1
8	Unknown	Unknown
9	Phillips Petroleum Co.	Davis "D" No. 1
10	Phillips Petroleum Co.	Louise "A" Unit No. 1
16	Phillips Petroleum Co.	Lasalo No. 1
20	Cockrell Corporation	Lowel Lemm No. 1

retrograde behavior. Subsequent pressure surveys in the field revealed that the aquifer underlying the field was providing pressure support to the reservoir. Estimates of the reservoir properties for both the hydrocarbon reservoir and the underlying aquifer are listed on Table 2.

### 2.3 Reservoir Dimensions

The simulation of the Northeast Hitchcock Field was limited to an areal study where the properties of the reservoir were allowed to vary along an X-Y axis projected upon the horizontal surface of the field. The structure map of the top of the Frio "A" sand was used to define the grid block representation of the reservoir. Figure 5 illustrates how the grid block configuration approximates the areal shape of the reservoir. This figure also reveals that the entire field was modeled using a grid block configuration that is 30 x 25 units in dimension. The individual grid blocks used in the hydrocarbon portion of the reservoir are all of equal size and have physical dimensions of 588.2 feet by 588.2 feet.

The properties of the reservoir which varied in the vertical direction were the amount of net gas sand, gross sand thickness, and the level of the gas-water contact. The amount of net gas sand for each grid block was determined from the isopach map of the original net gas sand. The net gas sand was defined as the amount of productive, hydrocarbon-filled reservoir rock above the gas-water contact. The gross sand thickness and the level of the gas-water contact were used to determine the amount of net pay which is connected between faults and was used to define the amount of reservoir rock in the aquifer which is interconnected between faults. Structural cross-sections were created to make these determinations and some of them are included in Appendix A.

TABLE 2

HYDROCARBON RESERVOIR AND AQUIFER PROPERTIES<sup>3</sup>

Pay Zone, at Discovery	
Pressure datum, ft subsea	9,070
Productive area, acres	1,450
Average net pay, ft	31
Productive gas volume, acre-ft	44,880
Porosity, % of bulk volume	30
Pore volume, Mbbl	104,450
Water saturation, % of bulk volume	25
Gas pore volume, Mbbl	78,340
Gas in place, MMcf @ 14.65 psia & 60°F	125,810
Condensate in place, MSTB	12,580
Gas, at Discovery	
Pressure at datum, psia	5,750
Temperature at datum, °F	216
Gas gravity, full wellstream (Air = 1.0)	0.94
Gas formation volume factor, Mcf/res bbl	1.606
Gas composition	Table 3
Condensate content, STB/MMcf	100
Condensate gravity, API	52.8
Cumulative production, 7-1-84	
Gas, MMcf	84,470
Condensate and oil, MSTB	5,265
Water, Mbbl	7,990
Producing Rate, First half of 1984	
Gas, Mcf per day	2,200
Condensate and oil, STB per day	129
Water, Bbl per day	5,814
Gross producing well count during period	5
Aquifer, at Discovery	
Productive area, acres	17,760
Average net sand, ft	70.4
Net volume, acre-feet	1,249,760
Porosity, % of net volume	32
Pore volume, Mbbl	3,100,000
Total dissolved solids in brine, ppm	40,000
Compressibility, 1/psi	
Above hydrostatic pressure	12E-6
Below hydrostatic pressure	6E-6

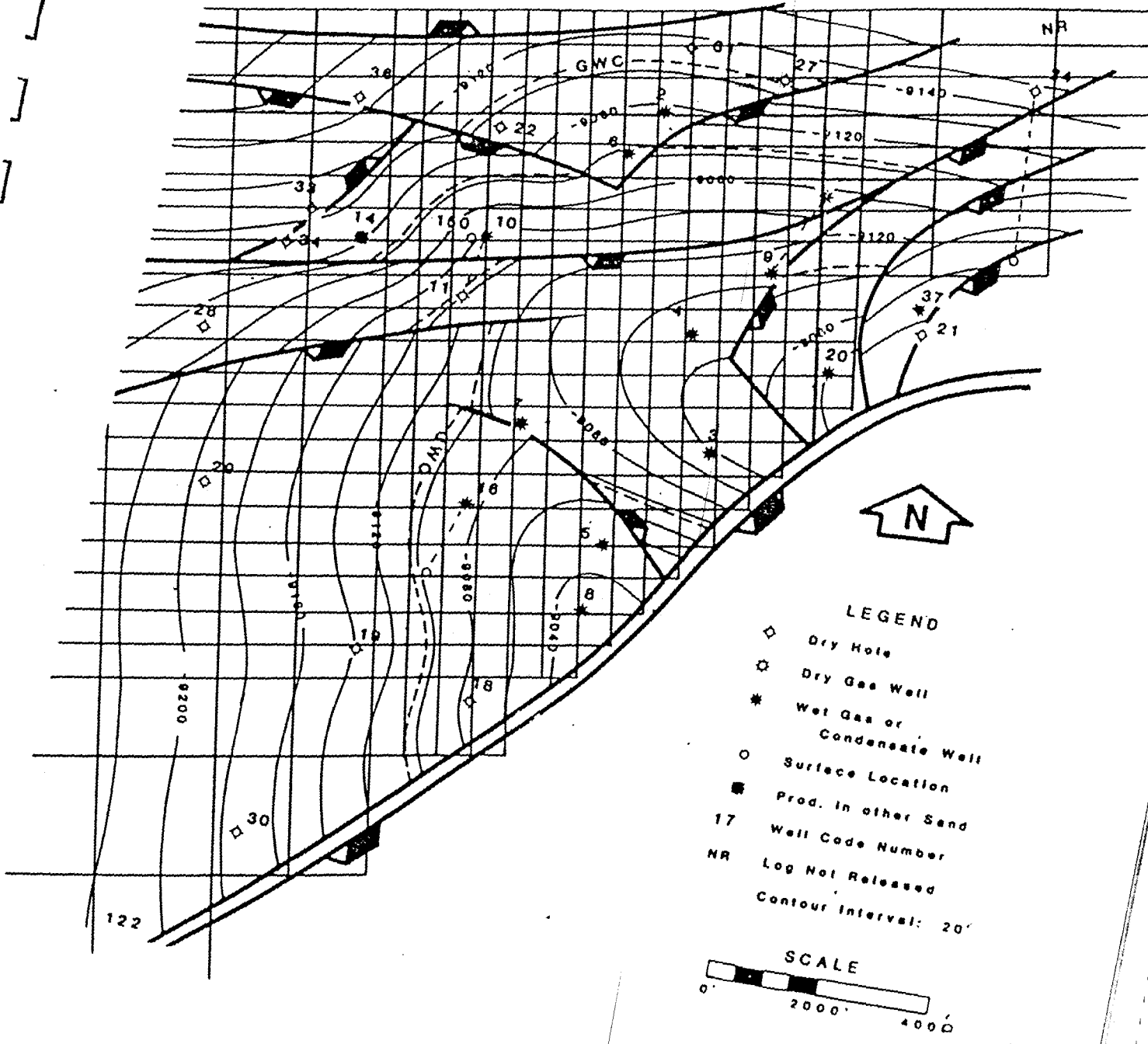


Figure 5. Grid Block Configuration of the Northeast Hitchcock Field

## 2.4 Aquifer Dimensions

The small decrease in reservoir pressure, along with large volumes of gas, condensate, and water production, gave indications that the aquifer underlying the Northeast Hitchcock Field was providing pressure support to the reservoir. The production histories of the Northeast Hitchcock Field in terms of condensate/gas ratio, subsurface pressures, and full wellstream gas production are listed in Tables 3, 4, and 5, respectively. The water production history of the field is listed in Table 6.

Studies were made to evaluate the size and effect of the aquifer prior to simulating the future performance of the field. Water influx calculations were made using the method of Fetkovitch.<sup>2,3</sup> The results of this analysis indicated that the aquifer volume should be approximately thirty times the size of the hydrocarbon reservoir volume. This aquifer volume was taken into account in the grid block configuration by increasing the size of the grid blocks which were lying outside of the hydrocarbon reservoir. More details concerning how much of an effect the aquifer has had on the reservoir pressures in the Northeast Hitchcock Field are delineated in the section describing efforts to match historical pressures.

## 3. FLUID DATA, PETROPHYSICAL DATA AND ITS USE AS INPUT DATA

### 3.1 Fluid Data

As early as September of 1959, it was known that the reservoir fluid of the Northeast Hitchcock Field was a retrograde condensate system. This information was disclosed through the only complete reservoir fluid analysis for the field, which was performed by P-V-T, Inc., Petroleum Analysts of Houston, Texas, on September 29, 1959.<sup>11</sup> The study was performed on a recombined sample from the Phillips Petroleum Company's

TABLE 3 - CONDENSATE/GAS RATIO HISTORY

STB Condensate/MMcf Full Well Stream Gas by Well													
Yr-Half	1	2	3	4	5	6	7	8	9	10	16	20	Total
58-2	96	92	--	92	--	93	--	--	--	94	--	--	93
59-1	92	90	--	94	--	98	--	--	--	94	--	--	95
59-2	88	86	--	94	--	86	--	--	--	84	--	--	87
60-1	90	87	88	92	--	99	--	--	--	92	--	--	93
60-2	84	85	86	86	86	91	--	--	--	93	--	--	88
61-1	91	83	86	84	85	92	--	--	71	89	--	--	86
61-2	--	84	85	86	87	88	--	--	80	91	91	--	86
62-1	--	83	80	81	83	83	--	--	80	85	87	--	82
62-2	--	103	82	77	85	84	--	--	77	90	94	--	85
63-1	--	77	76	67	77	80	86	--	75	90	95	--	78
63-2	--	74	72	58	77	72	76	--	78	88	108	--	74
64-1	--	82	72	53	76	73	76	--	70	85	101	--	73
64-2	--	70	67	52	73	70	73	--	72	83	69	--	69
65-1	--	68	60	63	67	68	71	--	66	76	45	--	66
65-2	--	68	63	61	65	65	68	--	65	74	--	--	65
66-1	--	57	60	61	63	61	53	--	62	67	--	--	62
66-2	--	54	58	57	60	63	57	--	61	59	--	--	63
67-1	--	47	56	54	57	55	45	--	57	56	--	--	56
67-2	--	43	54	51	53	48	33	--	56	35	--	--	52
68-1	--	36	52	51	55	50	--	--	50	22	--	--	51
68-2	--	31	52	46	56	58	--	--	49	--	--	--	51
69-1	--	38	49	43	47	45	--	--	53	--	--	--	48
69-2	--	36	47	42	48	33	--	--	53	--	--	--	47
70-1	--	36	47	45	49	119	--	--	40	--	--	--	48
70-2	--	51	45	42	60	33	--	--	32	--	--	--	46
71-1	--	38	45	42	64	56	--	--	44	--	--	--	47
71-2	--	44	46	41	65	40	--	--	79	--	--	--	46
72-1	--	38	47	44	52	42	--	--	56	--	--	--	46
72-2	--	--	45	43	39	--	--	--	--	--	--	--	44
73-1	--	--	54	30	56	--	--	--	--	--	--	--	46
73-2	--	--	44	51	--	--	--	--	--	--	--	--	46
74-1	--	--	45	49	--	--	--	--	--	--	--	--	46
74-2	--	--	48	68	--	--	--	--	--	--	--	--	50
75-1	--	--	56	31	--	--	--	--	--	--	--	--	52
75-2	--	--	55	56	--	--	--	--	--	--	--	--	56
76-1	--	--	55	57	--	--	--	--	--	--	--	--	56
76-2	--	--	56	76	--	--	--	--	--	--	--	--	56
77-1	--	--	57	--	--	--	--	--	--	--	--	--	57
77-2	--	--	57	--	--	--	--	--	--	--	--	--	58
78-1	--	--	55	--	--	--	--	--	--	--	--	--	55
78-2	--	--	64	--	--	--	--	--	--	--	--	--	64
79-1	--	--	71	--	--	--	--	--	--	--	--	--	70
79-2	--	--	64	--	--	--	--	--	--	--	--	--	64
80-1	--	--	70	--	--	--	--	57	--	--	--	--	66
80-2	--	--	68	--	--	--	--	63	--	--	--	--	66
81-1	--	--	73	--	--	--	--	60	--	--	--	--	61
81-2	--	--	68	--	--	--	--	73	--	--	--	--	71
82-1	--	--	75	--	--	--	--	68	--	--	--	55	61
82-2	--	--	61	--	--	--	--	69	--	--	--	43	52
83-1	--	--	53	125	--	--	--	79	--	--	--	30	66
Average	90	74	55	52	62	69	68	67	60	81	92	45	60

TABLE 4 - SUBSURFACE PRESSURE DATA

Subsurface pressure adjusted to 9070 feet subsea, psia								
Mo/Yr	Well 1	Well 2	Well 3	Well 4	Well 5	Well 6	Well 9	Average
09/57	--	--	--	--	--	5741	--	5741
12/57	5752	--	--	--	--	--	--	5752
05/58	--	5651	--	--	--	--	--	5651
12/58	--	--	--	5629	--	--	--	5629
04/59	5577	5566	--	5595	--	5573	--	5578
10/59	5517	5530	--	5542	--	5534	--	5531
01/60	--	--	5519	--	--	--	--	5519
09/60	5379	5384	--	--	5417	--	--	5393
01/61	5288	5300	5316	5316	5318	5296	--	5306
08/61	--	5283	5306	5311	5291	5316	--	5301
02/62	--	--	--	--	--	5229	--	5229
05/62	--	5222	5206	5216	5216	5198	5232	5215
07/62	--	--	--	--	--	5217	--	5217
08/62	--	--	--	--	--	5210	--	5210
10/62	--	--	--	--	5180	5172	--	5176
11/62	--	--	--	--	--	5146	--	5146
12/62	--	--	--	--	--	5168	--	5168
02/63	--	--	--	--	--	5125	--	5125
03/63	--	--	--	--	--	5103	--	5103
05/63	--	--	--	--	--	--	5031	5031
01/64	--	--	--	--	--	4908	4938	4923
08/64	--	--	--	4786	--	--	--	4786
12/64	--	--	--	--	4741	--	4752	4747
07/65	--	--	4621	--	--	--	--	4621
12/65	--	4558	--	4530	--	--	--	4544
04/66	--	--	--	4519	--	4504	--	4512
10/66	--	4425	--	--	4440	--	4432	4432
02/67	--	--	--	4343	--	--	--	4343
07/67	--	--	--	4274	--	--	--	4274
10/68	--	--	4106	--	4095	--	--	4100
10/69	--	--	--	3988	--	--	--	3988
07/70	--	--	3935	--	--	--	--	3935
03/71	--	--	--	--	--	3895	--	3895
04/72	--	--	--	--	3877	3884	3859	3875
05/72	--	3850	3854	3861	--	--	--	3855
08/73	--	--	--	3874	--	--	--	3874
01/74	--	--	--	3857	--	--	--	3857
05/76	--	--	--	3965	--	--	--	3965
08/81	--	--	4126	--	--	--	--	4126

SOURCE: Anderson, L.L., Peterson, K.P., and Parisi, W.A., "Enhanced Production from a Slightly Geopressured Water-Drive Gas Condensate Field," Proceedings 1984 Unconventional Gas Recovery Symposium, Pittsburgh, Pa., May 13-15, 1984 (SPE/DOE/GRI 12866) pp. 341-350.

TABLE 5 - GAS PRODUCTION HISTORY

Yr-Half	Mcf/Day Full Wellstream Gas by Well												Total
	1	2	3	4	5	6	7	8	9	10	16	20	
58-2	502	213	--	317	--	1,326	--	--	--	954	104	--	3,512
59-1	538	429	--	1,580	--	2,519	--	--	--	571	--	--	5,637
59-2	130	142	--	351	--	413	--	--	--	131	--	--	1,167
60-1	295	357	191	498	--	570	--	--	--	454	--	--	2,365
60-2	509	1,414	2,235	2,520	1,780	2,678	--	--	--	2,112	--	--	13,248
61-1	38	888	1,450	848	1,689	1,669	--	--	111	544	--	--	7,237
61-2	--	731	962	792	863	774	--	--	1,121	633	261	--	6,137
62-1	--	949	1,317	1,387	836	618	--	--	906	659	452	--	7,124
62-2	--	695	1,402	1,255	1,340	1,259	--	--	1,454	893	687	--	8,985
63-1	--	1,392	2,670	3,038	3,478	3,044	280	--	2,618	2,336	801	--	19,657
63-2	--	1,142	3,090	2,680	2,930	3,613	598	--	3,914	1,969	297	--	20,233
64-1	--	650	3,174	2,526	3,031	2,674	654	--	2,589	2,246	292	--	17,836
64-2	--	426	3,176	2,881	3,233	2,696	587	--	3,051	2,082	269	--	18,401
65-1	--	397	3,274	3,366	3,468	3,443	645	--	3,070	2,220	62	--	19,945
65-2	--	311	3,251	2,911	3,319	3,328	810	--	3,532	2,161	--	--	19,623
66-1	--	295	3,819	3,126	3,762	3,781	609	--	3,604	2,284	--	--	21,280
66-2	--	292	3,973	3,833	3,973	3,876	348	--	3,742	1,403	--	--	21,440
67-1	--	293	4,598	4,470	5,127	4,222	264	--	5,025	679	--	--	24,678
67-2	--	288	4,643	4,669	4,743	3,693	91	--	4,576	433	--	--	23,136
68-1	--	254	5,651	4,131	4,456	2,549	--	--	5,399	37	--	--	22,477
68-2	--	230	5,142	5,133	5,003	2,213	--	--	4,584	--	--	--	22,305
69-1	--	204	5,497	5,361	6,314	1,521	--	--	4,589	--	--	--	23,486
69-2	--	224	5,580	5,691	5,493	734	--	--	3,748	--	--	--	21,170
70-1	--	187	6,247	5,550	3,852	515	--	--	2,090	--	--	--	18,441
70-2	--	153	5,963	5,590	2,794	441	--	--	896	--	--	--	15,837
71-1	--	169	5,545	5,360	1,697	305	--	--	552	--	--	--	13,628
71-2	--	120	5,710	5,883	567	269	--	--	441	--	--	--	12,990
72-1	--	66	6,144	5,860	342	241	--	--	151	--	--	--	12,804
72-2	--	--	6,311	5,292	763	--	--	--	--	--	--	--	12,366
73-1	--	--	4,637	2,336	240	--	--	--	--	--	--	--	7,213
73-2	--	--	3,453	1,359	--	--	--	--	--	--	--	--	4,812
74-1	--	--	2,790	702	--	--	--	--	--	--	--	--	3,492
74-2	--	--	2,213	226	--	--	--	--	--	--	--	--	2,439
75-1	--	--	1,735	300	--	--	--	--	--	--	--	--	2,035
75-2	--	--	1,370	212	--	--	--	--	--	--	--	--	1,582
76-1	--	--	1,278	139	--	--	--	--	--	--	--	--	1,417
76-2	--	--	1,123	6	--	--	--	--	--	--	--	--	1,129
77-1	--	--	1,043	--	--	--	--	--	--	--	--	--	1,043
77-2	--	--	848	--	--	--	--	--	--	--	--	--	848
78-1	--	--	759	--	--	--	--	--	--	--	--	--	759
78-2	--	--	653	--	--	--	--	--	--	--	--	--	653
79-1	--	--	356	--	--	--	--	--	--	--	--	--	356
79-2	--	--	408	--	--	--	--	--	--	--	--	--	408
80-1	--	--	252	--	--	--	174	--	--	--	--	--	426
80-2	--	--	466	--	--	--	556	--	--	--	--	--	1,022
81-1	--	--	60	--	--	--	463	--	--	--	--	--	523
81-2	--	--	122	--	--	--	356	--	--	--	--	--	478
82-1	--	--	214	--	--	--	530	--	--	--	1,072	--	1,816
82-2	--	--	911	--	--	--	320	--	--	--	1,582	--	2,813
83-1	--	--	987	470	--	--	265	--	--	--	516	--	2,238
Cum. MMcf	367	2,356	23,176	18,733	13,705	10,071	892	486	11,272	4,526	570	579	86,733

SOURCE: Anderson, L.L., Peterson, K.P., and Parisi, W.A., "Enhanced Production from a Slightly Geopressured Water-Drive Gas Condensate Field," Proceedings 1984 Unconventional Gas Recovery Symposium, Pittsburgh, Pa., May 13-15, 1984 (SPE/DOE/GRI 12866) pp. 341-350.

TABLE 6 - WATER PRODUCTION HISTORY

Yr-Half	Barrels Water/Day by Well												Total
	1	2	3	4	5	6	7	8	9	10	16	20	
58-2	--	--	--	--	--	--	--	--	--	--	--	--	0
59-1	--	--	--	--	--	1	--	--	--	3	--	--	4
59-2	11	--	--	--	--	0	--	--	--	0	--	--	11
60-1	21	--	--	--	--	0	--	--	--	0	--	--	21
60-2	48	58	2	2	--	2	--	--	--	1	--	--	113
61-1	86	146	0	1	--	3	--	--	--	0	--	--	236
61-2	--	129	1	1	--	0	--	--	--	0	--	--	131
62-1	--	233	2	1	1	0	--	--	--	0	--	--	237
62-2	--	238	1	4	2	3	--	--	1	1	8	--	258
63-1	--	280	2	8	4	6	--	--	2	3	16	--	321
63-2	--	420	2	3	3	3	11	--	1	2	105	--	550
64-1	--	414	0	0	2	0	29	--	1	1	371	--	818
64-2	--	191	1	1	1	0	25	--	1	0	280	--	500
65-1	--	210	1	3	2	1	69	--	110	1	60	--	457
65-2	--	177	1	1	1	1	109	--	2	17	--	--	309
66-1	--	187	3	1	1	1	213	--	2	189	--	--	597
66-2	--	243	1	1	1	10	244	--	3	249	--	--	752
67-1	--	210	1	2	1	99	264	--	14	422	--	--	1,013
67-2	--	219	3	2	8	306	182	--	34	521	--	--	1,275
68-1	--	222	4	2	5	376	--	--	100	40	--	--	749
68-2	--	189	2	1	3	459	--	--	168	--	--	--	822
69-1	--	178	1	1	3	566	--	--	229	--	--	--	978
69-2	--	176	4	1	55	343	--	--	249	--	--	--	825
70-1	--	130	4	2	137	146	--	--	175	--	--	--	594
70-2	--	145	3	1	197	195	--	--	174	--	--	--	715
71-1	--	175	2	1	219	191	--	--	284	--	--	--	872
71-2	--	186	3	1	151	244	--	--	329	--	--	--	914
72-1	--	45	2	5	174	283	--	--	120	--	--	--	629
72-2	--	--	11	0	0	--	--	--	--	--	--	--	11
73-1	--	--	113	395	246	--	--	--	--	--	--	--	754
73-2	--	--	329	815	--	--	--	--	--	--	--	--	1,114
74-1	--	--	262	554	--	--	--	--	--	--	--	--	816
74-2	--	--	362	265	--	--	--	--	--	--	--	--	627
75-1	--	--	262	325	--	--	--	--	--	--	--	--	587
75-2	--	--	322	519	--	--	--	--	--	--	--	--	841
76-1	--	--	716	316	--	--	--	--	--	--	--	--	1,052
76-2	--	--	662	32	--	--	--	--	--	--	--	--	694
77-1	--	--	824	--	--	--	--	--	--	--	--	--	824
77-2	--	--	772	--	--	--	--	--	--	--	--	--	772
78-1	--	--	784	--	--	--	--	--	--	--	--	--	784
78-2	--	--	830	--	--	--	--	--	--	--	--	--	830
79-1	--	--	505	--	--	--	--	--	--	--	--	--	505
79-2	--	--	527	--	--	--	--	--	--	--	--	--	527
80-1	--	--	473	--	--	--	0	--	--	--	--	--	473
80-2	--	--	846	--	--	--	0	--	--	--	--	--	846
81-1	--	--	113	--	--	--	0	--	--	--	--	--	113
81-2	--	--	172	--	--	--	0	--	--	--	--	--	172
82-1	--	--	582	--	--	--	7	--	--	--	0	--	589
82-2	--	--	1,606	--	--	--	5	--	--	--	0	--	1,611
83-1	--	--	1,206	2,078	--	--	49	--	--	--	277	--	3,430
Cum MB	30	876	2,216	979	222	591	209	11	365	265	153	51	5,968

SOURCE: Anderson, L.L., Peterson, K.P., and Parisi, W.A., "Enhanced Production from a Slightly Geopressured Water-Drive Gas Condensate Field," Proceedings 1984 Unconventional Gas Recovery Symposium, Pittsburgh, Pa., May 13-15, 1984 (SPE/DOE/GRI 12866) pp. 341-350.

Thompson Trustee Well No. 1, herein referred to as Well No. 6.

The D.O.E. "BOAST" simulation model was designed to simulate the performance of oil reservoirs where three phases, oil, water, and gas, could be flowing. Oil comprises the major flowing phase. The "BOAST" model was not designed to account for retrograde phenomena but can be modified to simulate the performance of a gas reservoir. In order to use the "BOAST" model to simulate the gas reservoir performance of the Northeast Hitchcock Field, the fluid properties of the water from the aquifer were inputted into the oil property portion and water property portion of the program. The properties of the equilibrium gas were input in the gas phase portion of the program. The input required by the "BOAST" model for these two flowing phase were: the viscosity of the water and the equilibrium gas, the formation volume factors of water and the equilibrium gas, and the equilibrium gas-water ratios of both the flowing and stationary water phases. Plots of the equilibrium gas viscosity versus pressure and water viscosity versus pressure are shown on Figures 6 and 7, respectively. Plots of the formation factors for both the equilibrium gas and water are shown on Figures 8 and 9, respectively. In order to simplify matters, the equilibrium gas-water ratio for both the flowing and stationary water phases were set equal to zero. The fluid property values presented on Figures 6 through 9 were used as the input data in the "BOAST" model. Details concerning how the fluid properties of Figures 6 through 9 were determined can be seen in Appendix B.

### 3.2 Petrophysical Data

Average values for the porosity, connate water saturation, and absolute permeability were assigned to all of the grid blocks within the

FIGURE 6

N. E. HITCHCOCK FIELD  
GAS VISCOSITY VS. PRESSURE

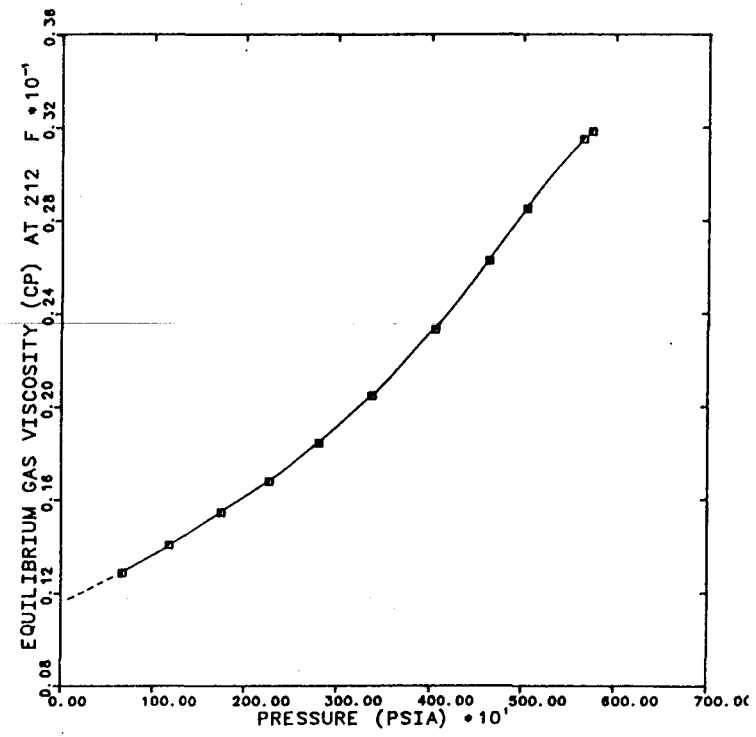


FIGURE 7

N. E. HITCHCOCK FIELD  
WATER VISCOSITY VS. PRESSURE

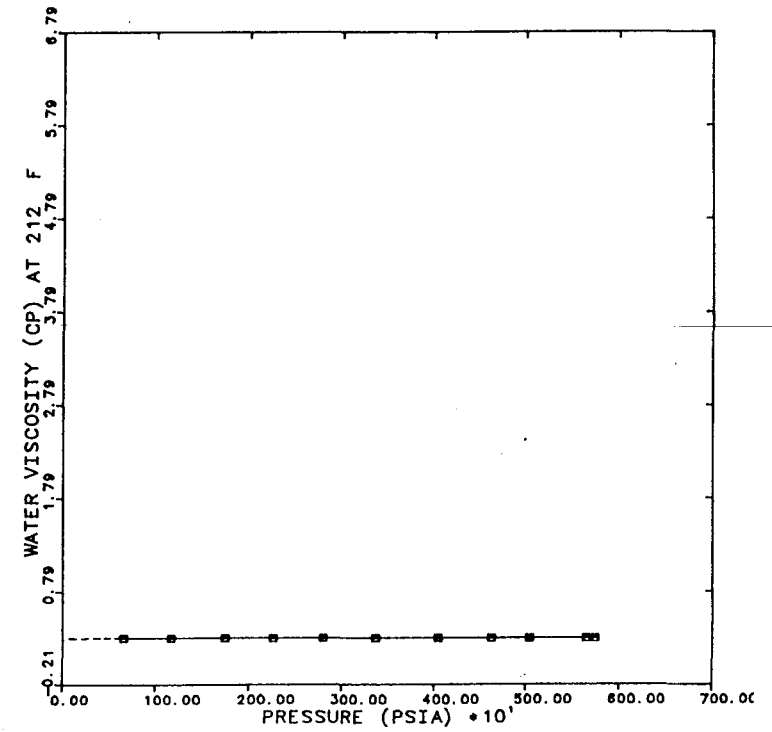


FIGURE 8

N.E. HITCHCOCK FIELD  
 BG (RCF/SCF) VS. PRESSURE

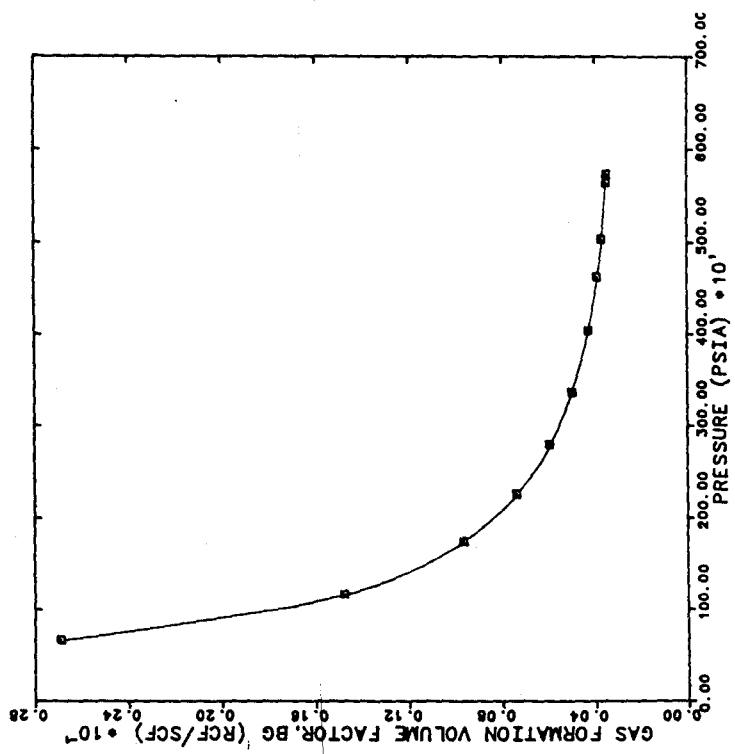
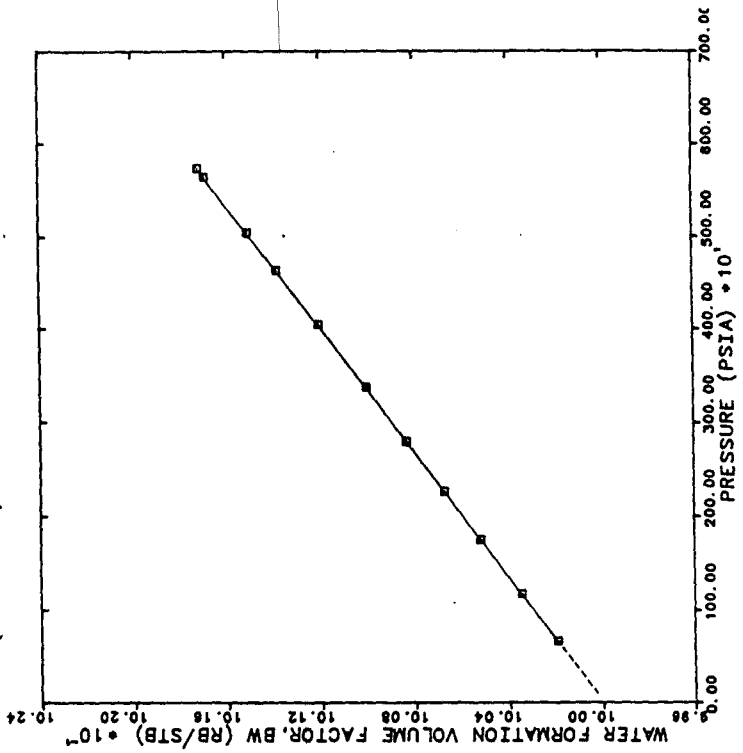


FIGURE 9

N.E. HITCHCOCK FIELD  
 BW (RB/STB) VS. PRESSURE



boundaries of the field. The exception occurred when the grid blocks were used to represent a fault. In these cases, the transmissibility was varied in order to account for complete sealing, partial sealing, or no sealing due to the fault. The average values used as input were as follows:

Porosity	30%
Connate water saturation	25%
Absolute permeability	1000 md (millidarcy) in the X-direction 1100 md in the Y-direction

The interphase behavior of the reservoir fluids within the pore space was defined by the imbibition-capillary pressure curve shown on Figure 10 and the relative permeability curves for gas and water, shown on Figure 11. The imbibition-capillary pressure curve was derived as an average curve for reservoir rock having 1000 md permeability. The data used in this determination were from the drainage capillary pressure curves of the Eaton Operating Co., Inc.'s S.G.R. No. 2 Louise Unit. The drainage capillary pressure curves used in creating Figure 10 had absolute permeabilities of 1120 md and 1140 md. No imbibition-capillary pressure curves were available for verification of the imbibition-capillary pressure curve found in Figure 10. The drainage capillary curves used as a basis for Figure 10 can be seen in Appendix C. The relative permeability curves were derived as average relative permeability curves for 30 percent porosity sands in the Texas Gulf Coast. The end points of the curves were set according to the results found in the March 6, 1985 Special Core Analysis report on the Eaton Operating Co., Inc.'s Louise Unit No. 2. The saturations (endpoint to endpoint) for the gas and water relative permeability curves ranged from 0.2 to 0.75. The residual gas saturation was determined to be 0.2 whereas the residual oil saturation was determined to be 0.25. The

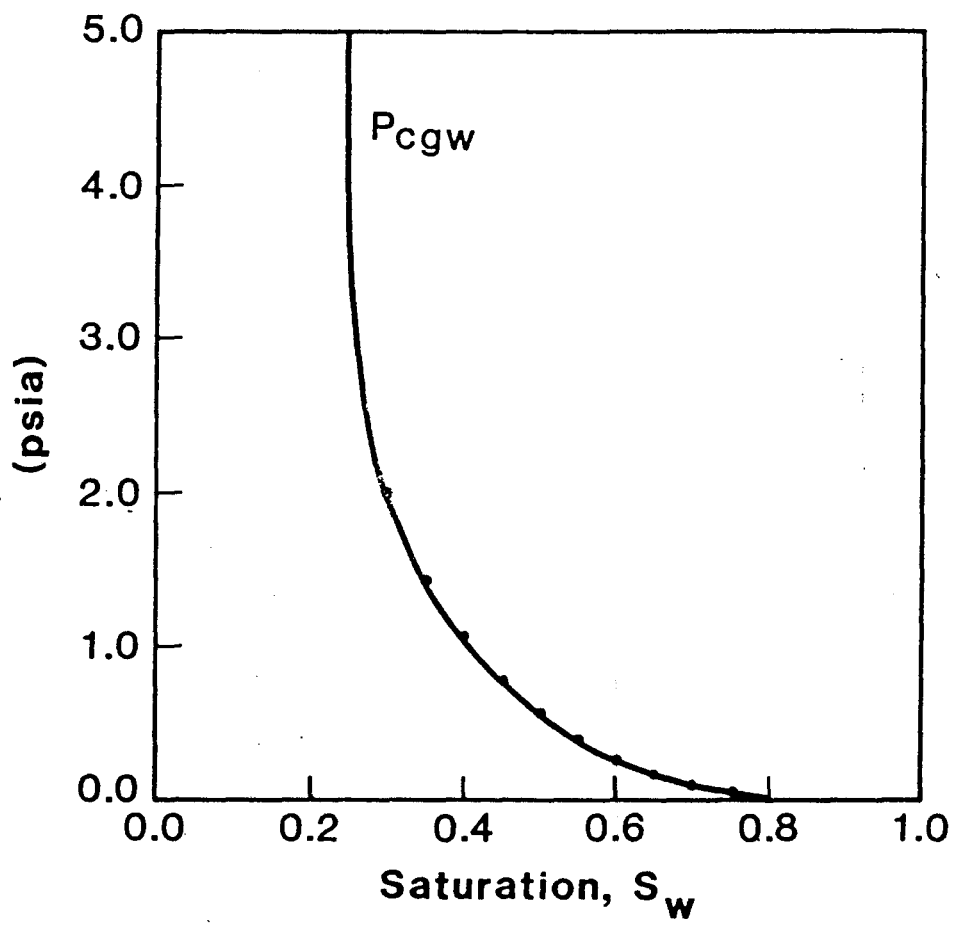


Figure 10. Imbibition-Capillary Pressure Curve  $P_{cgw}$  vs.  $S_w$

relative permeability curves used as input in the "BOAST" model are contained on Figure 11.

A major assumption was made in the decision to use the "BOAST" simulation model to simulate the performance of the Northeast Hitchcock Field. This assumption was that the liquid-dropout phenomenon, common to retrograde gas-condensate reservoirs, was not large enough to significantly reduce the permeability of the reservoir as the reservoir experienced pressure depletion. Two factors led the authors to believe that this assumption was reasonable in light of the quality and type of information available for this study. The first reason was that the aquifer appears to be large enough to prevent the reservoir from having significant pressure reduction before most of the hydrocarbons have been recovered. The second reason was that the maximum amount of liquid dropout is less than 8 percent of the pore space throughout the pressure range likely for pressure depletion. A review of the relative permeability curve for gas (Figure 11) reveals that an 8 percent increase in liquid saturation will have its most drastic effect in reducing the permeability of the rock to gas when the liquid saturation is initially at or near the connate water saturation. Since most of the wells in the field are at or near a watered-out status, the liquid saturation of the reservoir is expected to be close to 70 percent. In this range of liquid saturations on the relative permeability curve, an 8 percent increase in liquid saturation of the pore space would have a relatively insignificant effect on the permeability of the reservoir to gas when compared to the permeability of the reservoir to water. Hence, the liquid dropout phenomena associated with retrograde condensation is not expected to have a notable effect on the future performance of the Northeast Hitchcock Field at present.

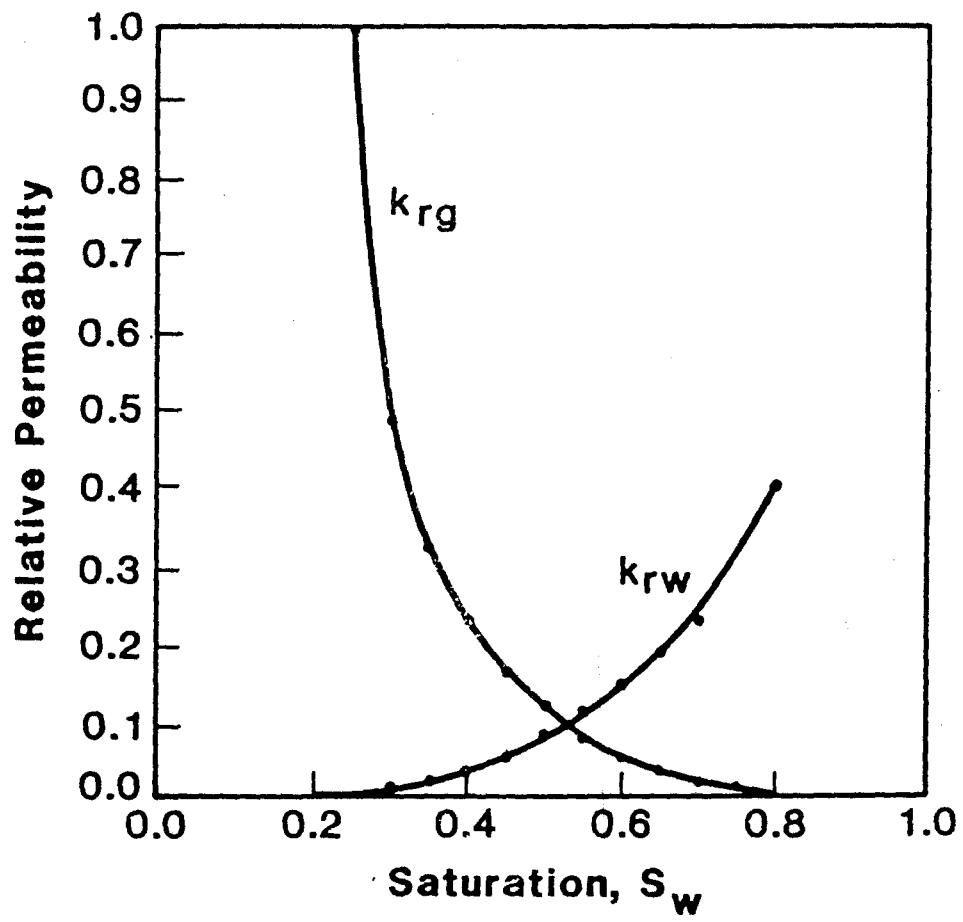


Figure 11. Relative Permeability Curve  $k_{rg}$ ,  $k_{rw}$  vs.  $S_w$

The liquid dropout curve for the Northeast Hitchcock Field's reservoir fluid under conditions similar to the isothermal depletion expected for the Northeast Hitchcock Field can be viewed in Figure 12. Appendix D details the calculations determining the amount of liquid dropout from the equilibrium gas as the reservoir fluid undergoes isothermal depletion.

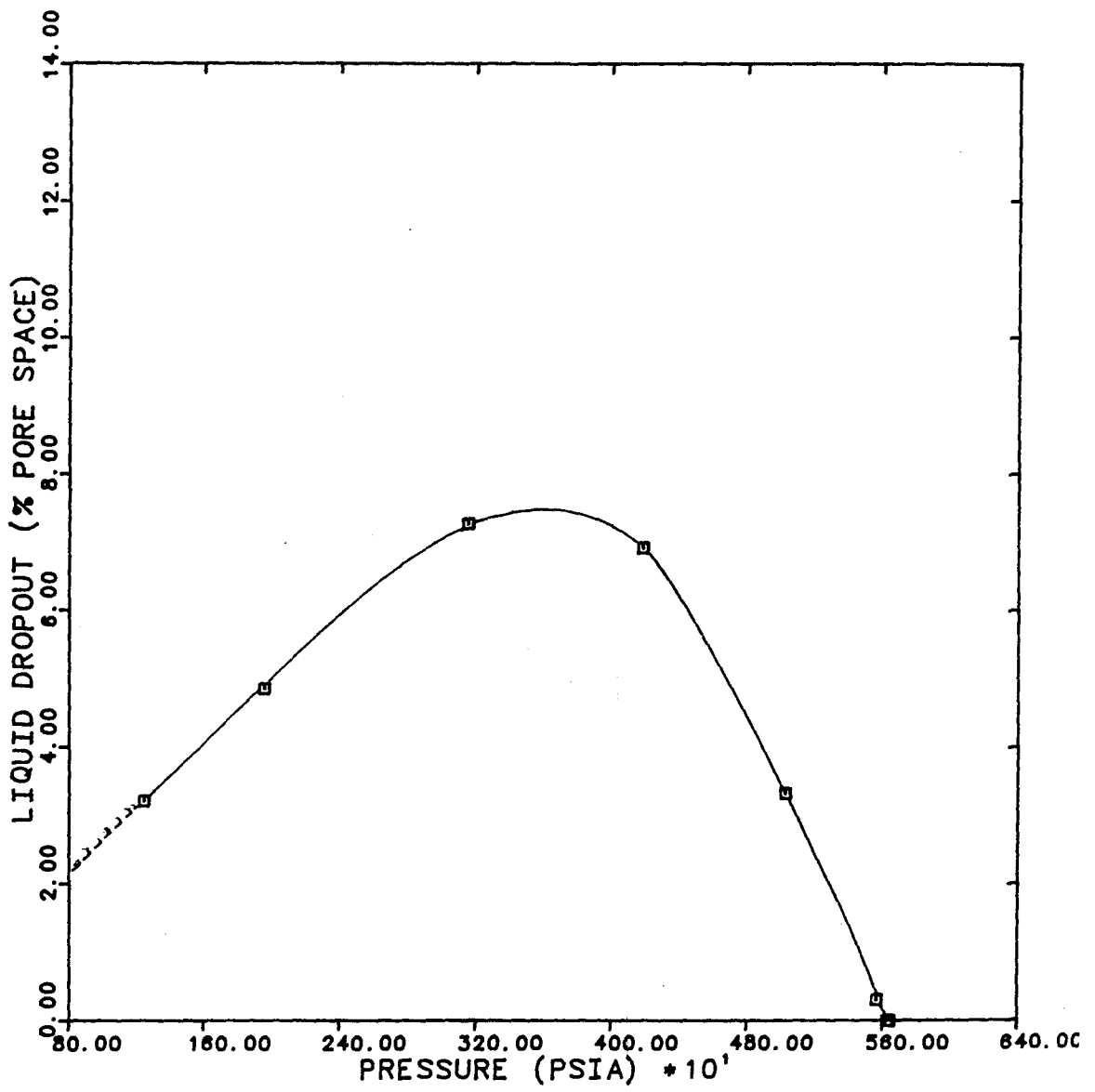


Figure 12. Northeast Hitchcock Field Liquid Dropout vs. Pressure

4. ADJUSTMENT OF RESERVOIR PROPERTIES AND GRID BLOCK CONFIGURATIONS  
TO MATCH HISTORICAL PRESSURES

Early attempts to match historical pressures were limited to evaluating the effects of sealing, partially sealing, and non-sealing faults surrounding the fault block containing Wells No. 2 and No. 6. Simulation runs incorporating totally sealing faults gave pressure histories which fell below historical pressures. This phenomenon suggested that the following could be true of the fault block containing Wells No. 2 and No. 6:

1. The reservoir volume being drained by Well No. 2 and No. 6 is larger than the volume contained within the fault block containing Wells No. 2 and 6.
2. The faults bounding the fault block are not completely sealing.
3. Additional pressure support, as indicated by the historical data, was being provided by the aquifer located outside the fault block.

For the above reasons, subsequent attempts to match historical pressures were made by adjusting the transmissibility between fault blocks. This method gave satisfactory pressure matches of historical data over short periods of time.

The successful results obtained from adjusting the fault block transmissibilities were carried over to the attempts to match historical pressures for the entire field. In the initial attempts to match pressure for the entire field, the hydrocarbon pore volume of the Northeast Hitchcock Field was set at 104,450 thousand reservoir barrels whereas the aquifer volume was set at 620,000 thousand reservoir barrels. Again, several combinations of sealing, partially sealing, and non-sealing faults

were evaluated. As in the single fault block evaluation, simulation runs using totally sealing faults gave pressures which fell below historical data. Simulation runs using both partially sealing and non-sealing faults gave pressures which were higher than historical data. The best pressure match had a maximum variation of 10 psi higher than historical data. All of these attempts to match historical pressures covered a five year period.

When history matching efforts were extended to cover a twelve year period, the simulated pressures during the first five years fell slightly above the historical pressures whereas during the last seven years the simulated pressures fell below historical pressures. Plots comparing simulated pressures to historical pressures for Wells Nos. 2, 3, 4, 5, 6, and 9 are shown on Figure 13 through 18. The downward trend of the simulated pressures from the point where they are higher than historical pressures indicates that the following could be true concerning the underlying aquifer:

1. The aquifer is large enough to prevent the pressure from declining after extended production from the hydrocarbon portion of the reservoir.
2. The permeability of the aquifer restricts flow into the hydrocarbon bearing fault blocks to the extent that pressure support from the aquifer is more dominant at pressures below 4000 psi.

An evaluation of the aquifer was made using the method of Fetkovitch.<sup>2,3</sup> This evaluation revealed that the aquifer was approximately thirty times the size of the hydrocarbon reservoir or five times the aquifer size indicated by the grid blocks shown in Figure 5. More details concerning the use of the method of Fetkovitch are described in Appendix E. The

FIGURE 13

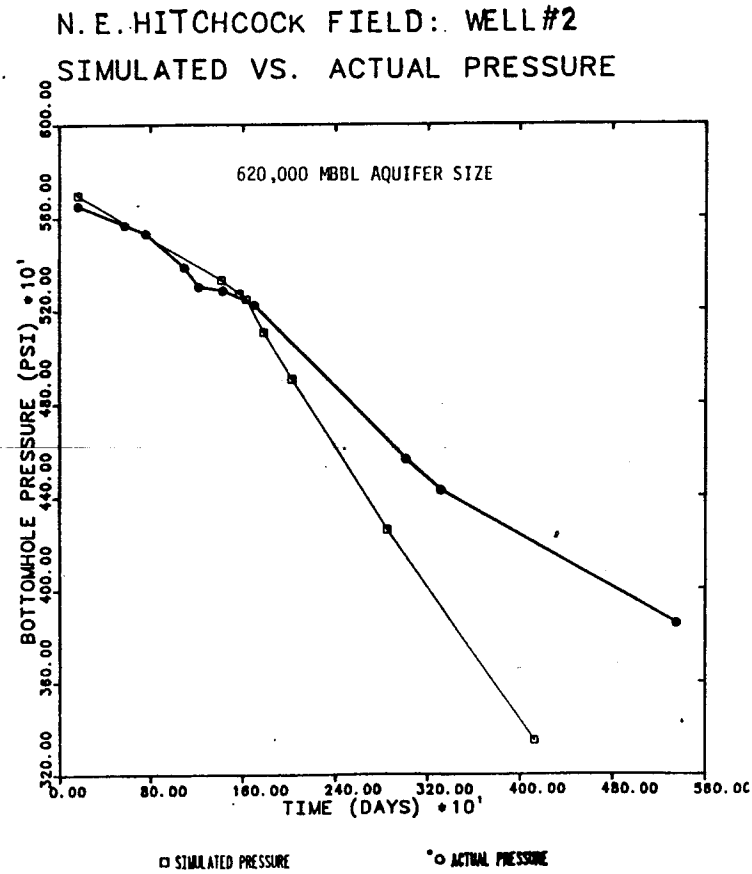


FIGURE 14

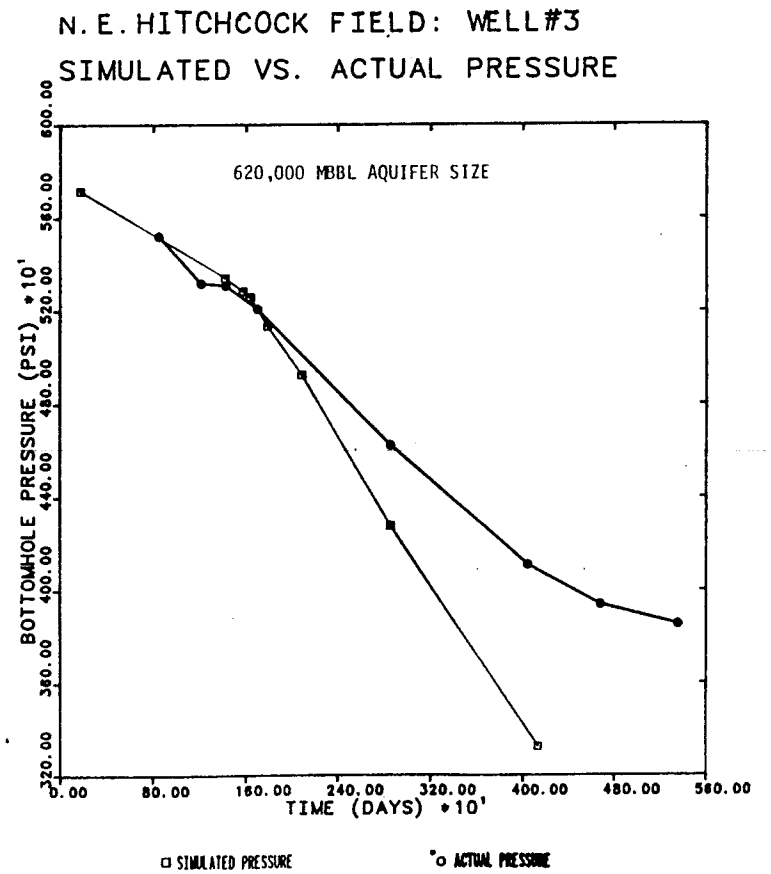


FIGURE 15

N. E. HITCHCOCK FIELD: WELL #4  
SIMULATED VS. ACTUAL PRESSURE

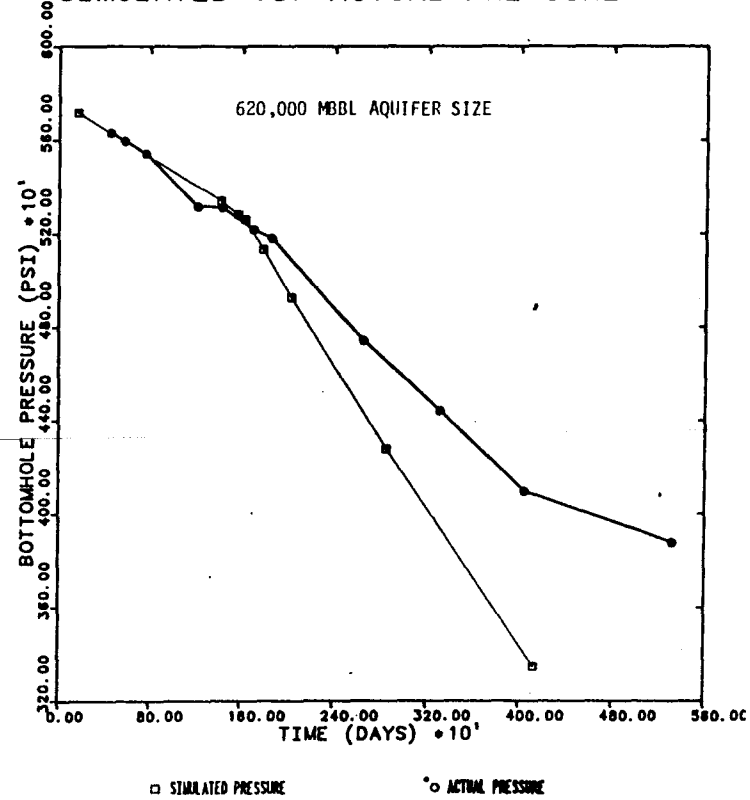


FIGURE 16

N. E. HITCHCOCK FIELD: WELL #5  
SIMULATED VS. ACTUAL PRESSURE

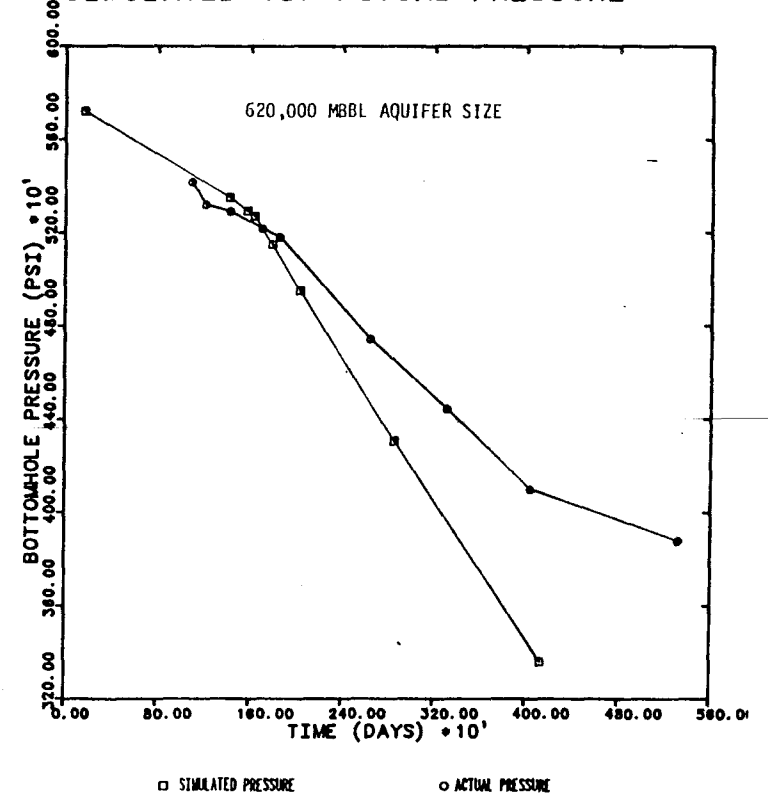


FIGURE 17

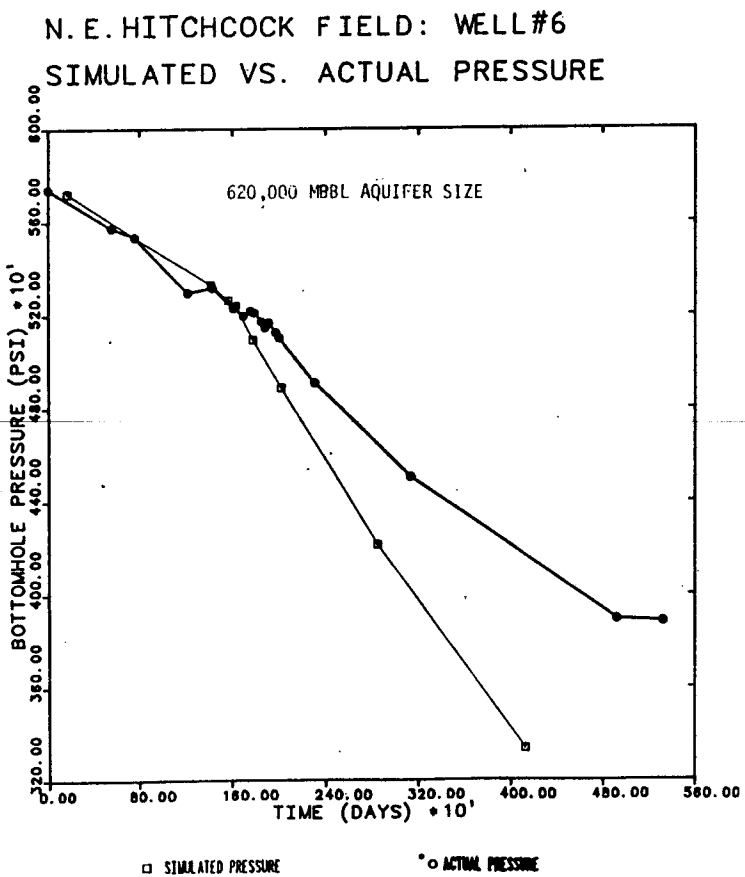
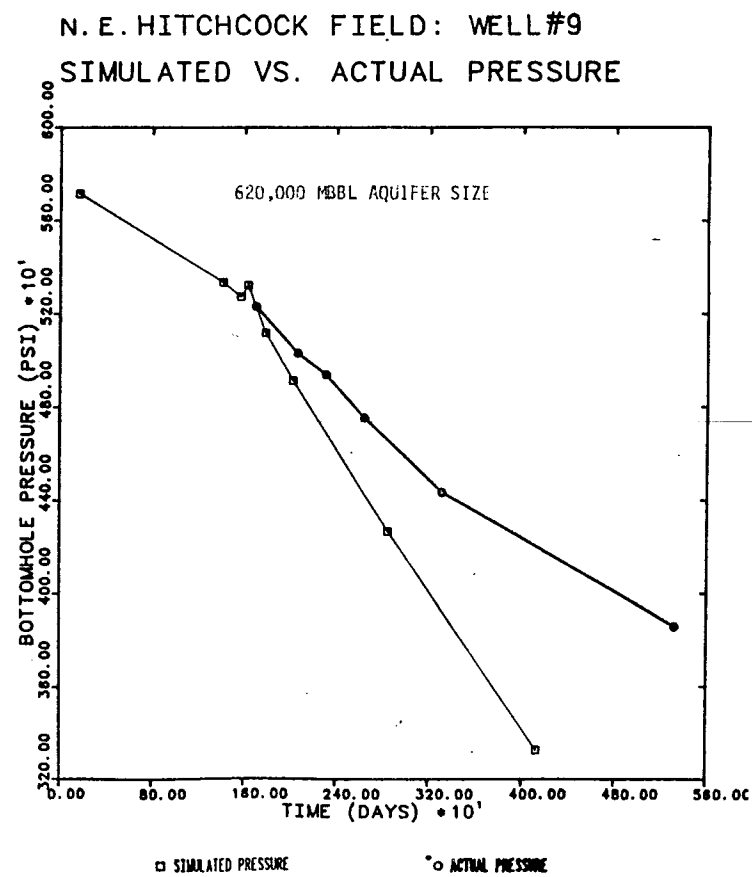


FIGURE 18



increased aquifer volume was taken into account by increasing the size of the grid blocks lying inside the aquifer. The study also revealed that the aquifer permeability was less than the permeability of the hydrocarbon reservoir. Subsequent simulation runs incorporated increased aquifer size and decreased aquifer permeability.

The latest pressure match was based on an aquifer size of 3,990,000 MBBL (1000 reservoir barrels) and an aquifer permeability of 400 millidarcies. Plots comparing the simulated pressures to historical pressures for this pressure match on Wells Nos. 2, 3, 4, 5, 6, and 9 are contained on Figures 14 through 24. The latest results indicate that the aquifer in the Northeast Hitchcock Field is smaller than 3,990,000 MBBL reservoir barrels because the simulated pressures appear to follow a trend which falls above the trend of historical pressures.

5. FINAL NOTE

Additional simulation runs are currently being processed using slightly smaller aquifer volumes in an effort to obtain better matches between simulated and historical pressures. Forecasts of the future performance of the Northeast Hitchcock Field under various production scenarios will be made and submitted in a final report after satisfactory pressure matches have been achieved.

FIGURE 19

N.E. HITCHCOCK FIELD: WELL #2  
SIMULATED VS. ACTUAL PRESSURE

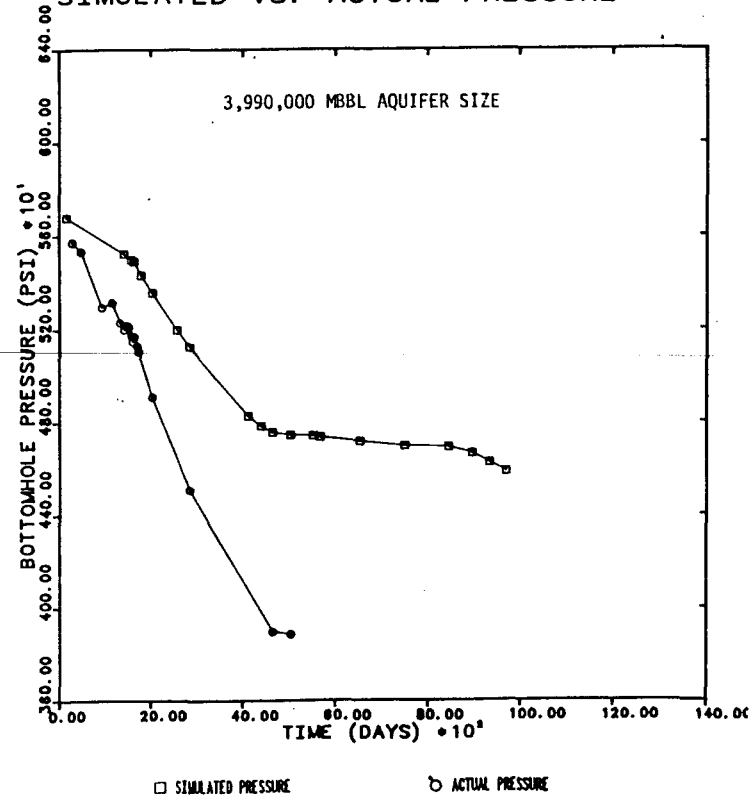


FIGURE 20

N.E. HITCHCOCK FIELD: WELL #3  
SIMULATED VS. ACTUAL PRESSURE

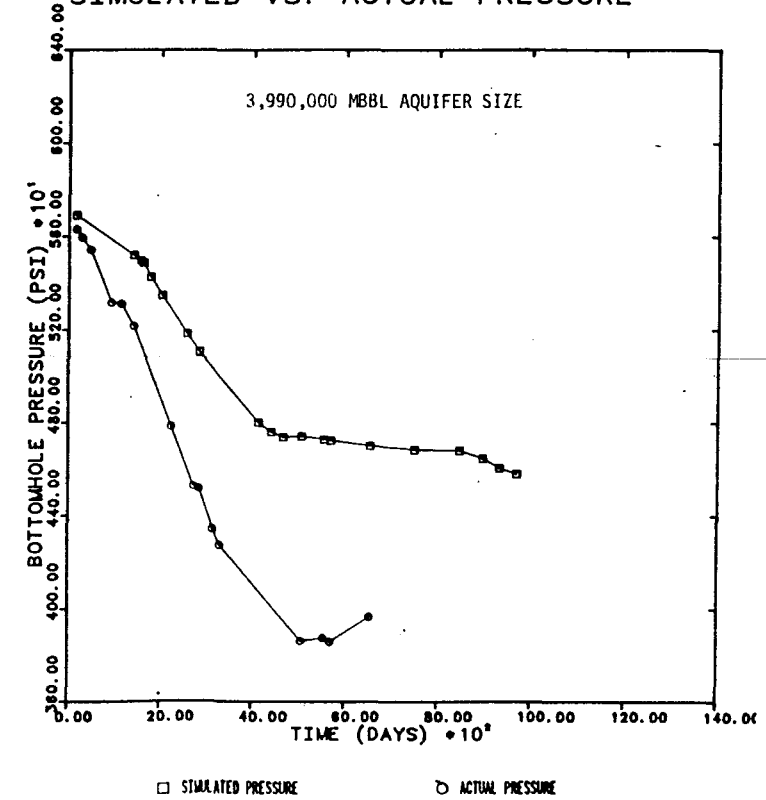


FIGURE 21

N.E. HITCHCOCK FIELD: WELL #4  
SIMULATED VS. ACTUAL PRESSURE

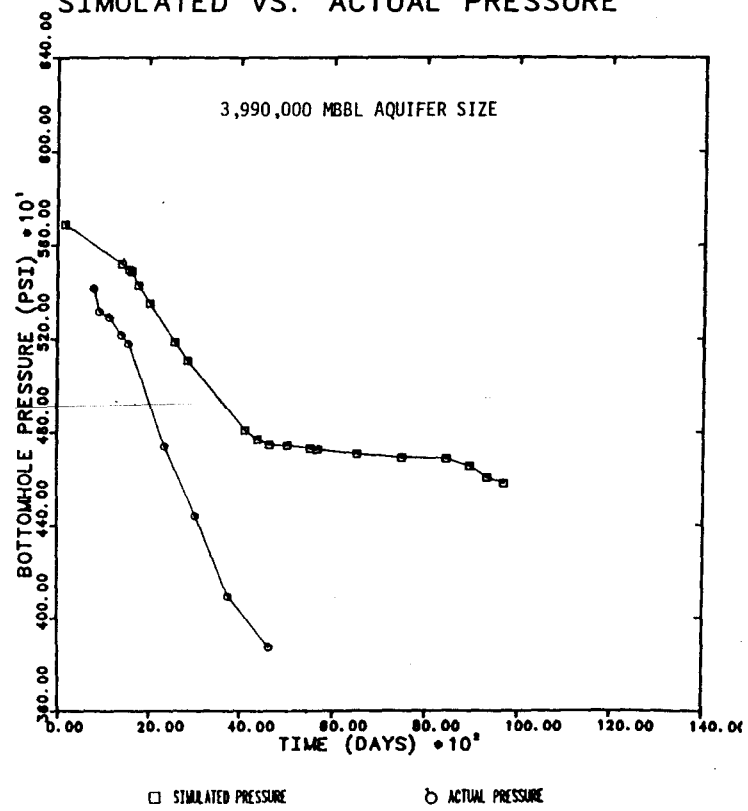


FIGURE 22

N.E. HITCHCOCK FIELD: WELL #5  
SIMULATED VS. ACTUAL PRESSURE

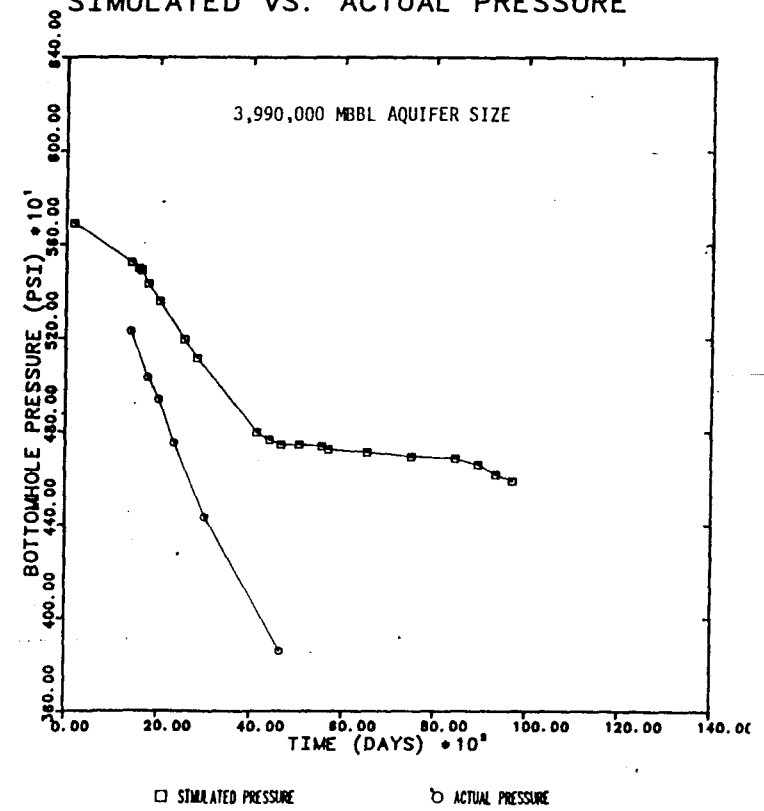


FIGURE 23

N. E. HITCHCOCK FIELD: WELL #6  
SIMULATED VS. ACTUAL PRESSURE

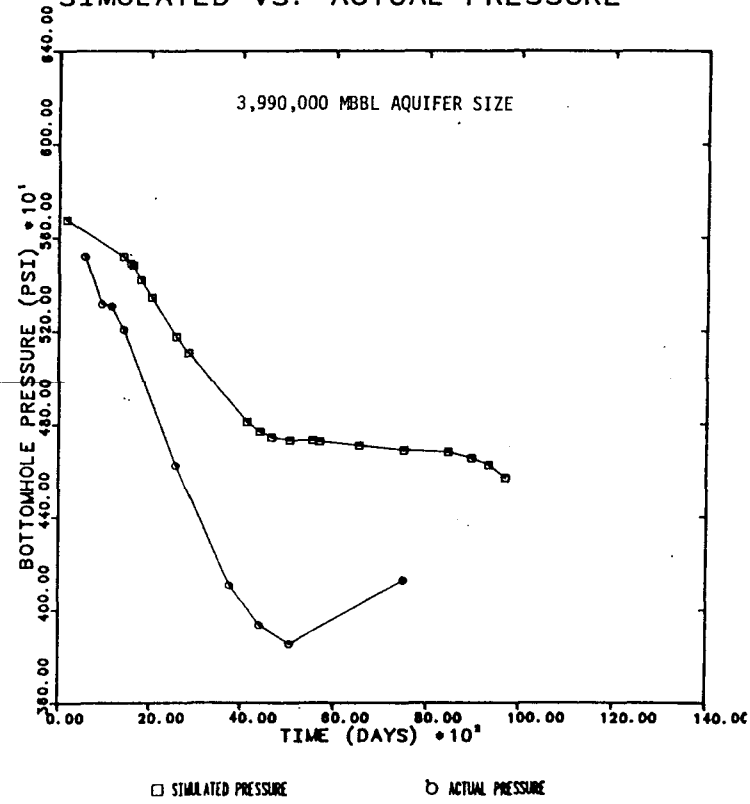
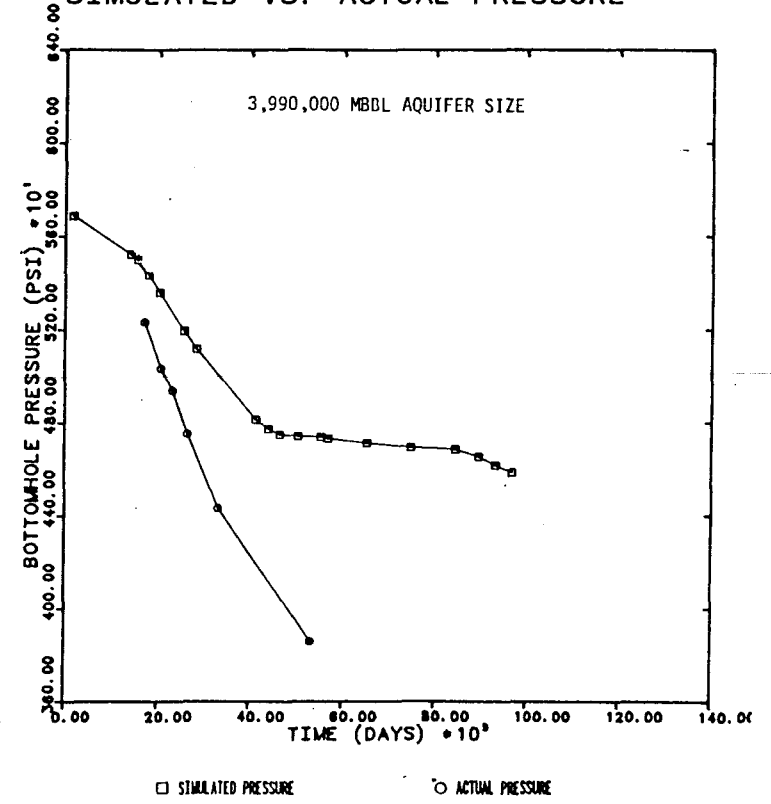


FIGURE 24

N. E. HITCHCOCK FIELD: WELL #9  
SIMULATED VS. ACTUAL PRESSURE



ACKNOWLEDGEMENTS

The work described by this report was funded by the Gas Research Institute (GRI) under Contract No. 5084-212-0924. Throughout this project, technical information and advice was required. Most all of the data used in this report were from the SPE/DOE/GRI 12866, "Enhanced Production from a Slightly Geopressured Water-Drive Gas Condensate Field," and the follow-up report to L. A. Rogers of GRI entitled, N.E. Hitchcock Co-Production Progress Report. Both documents were written by L. L. Anderson, K. P. Peterson, and W. A. Parisi.

The authors would also like to express their gratitude for the advice and information given by: Malcolm Light of the UT Bureau of Economic Geology; L. L. Anderson of Eaton Operating Co., Inc.; L. A. Rogers of Gas Research Institute; and P. Randolph of the Institute of Gas Technology.

## REFERENCES

1. Fanchi, J. R., Harpole, K. J., and Bujnowski, S. W., BOAST: A Three Dimensional, Three Phase Black Oil Applied Simulation Tool (Version 1.1), Volumes I and II. Oak Ridge, Tenn: US DOE Technical Information Center, 1982.
2. Anderson, L. L., Peterson, K. P., and Parisi, W. A., "Enhanced Production from a Slightly Geopressured Water-Drive Gas Condensate Field," in Proceedings 1984 Unconventional Gas Recovery Symposium, Pittsburgh, Pa., May 13-15, 1984, (SPE/DOE/GRI 12866), pp. 341-350.
3. Anderson, L. L., Peterson, K. P., and Parisi, W. A., N.E. Hitchcock Co-Production Progress Report. Report to L. A. Rogers of Gas Research Institute, March, 1985.
4. Fetkovitch, M. J., "A Simplified Approach to Water Influx Calculations - Finite Aquifer Systems," J. Pet. Tech., July, 1971, pp. 814-828.
5. Dake, L. P., Fundamentals of Reservoir Engineering, Amsterdam, The Netherlands: Elsevier Scientific Publishing Company, 1978.
6. Ikoku, C. U., Natural Gas Engineering: A Systems Approach, Tulsa, Oklahoma, Penn Well Publishing Company, 1980.
7. Katz, D. L., et al., Handbook of Natural Gas Engineering, New York: McGraw-Hill Book Co., 1959.
8. Dempsey, J. R., "Computer Routine Treats Gas Viscosity as a Variable," Oil and Gas Journal, August 16, 1965, pp. 141-143.
9. Brown, K. W., and Beggs, H. D., The Technology of Artificial Lift Methods - Volume I, Petroleum Publishing Company, Tulsa, Oklahoma, 1977.
10. Malcolm Light, et al., Set of Subsurface Maps of the Northeast Hitchcock Field, Bureau of Economic Geology, The University of Texas at Austin, December, 1984.
11. P\_V-T, Inc., Petroleum Analysts of Houston, unpublished reservoir fluid study, Thompson Trustee Well No. 1, September 29, 1959.

APPENDIX A

The appendix contains structural cross sections which were used to determine the amount of reservoir rock which was interconnected above and below the gas water contact. These cross sections were aligned according to the grid columns or the grid rows of the grid block representation of the reservoir. The grid block configuration and the structural cross sections contained in this appendix are listed on the following page.

Figure A-1	Grid Block Configuration of the Northeast Hitchcock Field . . . . .	158
Figure A-2	Cross Section: grid column #13 . . . . .	159
Figure A-3	Cross Section: grid column #15 . . . . .	160
Figure A-4	Cross Section: grid column #17 . . . . .	161
Figure A-5	Cross Section: grid column #21 . . . . .	162
Figure A-6	Cross Section: grid row #12 . . . . .	163

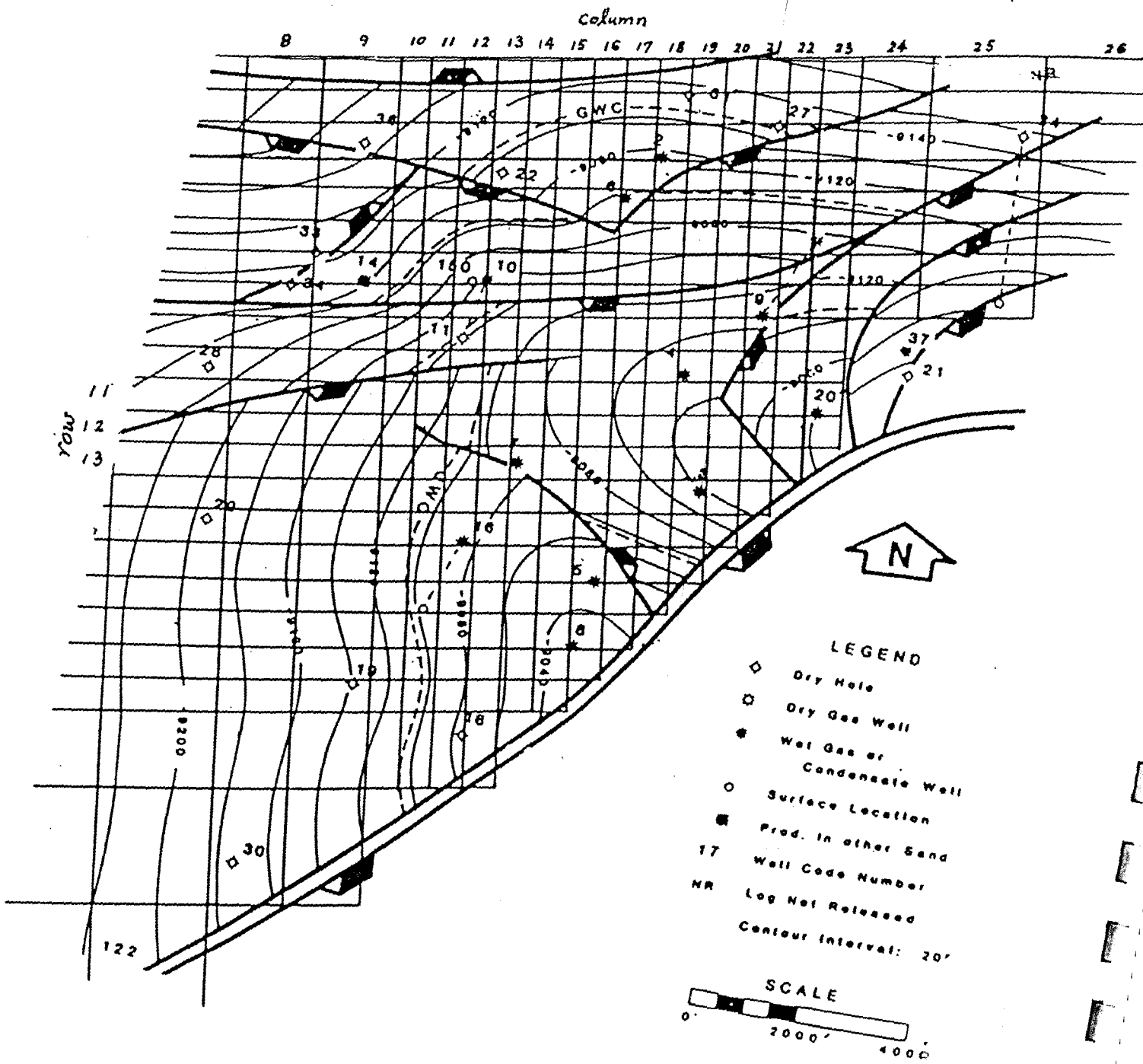
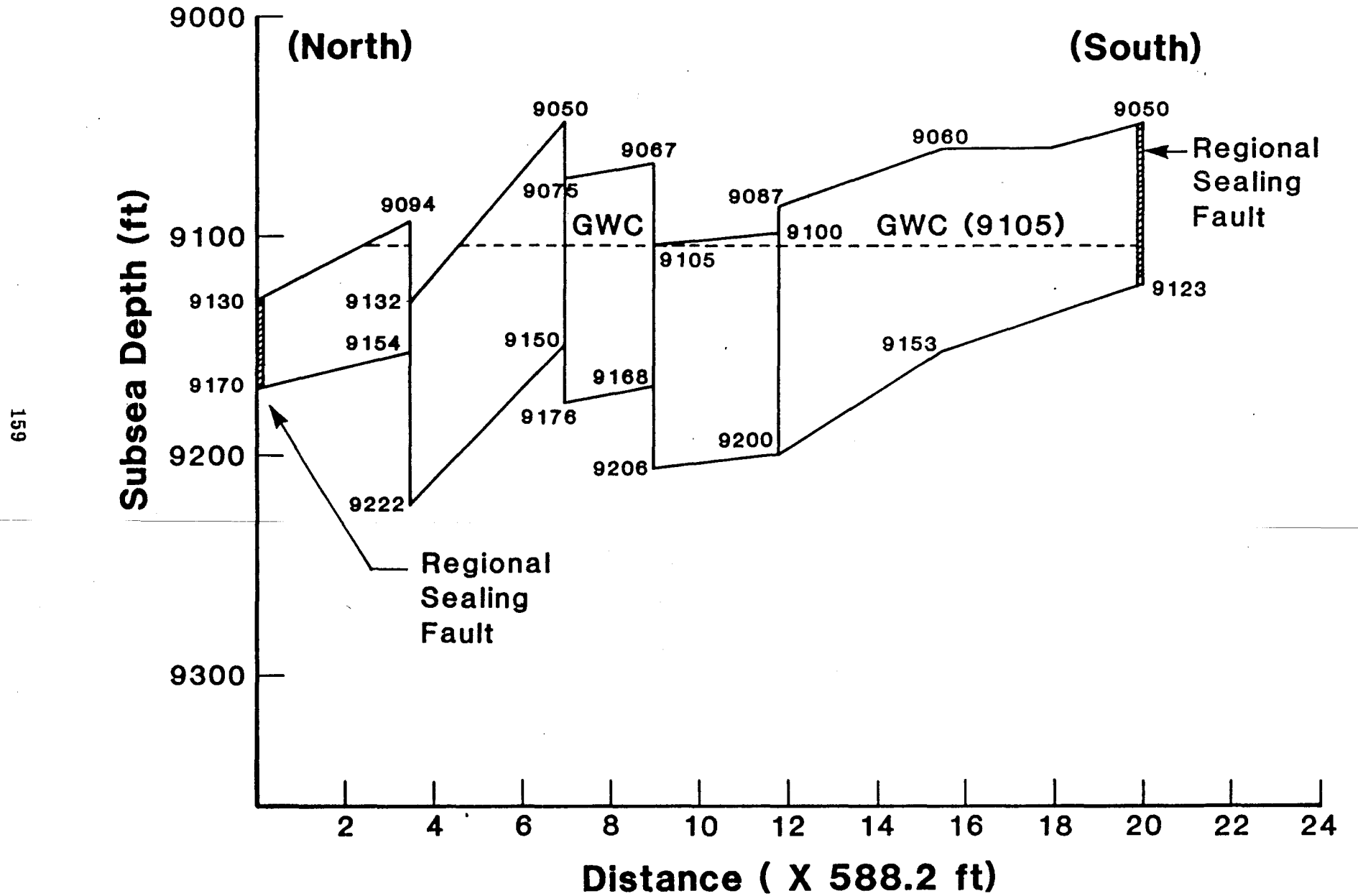


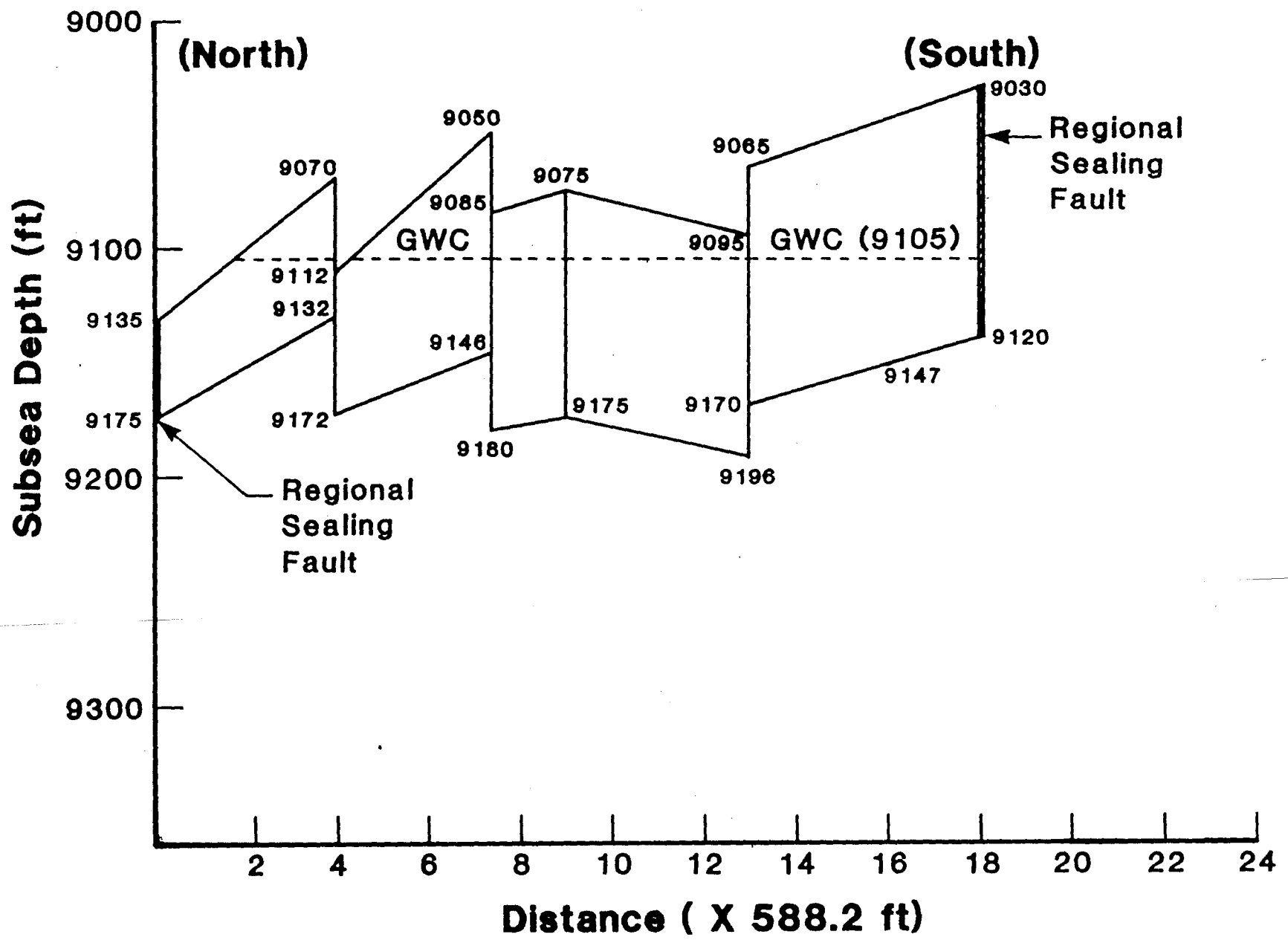
Figure A-1 Grid Block Configuration of the  
 Northeast Hitchcock Field

Figure A-2 Cross-Section: Grid Column #13



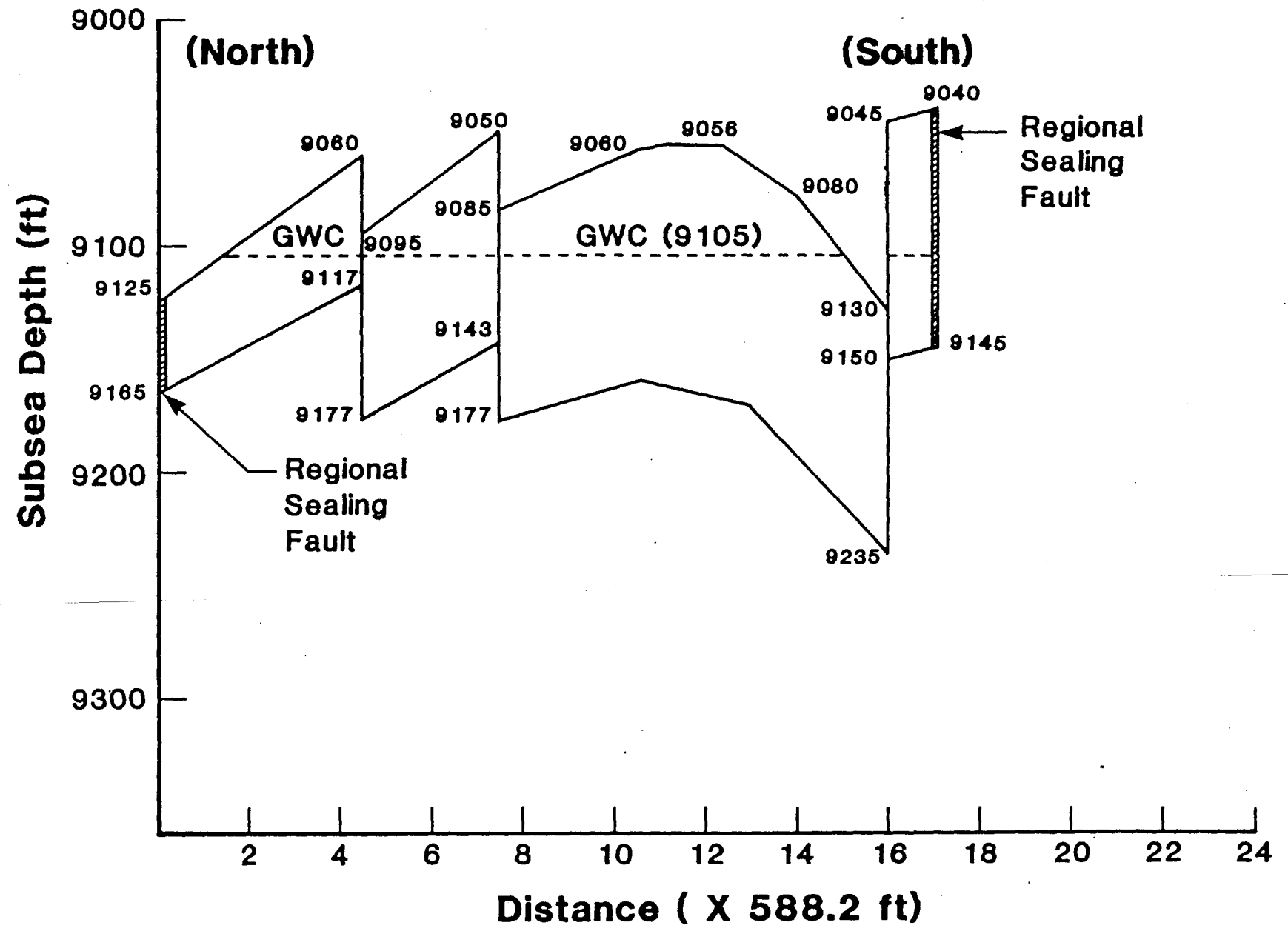
159

Figure A-3 Cross-Section: Grid column #15



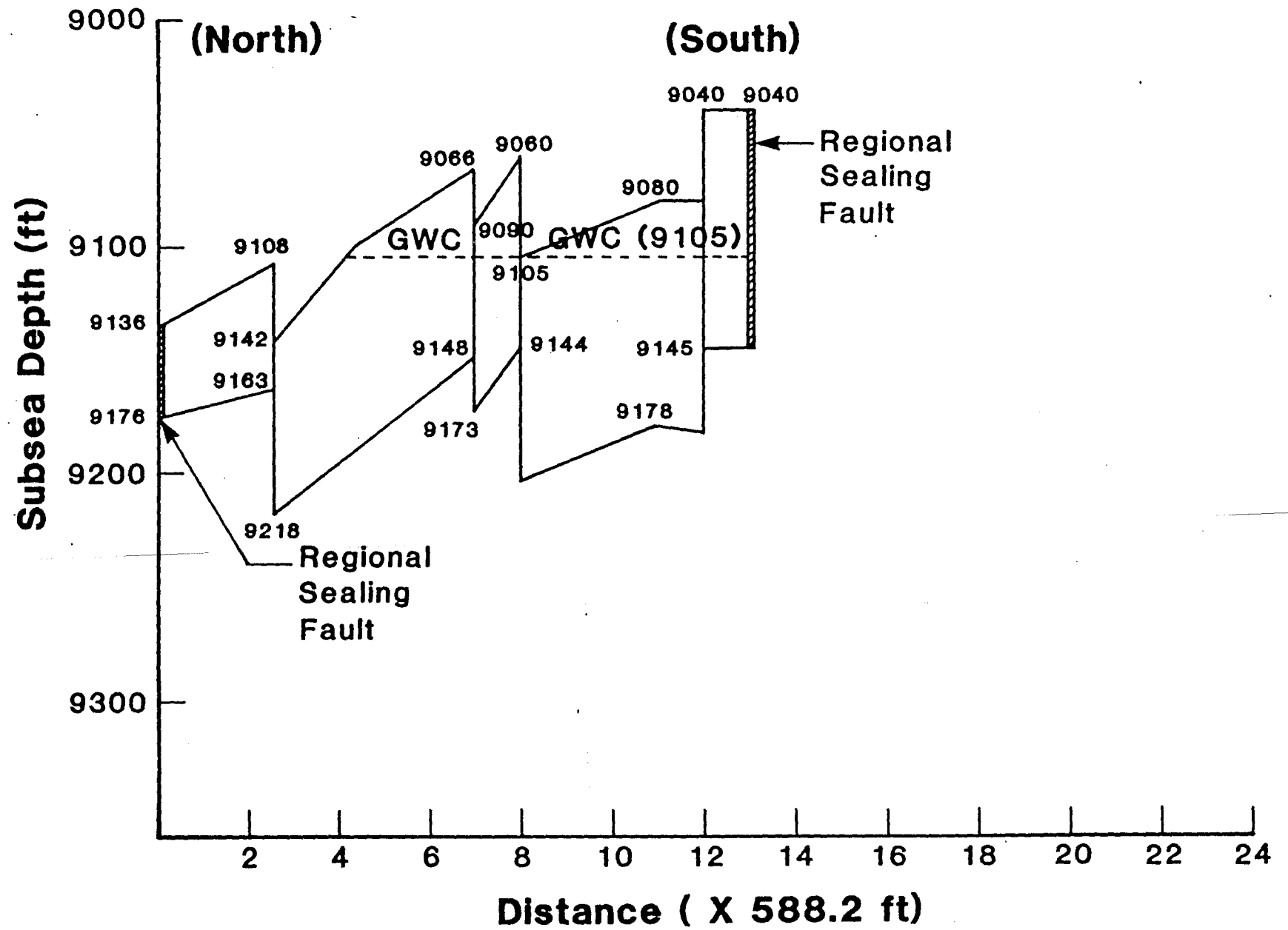
160

Figure A-4 Cross-Section: Grid Column #17



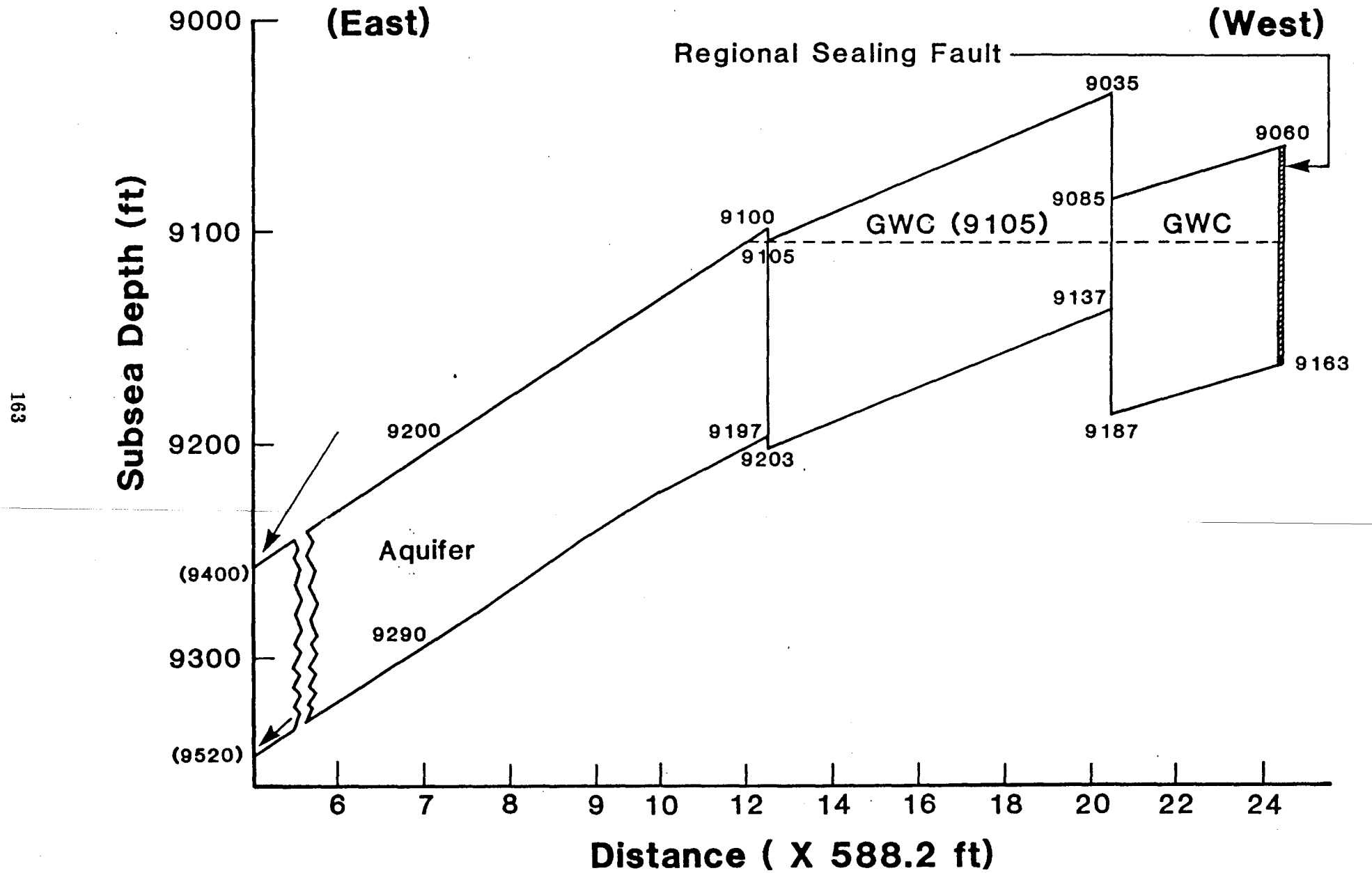
161

Figure A-5 Cross-Section: Grid Column #21



162

Figure A-6 Cross-Section: Grid Row #12



APPENDIX B

The following pages describe the calculations required to determine the formation volume factors and viscosities of the flowing gas and water phases. The flowing gas phase is assumed to be 100 percent equilibrium gas whereas the flowing water phase is assumed to be 100 percent aquifer water. The calculations are divided into two sections. The first section presents the calculations required for the equilibrium gas and the second section presents the calculations for the aquifer water.

Eleven tables are included to describe the calculations of fluid properties.

## I. Equilibrium Gas:

The depletion study found on page 9 of the reservoir fluid analysis performed by P-V-T, Inc. served as the basic data for these fluid property calculations.<sup>6,7</sup> These calculations required determination of the pseudo-critical temperature, pseudo-critical pressure, and specific gravity for each molecular composition at the various pressures in the depletion study. The equations used to determine these properties are as follows:

Pseudo-Critical Temperature,  $T_{pc}$

$$T_{pc} = \frac{\sum_{i=1}^n (Y_i \cdot T_{ci})}{100}$$

where  $n$  = total number of molecular components,  $i$

$Y_i$  = mole percent of component  $i$

$T_{ci}$  = critical temperature of component  $i$   
in degrees Rankine

Pseudo-Critical Pressure,  $P_{pc}$

$$P_{pc} = \frac{\sum_{i=1}^n (Y_i \cdot P_{ci})}{100}$$

where  $n$  = total number of molecular components,  $i$

$Y_i$  = mole percent of component  $i$

$P_{ci}$  = critical pressure of component  $i$   
in pounds per square in absolute

Specific Gravity,  $SG_T$

$$SG_T = \frac{\sum_{i=1}^n (Y_i \cdot SG_i)}{100}$$

where  $n$  = total number of molecular components,  $i$

$Y_i$  = mole percent of component  $i$

$SG_i$  = specific gravity of component  $i$

Treatment of the Heptanes Plus:

It should be noted that the specific gravity of the heptanes plus found in the depletion study was calculated via the following equation.

$$SG_{\text{Heptanes Plus}} = \frac{\text{Molecular Weight of Heptanes Plus}}{\text{Molecular Weight of Air}}$$

In the above equation, air was assumed to have a molecular weight of 28.97 lb/mole. Tables listing the calculations of specific gravity and the pseudo-critical temperatures and pressures of the equilibrium gas can be found on Tables B-1 through B-11.

The pseudo-critical properties of the heptanes plus components were determined from correlation charts developed by Katz et al. found on page 111 of the Handbook of Natural Gas Engineering.<sup>7</sup>

After determining the specific gravities, the pseudo-critical temperatures and the pseudo-critical pressures, the pseudo-reduced temperatures and pressures were evaluated. The pseudo-reduced temperatures and pressures were calculated through use of the following expressions.

Pseudo-Reduced Temperature,  $T_{PR}$

$$T_{PR} = \frac{\text{Reservoir Temperature (degrees Rankine)}}{\text{Pseudo-Critical Temperature (degrees Rankine)}}$$

Pseudo-Reduced Pressure,  $P_{PR}$

$$P_{PR} = \frac{\text{Reservoir Temperature (psia)}}{\text{Pseudo-Critical Pressure (psia)}}$$

The values of the pseudo-reduced temperature and pressure and the specific gravity were then used to determine the gas deviation factor, the gas viscosity, and the gas formation volume factor. The gas deviation factor,  $Z$ , was calculated using the method developed by Hall and Yarborough.<sup>5</sup> This method involved solving a non-linear equation for the "reduced" gas density, then substituting the "reduced" density into an equation representing the gas deviation factor. These equations were developed from the Starling-Carnahan equation of state and they are as follows:

$$Z = \frac{0.06125 P_{PR} (1/T_{PR}) \exp(-1.2(1-(1/T_{PR}))^2)}{Y}$$

where  $Z$  = gas deviation factor  
 $P_{PR}$  = pseudo reduced pressure  
 $T_{PR}$  = pseudo reduced temperature  
 $Y$  = "reduced" gas density

The non-linear equation defining the reduced gas density is as follows:

$$0.06125 P_{PR} (1/T_{PR}) \exp(-1.2(1-(1/T_{PR}))^2) + \frac{Y + Y^2 + Y^3 - Y^4}{(1 - Y)^3} - (14.76(1/T_{PR}) - 9.76(1/T_{PR})^2 + 4.58(1/T_{PR})^3)Y^2$$

$$+ (90.7(1/T_{PR}) - 242.2(1/T_{PR})^2 + 42.4(1/T_{PR})^3)Y^{(2.18 + 2.82(1/T_{PR}))} = 0.0$$

The gas viscosity was calculated using a computer algorithm listed in the August 16, 1965, Oil and Gas Journal article, "Computer Routine Treats Gas Viscosity as a Variable," by John R. Dempsey.<sup>8</sup> The computer algorithm presented by this article represents a multivariant regression equation of the gas viscosity correlations developed by Carr, Kobayashi, and Burrows. The gas properties required as parameters in this regression equation were the specific gravity of the gas, and the pseudo-reduced temperature and pressure of the equilibrium gas.

The formation volume factor of the equilibrium gas was determined by expressing the real gas equation of state<sup>6</sup> as follows:

$$B_g = 0.0283 \frac{zT}{p}$$

- where
- $B_g$  = gas formation volume factor in units of reservoir cubic feet per standard cubic feet
  - $Z$  = gas deviation factor
  - $T$  = reservoir temperature in degrees Rankine
  - $p$  = reservoir pressure in psia

## II. Aquifer Water:

The viscosity of the aquifer water was determined from a correlation developed by Carlton Beal.<sup>9</sup> This correlation determines the water viscosity as a function of temperature and is expressed through the following equation.

$$\mu_w = \exp(1.003 - 1.479 \times 10^{-2} T + 1.982 \times 10^{-5} T^2)$$

where  $\mu_w$  = water viscosity in centipoise  
T = reservoir temperature in degrees Fahrenheit  
Y = "reduced" gas density

The formation volume factor of the aquifer water was determined by means of the following equation:

$$B_{wi} = B_{w_{sc}} (1 - CW(P_{sc} - P_i))$$

where

$B_{wi}$  = formation volume factor of the aquifer water at the average reservoir pressure,  $p_i$  (psia)  
 $B_{w_{sc}}$  = formation volume factor of the aquifer water at 1.465 psia and 60 degrees Fahrenheit  
CW = water compressibility,  $3.0 \times 10^{-6}$  psi<sup>-1</sup>  
 $P_{sc}$  = pressure at standard conditions, 14.65 psia  
 $P_i$  = average reservoir pressure (psia).

TABLE B-1: Equilibrium Gas Properties at 5742 and 5649 psia, 212°F

COMPONENT	MOLE FRACTION, $Y_i$	CRITICAL TEMP. ( $^{\circ}$ R) $T_c$	CRITICAL PRESSURE (psia) $P_c$	SPECIFIC GRAVITY (SG)	$Y_i T_c$	$Y_i P_c$	$Y_i$ (SG)
Nitrogen	1.57	227	493	0.9672	3.564	7.740	0.0152
Carbon Dioxide	0.18	548	1071	1.5195	0.986	1.928	0.0027
Methane	81.11	343	668	0.5539	278.207	541.815	0.4493
Ethane	5.05	550	708	1.0382	27.775	35.754	0.0524
Propane	2.88	666	616	1.5225	19.181	17.741	0.0438
I-Butane	1.11	735	529	2.0068	8.159	5.872	0.0223
N-Butane	1.03	765	551	2.0068	7.880	5.675	0.0207
I-Pentane	0.52	829	490	2.4911	4.311	2.548	0.0130
N-Pentane	0.54	845	489	2.4911	4.563	2.641	0.0135
Hexanes	1.18	913	437	2.9753	10.733	5.157	0.0351
Heptanes + (156)	4.83	1240	400	5.3849	59.892	19.320	0.2601
TOTALS	100.00%				425.291	646.191	0.9281

170

$$p = 5649 \text{ psia, } Z_{\text{(Hall-Yarborough)}} = 1.0482$$

$$\rho_{\text{gas}} = 20.1185 \text{ lbm/ft}^3$$

$$p = 5742 \text{ psia, } Z_{\text{(Hall-Yarborough)}} = 1.0576$$

$$\rho_{\text{gas}} = 20.2680 \text{ lbm/ft}^3$$

TABLE B-2: Equilibrium Gas Properties at 5045 psia and 212°F

COMPONENT	MOLE FRACTION, $Y_i$	CRITICAL TEMP. ( $^{\circ}$ R) $T_c$	CRITICAL PRESSURE (psia) $P_c$	SPECIFIC GRAVITY (SG)	$Y_i T_c$	$Y_i P_c$	$Y_i$ (SG)
Nitrogen	1.57	227	493	0.9672	3.564	7.740	0.0152
Carbon Dioxide	0.18	548	1071	1.5195	0.986	1.928	0.0027
Methane	81.55	343	668	0.5539	279.717	544.754	0.4517
Ethane	5.55	550	708	1.0382	29.920	38.515	0.0565
Propane	2.85	666	616	1.5225	18.981	17.556	0.0434
I-Butane	0.96	735	529	2.0068	7.056	5.078	0.0193
N-Butane	1.15	765	551	2.0068	8.798	6.337	0.0231
I-Pentane	0.48	829	490	2.4911	3.979	2.352	0.0120
N-Pentane	0.44	845	489	2.4911	3.718	2.152	0.0110
Hexanes	1.04	913	437	2.9753	9.495	4.545	0.0309
Heptanes + (156)	4.43	1220	390	5.2813	52.948	16.926	0.2292
TOTALS	100.00%				419.162	647.883	0.8950

171

$$Z_{\text{(Hall-Yarborough)}} = 0.9904$$

$$\rho_{\text{gas}} = 18.3378 \text{ lbm/ft}^3$$

TABLE B-3: Equilibrium Gas Properties at 4633 psia and 212°F

COMPONENT	MOLE FRACTION, $Y_i$	CRITICAL TEMP. ( $^{\circ}$ R) $T_c$	CRITICAL PRESSURE (psia) $P_c$	SPECIFIC GRAVITY (SG)	$Y_i T_c$	$Y_i P_c$	$Y_i$ (SG)
Nitrogen	1.57	227	493	0.9672	3.564	7.740	0.0152
Carbon Dioxide	0.18	548	1071	1.5195	0.986	1.928	0.0027
Methane	82.28	343	668	0.5539	282.220	549.630	0.4557
Ethane	5.43	550	708	1.0382	29.865	38.444	0.0564
Propane	2.76	666	616	1.5225	18.382	17.002	0.0420
I-Butane	1.06	735	529	2.0068	7.791	5.607	0.0213
N-Butane	1.01	765	551	2.0068	7.727	5.565	0.0203
I-Pentane	0.52	829	490	2.4911	4.311	2.548	0.0130
N-Pentane	0.46	845	489	2.4911	3.887	2.249	0.0115
Hexanes	0.69	913	437	2.9753	6.300	3.015	0.0205
Heptanes + (145)	4.04	1175	380	5.0052	47.470	15.352	0.2022
TOTALS	100.00%				412.503	649.080	0.8608

172

$$Z_{(\text{Hall-Yarborough})} = 0.9570$$

$$\rho_{\text{gas}} = 16.7620 \text{ lbm/ft}^3$$

TABLE B-4: Equilibrium Gas Properties at 4045 psia and 212°F

COMPONENT	MOLE FRACTION, $Y_i$	CRITICAL TEMP. ( $^{\circ}$ R) $T_c$	CRITICAL PRESSURE (psia) $P_c$	SPECIFIC GRAVITY (SG)	$Y_i T_c$	$Y_i P_c$	$Y_i$ (SG)
Nitrogen	1.57	227	493	0.9672	3.564	7.740	0.0152
Carbon Dioxide	0.18	548	1071	1.5195	0.986	1.928	0.0027
Methane	83.35	343	668	0.5539	285.891	556.778	0.4617
Ethane	5.45	550	708	1.0382	29.975	38.586	0.0556
Propane	2.71	666	616	1.5225	18.049	16.694	0.0413
I-Butane	1.02	735	529	2.0068	7.497	5.396	0.0205
N-Butane	0.96	765	551	2.0068	7.344	5.290	0.0193
I-Pentane	0.45	829	490	2.4911	3.731	2.205	0.0112
N-Pentane	0.43	845	489	2.4911	3.634	2.103	0.0107
Hexanes	0.58	913	437	2.9753	5.295	2.535	0.0173
Heptanes + (136)	3.30	1120	375	4.6945	36.960	12.375	0.1549
TOTALS	100.00%				402.926	651.630	0.8114

173

$$Z_{\text{(Hall-Yarborough)}} = 0.9181$$

$$\rho_{\text{gas}} = 14.3793 \text{ lbm/ft}^3$$

TABLE B-5: Equilibrium Gas Properties at 3371 psia and 212°F

COMPONENT	MOLE FRACTION, $Y_i$	CRITICAL TEMP. ( $^{\circ}$ R) $T_c$	CRITICAL PRESSURE (psia) $P_c$	SPECIFIC GRAVITY (SG)	$Y_i T_c$	$Y_i P_c$	$Y_i$ (SG)
Nitrogen	1.57	227	493	0.9672	3.564	7.740	0.0152
Carbon Dioxide	0.18	548	1071	1.5195	0.986	1.928	0.0027
Methane	84.38	343	668	0.5539	289.423	563.658	0.4674
Ethane	5.49	550	708	1.0382	30.195	38.869	0.0570
Propane	2.70	666	616	1.5225	17.982	16.632	0.0411
I-Butane	1.03	735	529	2.0068	7.571	5.449	0.0207
N-Butane	0.92	765	551	2.0068	7.038	5.069	0.0185
I-Pentane	0.46	829	490	2.4911	3.813	2.254	0.0115
N-Pentane	0.38	845	489	2.4911	3.211	1.858	0.0095
Hexanes	0.66	913	437	2.9753	6.026	2.884	0.0196
Heptanes + (128)	2.23	1070	360	4.4184	23.861	8.0280	0.0985
TOTALS	100.00%				393.670	654.369	0.7617

174

$$Z_{\text{(Hall-Yarborough)}} = 0.8883$$

$$\rho_{\text{gas}} = 11.6267 \text{ lbm/ft}^3$$

TABLE B-6: Equilibrium Gas Properties at 2801 psia and 212°F

COMPONENT	MOLE FRACTION, $Y_i$	CRITICAL TEMP. ( $^{\circ}$ R) $T_c$	CRITICAL PRESSURE (psia) $P_c$	SPECIFIC GRAVITY (SG)	$Y_i T_c$	$Y_i P_c$	$Y_i$ (SG)
Nitrogen	1.57	227	493	0.9672	3.564	7.740	0.0152
Carbon Dioxide	0.18	548	1071	1.5195	0.986	1.928	0.0027
Methane	85.40	343	668	0.5539	292.922	570.472	0.4730
Ethane	5.32	550	708	1.0382	29.260	37.666	0.0552
Propane	2.69	666	616	1.5225	17.915	16.570	0.0410
I-Butane	0.98	735	529	2.0068	7.203	5.184	0.0197
N-Butane	0.85	765	551	2.0068	6.503	4.684	0.0171
I-Pentane	0.42	829	490	2.4911	3.482	2.058	0.0105
N-Pentane	0.35	845	489	2.4911	2.958	1.712	0.0087
Hexanes	0.56	913	437	2.9753	5.113	2.447	0.0167
Heptanes + (124)	1.68	1025	335	4.2803	17.220	5.6280	0.0719
TOTALS	100.00%				387.126	656.089	0.7317

175

$$Z_{\text{(Hall-Yarborough)}} = 0.8777$$

$$\rho_{\text{gas}} = 9.39240 \text{ lbm/ft}^3$$

TABLE B-7: Equilibrium Gas Properties at 2262 psia and 212°F

COMPONENT	MOLE FRACTION, $Y_i$	CRITICAL TEMP. ( $^{\circ}$ R) $T_c$	CRITICAL PRESSURE (psia) $P_c$	SPECIFIC GRAVITY (SG)	$Y_i T_c$	$Y_i P_c$	$Y_i$ (SG)
Nitrogen	1.57	227	493	0.9672	3.564	7.740	0.0152
Carbon Dioxide	0.18	548	1071	1.5195	0.986	1.928	0.0027
Methane	86.00	343	668	0.5539	294.980	574.480	0.4764
Ethane	5.50	550	708	1.0382	30.250	38.940	0.0571
Propane	2.71	666	616	1.5225	18.049	16.694	0.0413
I-Butane	0.97	735	529	2.0068	7.130	5.131	0.0195
N-Butane	0.88	765	551	2.0068	6.732	4.849	0.0177
I-Pentane	0.34	829	490	2.4911	3.233	1.911	0.0097
N-Pentane	0.36	845	489	2.4911	3.042	1.760	0.0090
Hexanes	0.46	913	437	2.9753	4.200	2.010	0.0137
Heptanes + (119)	0.98	1005	335	4.1077	9.8490	3.2830	0.0403
TOTALS	100.00%			382.015	658.726	0.7026	

176

$$Z_{\text{(Hall-Yarborough)}} = 0.8807$$

$$\rho_{\text{gas}} = 7.2713 \text{ lbm/ft}^3$$

TABLE B-8: Equilibrium Gas Properties at 1753 psia and 212°F

COMPONENT	MOLE FRACTION, $Y_i$	CRITICAL TEMP. ( $^{\circ}$ R) $T_c$	CRITICAL PRESSURE (psia) $P_c$	SPECIFIC GRAVITY (SG)	$Y_i T_c$	$Y_i P_c$	$Y_i$ (SG)
Nitrogen	1.57	227	493	0.9672	3.564	7.740	0.0152
Carbon Dioxide	0.18	548	1071	1.5195	0.986	1.928	0.0027
Methane	86.10	343	668	0.5539	295.323	575.148	0.4769
Ethane	5.43	50	708	1.0382	29.865	38.444	0.0564
Propane	2.74	666	616	1.5225	18.248	16.878	0.0417
I-Butane	0.97	735	529	2.0068	7.130	5.131	0.0195
N-Butane	0.88	765	551	2.0068	6.732	4.849	0.0177
I-Pentane	0.39	829	490	2.4911	3.233	1.911	0.0097
N-Pentane	0.33	845	489	2.4911	2.789	1.614	0.0082
Hexanes	0.51	913	437	2.9753	4.656	2.229	0.0152
Heptanes + (115)	0.90	980	335	3.9696	8.820	3.0150	0.0357
TOTALS	100.00%				381.346	658.887	0.6989

177

$$Z_{\text{(Hall-Yarborough)}} = 0.8903$$

$$\rho_{\text{gas}} = 5.5352 \text{ lbm/ft}^3$$

TABLE B-9: Equilibrium Gas Properties at 1177 psia and 212°F

COMPONENT	MOLE FRACTION, $Y_i$	CRITICAL TEMP. ( $^{\circ}$ R) $T_c$	CRITICAL PRESSURE (psia) $P_c$	SPECIFIC GRAVITY (SG)	$Y_i T_c$	$Y_i P_c$	$Y_i$ (SG)
Nitrogen	1.57	227	493	0.9672	3.564	7.740	0.0152
Carbon Dioxide	0.18	548	1071	1.5195	0.986	1.928	0.0027
Methane	85.98	343	668	0.5539	294.911	574.346	0.4762
Ethane	5.62	550	708	1.0382	30.910	39.790	0.0583
Propane	2.77	666	616	1.5225	18.448	17.063	0.0422
I-Butane	0.99	735	529	2.0068	7.277	5.237	0.0199
N-Butane	0.87	765	551	2.0068	6.656	4.794	0.0175
I-Pentane	0.40	829	490	2.4911	3.316	1.960	0.0100
N-Pentane	0.32	845	489	2.4911	2.704	1.565	0.0080
Hexanes	0.46	913	437	2.9753	4.200	2.010	0.0137
Heptanes + (111)	0.84	975	335	3.8315	8.1900	2.8140	0.0322
TOTALS	100.00%				381.162	659.247	0.6959

178

$$Z_{\text{(Hall-Yarborough)}} = 0.9148$$

$$\rho_{\text{gas}} = 3.6014 \text{ lbm/ft}^3$$

TABLE B-10: Equilibrium Gas Properties at 668 psia and 212°F

COMPONENT	MOLE FRACTION, $Y_i$	CRITICAL TEMP. ( $^{\circ}$ R) $T_c$	CRITICAL PRESSURE (psia) $P_c$	SPECIFIC GRAVITY (SG)	$Y_i T_c$	$Y_i P_c$	$Y_i$ (SG)
Nitrogen	1.57	227	493	0.9672	3.564	7.740	0.0152
Carbon Dioxide	0.18	548	1071	1.5195	0.986	1.928	0.0027
Methane	84.94	343	668	0.5539	291.344	567.399	0.4705
Ethane	5.95	550	708	1.0382	32.725	42.126	0.0618
Propane	3.09	666	616	1.5225	20.579	19.034	0.0470
I-Butane	1.11	735	529	2.0068	8.159	5.872	0.0223
N-Butane	1.07	765	551	2.0068	8.186	5.896	0.0215
I-Pentane	0.42	829	490	2.4911	3.482	2.058	0.0105
N-Pentane	0.29	845	489	2.4911	2.451	1.418	0.0072
Hexanes	0.48	913	437	2.9753	4.382	2.098	0.0143
Heptanes + (105)	0.90	980.0	400.0	3.6244	8.8200	3.6000	0.0326
TOTALS	100.00%				384.678	659.169	0.7056

179

$$Z_{\text{(Hall-Yarborough)}} = 0.9449$$

$$\rho_{\text{gas}} = 2.0020 \text{ lbm/ft}^3$$

TABLE B-11: Separator Gas Properties

SEPARATOR PRESSURE = 870 psig  
 SEPARATOR TEMPERATURE = 88°F

COMPONENT	MOLE FRACTION, $Y_i$	CRITICAL TEMP. (°R) $T_c$	CRITICAL PRESSURE (psia) $P_c$	SPECIFIC GRAVITY (SG)	$Y_i T_c$	$Y_i P_c$	$Y_i$ (SG)
Nitrogen	1.77	227	493	0.3672	4.9029	8.7261	0.0171
Carbon Dioxide	0.20	548	1071	1.5195	1.0960	2.1420	0.0030
Methane	88.53	343	668	0.5539	303.6579	591.3804	0.4904
Ethane	5.15	550	708	1.0382	28.3250	36.4620	0.0531
Propane	2.36	666	616	1.5225	15.7176	14.5376	0.0359
I-Butane	0.73	735	529	2.0068	5.3655	3.8617	0.0146
N-Butane	0.60	765	551	2.0068	4.5900	3.3060	0.0120
I-Pentane	0.21	829	490	2.4911	1.7409	1.0290	0.0052
N-Pentane	0.16	845	489	2.4911	1.3520	0.7824	0.0040
Hexanes	0.20	913	437	2.9753	1.8260	0.8740	0.0060
Heptanes +	0.09	972.3	396.9	3.4596	0.8751	0.3572	0.0031
TOTALS	100.00%				369.4489	663.4584	0.6444

180

$Z_{SEPARATOR CONDITIONS} = 0.8681$

$\rho_{gas} = 2.5976 \text{ lbm/cu ft}$

APPENDIX C

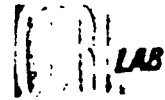
The following pages contain the relevant capillary pressure test results and the capillary pressure curves from the December 5, 1984 Special Core Analysis Report on core samples from the Eaton Operating Co., Inc.'s Louise Unit No. 2.

SPECIAL CORE ANALYSIS STUDY

FOR

Eaton Operating Co., Inc.  
Secondary Gas Recovery Inc. No. 2 Louise  
Hitchcock Field  
Frio Sand Formation  
Galveston County, Texas  
File Number: SCAL 305-84092

Special Core Analysis



**CORE LABORATORIES, INC.**  
Special Core Analysis

**LAB**

December 5, 1984

Eaton Operating Co., Inc.  
3104 Edloe, Suite 200  
Houston, Texas 77027

Attention: Mr. Lonnie L. Anderson

Subject: Special Core Analysis Study  
Secondary Gas Recovery Inc. No.2 Louise Unit  
Hitchcock Field  
Frio Sand Formation  
Galveston County, Texas  
File Number: SCAL 305-84092

Gentlemen:

In a letter dated August 10, 1984, Mr. Lonnie L. Anderson of Eaton Operating Co., Inc. requested that Core Laboratories, Inc. perform the following special core analysis on core material recovered from the subject well: (1) Formation Resistivity Factor and Formation Resistivity Index determinations, (2) Porous-Plate method Air-Brine Capillary Pressure tests, and (3) Steady-State Water-Gas Relative Permeability Tests. The samples used for testing are lithologically described and identified as to sample number and depth interval on page 1 of this report.

Full diameter core material representing three coring intervals Core No. 1 9065.0 to 9109.7 feet, Core No. 2, 9113.0 to 9171.0 feet and Core No. 3, 9173.0 to 9194.6 feet; was submitted for use in this study. Sixteen one-inch and fifteen one and one half-inch diameter cylindrical core plugs were obtained using a diamond drill bit with water as the bit coolant and lubricant. The samples were extracted of hydrocarbons using toluene, leached of salts with methanol, and oven-dried at a temperature of 180 degrees Fahrenheit. Permeability to air and Boyle's law porosities (using helium as the gaseous medium) were measured on the cleaned and dried samples. These results are presented on page 2.

The samples selected for electrical properties and capillary pressure tests were evacuated and pressure saturated with a 40,000 ppm sodium chloride brine. The resistivity of the brine and brine saturated core plugs were measured over a period of several days until the resistivity values stabilized, indicating that ionic equilibrium within the core plugs had been attained.

The samples were desaturated using humidified air in a porous plate cell. At selected pressures, equilibrium saturations were attained and the sample resistivities were measured. The results of the formation factor measurements and resistivity index determinations are presented in tabular form on page 3 and in graphical form on pages 4 through 13. The capillary pressure test results are presented in tabular form on page 14 and in graphical form on pages 15 through 24.

21

30

185

20

Eaton Operating Co., Inc.

Page two

Using Archie's equation, a cementation exponent "m" of 1.93 is calculated for this suite of samples. The formation resistivity index versus saturation relationships yield saturation exponents "n" ranging from 1.78 to 2.36. For your convenience, a composite plot of the resistivity-saturation relationships for this suite of samples, yielding an "n" value of 2.03 is presented on page 25. /

The core plugs selected for steady-state water-oil relative permeability tests are currently in our Dallas facility for testing. When the analysis is completed, the results will be forwarded in an addendum to this report.

It has been a pleasure to provide Eaton Operating Co., Inc. with this study. Should you have any questions or require further assistance, please feel free to contact us.

Very truly yours,

CORE LABORATORIES, INC.



W.K. Hudson  
Laboratory Supervisor  
Special Core Analysis  
Houston, Texas

WKH/grm/sle

SUMMARY OF CAPILLARY PRESSURE TEST RESULTS

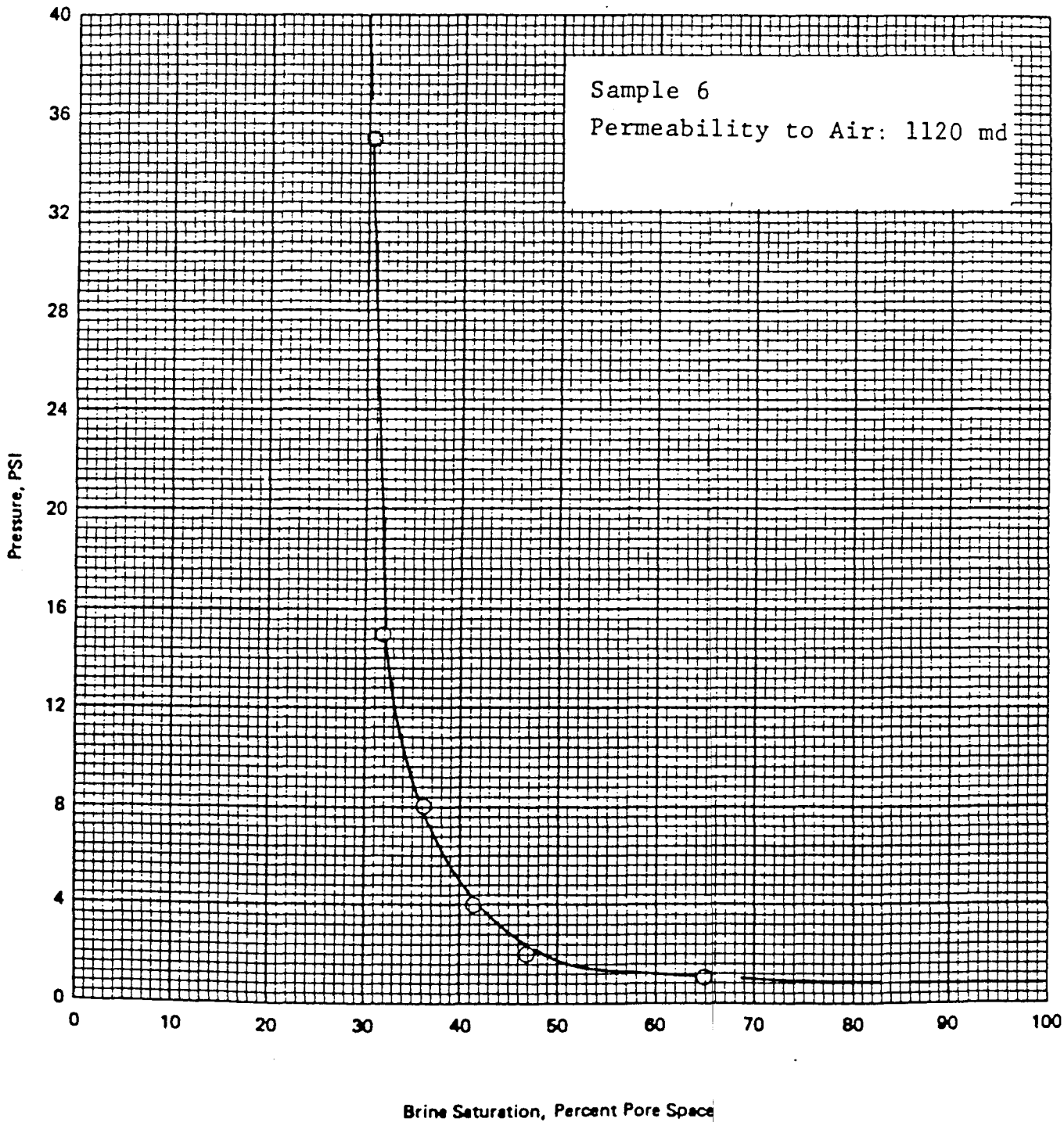
Eaton Operating Company, Inc.  
S.G.R. Inc. No. 2 Louise Unit  
Frio Sand Formation  
Hitchcock Field  
Galveston County, Texas

Fluid System: Air-Water

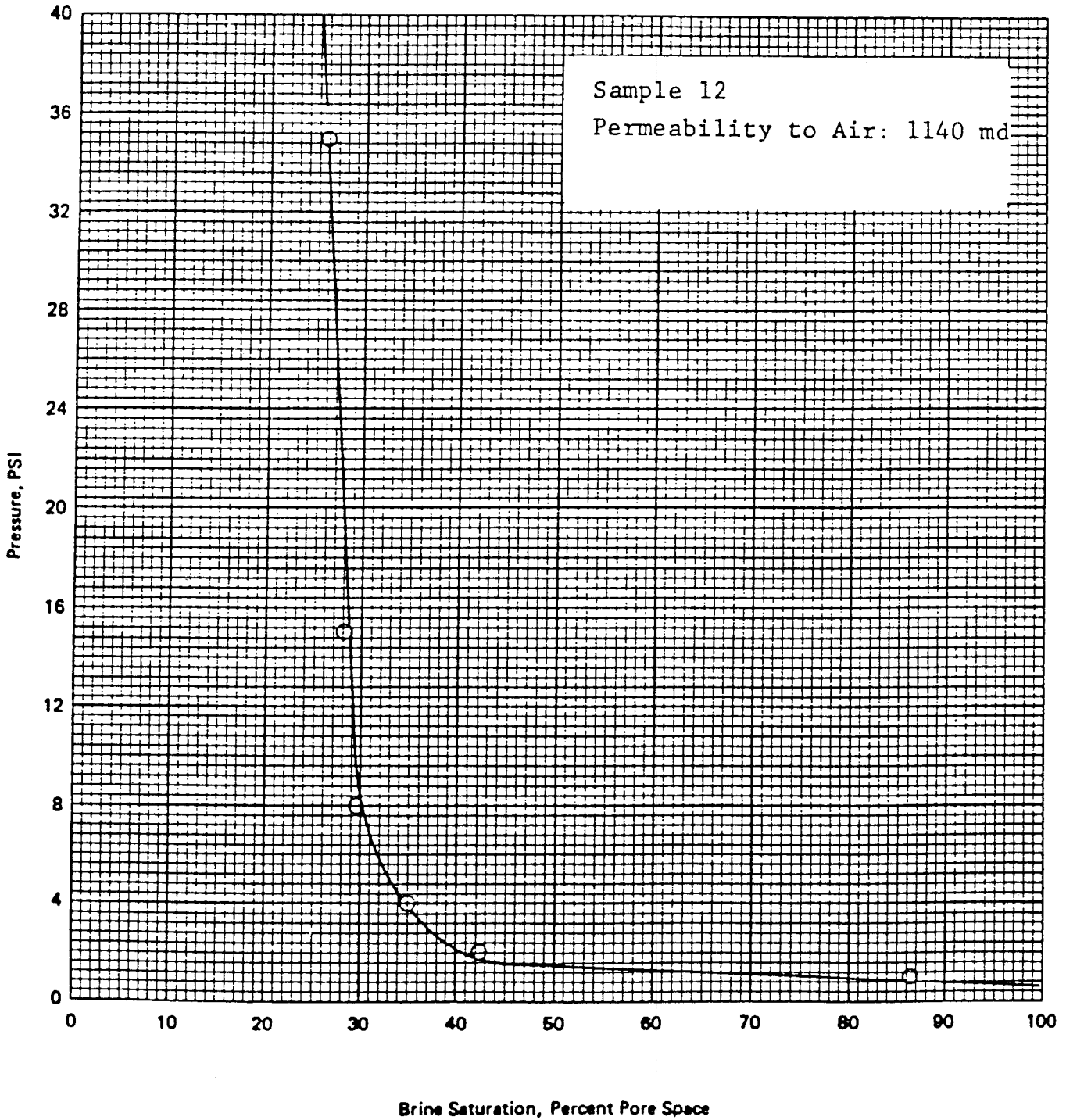
Test Method: Porous-Plate Cell

Sample I.D.	Depth, feet	Permeability to Air, millidarcys	Porosity percent	Pressure, psi					
				1	2	4	8	15	35
				Brine Saturation, percent pore space					
2	9106	419	28.7	88.6	53.6	44.5	36.8	32.3	30.8
4	9113	301	29.7	79.0	58.1	53.5	48.0	42.0	39.8
6	9119	1120	30.1	65.0	47.1	41.5	36.3	32.1	30.7
8	9125	167	28.2	100.0	91.3	65.9	54.5	48.4	47.2
10	9131	592	29.8	85.8	61.8	50.6	42.3	38.1	37.9
12	9137	1140	30.3	86.6	42.5	35.2	29.8	28.3	26.0
16	9149	3500	32.8	46.1	27.1	23.1	20.3	18.8	18.3
18	9155	204	27.5	100.0	96.8	66.1	48.0	44.1	44.0
24	9173	1590	32.3	80.8	43.2	36.6	20.6	28.4	27.8
30	9192	1510	31.3	99.3	41.2	28.6	23.6	21.4	21.2

Company Eaton Operating Co., Inc. Formation Frio  
Well S.G.R. No. 2 Louise Unit County Galveston  
Field Hitchcock State Texas



Company Eaton Operating Co., Inc. Formation Frio  
Well S.G.R. No. 2 Louise Unit County Galveston  
Field Hitchcock State Texas



APPENDIX D

The following page contains a table detailing the calculations of the amount of liquid dropout from the equilibrium gas as it undergoes isothermal depletion. The experimental data listed in the table were taken from page 7 of the September 29, 1959, Reservoir Fluid Study of the Thompson Trustee Well No. 1.<sup>11</sup>

TABLE D-1

CALCULATION TABLE FOR LIQUID-DROPOUT OF THE  
NORTHEAST HITCHCOCK FIELD RESERVOIR FLUID  
AT 212°F

GIVEN: Equilibrium Cell charge with 0.48025 lbs. of Reservoir Fluid

<u>EQUILIBRIUM CELL PRESSURE (PSIA)</u>	<u>EQUILIBRIUM CELL VOLUME (CC)</u>	<u>OBSERVED LIQUID VOLUME (CC)</u>	<u>PERCENT LIQUID IN CELL VOLUME</u>	<u>PERCENT LIQUID IN (1-S<sub>w</sub>) RESERVOIR PORE VOLUMES</u>
1252	2284	97.88	4.29	3.22
1962	1569	101.74	6.48	4.86
3155	997	96.68	9.70	7.28
4190	796	73.50	9.23	6.92
5035	708	31.45	4.44	3.33
5572	670	2.78	0.41	0.31
5630	666	0.05	0.008	0.006
5649	665	0.0	0.0	0.0

NOTE: The liquid referred to in the above table is hydrocarbon liquid. Also, the greatest amount of hydrocarbon liquid dropout occurs around 3155 psia. Also,  $S_w = 0.25$ .

## APPENDIX E

The method of Fetkovitch<sup>4,5</sup> for finite aquifers was used to evaluate the size of the aquifer in the Northeast Hitchcock Field. This method modeled the reservoir as a single well field having either a radial or linear aquifer. In the case of the Northeast Hitchcock Field, a finite radial model was chosen to describe the relationship between the hydrocarbon reservoir and the aquifer. In order to obtain a representative model, the model's reservoir characteristics and geometric dimensions were adjusted through a trial-and-error process until the model was capable of matching the field's production and pressure history. The approximate size of the aquifer in the Northeast Hitchcock Field was determined through this trial-and-error process.

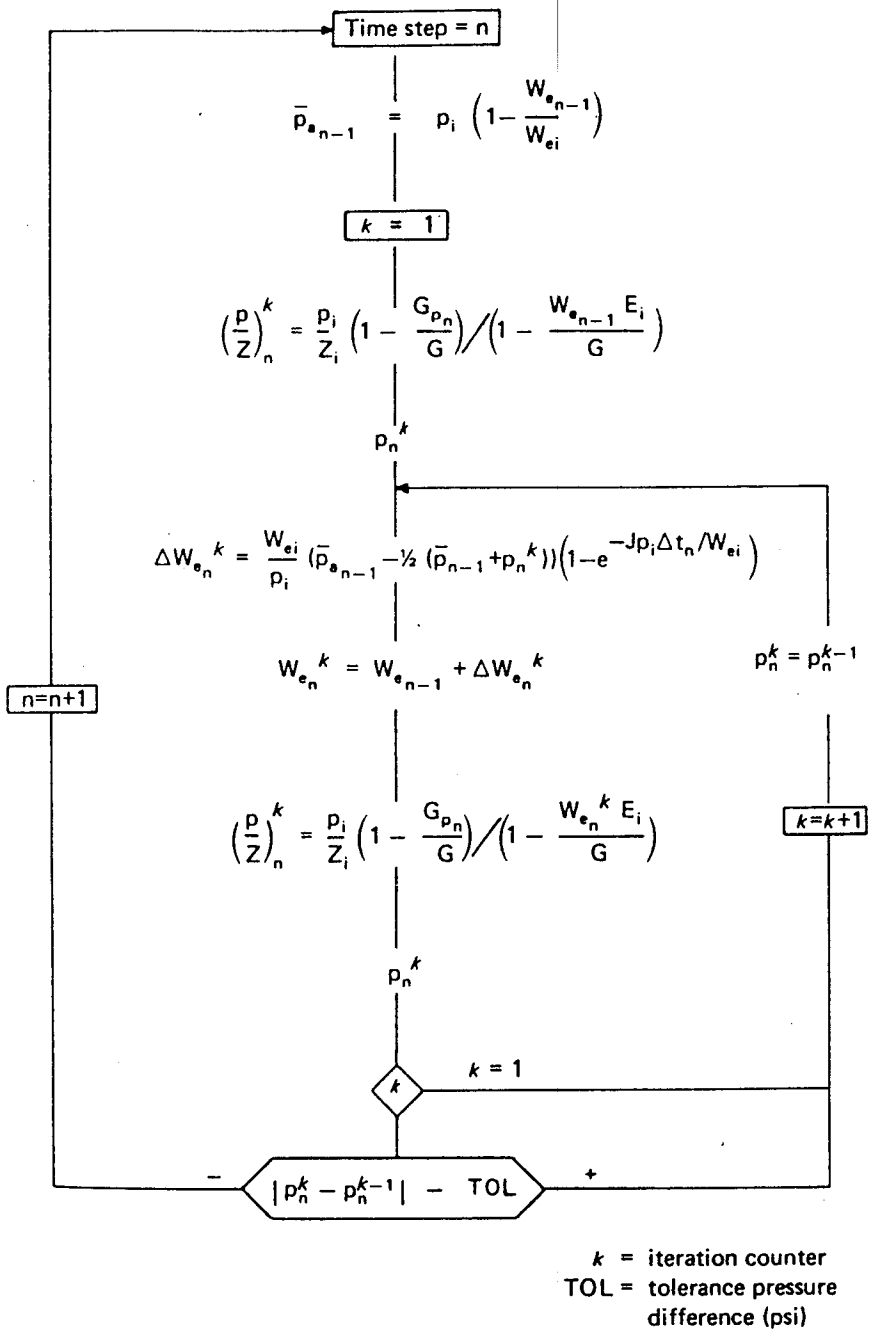
A computer algorithm was used to facilitate the trial-and-error process. This algorithm evaluated the gas reservoir pressures resulting from fluid production and water influx, and it can be seen on the following page (Figure E-1). The basic equations used in the method proposed by Fetkovitch are described below.

Inflow equation describing the flow of the aquifer into a hydrocarbon reservoir:

$$q_w = \frac{dW_e}{dt} = J(\bar{p}_a - p)$$

where

- $q_w$  = water influx rate (BBL's of Water Per Day)
- $J$  = aquifer productivity index (BBL's of Water Per Day/PSI)
- $p$  = reservoir pressure at the hydrocarbon-water contact (PSI)
- $\bar{p}_a$  = average pressure in the aquifer (PSI).



Prediction of gas reservoir pressures resulting from fluid withdrawal and water influx (Fetkovitch).

SOURCE: Dake, L.P., *Fundamentals of Reservoir Engineering*, Amsterdam, The Netherlands, Elsevier Scientific Publishing Company, 1978, p.337.

Figure E-1. Flowchart Describing the Computer Algorithm For the Method of Fetkovitch

Aquifer Material Balance equation representing the amount of water encroachment as the maximum possible expansion of the aquifer minus the expansion of the aquifer when the aquifer pressure equals  $\bar{p}_a$ :

$$W_e = \bar{c}W_i(p_i - \bar{p}_a)$$

where

$W_e$  = water encroachment volume (BBL's)

$\bar{c}$  =  $c_w + c_f$ , or the compressibility of the aquifer water plus the formation compressibility ( $\text{PSI}^{-1}$ )

$W_i$  = initial water volume (BBL's)

$p_i$  = initial aquifer pressure (PSI)

$\bar{p}_a$  = average pressure in the aquifer (PSI)

The method of Fetkovitch uses the two basic equations above in a form that represents the average pressure and the amount of water influx during discrete time intervals. These equations are:

#### AQUIFER MATERIAL BALANCE

$$\bar{p}_{a_{n-1}} = p_i \left[ 1 - \frac{\sum_{j=1}^n \Delta W_{ej}}{W_{ei}} \right]$$

where

$\bar{p}_{a_{n-1}}$  = average reservoir pressure for time interval n-1 (PSI)

$p_i$  = initial reservoir pressure (PSI)

$\Delta W_{ej}$  = water encroachment volume during time interval j (BBL's)

$W_{ei}$  =  $\bar{c}W_i p_i$ , the aquifer size (BBL's).

### WATER INFLUX

$$W_{e_n} = \frac{We_i}{P_i} (\bar{p}_{a_{n-1}} - \bar{p}_n) (1 - e^{(-Jpi\Delta t_n/Wei)})$$

where

$\bar{p}_{a_{n-1}}$  = average aquifer pressure at the end of the (n-1)<sup>th</sup> time interval (PSI)

$\bar{p}_n$  =  $\frac{1}{2}(p_{n-1} + p_n^k)$ , average reservoir-aquifer boundary pressure during the nth time interval (PSI)

### RADIAL FLOW MODEL (Semisteady State)

$$J = \frac{7.8 \times 10^{-3} fkh}{(\frac{r_e}{r_g} - 3/4)}, \text{ productivity index for a finite radial aquifer (BBL's of Water Per Day/PSI)}$$

where

f =  $\theta/360$ , where  $\theta$  was taken to be 60 degrees for the Northeast Hitchcock Field

h = aquifer height (ft)

k = aquifer permeability (md)

$r_e$  = radial distance from aquifer boundary to producing well in feet

$r_g$  = radial distance from boundary of the hydrocarbon reservoir to the producing well in feet.

The iterative method of Fetkovitch also considers the effect of gas withdrawals and water influx into the reservoir through use of the following reservoir material balance equation.

## RESERVOIR MATERIAL BALANCE

$$\left(\frac{p}{z}\right)^k = \frac{p_i}{z_i} \left(1 - \frac{G_{p_n}}{G}\right) / \left(1 - \frac{W_{e_n}^k E_i}{G}\right)$$

where

$z$  = gas deviation factor at pressure  $p_n$

$G_{p_n}$  = gas produced at time  $n$  (standard cubic feet)

$G$  = original gas in place (standard cubic feet)

$W_{e_n}$  = water encroachment at time  $n$  (BBL's)

$E_i$  =  $1/B_{g_i}$ , initial gas expansion factor  
(standard cubic feet/reservoir cubic feet)

$p_i$  = initial reservoir pressure (PSI)

$z_i$  = initial gas deviation factor

$B_{g_i}$  = initial gas formation volume factor (See Appendix B)

Several runs were made using the computer algorithm before satisfactory matches between historical pressures were obtained. The trial-and-error runs were made by varying the  $r_e/r_g$  ratio in the radial flow model representation of the reservoir. The reservoir characteristics assumed to be constant throughout the matching process were:

theta,  $\theta$  = 60 degrees

porosity,  $\phi$  = 0.30

permeability,  $k$  = 400 md

total compressibility,  $\bar{C}$  =  $9.6 \times 10^{-6}$  psi<sup>-1</sup>

An adequate match of historical pressures was obtained when the  $r_e/r_g$  ratio was set to 5.5. At this ratio, the aquifer pore volume calculated to be 3,100,000 MBBL. The hydrocarbon reservoir pore volume was taken to be 104,450 MBBL. These calculations indicated that the aquifer is approximately 30 times the size of the hydrocarbon reservoir pore volume.

Most of the equations and the computer algorithm presented in this Appendix are described in greater detail in Chapter 9 of the Fundamentals of Reservoir Engineering by L. P. Dake.<sup>5</sup>

APPENDIX F

In order to predict the amount of condensate produced by each well, the relationship between the amount of liquid hydrocarbons dissolved in the equilibrium gas (wellstream gas) and the reservoir pressure need to be determined. This relationship could then be used to determine the liquid production from a well as a function of the equilibrium gas produced and the average reservoir pressure of the well's drainage area.

The relationship described above was determined using equilibrium cell data found on page 7 of the September 29, 1959, Reservoir Fluid Study on a recombined fluid sample from the Thompson Trustee Well No. 1.<sup>11</sup> Calculations determining the amount of liquid hydrocarbon dissolved in the equilibrium gas are contained on the following page.

TABLE F-1

DETERMINATION OF THE AMOUNT OF DISSOLVED HYDROCARBON  
LIQUID CARRIED IN THE EQUILIBRIUM GAS

GIVEN: Page 7 of 1985 Reservoir Fluid Study - Liquid Phase Volume Observations

Volumes charged into the equilibrium cell:

121.19 cc liquid at 80°F and 1200 psia  
5.94661 cu. ft. gas at 60°F and 14.65 psia

MAJOR ASSUMPTION: The effects of liquid compressibility are considered negligible.

CELL PRESSURE (psia)	A. Initial Liquid Volume (cc)	B. Observed Liquid Volume (cc)	(A-B) Dissolved liquid Volume		BBL (5.94661 cu ft)	BBL (MMCF)
			cc	BBL*		
1252	121.19	97.88	23.31	$1.599 \cdot 10^{-4}$	$2.690 \cdot 10^{-5}$	26.9
1962	121.19	101.74	19.45	$1.335 \cdot 10^{-4}$	$2.245 \cdot 10^{-5}$	22.4
3155	121.19	96.68	24.51	$1.682 \cdot 10^{-4}$	$2.829 \cdot 10^{-5}$	28.3
4190	121.19	73.50	47.69	$3.273 \cdot 10^{-4}$	$5.504 \cdot 10^{-5}$	55.0
5035	121.19	31.45	89.74	$6.159 \cdot 10^{-4}$	$1.036 \cdot 10^{-4}$	103.6
5572	121.19	2.78	118.41	$8.126 \cdot 10^{-4}$	$1.336 \cdot 10^{-4}$	136.6
5630	121.19	0.05	121.14	$8.313 \cdot 10^{-4}$	$1.398 \cdot 10^{-4}$	139.8
5649	121.19	0	121.19	$8.314 \cdot 10^{-4}$	$1.398 \cdot 10^{-4}$	139.8
5899	121.19	0	121.19	$8.314 \cdot 10^{-4}$	$1.298 \cdot 10^{-4}$	139.8

\*CONVERSION FACTOR:  $6.86268 \cdot 10^{-6}$  BBL/cc

PART 3  
RESEARCH IN WELL LOGGING

by H. F. Dunlap, James H. Dupree, Jr., and Tom A. Lowe

July 1985

Center for Energy Studies  
The University of Texas at Austin  
Austin, Texas 78713

## DISCUSSION

### Research in Well Logging

Our original research objectives were to: (1) evaluate the possibility of quantitative gas saturation calculation using the density log, neutron log, lithodensity log, and the gamma spectrometry tool logs run in open hole; (2) evaluate sanding prediction using compressional and shear wave velocities from the digital sonic log run in open hole; (3) continue our study of short term variation in mud and mud filtrate resistivity; and (4) generally advise on logging programs and interpretation in the Delee #1 well.

Unfortunately, no open hole logs were run in the Delee #1 well, due to the occurrence of unexpected high pressure gas stringers near total depth. This ruled out items (1) and (2) of our original objectives. The cement job over the Frio "A" zone of interest was poor, as indicated by the cement bond log and the cement evaluation tool. This meant that the density log, if run in the cased hole, could not be corrected for cement effects in the casing-formation annulus, so the density log was not run.

In addition to the cement bond log and the cement evaluation tool, Schlumberger ran the digital sonic (long linear array) log, compensated neutron log, natural gamma ray spectroscopy log, and the gamma ray spectroscopy tool (uses gamma ray spectroscopy from neutron capture and inelastic neutron scattering to estimate C, O, H, Si, Ca, S, Cl, and Fe content).

We hoped that it would be possible to estimate shear velocity, as well as compressional velocity, from the cased hole digital sonic log. To date this has not been possible. We have suggested to Schlumberger that they

try to derive the shear velocity values from the Stonely wave velocities (which are obtainable from the Delee Logs) and the wellbore geometry. They have said they would attempt this, but no results are available to date. If we can get both shear and compressional wave velocities in the Delee well, we can check sanding prediction methods against the actual sanding behavior in this well. It is quite possible that sanding will be a problem at high production rates in this well.

We were able to get data on research objective (3) - study of short term variation in mud and mud filtrate resistivity in the Delee well. A paper on this subject was presented at the 6th U. S. Gulf Coast Geopressured-Geothermal Energy Conference at the University of Texas, February 4-6, 1985 (copy attached). We were able for the first time to obtain data on effect of makeup water resistivity (but not makeup water volume) on mud and mud filtrate resistivity. In the Delee well, barite is not a major contributor to NaCl in the mud, as compared to lignosulfonate, NaOH, and other additives.

We found the boron concentration in the Frio A sand was unexpectedly high (10 to 44 ppm). These high concentrations must be corrected for when using the gamma spectroscopy tool sigma data (neutron capture cross section data).

## EFFECT OF MAKEUP WATER AND MUD ADDITIVES ON DRILLING FLUID RESISTIVITY\*

H. F. Dunlap, James H. Dupree Jr., and Tom A. Lowe  
The University of Texas at Austin  
Petroleum Engineering Department  
Austin, Texas 78712

### ABSTRACT

Recent studies show that there are large short term variations in mud and mud filtrate resistivity in drilling wells. Standard deviation of Rmf (log header) vs. Rmf (actual) averaged 50% in five wells studied (Williams and Dunlap, 1984). There are several causes of these short term fluctuations, one of which is short term variation in mud makeup water resistivity and volume. Data on variation in mud makeup water resistivity (but not volume) were obtained for the first time in the DeLee #1 well, Hitchcock Field, Galveston County, Texas. In this well, at least, makeup water resistivity correlates well with mud resistivity. Data are now being collected for the Texas Oil and Gas Co. Bruce #1 well, N. Alta Loma Field, which will include both makeup water resistivity and volume.

### INTRODUCTION

It is important in log interpretation to know the value of the mud filtrate resistivity (Rmf) at the time a zone is drilled. A large part of the mud filtrate, probably one-half or more, is lost to porous and permeable zones at the time they are drilled (spurt loss). The remainder of the filtrate is lost gradually over a period of days or weeks as the well is drilled deeper. Knowledge of the mud filtrate resistivity is important in log interpretation, being needed in the calculation of formation water resistivity from the SP log, and in calculation of formation factor, porosity, and water saturation using the shallow investigation resistivity logs (Rxo logs).

SP-derived formation water salinities were used as a major screening factor by the Department of Energy, Geothermal Energy Division, in testing the feasibility of dissolved methane production from deep, hot geopressed aquifers in South Texas and Louisiana. Dissolved methane decreases with increases in salinity, and zones with relatively fresh water were desired for testing; however, the waters of zones chosen on the basis of SP-derived salinities were usually far more saline than calculated.

In the course of research designed to improve the accuracy of SP-derived water salinity predictions, Dunlap and Dorfman (1981) suggested that the errors could be due in part to large short term variations in Rm and Rmf values which differ

\*Presented at 6th U.S. Gulf Coast Geopressed-Geothermal Energy Conference, Austin, Texas, February, 1985.

significantly from log header values, which are traditionally used in log interpretation. Further work by Williams and Dunlap (1984) showed that large short term (daily) variations in  $R_m$  and  $R_{mf}$  indeed occurred in five wells for which data were available. Average standard deviation between actual  $R_m$  and log header  $R_m$  was 40%. For  $R_{mf}$ , the standard deviation in these wells was 50%.

The causes of these large short term variations in mud properties are complex, but the following factors are certainly involved.

1. The addition of soluble salts, some present as impurities, in common mud additives such as bentonite, barite, lignosulfonate, etc.
2. Inflows of relatively salty formation water when the mud pressure momentarily falls below formation pressure during drilling, when pulling pipe, or when drilling into a high pressure zone.
3. Variations in resistivity and volume of makeup water added to the mud during drilling.

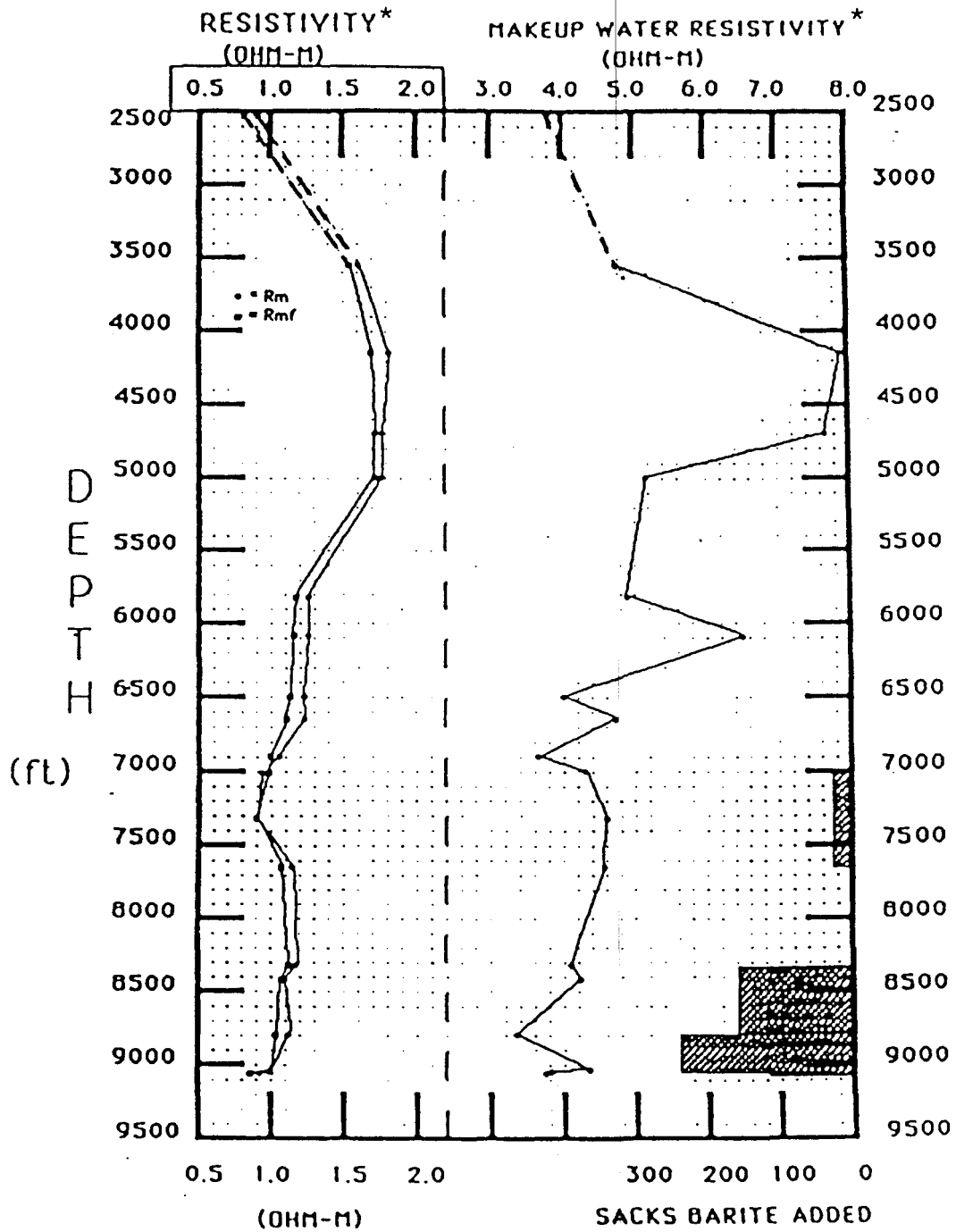
Williams and Dunlap (1984) discuss factor #1 in some detail. No data on factor #2 are presently available to us. Such data might be obtained by continuously monitoring mud resistivity in and out of hole. The present paper reports for the first time the effect of makeup water on mud resistivity.

### THE EXPERIMENT

During the drilling of Secondary Gas Recovery DeLee #1 well, Hitchcock Field, Galveston County, Texas, it was possible to sample the mud and makeup water daily, and also to obtain samples of barite, bentonite, lignosulfonate, and other additives used in the mud. However, it proved impossible to monitor the volume of mud makeup water added. Water was added to the mud in several places, and we were not able to devise a system for measuring daily water additions. An ideal system would use a water meter installed so as to measure only mud makeup water, not water used in washing down the rig floor, etc. We hope to obtain such data in the Texas Oil and Gas Co. Bruce #1 well, N. Alta Loma Field, Galveston County, Texas.

The resistivities of the makeup water, mud, and mud filtrate for the DeLee #1 well are shown as a function of depth in Fig. 1. There is an obvious correlation between mud and mud filtrate resistivity, and makeup water resistivity. We suspect that if makeup water volumes had been known, the correlation would be even stronger. From 2500' to approximately 3600', and from approximately 6100' to TD, water from a nearby water well was used for mud makeup. From approximately 3600' to about 6100', public utility water was used due to maintenance operations on the water well. The larger variations in makeup water resistivity can be attributed to using different makeup water. The smaller variations can be attributed to short term variations naturally occurring within each makeup water type.

Mud additives used in the DeLee #1 well were analyzed for salt content. Table 1 shows salt contributions, expressed as sodium, for the additives that were used in significant amounts. For barite, bentonite, and lignosulfonate, amounts of sodium contributed to the drilling fluid were obtained by resistivity measurements on mixtures of each additive with distilled water and assuming negligible contributions from other cations (the effects of which are yet to be analyzed). Sodium contribution from caustic soda (NaOH) was calculated directly. Table 1 indicates that for the DeLee #1 well, caustic soda was the principal contributor of sodium, while lignosulfonate and bentonite also contributed significant amounts. Barite data from Table 1 show that for the DeLee #1 well, sodium addition by contamination



\*Normalized to 75°F

Fig. 1 Resistivity of mud, mud filtrate, and makeup water vs. depth, DeLee #1 well, Hitchcock Field.

TABLE 1 Sodium Contributions by Mud Additives, DeLee #1 Well

Additive	Weight % Sodium	Total Sacks Added	Total lbs Sodium Added
Barite	<0.01%	4902	< 39
Bentonite	0.43%	384	163
Lignosulfonate	3.73%	423	782
Caustic Soda	57.5%	107	3076

in barite is negligible. Added together, caustic soda, lignosulfonate, and bentonite additions to the drilling fluid contributed more than enough sodium (if present as Na<sup>+</sup> in solution), to account for all conductivity and resultant R<sub>m</sub> and R<sub>mf</sub>. Clearly, sodium content in drilling fluid additives affects R<sub>m</sub> and R<sub>mf</sub> significantly, and large additions over a short period of time will cause changes in R<sub>m</sub> and R<sub>mf</sub>, as noted by Williams and Dunlap (1984).

Chemical reactions within the drilling fluid system must be accounted for also, as they play an important role in determining the amount of ions actually in solution and hence R<sub>m</sub> and R<sub>mf</sub>. Currently, a model accounting for chemical reactions is being developed to quantify all factors, including makeup water and additives, which result in short term variations in R<sub>m</sub> and R<sub>mf</sub> in drilling wells.

In the DeLee #1 well, no open hole log runs were made, so no comparisons with log header values of R<sub>m</sub> and R<sub>mf</sub> were possible.

#### USE OF ION SELECTIVE ELECTRODES

Williams and Dunlap (1984) presented data suggesting it might be possible to infer R<sub>mf</sub> from ion selective electrode measurements on the mud, without filtering the mud. Figure 2 (Williams and Dunlap, 1984) shows their data on laboratory muds and filtrates using a Na<sup>+</sup> ion selective electrode. The correlation is excellent. Measurements on the field mud sampled in the DeLee #1 well are shown in Fig. 3. The salinity correlation based on the Na<sup>+</sup> ion selective electrode between mud and mud filtrate is again excellent. However, we suspect that it may not be practical to infer accurate values of R<sub>mf</sub> using ion selective electrodes in mud. Other ions in addition to Na<sup>+</sup> may be present in the filtrate in amounts that would significantly affect R<sub>mf</sub> and would not be accounted for by the Na<sup>+</sup> electrode. A different ion selective electrode must be used to measure the activity of each ion in the mud (Ca<sup>++</sup>, Mg<sup>++</sup>, Cl<sup>-</sup>, etc.). Hence, several electrodes may be needed to accurately obtain R<sub>mf</sub>. If more than two ion selective electrodes need to be used to obtain accurate R<sub>mf</sub>, it may be quicker and simpler to obtain a reasonable approximation of R<sub>mf</sub> using the conventional method of filtration and direct measurement using an ohmmeter, as we have done for the DeLee #1 well in Fig. 1. Further research is necessary to determine the suitability of ion selective electrodes in determining mud filtrate resistivity in drilling wells.

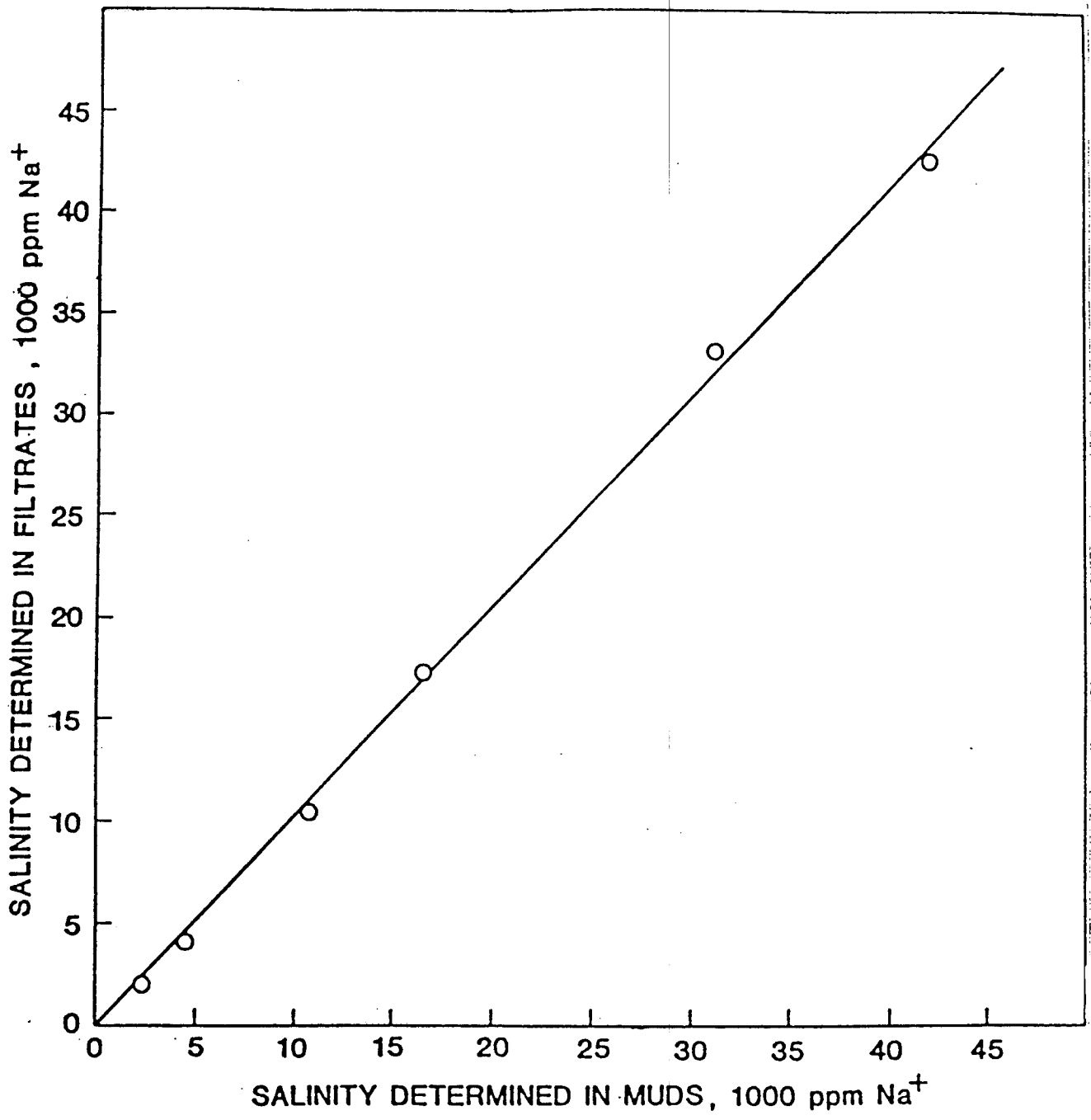


Fig. 2 A comparison of salinities determined in muds and their filtrates by Na<sup>+</sup> ion selective electrode (Williams and Dunlap, 1984).

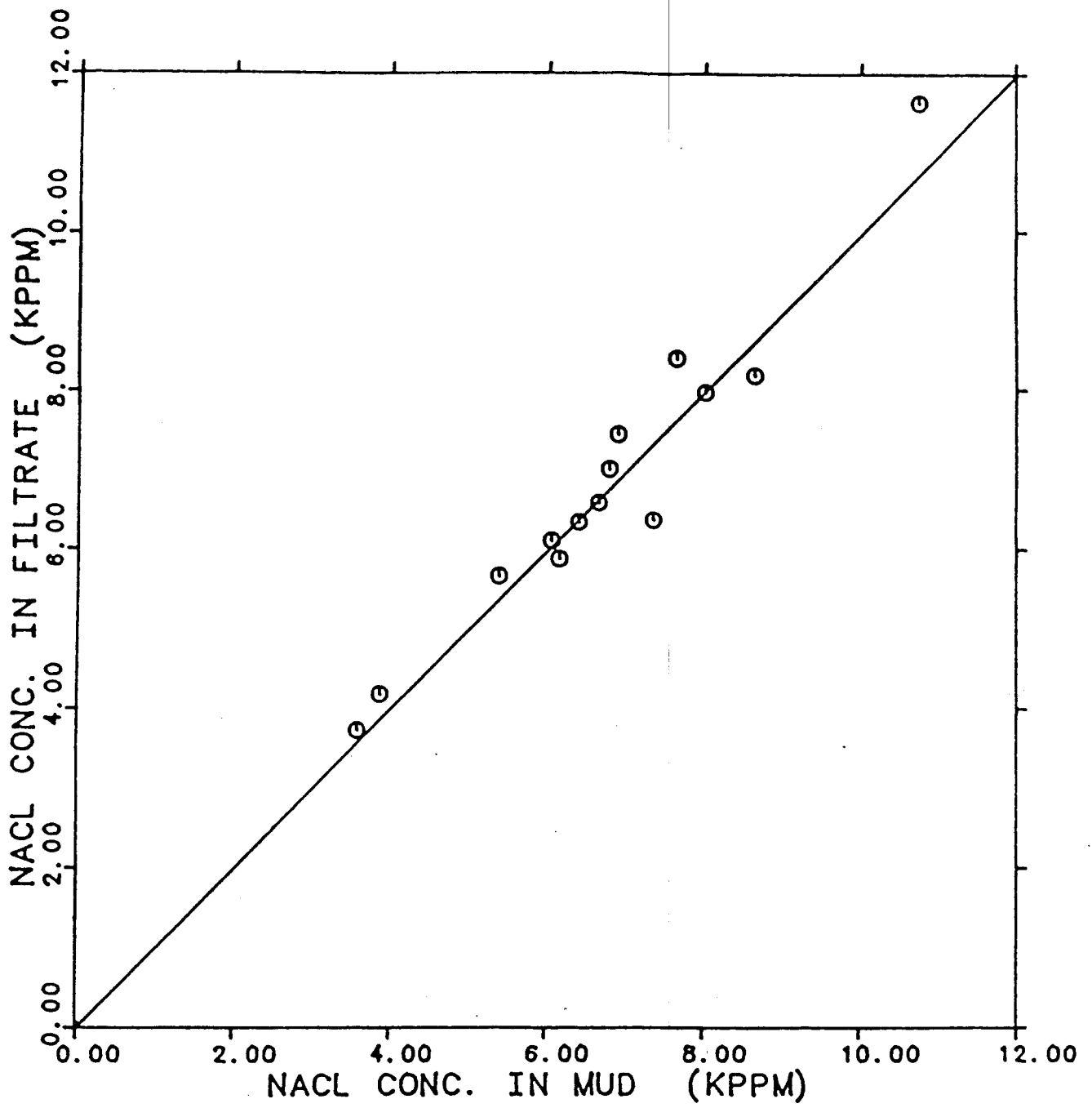


Fig. 3 Comparison of salinities determined in muds and their filtrates by sodium ion selective electrode, DeLee #1 well, Hitchcock Field.

## CONCLUSIONS

1. Variations in makeup water resistivity correlate with variations in mud and mud filtrate resistivity in the DeLee #1 well. Variations in makeup water resistivity should be measured daily and these variations controlled to obtain more uniform mud properties.
2. Sodium content in mud additives significantly affects  $R_m$  and  $R_{mf}$  in the DeLee #1 well. In this well, caustic soda contributed the largest amount of sodium, and lignosulfonate and bentonite also contributed significant amounts. Salt contamination in the barite used was negligible.
3. It will be necessary to plan the system for obtaining mud makeup water volume several days in advance of spudding the well, so the necessary water meter and piping layout can be installed.

## ACKNOWLEDGEMENTS

This work was supported by The Gas Research Institute, and data were provided by them and Secondary Gas Recovery, Inc. The encouragement and assistance of Dr. Myron Dorfman of The University of Texas is gratefully acknowledged.

## REFERENCES

- Bauer, H. H., G. D. Christian, and J. E. O'Reilly (1978). Instrumental Analysis, Allyn and Bacon, Inc., Boston, Chapt. 1-2.
- Dunlap, H. F., and M. H. Dorfman (1981). Problems and partial solutions in using the S.P. log to predict water salinity in deep hot wells. Trans. Geothermal Resources Council, 5, 283-286.
- Log Interpretation Charts (1972). Schlumberger Ltd., U.S.A.
- Williams, H., and H. F. Dunlap (1984). Short term variations in drilling fluid parameters: their measurement and implications. Log Analyst, 25(5), 3-9.